Molecular Mechanism of Active Photoprotein Complex Formation

Elena V. Eremeeva

Thesis committee

Promotors
Prof. dr. W.J.H. van Berkel
Personal Chair at the Laboratory of Biochemistry

Prof. dr. A.J.W.G. Visser
Emeritus Professor of Microspectroscopy

Co-promotor
Dr. E.S. Vysotski
Associate professor
Institute of Biophysics, Russian Academy of Sciences, Krasnoyarsk

Other members
Prof. dr. H. van Amerongen, Wageningen University
Prof. dr. S. de Vries, Delft University of Technology
Dr. J.T.M. Kennis, VU University Amsterdam
Dr. S. J.J. Brouns, Wageningen University

This research was conducted under the auspices of the Graduate School VLAG (Advanced studies in Food Technology, Agrobiotechnology, Nutrition and Health Sciences).

Molecular Mechanism of Active Photoprotein Complex Formation

Elena V. Eremeeva

Thesis
submitted in fulfilment of the requirements for the degree of doctor
at Wageningen University
by the authority of the Rector Magnificus
Prof. dr. M.J. Kropff,
in the presence of the
Thesis Committee appointed by the Academic Board
to be defended in public
on Wednesday 16 January 2013
at 4 p.m. in the Aula.

Elena V. Eremeeva
Molecular mechanism of active photoprotein complex formation
195 pages

Thesis, Wageningen University, Wageningen, NL (2013)
With references, with summaries in English and Dutch

ISBN 978-94-6173-458-7

Table of contents

Chapter 1	General Introduction	7
Chapter 2	Ligand binding and conformational states of the photoprotein obelin	25
Chapter 3	The intrinsic fluorescence of apo-obelin and apo-aequorin and use of its quenching to characterize coelenterazine binding	43
Chapter 4	Oxygen activation of apo-obelin-coelenterazine complex	59
Chapter 5	Molecular mechanism of active photoprotein formation	77
Chapter 6	Bioluminescent and spectroscopic properties of obelin and aequorin coelenterazine-binding pocket mutants	109
Chapter 7	Picosecond fluorescence relaxation spectroscopy of the calcium-discharged photoproteins aequorin and obelin	125
Chapter 8	Fast kinetics of W92F obelin emitting species	141
Chapter 9	Summary and General Discussion	153
	References	163
	Samenvatting en Algemene Discussie	181
	Acknowledgements	190
	Curriculum Vitae	192
	List of publications	193
	Overview of completed training activities	194

Chapter 1

General Introduction

Bioluminescence

Bioluminescence is the production and emission of light by a living organism, a phenomenon which is widespread in the biosphere. Bioluminescence occurs in marine organisms, in bacteria, fungi and algae, and in many animals (Lee, 2001; Shimomura, 2006; Haddock ***et al.***, 2010). In the deep ocean, almost all species are bioluminescent. On land, bioluminescent species comprise fireflies and some other beetles, insects like flies and springtails, fungi, centipedes and millipedes, certain snails and earthworms. Bioluminescence is almost absent in freshwater, except for some insect larvae and a freshwater limpet.

Bioluminescence serves a number of crucial functions. These include: i) defense such as startle, production of a smoke screen or distractive body part, ii) offence such as prey attraction or illumination, iii) communication and iv) mating. Yet, in many cases the survival value of bioluminescence remains a puzzle. Bioluminescence may be important at a particular developmental state, such as the plankton larva of a benthic worm or the medusa stage of a hydroid, or during a particular reproductive period, as with the female octopod *Japetella* (Haddock ***et al.***, 2010).

Bioluminescence is an extremely attractive analytical tool for many areas of research. A main advantage of bioluminescence is the high sensitivity of the emitted light, which can be measured down to a few photons using either a photomultiplier or a charge-coupled device (CCD) camera. Starting from the luciferase firefly system (Shropshire and Gettens, 1966) application of bioluminescence has increased tremendously in the past decades and has significantly contributed to the advances of biology and medicine. Various bioluminescent proteins are successfully used in immuno- and nucleic acid hybridization assays, and as reporters or probes in living cells to monitor Ca^{2+} concentrations, protein-protein interactions or gene expression levels (Roda ***et al.***, 2004, Rowe ***et al.***, 2009; Grienberger and Konnerth, 2012).

Ca^{2+}-regulated photoproteins

Bioluminescence of a variety of marine organisms, mostly coelenterates, is caused by Ca^{2+}-regulated photoproteins. The best known of these is aequorin, first isolated some 50 years ago by Shimomura (Shimomura *et al.*, 1962), from the jellyfish *Aequorea*. Ca^{2+}-regulated photoproteins use coelenterazine (Fig. 1.1A) as a substrate, which is widely distributed in luminous and non-luminous marine organisms, and has been identified as a luciferin in many bioluminescent systems.

Ca^{2+}-regulated photoproteins consist of a single polypeptide chain of about 22 kDa to which the "pre-activated" coelenterazine, 2-hydroperoxycoelenterazine, is tightly bound (Fig. 1.1B) (Shimomura and Johnson, 1978; Head *et al.*, 2000; Liu *et al.*, 2000). Therefore it was proposed that aequorin and some other bioluminescent proteins should be classified as "photoproteins", capable of emitting light in proportion to the concentration of protein, distinguishing them from luciferases where the amount of light emitted is proportional to the concentration of the substrate luciferin (Hastings, 1996). Consequently, in an assay each photoprotein molecule can react only once.

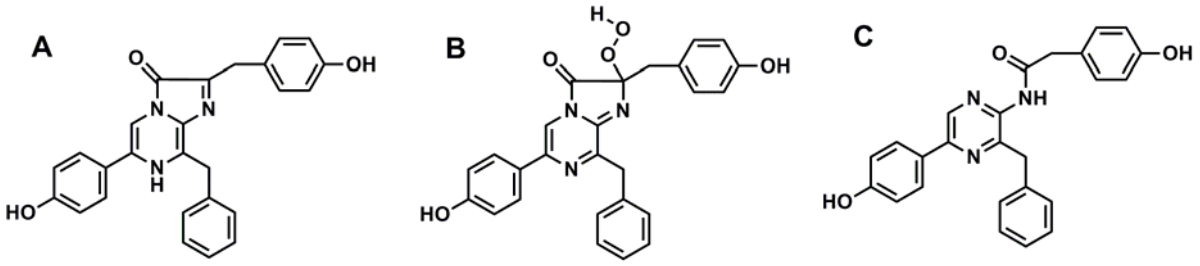

Figure 1.1 Coelenterazine (A), 2-hydroperoxycoelenterazine (B) and coelenteramide (C) structures.

Recombinant apo-photoproteins can be converted to their active 2-hydroperoxy-coelenterazine-liganded forms upon incubation under calcium-free conditions with coelenterazine, molecular oxygen and thiol-reducing agents (Shimomura and Johnson, 1975). Binding of calcium initiates oxidative decarboxylation of 2-hydroperoxy-coelenterazine resulting in the excited state of the product, coelenteramide (Fig. 1.1C). The excited coelenteramide relaxes to its ground state with the production of blue light with emission maximum around 465-495 nm depending on the type of photoprotein (Vysotski and Lee, 2004). Calcium is not essential for the bioluminescence of photoproteins because

even without this trigger they display a very low level of light emission called the "calcium-independent luminescence" (Allen *et al.*, 1977). However, light intensity is increased up to 1 million-fold or more in the presence of calcium.

Ca^{2+}-regulated photoproteins have been detected in more than 25 different coelenterates and probably there are many other organisms containing photoproteins (Morin, 1974). So far seven photoproteins have been isolated and purified: aequorin, halistaurin (mitrocomin) and phialidin (clytin) from the jellyfishes *Aequorea, Halistaura (Mitrocoma),* and *Phialidium (Clytia)* (Shimomura, 2006); obelins from the marine hydroids *Obelia longissima* (Vysotski *et al.*, 1989) and *Obelia geniculata* (Campbell, 1974) and mnemiopsin and berovin from the ctenophores *Mnemiopsis* and *Beroe* (Ward and Seliger, 1974).

Three-dimensional structures of Ca^{2+}-regulated photoproteins

To date cDNA sequence information is available for all purified photoproteins: aequorin (Prasher *et al.*, 1985; Inouye *et al.*, 1985), halistaurin (Fagan *et al.*, 1993), clytin (Inouye and Tsuji, 1993), *Ol*-obelin (Illarionov *et al.*, 1995), *Og*-obelin (Markova *et al.*, 2002), mnemiopsin (Aghamaali *et al.*, 2011) and berovin (Markova *et al.*, 2012). They show similar amino acid sequences with three conserved calcium-binding motifs (Fig. 1.2) (Tsuji *et al.*, 1995).

The spatial structures of obelin and aequorin were first determined in 2000 (Head *et al.*, 2000; Liu *et al.*, 2000). As expected, both photoproteins share the same fold. The compact globular tertiary structure contains two sets of four helices comprising helix-turn-helix motifs known as EF-hands (Fig. 1.3). The 2-hydroperoxycoelenterazine binding pocket is located in the interior hydrophobic part of the photoprotein and is formed by residues originating from each of the helices (Liu *et al.*, 2000). From the multiple sequence alignment depicted in Figure 1.2 it can be seen that almost all residues forming the substrate binding pocket in each type of photoprotein are conserved (Vysotski and Lee, 2004).

Ca^{2+}-regulated photoproteins contain less Trp residues than other members of the EF-hand calcium-binding protein superfamily (Moncrief *et al.*, 1990). All photoproteins

with known amino acid sequence contain six tryptophans. Four strictly conserved residues (Trp92, 114, 135, and 179; numbered according to the obelin sequence (Liu *et al.*, 2000) are found in the coelenterazine-binding pocket.

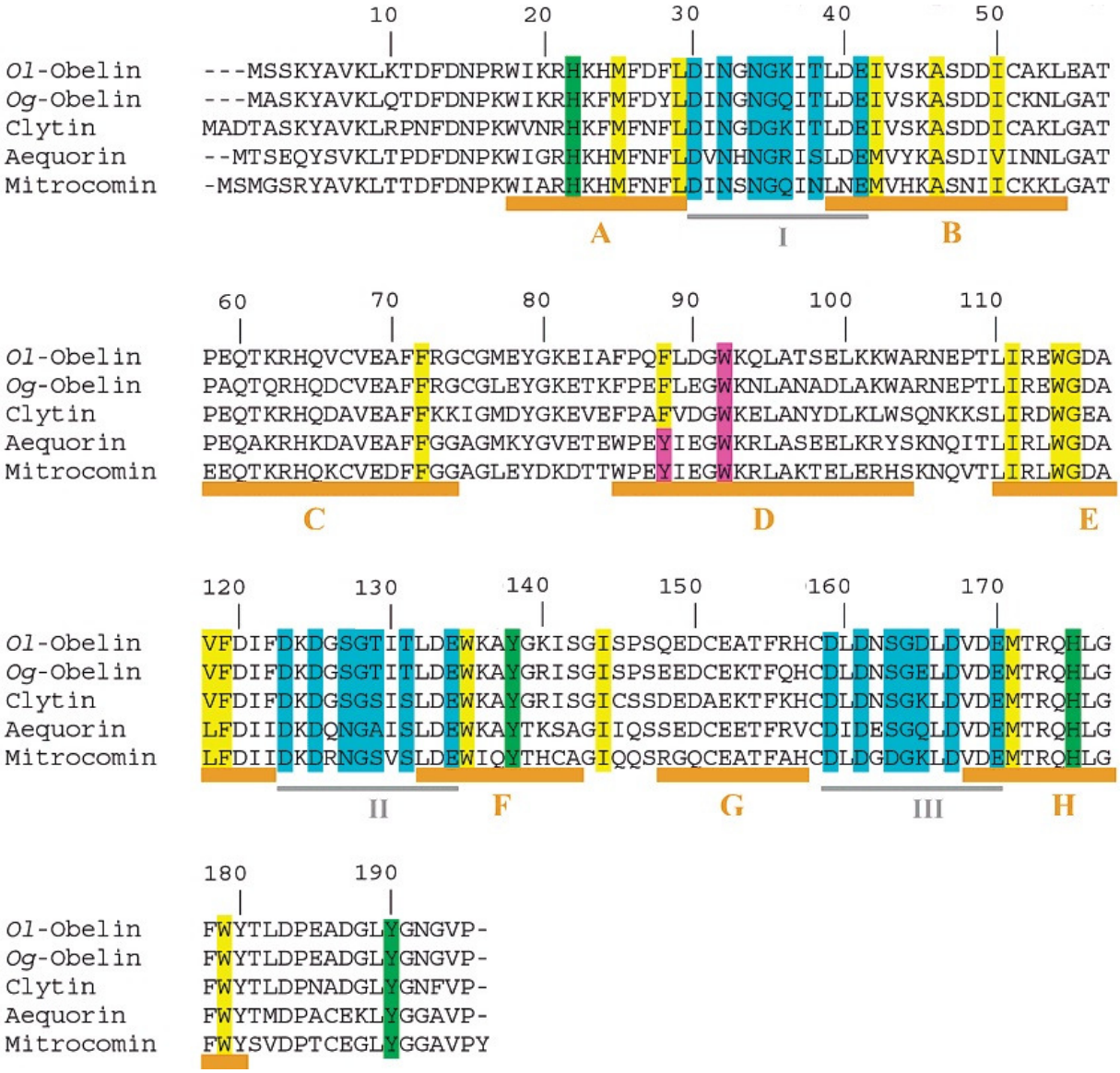

Figure 1.2 Multiple sequence alignment among the Ca^{2+}-regulated photoproteins: aequorin, mitrocomin, clytin and obelins from *O. longissima* and *O. geniculate.* The residues found from spatial structures of aequorin and obelins to be around the active site are shown in yellow, green, and pink. The residues participating presumably in bioluminescent reaction are marked in green. The residues that probably take part in formation of light emitter through their hydrogen bonds are shown in pink. Helices A-H are shown in brown underbars according to the *Ol*-obelin 3D structure. Calcium-binding loops I-III are shown as gray underbars. The calcium-binding consensus sequences within the loops are marked in cyan.

Figure 1.3 Spatial structure of obelin (PDB code 1QV0). The 2-hydroperoxycoelenterazine molecule (gray) is shown in the center as a stick model.

The importance of certain amino acid residues for the photoprotein bioluminescence was obvious before the three-dimensional structures were solved. Studies of Trp92 and His175 variants of obelin and aequorin (Ohmiya et al., 1992; Ohmiya and Tsuji, 1993; Bondar et al., 1999) suggested that these residues can be involved in the generation of the photoprotein excited state and are located near coelenterazine in the active center. Further replacements of aromatic and histidine residues allowed the conclusion that Trp138, His175, Trp179 and Tyr190 are important for positioning and stabilizing of 2-hydroperoxycoelenterazine and could be involved in triggering of photoprotein bioluminescence (Fig. 1.4).

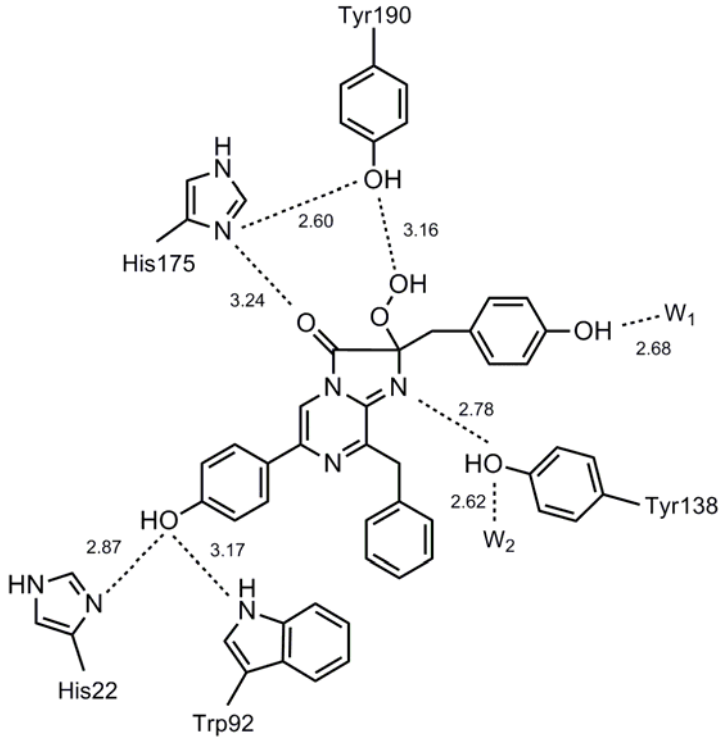

Figure 1.4 Two-dimensional representation to illustrate the hydrogen bond network (dashed lines) in the binding cavity of obelin. W_1 and W_2 – water molecules. Distances are shown in Å.

Proton-relay mechanism for Ca^{2+}-triggered photoprotein bioluminescence

McCapra and Chang suggested a mechanism for the bioluminescence reaction from a model study of the chemiluminescence of 6-phenyl-2-methyl-imidazopyrazinone in aprotic solvent (McCapra and Chang, 1967). They suggested that the oxidative decarboxylation of this coelenterazine analog occurs through several steps (Fig. 1.5). The initial reaction with oxygen produces a primary oxygenation product, the 2-hydroperoxide (1), which is deprotonated and ring-closed to a dioxetanone (2). In DMSO and a strong base such as potassium *tert*-butoxide, the chemiluminescence reaction in Fig. 1.5 has a spectral emission maximum at 455 nm. The fluorescent species was identified as the excited amide anion because without base added the fluorescence maximum is at 380 nm, assigned to the neutral species.

Later this model was extended with a study of the chemiluminescence properties of a number of other coelenterazine analogs (Hori *et al.*, 1973). Since fluorescence and bioluminescence spectral properties are similar for the amide anion of aequorin, it has been

generally agreed until recently that the excited amide anion was the origin of the aequorin bioluminescence.

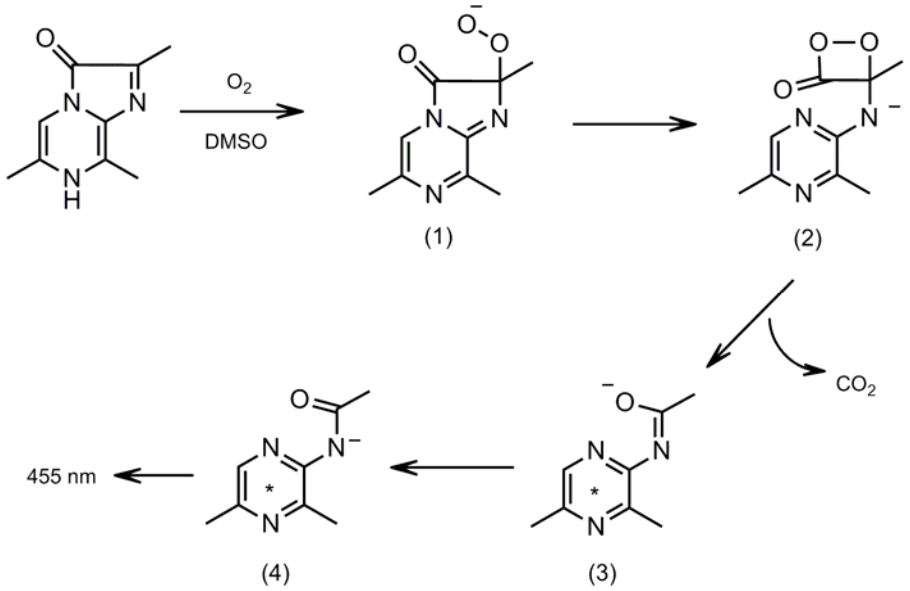

Figure 1.5 The McCapra/Chang mechanism of chemiluminescence of 6-phenyl-2-methyl-imidazopyrazinone (McCapra and Chang, 1967).

Shimomura and Teranishi proposed that coelenteramide can form five distinguishable excited states: neutral, amide anion, phenolate/pyrazine-N(4) anion resonance structure, and an ion-pair with a proton acceptor (Fig. 1.6) (Shimomura and Teranishi, 2000). The addition of *n*-butylamine to a benzene solution of coelenteramide was shown to produce a bimodal fluorescence spectrum with maxima at 397 and 467 nm. The fluorescence at 467 nm was assigned as being from an ion-pair excited state. In the ground state, the phenolic OH is hydrogen-bonded to the amine without ionic dissociation; thus, the excitation peaks (302 and 337 nm) closely correspond to those of the neutral coelenteramide. On excitation however, the phenolic OH proton transfers to the amine and the resulting fluorescence emission (465-479 nm) of the ion pair becomes close to, but not identical with, that of the phenolate ion (480-490 nm). The excited state proton transfer is feasible because it is well known that the phenolic OH in the excited state is a much stronger acid than that in its ground state.

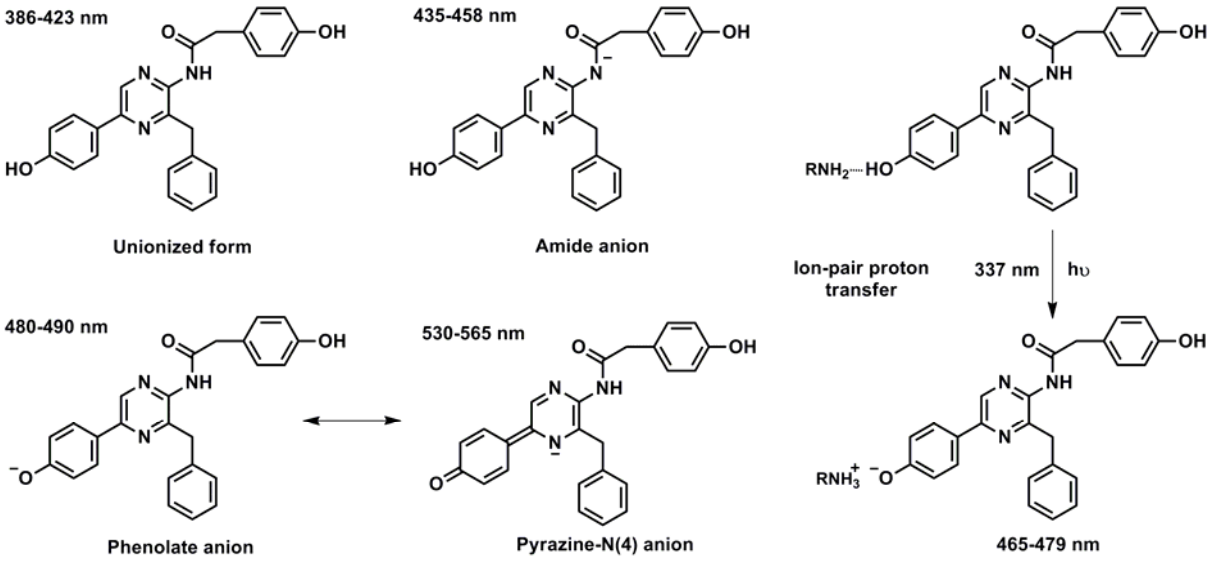

Figure 1.6 Fluorescent forms of coelenteramide. The range of fluorescence maxima is indicated.

Hirano and co-workers made a systematic study of the fluorescence of coelenteramide analogs and came to similar conclusions about ion pairing with amines (Imai *et al.*, 2001). They suggested that the singlet-excited state of the phenolate ion has an intramolecular charge-transfer character and that this phenolate anion state, rather than the amide anion, is the light emitter in aequorin bioluminescence. Based on these studies the mechanism for the chemiluminescence reaction of *Cypridina* luciferin analogs was suggested later (Kondo *et al.*, 2005).

According to the suggested reaction mechanism, the first step is deprotonation of the N7 of imidazopyrazinone with a base yielding the imidazopyrazinone anion (Fig. 1.7). Then, single electron transfer (SET) from imidazopyrazinone anion to triplet oxygen affords the imidazopyrazinone radical and the superoxide anion of oxygen. The SET process requiring spin conversion is considered to be rate-limiting. The radical coupling of imidazopyrazinone radical and superoxide anion leads to the peroxide anion of imidazopyrazinone. In case of bioluminescent reactions catalyzed by luciferases the cyclization of imidazopyrazinone peroxide anion then will take place. The cyclization gives dioxetanone which decomposes with loss of CO_2 generating the singlet excited state of a product (Kondo *et al.*, 2005).

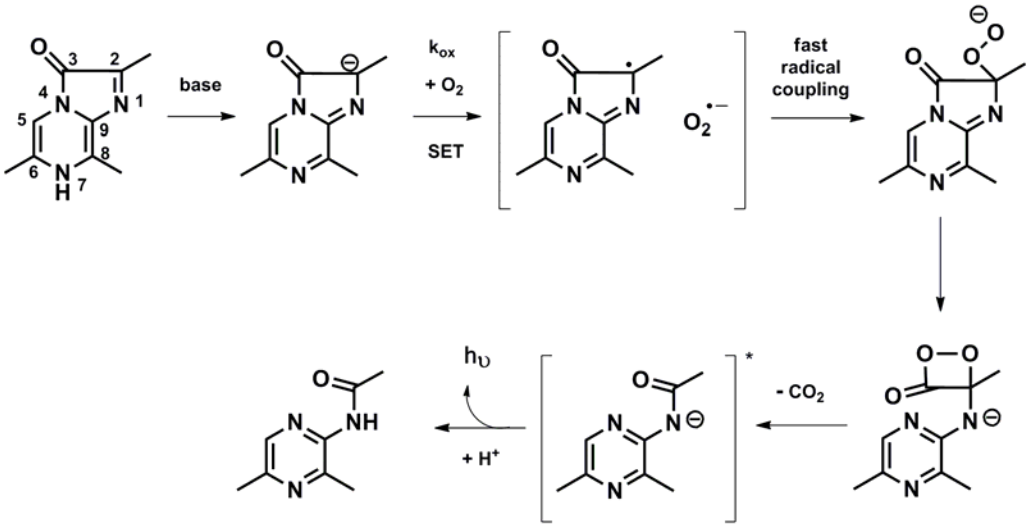

Figure 1.7 Mechanism for the chemiluminescence reaction of *Cypridina* luciferin analogs (Kondo *et al.*, 2005).

In the McCapra/Chang chemiluminescence mechanism, the primary excited state is clearly the amide anion of coelenteramide. However, the bioluminescence reaction of photoproteins occurs within a hydrophobic internal active site where the 2-hydroperoxycoelenterazine is stabilized by hydrogen bonds with various amino acid residues and where the substrate is isolated from solvent (Fig. 1.8).

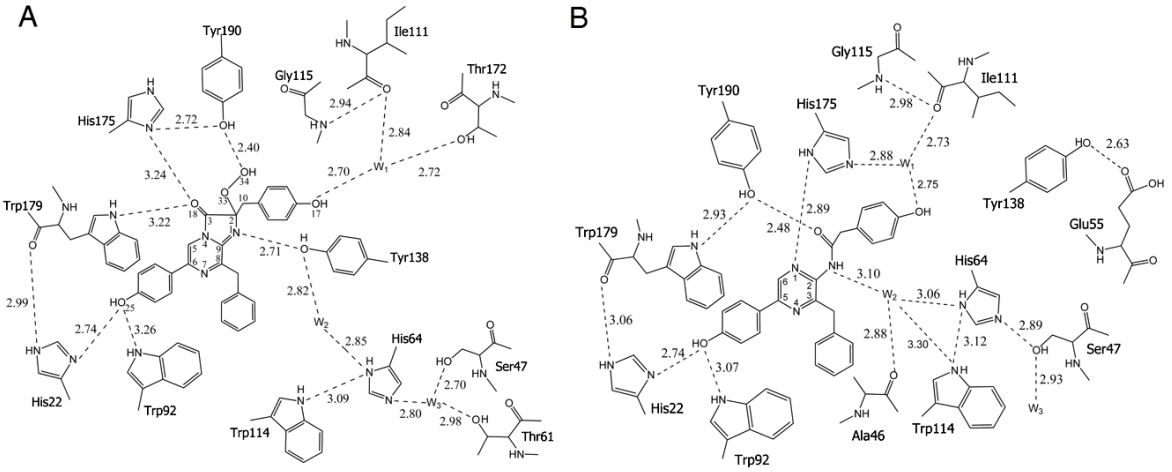

Figure 1.8 Two-dimensional comparison of the hydrogen bond network (dashed lines) in the active sites of obelin (*A*) and Ca^{2+}-discharged obelin (*B*). Upon formation of coelenteramide, the Tyr138 side chain hydrogen bonded to N1 moves away to be replaced by a water molecule W2 (Liu *et al.*, 2006).

These conditions are very favourable for proton transfer to occur. Thus, on the basis of structural studies of photoproteins (Liu *et al.,* 2000; Deng *et al.,* 2004; Liu *et al.,* 2006) and chemical studies of coelenterazine and its analogs (McCapra and Chang, 1967; Hori *et al.,* 1973; Imai *et al.,* 2001; Kondo *et al.,* 2005), a proton-relay hypothesis has been formulated as to how Ca^{2+} binding could trigger the bioluminescence reaction and how the product excited states form (Vysotski and Lee, 2004; Vysotski and Lee, 2007).

According to the suggested mechanism, the triggering step in photoprotein bioluminescence reaction involves transfer of a proton from Tyr190 to His175 as a direct result of Ca^{2+} binding, followed by deprotonation of the hydroperoxide (step 1 in Fig. 1.9) and subsequent formation of the dioxetanone anion (step 2). Comparison of the obelin spatial structures before and after bioluminescent reaction supports the plausibility of this mechanism (Liu *et al.,* 2006). If the p*K* of the N-anion is higher than the p*K* of the water molecule in this environment, protonation from W2 (step 3A) would lead to the neutral dioxetanone. This would be made more energetically feasible by a proton relay from His64 if that His was initially in a protonated state. Hence the critical function of the water molecule W2 is to catalyze the decarboxylation reaction by protonating the dioxetanone anion (step 3 in Fig. 1.9). Step 4 then yields the neutral coelenteramide as the primary excited product of bioluminescence.

Step 5 of the suggested mechanism explains the formation of excited states of coelenteramide emitting light at longer wavelength (Fig. 1.9). For coelenterazine having the dissociable 6-(*p*-hydroxyphenyl) group, the longer wavelength bioluminescence band was proposed to arise from the excited phenolate anion after excited state proton transfer to His22. This histidine was found to be in hydrogen bond distance with the oxygen of the 6-(*p*-hydroxyphenyl) group of coelenterazine before and after the bioluminescence reaction (Fig. 1.8).

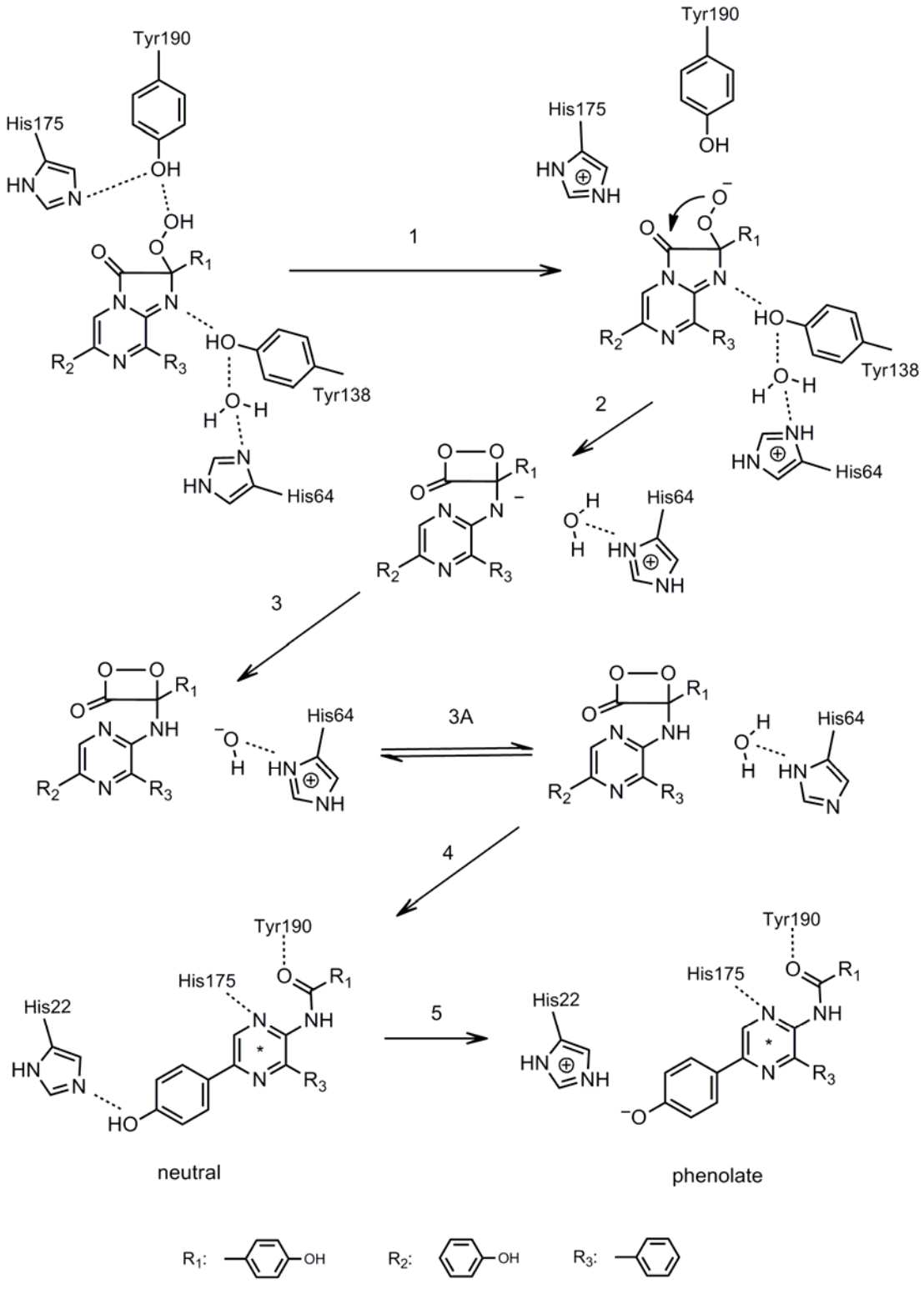

Figure 1.9 Proton-relay mechanism of the photoprotein Ca^{2+} trigger and formation of the product excited states (Vysotski and Lee, 2007).

Biological partners of Ca^{2+}-regulated photoproteins

Many bioluminescence systems contain supplemental proteins in addition to luciferases or photoproteins. One of the most famous examples of such partnership is the so-called antenna protein - green-fluorescent protein (GFP), first isolated from the jellyfish *Aequorea* (Shimomura *et al*, 1962). GFP was found to be a bioluminescence color modulator in various bioluminescent coelenterates containing Ca^{2+}-regulated photoproteins such as *Aequorea, Obelia, Clytia, Mitrocoma* (Shimomura, 2006).

One of the relatively well-studied examples is the clytin-*cg*GFP complex from *Clytia gregaria,* the jellyfish with green bioluminescence (maximum at 509 nm) containing both the photoprotein clytin and *cg*GFP (Fig. 1.10) (Titushin *et al.*, 2010). With no *cgG*FP present, the bioluminescence emission has a maximum around 470 nm originating from clytin alone (Levine and Ward, 1982; Inouye and Tsuji, 1993). Binding of Ca^{2+} to clytin

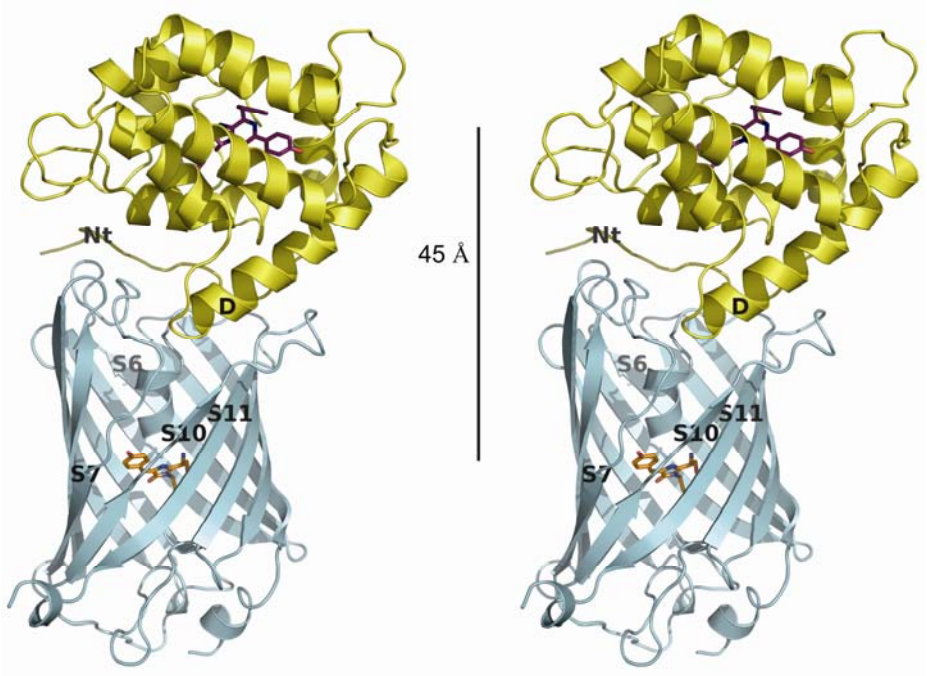

Figure 1.10 Stereoview representation of the spatial structure of the clytin-*cg*GFP complex derived from X-ray structures of clytin and *cg*GFP, NMR mapping of the interaction surfaces and computational docking in HADDOCK. 45 Å is the distance between the two chromophores. Structural elements of clytin and *cg*GFP comprising the interaction surface are labeled (Titushin *et al.*, 2010).

triggers the bioluminescence reaction to produce the excited state product coelenteramide and CO_2. In the clytin-*cg*GFP complex, the excitation energy is passed via resonance energy transfer to the *cg*GFP's fluorophore resulting in green fluorescence with maximum around 500 nm.

The interaction between the partners in the photoprotein-GFP complex is of transient nature, with dissociation constants (K_D) in the range of 10^{-4} to 10^{-3} M, which hampers investigation of the complexes with X-ray crystallographic or NMR methods (Malikova *et al.*, 2011; Titushin *et al.,* 2011).

Applications of Ca^{2+}-regulated photoproteins

The first use of Ca^{2+}-regulated photoproteins has been for the detection of calcium ions in biological systems (Blinks *et al.,* 1982; Knight *et al.,* 1991; Rizzuto *et al.,* 1992; Baubet *et al.,* 2000; Mithofer and Mazars, 2002; Moscatiello *et al.,* 2009). The emission from photoproteins is characterized by a high signal-to-noise ratio and a wide dynamic range allowing monitoring changes in the cytosolic calcium concentration from 10^{-7} to 10^{-3} M. Besides photoproteins do not require external illumination, so problems, such as phototoxicity, photobleaching, autofluorescence, and undesirable stimulation of photobiological processes are avoided (Grienberger and Konnerth, 2012). That is why photoproteins have been successfully applied in many different types of living cells, both to estimate the intracellular Ca^{2+} concentration under steady-state conditions and to study the role of calcium transients in the regulation of cellular function. Genetically encoded peptide or protein tags within photoproteins that target specific organelles could provide *in vivo* measuring of Ca^{2+} level in discrete cellular locations, for example, in mitochondria (de la Fuente *et al.,* 2012). Fusing photoproteins with long wavelength emitting GFPs (such as red fluorescent proteins RFPs) can significantly improve the quality of the Ca^{2+} activity visualization *in vivo* (Bakayan *et al.,* 2011).

Bioluminescent proteins achieve very low detection limits providing a distinct advantage when an analyte is present in very low concentrations or when an analytical technique is being miniaturized (lab-on-chip) (Rowe *et al.,* 2009). Ca^{2+}-regulated photoproteins have been used extensively as reporters or labels in various binding assays,

such as ELISA-type, homogeneous, and DNA-hybridization assays and whole cell sensing systems. Moreover, several methods have been described in which multiple luminescent signals are generated simultaneously and differentiated by differences in the properties of the luminescent reactions (kinetics, wavelengths, combination of bioluminescence and chemiluminescence, etc).

For instance, a dual-analyte assay using tandem flash luminescence from the photoprotein aequorin and acridinium-9-carboxamide label has been described. The assay enabled quantification of two analytes in one tube, by sequential triggering and measuring the two luminescent reactions. Because it is based on flash-type kinetics, the assay requires very short measurement times and is therefore suitable for high-throughput screening (Adamczyk ***et al.***, 2002).

A different approach for dual analyte detection using photoproteins has been reported recently. Dual-analyte single-well bioluminescence immunoassay (BLIA) for total and IgG-bound prolactins was developed on the base of Ca^{2+}-regulated photoprotein obelin mutants with altered color and kinetics of bioluminescence signal as reporters (Kudryavtsev ***et al.***, 2012). The violet W92F-H22E and greenish Y138F obelin mutants were chemically conjugated with monoclonal mouse anti-hPRL and anti-hIgG immunoglobulins and thus displayed signals from total prolactin and IgG-bounded prolactin (macroprolactin) correspondingly.

Aim and outline of the thesis

This thesis describes the work performed as a joint project between Enzymes@Work group (Biochemistry, Wageningen University) and Photobiology Lab (Institute of Biophysics, Krasnoyarsk). The goal of the project was to cast light on the mechanism of active photoprotein complex formation, and to reveal the role of key amino acid residues involved in photoprotein bioluminescence.

This thesis focuses on the properties of the Ca^{2+}-regulated photoprotein obelin from the hydroid *Obelia longissima*. The first part of the thesis (chapters 2-5) mainly deals with characterization of different obelin conformation states and describes the process of active photoprotein formation from apo-protein, coelenterazine and oxygen. The second part of this thesis (chapters 6-8) presents the study on obelin bioluminescence. The knowledge obtained provides the fundamental basis for improving intracellular assays involving photoproteins.

Chapter 2 describes the conformational stability of different forms of obelin. Thermal unfolding of the free and ligand-bound photoprotein is studied by fluorescence and far-UV circular dichroism (CD) spectroscopy.

Chapter 3 reports on the intrinsic fluorescence of two photoproteins, apo-obelin and apo-aequorin, and use of its quenching to characterize coelenterazine binding. The apparent dissociation constants for coelenterazine binding with both apo-photoproteins are determined and the rate-limiting step of active photoprotein complex formation is discussed.

In **Chapter 4** the spectral properties of the anaerobic coelenterazine and apo-obelin-coelenterazine complex and their reactivity with oxygen are investigated. Kinetics of conversion of apo-obelin-coelenterazine complex into active photoprotein is studied using two different approaches, via absorbance and bioluminescence.

Chapter 5 presents a mechanism of 2-hydroperoxycoelenterazine formation as well as the function of two key residues (His175 and Tyr138) involved in this process. Activation kinetics for obelin and its mutants were investigated and detailed quantum chemical calculations were performed in order to understand how oxygen activation occurs and what coelenterazine derivatives might be involved in the formation of active obelin.

In **Chapter 6** bioluminescent and spectroscopic properties of obelin and aequorin coelenterazine-binding pocket mutants are characterized. Replacements of His175, Trp179 and Tyr190 by residues with different hydrogen bond donor-acceptor capacity revealed significant changes in the yield of active complex and bioluminescence. Possible roles of these residues in stabilizing reaction intermediates and in the emitter formation process are discussed.

In **Chapter 7** picosecond fluorescence relaxation spectroscopy is applied to investigate the excited state dynamics of coelenteramide bound in the active site cavity of the calcium-discharged photoproteins aequorin and obelin. Two excited states are suggested to be formed in the product-binding pocket, i.e. the neutral coelenteramide, which reverts to the anion on a picosecond time scale.

Chapter 8 presents a different approach to study the nature of light emitters involved in photoprotein bioluminescence. Rapid mixing stopped-flow kinetics of W92F obelin, a mutant with bimodal bioluminescence, are applied to investigate the emitting components with different emission maxima. Again, indications are found that a mixture of neutral and ion-pair excited states is involved in photoprotein bioluminescence. These emitters probably result from different pathways of dioxetanone decomposition.

In **Chapter 9** the findings described in this thesis are summarized and discussed and some final conclusions are drawn.

Chapter 2

Ligand binding and conformational states of the photoprotein obelin

Eremeeva, E.V.; Vysotski, E.S.; Westphal, A.H.; van Mierlo, C.P.M.; and van Berkel, W.J.H. (2012) *FEBS Letters*, 586, 4173–4179.

Abstract

Many proteins require a non-covalently bound ligand to be functional. How ligand binding affects protein conformation is often unknown. Here we address thermal unfolding of the free and ligand-bound forms of photoprotein obelin. Fluorescence and far-UV circular dichroism (CD) data show that the various ligand-dependent conformational states of obelin differ significantly in stability against thermal unfolding. Binding of coelenterazine and calcium considerably stabilizes obelin. In solution, all obelin structures are similar, except for apo-obelin without calcium. This latter protein is an ensemble of conformational states, the populations of which alter upon increasing temperature.

Keywords*:* bioluminescence, coelenterazine, photoprotein, thermostability

Abbreviations: DTT, dithiothreitol; EDTA, ethylenediaminetetraacetate; IPTG, isopropyl thio-β-D-galactopyranoside

Introduction

Many proteins require binding of a ligand to be functional. These ligands vary in size and complexity from a single metal ion to large organic molecules. Ligand binding can influence protein structure in different ways. For example, apocytochrome *c* is largely unstructured but upon incorporation of heme it turns into a well-ordered helical protein (Fisher *et al.,* 1973). In contrast, apoflavodoxin is structurally identical to holoflavodoxin, except for increased dynamics (Steensma *et al.,* 1998; Steensma and van Mierlo, 1998; Bollen et al., 2012).

Ca^{2+}-regulated photoproteins responsible for bioluminescence of various coelenterates consist of a single polypeptide chain of about 22 kDa. The substrate of the photoprotein bioluminescence reaction, coelenterazine, is widely distributed in luminous and non-luminous marine organisms, and has been identified as a luciferin in various luminous organisms (Shimomura, 2006). Recombinant apo-photoproteins are converted to their active 2-hydroperoxycoelenterazine-liganded forms upon incubation under calcium-free conditions with coelenterazine in presence of oxygen and thiol-reducing agents (Shimomura and Johnson, 1975).

Photoproteins contain three canonic EF-hand Ca^{2+}-binding sites. Calcium binding initiates oxidative decarboxylation of 2-hydroperoxycoelenterazine, resulting in the excited state of the product, coelenteramide (Shimomura and Johnson, 1972), which relaxes to its ground state by emitting blue light with, depending on the type of photoprotein involved, emission maximum of 465-495 nm (Vysotski and Lee, 2004). Coelenteramide remains bound after the bioluminescence reaction and the resulting protein-ligand complex is generally referred to as "Ca^{2+}-discharged photoprotein". Without calcium, photoproteins display a very low level of light emission called "calcium-independent luminescence" (Allen *et al.,* 1977). Upon calcium binding light intensity increases by six orders of magnitude or more.

Photoprotein obelin populates five conformational states (Fig. 2.1): apo-protein (**I**), active photoprotein with 2-hydroperoxycoelenterazine (**II**), Ca^{2+}-discharged photoprotein containing coelenteramide and calcium (**III**), Ca^{2+}-discharged photoprotein containing coelenteramide (**IV**), and apo-protein containing calcium (**V**) (Lee *et al.,* 2001). To date the

spatial structures of four conformational states (II, III, IV, and V) have been determined by X-ray crystallography (Liu *et al.*, 2006).

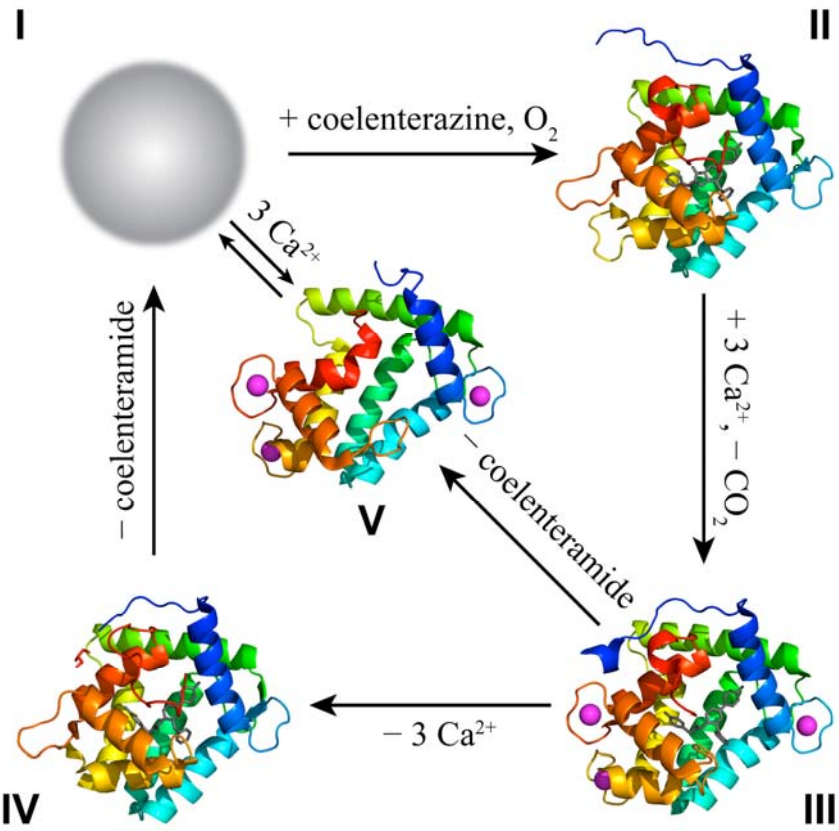

Figure 2.1 Conformational states of obelin. **I**, apo-obelin; **II**, active obelin containing 2-hydroperoxycoelenterazine (PDB ID code 1EL4); **III**, Ca^{2+}-discharged obelin containing both coelenteramide and calcium (PDB ID code 2F8P); **IV**, Ca^{2+}-discharged obelin containing coelenteramide (PDB ID code 1S36); **V**, calcium-loaded apo-obelin (PDB ID code 1SL7). The structure of apo-obelin is unknown. 2-hydroperoxycoelenterazine and coelenteramide are displayed in stick representation; calcium ions are shown as magenta balls.

In this paper, we report the effects ligands have on conformational states of obelin by using fluorescence and far-UV CD spectroscopy. We demonstrate that the binding of these ligands considerably stabilizes obelin against thermal unfolding. Apo-obelin containing no ligand (**I**) turns out to be an ensemble of conformational states and it is the least stable obelin conformation.

Materials and Methods

Chemicals - Coelenterazine was obtained from Prolume Ltd. (Pinetop, USA). Other chemicals were obtained at the purest grade available from Sigma-Aldrich, unless mentioned otherwise.

Protein expression and purification - Recombinant apo-obelin was expressed as reported (Illarionov *et al.*, 2000; Vysotski *et al.*, 2001). For protein production, transformed *E. coli* BL21-Gold was cultivated under vigorous shaking at 37 ºC in LB medium containing 200 µg/ml ampicillin. Induction was initiated by adding 0.5 mM IPTG once the culture reached an OD_{600} of 0.5-0.6, and cultivation continued for another 3 h. Apo-obelin predominantly accumulated as inclusion bodies.

Apo-obelin (**I**) was purified from inclusion bodies as described (Illarionov *et al.*, 2000; Vysotski *et al.*, 2001) and concentrated by using Amicon Ultra Centrifugal Filters (Millipore). To fold apo-obelin, concentrated protein samples in 6 M urea were diluted approximately 20-fold with buffer, which contains 1 mM EDTA and 20 mM Tris–HCl pH 7.0. Subsequently, the protein was concentrated, diluted, and concentrated again. This washing procedure was repeated several times to remove all urea and excess salt. Next, apo-obelin was passed through a Superdex 200 column (Amersham Bioscience) equilibrated with 5 mM EDTA, 20 mM Tris-HCl pH 7.0 to produce monomeric apo-photoprotein.

Active obelin containing 2-hydroperoxycoelenterazine (**II**) was produced as reported (Illarionov *et al.*, 2000; Vysotski *et al.*, 2001). To prepare Ca^{2+}-discharged obelin with coelenteramide and calcium bound (**III**), active obelin was diluted in 1 mM $CaCl_2$, 20 mM Tris–HCl, pH 7.0. After bioluminescence ceased, the sample was concentrated and passed through a Bio Gel P2 column equilibrated with 1 mM $CaCl_2$, 20 mM Tris–HCl, pH 7.0. Ca^{2+}-discharged obelin containing only coelenteramide (**IV)** was produced by addition of 5 mM EDTA to obelin conformation state (**III**) and passing through the same column but now equilibrated with 5 mM EDTA, 20 mM Tris–HCl, pH 7.0. All obelin samples were of high purity according to 12.5% SDS-PAGE.

Coelenterazine concentration was determined by measuring absorbance at 435 nm, using a molar absorption coefficient of 9800 $M^{-1}cm^{-1}$ (Shimomura, 2006). Concentrations of apo-obelin and obelin were determined by measuring absorbance at 280 nm, using molar absorption coefficients of 40450 M^{-1} cm^{-1} and 55500 M^{-1} cm^{-1}, respectively (Eremeeva ***et al.***, 2009).

Fluorescence spectroscopy - Obelin fluorescence was measured at 20 °C with a Varian Cary Eclipse spectrofluorimeter. Excitation was set at 295 nm and emission was recorded between 305 and 550 nm at 1 nm intervals with a scan rate of 600 $nm \cdot min^{-1}$ and 0.1 s averaging time.

Protein thermal unfolding was followed by recording fluorescence emission at 330, 340 and 350 nm, respectively. Temperature was increased at a rate of 1 °C/min from 16 to 80 °C in a 1.5 mL stirred quartz cuvette (path length 0.4 cm). Cooling down was achived with a rate of 1°C/min. In all fluorescence experiments, excitation and emission slits were set to a width of 5 nm. Protein concentration was 1.2 μM in 25 mM HEPES, pH 7.0, containing either 1 mM EDTA or 1 mM $CaCl_2$.

Far-UV CD - Far-UV CD spectra of ligand-dependent obelin conformations were recorded with a Jasco J-715 spectropolarimeter (Tokyo, Japan) equipped with a PTC-348WI Peltier temperature control system. Thermal unfolding of ligand-dependent obelin conformations was followed at 220 nm. Temperature was increased from 12 to 80 °C at a rate of 1 °C/min in a 1 mL stirred quartz cuvette (path length 0.1 cm). Protein concentration was 4 μM in 25 mM HEPES, pH 7.0, containing either 1 mM EDTA or 1 mM $CaCl_2$. Before and after thermal unfolding, far-UV CD spectra were recorded at 20 °C by averaging 20 scans. Sample spectra were corrected by subtracting spectra of corresponding blank solutions.

Data analysis - Thermal unfolding data were fitted to a two-state mechanism of unfolding, in which only the native and denatured states are populated. The change in free energy for thermal-induced protein unfolding, $\Delta G(T)$, is described by the modified Gibbs-Helmholtz equation:

$$\Delta G(T) = \Delta H_m(1 - T/T_m) - \Delta C_p\left[(T_m - T) + T\ln(T/T_m)\right] \quad (2.1)$$

where ΔH_m is the enthalpy change for unfolding measured at T_m, T is the absolute temperature, T_m is the temperature at the midpoint of transition, and ΔC_p is the difference in heat capacity between unfolded and folded states (Pace and Laurents, 1989; Becktel and Schellman, 1987). Under the assumption that ΔC_p is temperature independent (Privalov and Khechinashvili, 1974), a two-state mechanism of unfolding can be fitted to individual thermal unfolding curves:

$$Y_{obs} = (a_U + b_U T) + \frac{((a_N + b_N T) - (a_U + b_U T))}{(1 + \exp(((-\Delta H_m / R)(1/T - 1/T_m)) + ((\Delta C_p / R)(((T_m / T) - 1) + \ln(T/T_m)))))} \quad (2.2)$$

where Y_{obs} is the measured far-UV CD or fluorescence signal, *R* is the gas constant, and a and b are the intercepts and slopes of pre- and post unfolding baselines that linearly depend on temperature, respectively. Equation 2.2 was fitted to the thermal unfolding data by using the non-linear least-squares algorithm provided in the Microsoft Excel package. While fitting the thermal unfolding data obtained by both CD and fluorescence, ΔC_p was used as an adjustable parameter. Data shown present repetitive studies carried out on independently produced and purified protein samples.

Results and Discussion

Thermal unfolding of obelin studied by fluorescence spectroscopy - Tryptophan fluorescence of apo-obelin (**I)** has a maximum at 340 nm (Eremeeva *et al.*, 2009). Upon denaturant-induced unfolding of apo-obelin with 6.0 M GuHCl, the emission maximum shifts to 350 nm while fluorescence intensity slightly increases (Fig. 2.2). Upon heat-induced unfolding of apo-obelin (**I)** by increasing temperature to 80 °C and subsequent cooling down to 20 °C, fluorescence intensity of refolded protein has its maximum at 343 nm and has 17 % reduction of fluorescence intensity as compared to starting material (Fig. 2.2). This observation suggests that thermal unfolding of apo-obelin (**I)** is not fully reversible. Reversibility of thermal unfolding of apo-obelin loaded with calcium (**V**, Fig. 2.1) is less effecient (up to 50% reduction of fluorescence intensity at 343 nm, data not shown).

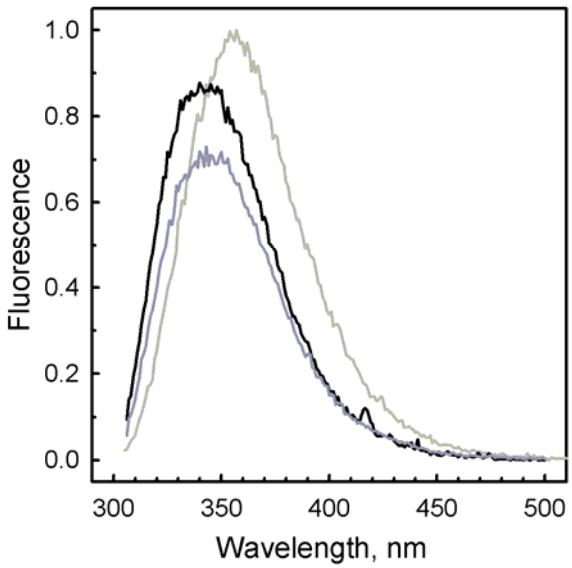

Figure 2.2 Reversibility of thermal unfolding of apo-obelin (**I**). Normalized fluorescence emission spectra of apo-obelin are shown before thermal unfolding (black line), after increasing temperature up to 80 °C and subsequent cooling down (dark gray line), and of apo-obelin in 6.0 M GuHCl (light gray line). Excitation is at 295 nm and temperature is 20 °C.

Upon binding of coelenterazine, tryptophan fluorescence of apo-obelin is quenched (Eremeeva *et al.*, 2009). Bound 2-hydroperoxycoelenterazine is weakly fluorescent (Fig. 2.3A, black line), whereas bound coelenteramide is highly fluorescent with an emission

maximum around 500 nm upon excitation at 295 nm (Fig. 2.3B and 2.3C, black lines). The green fluorescence of coelenteramide bound to obelin is mainly due to Förster resonance energy transfer from tryptophans. This is concluded from the observed quenching of tryptophan fluorescence of obelin upon binding of coelenteramide (3C, left panel).

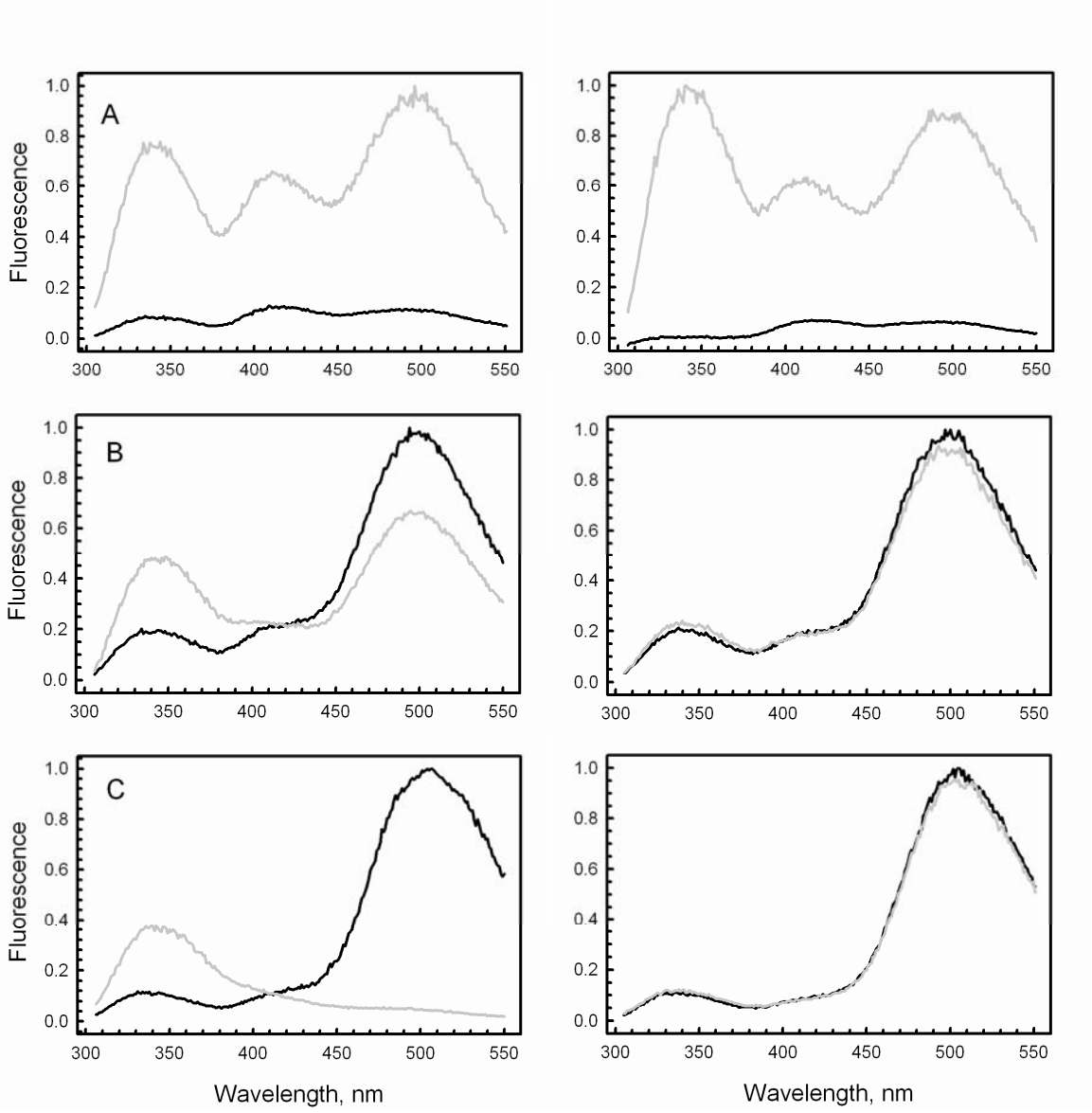

Figure 2.3 Fluorescence of ligand-dependent conformations of obelin. Left panels show spectra of protein before (black line) and after thermal unfolding by increasing temperature to 80 °C and subsequent cooling to 20 °C (gray line). Right panels show spectra of protein before (black line) and after heating to their midpoints of thermal unfolding (i.e., 52, 31, and 54 °C, respectively) and subsequent cooling to 20 °C. (A) active obelin containing 2-hydroperoxycoelenterazine (**II**); (B) Ca^{2+}-discharged obelin containing coelenteramide (**IV**); (C) Ca^{2+}-discharged obelin containing both coelenteramide and calcium (**III**). Excitation is at 295 nm and temperature is 20 °C.

We also studied reversibility of thermal unfolding of active obelin (**II**) and Ca^{2+}-discharged obelins, both with and without calcium (**III** and **IV**), by using fluorescence spectroscopy. Samples are heated to 80 °C and subsequently cooled to 20 °C and display no visible turbidity. Tryptophan fluorescence of these obelin conformational states increases after this heating procedure (Fig. 2.3, left panels).

In case of active obelin (**II**), a strong increase of fluorescence occurs at 420 and 500 nm (Fig. 2.3A, left panel) that might be attributed to heat-induced, calcium-independent oxidation of 2-hydroperoxycoelenterazine yielding bound coelenteramide (500 nm) (Ray *et al.*, 1985) and probably some side-product (420 nm) (Shimomura and Johnson, 1973) or to an obelin conformational state that assists in the formation of excited coelenteramide in its neutral state (Shimomura and Teranishi, 2000). In case of Ca^{2+}-discharged obelin with coelenteramide bound (**IV**) the heating procedure causes a decrease in fluorescence at 500 nm (Fig. 2.3B, left panel). This fluorescence completely vanishes in case of Ca^{2+}-discharged obelin with both coelenteramide and calcium bound (**III**) (Fig. 2.3C, left panel). Because free coelenteramide is non-fluorescent in solution, these observations suggest that coelenteramide dissociates from obelin during heating and that in presence of calcium this dissociation is irreversible.

The various ligand-dependent conformational states of obelin differ significantly in stability against thermal unfolding (Fig. 2.4). Both apo-obelin forms (**I** and **V**) have thermal unfolding curves that display no distinct midpoints of unfolding (Fig. 2.4A). These curves show highly non-cooperative unfolding behaviour, suggesting that apo-obelin is an ensemble of multiple conformational states, the populations of which alter upon increasing temperature. In case of calcium-loaded apo-obelin (**V**), the unfolding curve shifts to slightly higher temperature (Fig. 2.4A).

Thermal unfolding of active obelin (**II**) is highly cooperative (Fig. 2.4A), which suggests that active obelin is in a single conformational state. Fitting of a two-state unfolding model to the thermal unfolding data of state **II** shows that its thermal midpoint of unfolding (T_m) is 52.1 ± 0.1 °C (Fig. 2.4A). Active obelin containing 2-hydroperoxy-coelenterazine is thus a relatively stable protein. Upon thermal unfolding of active obelin, its tryptophan fluorescence significantly increases (Figs. 2.3A (left panel) and 2.4A), because 2-hydroperoxycoelenterazine is no longer bound and thus does not quench

fluorescence.

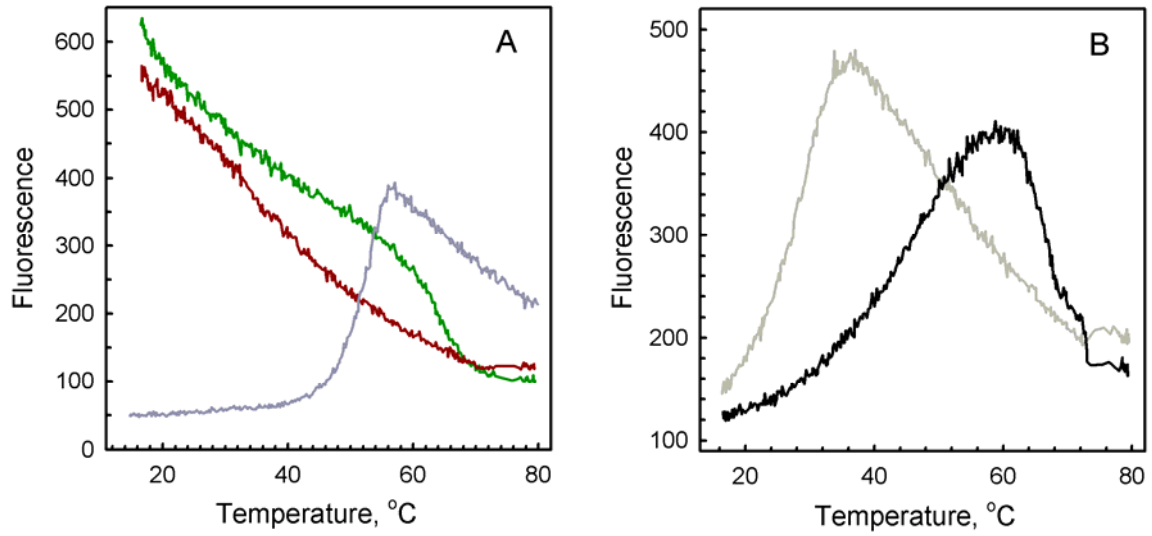

Figure 2.4 Thermal unfolding of ligand-dependent obelin conformations followed by fluorescence spectroscopy. Shown are changes in fluorescence emission at 340 nm. (A) apo-obelin (**I**) (dark red line), calcium-loaded apo-obelin (**V**) (dark green line) and active obelin (**II**) (dark gray line); (B) Ca^{2+}-discharged obelin containing both coelenteramide and calcium (**III)** (black line) and Ca^{2+}-discharged obelin containing only coelenteramide (**IV)** (light gray line).

Ca^{2+}-discharged obelin with both coelenteramide and calcium bound (**III**) has a thermal unfolding curve with a midpoint of unfolding of 54.5 ± 0.2 °C (Fig. 2.4B), i.e., similar to the value that characterizes active obelin. However, the curvature of the native baseline part of this unfolding curve suggests that Ca^{2+}-discharged obelin with both coelenteramide and calcium bound comprises some interconverting conformational states. Removal of calcium and thus generating state **IV** decreases protein stability considerably, because now T_m becomes 31.4 ± 1.0 °C (Fig. 2.4B).

The protein conformations of which thermal midpoints could be determined (**II, III** and **IV**) were heated to their respective T_m-values and subsequently cooled down to 20 °C (Fig. 2.3, right panels). This procedure does not alter fluorescence of obelin states **III** and **IV** (Fig. 2.3B and 2.3C, right panels). It shows that both obelin states are capable of reversibly binding coelenteramide up to their respective T_m-values. At higher temperatures, however, both conformations lose their coelenteramide binding capacity (Fig. 2.3). In case

of active obelin (**II**), applying the mentioned heating procedure leads to strong fluorescence at 500 nm (Fig. 2.3A, right panel). This clearly shows that for state **II** irreversible processes happen at T_m, which is due to conversion of 2-hydroperoxycoelenterazine into coelenteramide as a result of Ca^{2+}-independent light emission upon heating. Midpoints of thermal unfolding are summarized in Table 2.1.

Far-UV CD spectra of ligand-dependent obelin conformations- Far-UV CD spectra of ligand-dependent obelin conformations are typical for those of helical proteins, and thus these spectra have ellipticity minima at 208-210 nm and 222 nm (Fig. 2.5). Active obelin (**II**) shows the highest helical content. Far-UV CD spectra of Ca^{2+}-discharged forms of obelin (containing both coelenteramide and calcium (**III**) or containing only coelenteramide (**IV**)) are virtually indistinguishable. Both spectra display less negative ellipticies as compared to the far-UV CD spectrum of state **II**. Calcium-loaded apo-obelin (**V)** has the lowest helical content of all obelin conformations containing ligands, because it has the lowest ellipticity at 220 nm. Apo-obelin (**I)** is structurally distinct from the other obelin states, because its far-UV CD spectrum has a zero crossing at 202.5 nm, whereas the other obelin conformational states have their zero crossing around 204 nm (Fig. 2.5).

Thermal unfolding of obelin studied by far-UV CD - Thermal unfolding of ligand-dependent obelin conformations causes significant changes in ellipticities at 220 nm (Fig. 2.6). Fitting of a two-state unfolding model to these data gives T_m-values of 34.5 ± 1.2 °C for apo-obelin (**I**), 42.5 ± 0.3 °C for apo-obelin loaded with calcium (**V**), 54.8 ± 0.2 °C for active obelin (**II**), 78.2 ± 0.3 °C for Ca^{2+}-discharged obelin containing coelenteramide and Ca^{2+} (**III**), and 37.1 ± 0.5 °C for Ca^{2+}-discharged obelin containing only coelenteramide (**IV**) (Table 2.1). It should be noted that, according to far-UV CD spectra of ligand-dependent obelin conformations before and after thermal unfolding at 80 °C and subsequent cooling to 20 °C, the temperature-induced unfolding of all these conformations is not fully reversible.

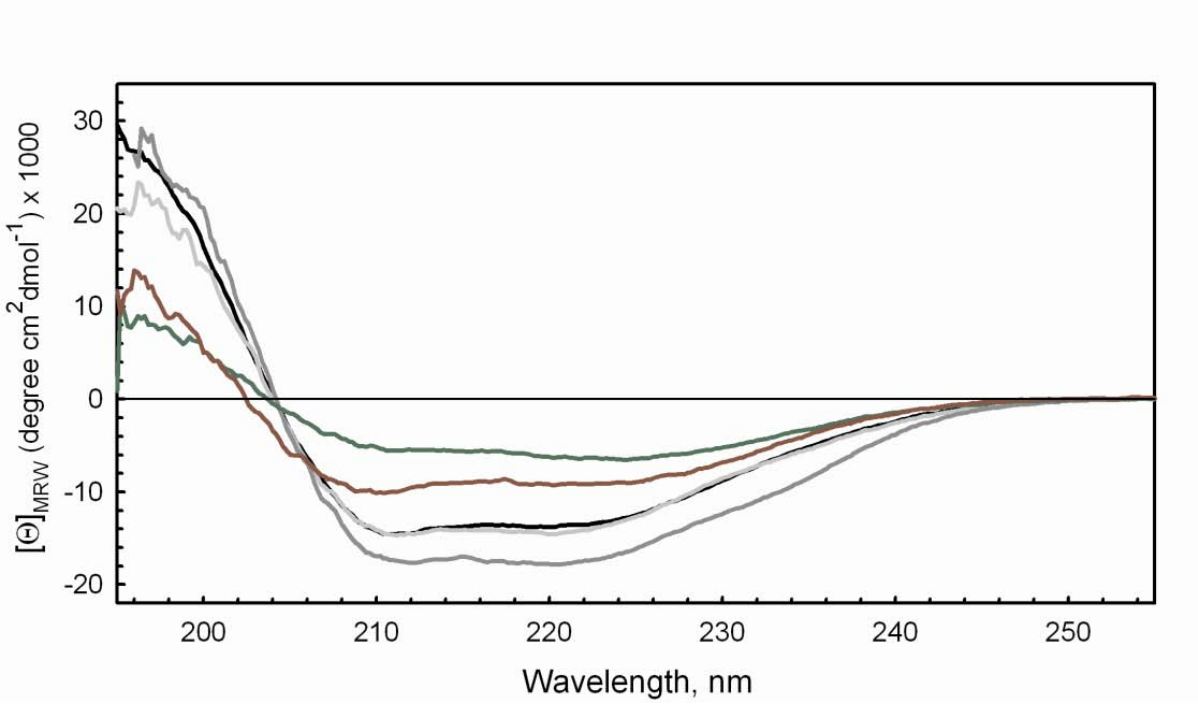

Figure 2.5 Far-UV CD spectra of ligand-dependent obelin conformations. Spectra are of apo-obelin (**I)** (dark red line), calcium loaded apo-obelin (**V)** (dark green line), active obelin (**II)** (dark gray line), Ca^{2+}-discharged obelin containing both coelenteramide and calcium (**III)** (black line) and Ca^{2+}-discharged obelin containing only coelenteramide (**IV)** (light gray line). Protein concentration is 4 μM in 5 mM Tris-HCl, pH 7.0, with addition of either 1 mM EDTA or 1 mM $CaCl_2$. Temperature is 20 °C.

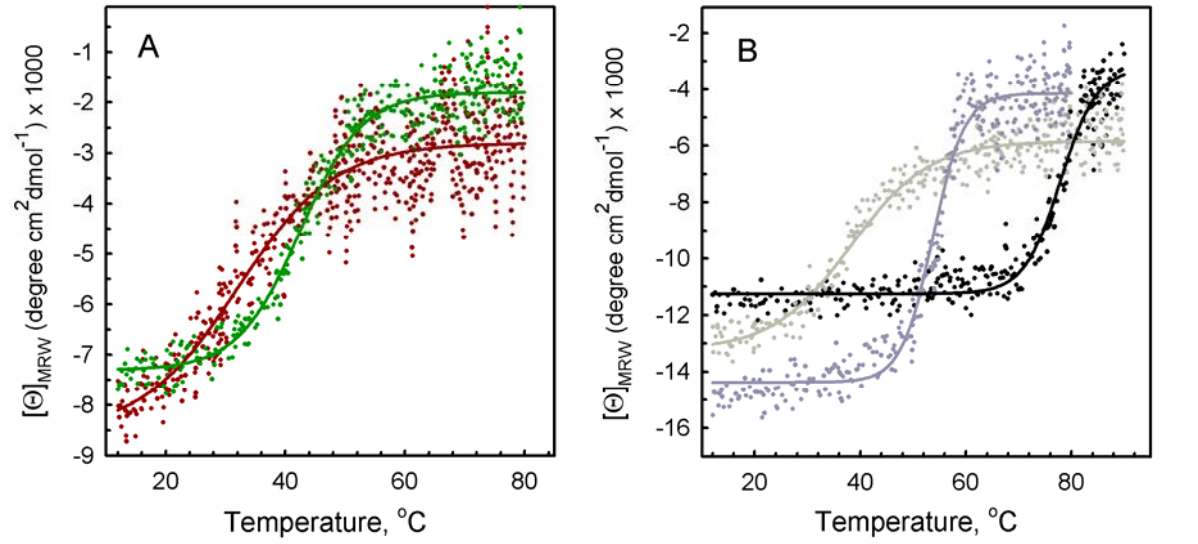

Figure 2.6 Thermal unfolding of ligand-dependent obelin conformations followed by far-UV CD. Shown are changes in ellipticities at 220 nm. (A) apo-obelin (**I)** (dark red line), calcium-loaded apo-obelin (**V**) (dark green line); (B) active obelin (**II)** (dark gray line), Ca^{2+}-discharged obelin containing both coelenteramide and calcium (**III)** (black line) and Ca^{2+}-discharged obelin containing only coelenteramide (**V**) (light gray line). Protein concentration is 4 μM in 25 mM HEPES, pH 7.0 with addition of either 1 mM EDTA or 1 mM $CaCl_2$.

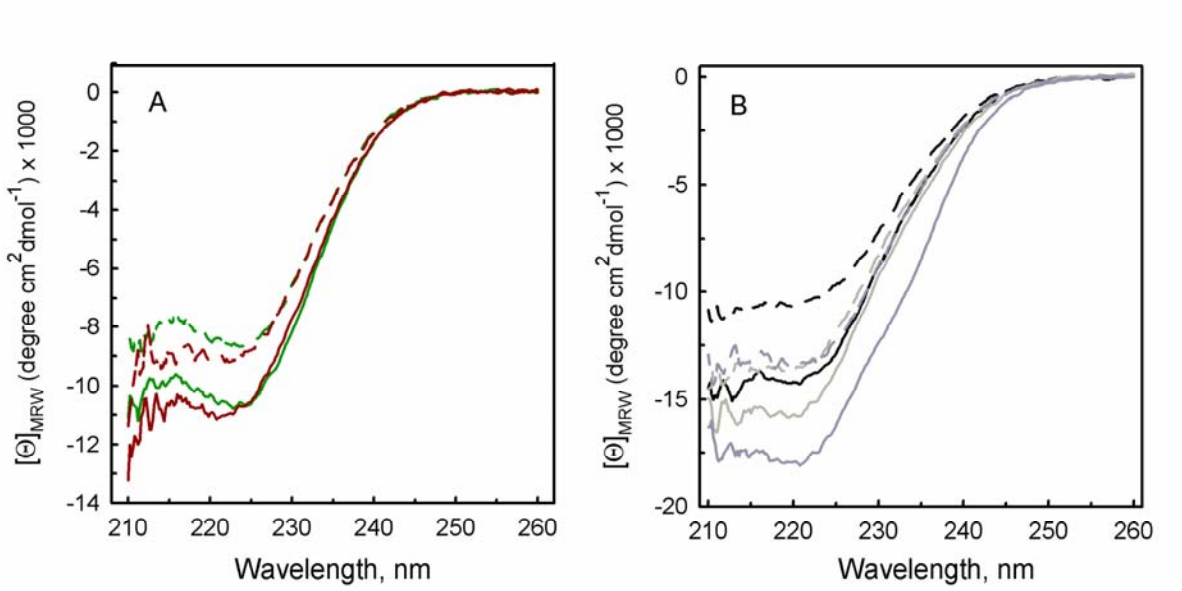

Figure 2.7 Far-UV CD spectra of ligand-dependent obelin conformations before (solid line) and after thermal unfolding at 80 °C (dashed line). (A) apo-obelin (**I**) (dark red line), calcium-loaded apo-obelin (**V**) (dark green line); (B) active obelin (**II**) (dark gray line), Ca^{2+}-discharged obelin containing both coelenteramide and calcium (**III)** (black line) and Ca^{2+}-discharged obelin containing only coelenteramide (**IV**) (light gray line). Protein concentration is 4 μM in 25 mM HEPES, pH 7.0, with addition of either 1 mM EDTA or 1 mM $CaCl_2$. Temperature is 20 °C.

Table 2.1 Midpoints of thermal unfolding of ligand-dependent obelin conformations, derived from changes in fluorescence emission at 340 nm and ellipticity at 220 nm.

Obelin state	T_m via fluorescence at 340 nm, °C	T_m via CD at 220 nm °C
Apo-obelin, no Ca^{2+} (**I**)	n.d.	34.5 ± 1.2
Apo-obelin, Ca^{2+} (**V**)	n.d.	42.5 ± 0.3
Active obelin, no Ca^{2+} (**II**)	52.1 ± 0.1	54.8 ± 0.2
Discharged obelin, Ca^{2+} (**III**)	54.5 ± 0.2	78.2 ± 0.3
Discharged obelin, no Ca^{2+} (**IV**)	31.4 ± 1.0	37.1 ± 0.5

n.d. = not determinable

Conclusion

X-ray crystallography yielded spatial structures for four of five ligand-dependent obelin conformations (Fig. 2.1). These structures have the same compact two-domain fold, which consists of four sets of helix-turn-helix structural motifs specific for EF-hand calcium-binding domains (Liu *et al.,* 2000). The coelenterazine-binding pocket of obelin is highly hydrophobic and is formed by residues originating from all eight helices. In addition, several hydrophilic side chains are directed into this pocket. Upon going from substrate-containing obelin state **II** to product-containing obelin state **IV**, the largest structural change observed concerns the position of the key amino acid residues in the reaction center around the C2-carbon of coelenterazine (Deng *et al.,* 2004).

Both N- and C-termini of calcium-loaded apo-obelin are not observed in the electron density map of the protein, because of their flexibility. In contrast, the C-terminus caps the substrate-binding cavity containing 2-hydroperoxycoelenterazine in active obelin (**II**) and the ligand cavity containing coelenteramide in Ca^{2+}-discharged obelin (**III**), which results in its solvent-inaccessibility and, therefore, in nonpolar environment of substrate or product.

In the calcium-loaded forms of Ca^{2+}-discharged obelin and apo-obelin (**III** and **V**, respectively) twelve residues of the EF-hand calcium-binding loops I, III, and IV shift their relative positions (Deng *et al.,* 2005). Among these loops, loop IV undergoes the largest change in terms of residue reorientation and repositioning. In addition, calcium binding to active obelin results in a reorganization of the protein's hydrogen-bond network (Deng *et al.,* 2005). However, overall inspection of the crystal structures shows that calcium binding to obelin does not result in large changes in protein conformation. This observation suggests that Ca^{2+}-regulated photoproteins are calcium-signal modulators (like for example parvalbumin) rather than being calcium-sensors (like for example calmodulin) (Nelson, M.R. and Chazin, 1998).

The fluorescence and far-UV CD data reported in this study show that coelenterazine binding considerably stabilizes obelin against thermal unfolding. Whereas apo-obelin (**I)** shows non-cooperative temperature-induced unfolding behaviour detected by fluorescence spectroscopy, active obelin containing 2-hydroperoxycoelenterazine (**II**) has a

distinct unfolding transition at 52.1 ± 0.1 °C (Table 2.1). Calcium binding also stabilizes apo-obelin against thermal unfolding, as fluorescence spectroscopy shows (Fig. 2.4A), and according to far-UV CD spectroscopy (Fig. 2.6A) the thermal midpoint of secondary structure unfolding increases by 8 °C (Table 2.1).

Whereas unfolding experiments using fluorescence predominantly report about changes in microenvironments of tryptophans, reflecting distortion of tertiary structure, far-UV CD reports about alterations in protein secondary structure. In case of Ca^{2+}-discharged obelin containing coelenteramide and calcium (**III**), fluorescence and far-UV CD spectroscopy report midpoints of thermal unfolding differing by 23.7 °C (Table 2.1). Upon thermal unfolding of Ca^{2+}-discharged obelin (**III)**, tertiary side-chain packing involving tryptophans is apparently lost before protein secondary structure is disrupted. This phenomenon is typical for formation of molten globules, which are ensembles of interconverting protein conformers that have a substantial amount of secondary structure, but lack virtually all tertiary side-chain packing of natively folded proteins. In this molten globule, calcium possibly remains bound to the EF-hand Ca^{2+}-binding loops I, III, and IV, which do not contain tryptophans (Deng *et al.,* 2005). Far-UV CD would report the structuring of these protein regions, whereas it would remain undetected by tryptophan fluorescence, which reports the unfolding behavior of other parts of the protein.

This study shows that calcium-loaded apo-obelin (**V)** has a rather low helical content as it has a low ellipticity at 220 nm (Fig. 2.5). This observation differs from the one obtained from crystallography, which shows that this state has 101 out of 195 residues involved in helices compared to 115 helical residues in case of active obelin (Deng *et al.,* 2005). However, as thermal unfolding monitored by fluorescence shows (Fig. 2.4), in solution calcium-loaded apo-obelin (**V)** is an ensemble of conformational states, which apparently involves less structured ones as well. Apo-obelin (**I)** is also an ensemble of conformational states. It differs structurally from the other obelin states, because its far-UV CD spectrum has a zero crossing at 202.5 nm, whereas the other obelin conformational states have their zero crossing at 204 nm (Fig. 2.5). These characteristics of apo-obelin (**I**) possibly prevented its crystallization to date.

Acknowledgements

The work was supported by RFBR grant 12-04-00131, by the Program of the Government of Russian Federation “Measures to Attract Leading Scientists to Russian Educational Institutions” (grant 11.G34.31.058), by the Program “Molecular and Cellular Biology” of RAS. The Wageningen University Sandwich PhD-Fellowship Program supported E.V.E.

Chapter 3

The intrinsic fluorescence of apo-obelin and apo-aequorin and use of its quenching to characterize coelenterazine binding

Eremeeva, E.V.; Markova, S.V.; Westphal, A.H.; Visser, A.J.W.G.; van Berkel, W.J.H.; and Vysotski, E.S. (2009) *FEBS Letters*, 583, 1939-1944.

Abstract

The intrinsic fluorescence of two apo-photoproteins has been characterized and its concentration-dependent quenching by coelenterazine has been for the first time applied to determine the apparent dissociation constants for coelenterazine binding with apo-aequorin (1.2 ± 0.12 M) and apo-obelin (0.2 ± 0.04 M). Stopped-flow measurements of fluorescence quenching showed that coelenterazine binding is a millisecond-scale process, in contrast to the formation of an active photoprotein complex taking several hours. This finding evidently shows that the rate-limiting step of active photoprotein formation is the conversion of coelenterazine into its 2-hydroperoxy derivative.

Keywords: bioluminescence, photoprotein, Trp fluorescence

Abbreviations: DTT, dithiothreitol; EDTA, ethylenediaminetetraacetate; IPTG, isopropyl thio-β-D-galactopyranoside

Introduction

The Ca^{2+}-regulated photoproteins consist of a single polypeptide chain of about 22 kDa to which the substrate, 2-hydroperoxycoelenterazine, is tightly though not covalently bound (Shimomura, 2006). Photoprotein bioluminescence is triggered by Ca^{2+} binding which induces the generation of protein-bound coelenteramide in its excited state. Because photoproteins are highly sensitive to detect calcium and harmless when injected into living cells, they have been widely used as probes of intracellular Ca^{2+}. The successful cloning of cDNAs encoding photoproteins has opened a new way of utilizing photoproteins, by expressing the recombinant apo-photoprotein intracellularly, then adding coelenterazine externally which diffuses into the cell and forms the active photoprotein (Knight *et al.*, 1991; Rizzuto *et al.*, 1992). This technique is highly valuable, because it does not require microinjection.

Our previous studies have been focused on the mechanism of photoprotein bioluminescence (Vysotski and Lee, 2007). At the same time much less is known about the mechanism of formation of the active photoprotein complex (Scheme 3.1); there are investigations on relative rates of the regeneration *in vitro* of wild-type aequorin with coelenterazine and its analogs as well as the effect of temperature, pH, incubation time, reducing agent concentrations, and some additives on this process (Shimomura and Johnson, 1975; Shimomura *et al.*, 1993; Knight *et al.*, 1993; Inouye *et al.*, 1986). It was also shown that DTT (or -mercaptoethanol) is required to reduce disulfide bonds in the recombinant apo-aequorin (Ohmiya *et al.*, 1993).

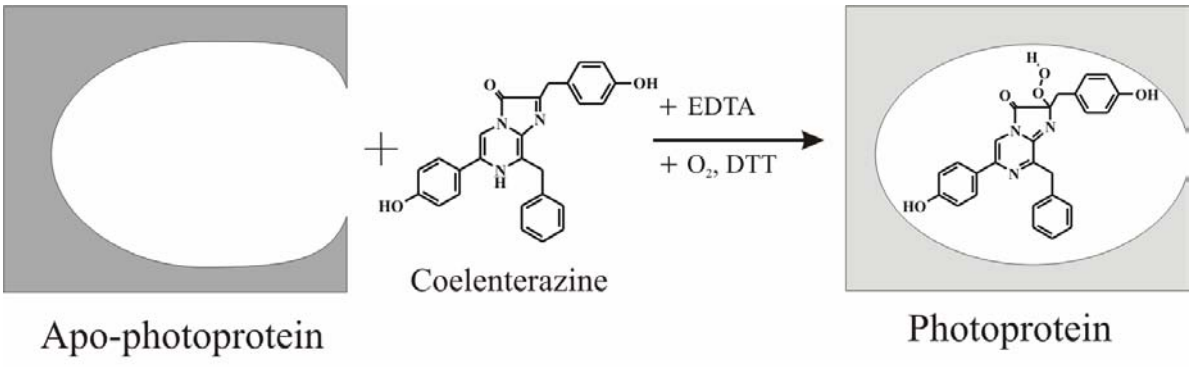

Scheme 3.1 Formation of active photoprotein complex

All photoproteins with known amino acid sequence contain six tryptophans. Four residues (Trp92, 114, 135, and 179; numbered according to the obelin sequence (Liu ***et al.,*** 2000)) are found in the coelenterazine-binding pocket (Fig. 3.1). Trp18 and Trp103 are situated away from the binding cavity in the first and fourth -helix, respectively (Fig. 3.1C). The side chains of Trp92 and Trp179 sandwich the 6-(*p*-hydroxyphenyl) ring of coelenterazine; the side chains of Trp114 and Trp135 are localized near the 2-(*p*-hydroxybenzyl) group of coelenterazine (Fig. 3.1). The nitrogen atoms of the Trp92 and Trp179 indole rings interact dipolarly with the oxygen atoms of the 6-(*p*-hydroxyphenyl) group and the C3 carbonyl of coelenterazine (Vysotski and Lee, 2004). It has been shown that Trp92 affects the bioluminescence emitter because its replacement with Phe or some other residue leads to a change in the light emission spectrum of photoproteins (Ohmiya ***et al.,*** 1992; Deng ***et al.,*** 2001; Vysotski ***et al.,*** 2003; Malikova ***et al.,*** 2003). Five Trp residues occupy the same positions in obelin and aequorin. The Trp103 of obelin (Fig. 3.1A) and Trp78 of aequorin (Fig. 3.1B) are found in the fourth -helix but at the opposite termini (Fig. 3.1) (Liu ***et al.,*** 2000; Head ***et al.,*** 2000). The spatial structures of different ligand-dependent conformational states of obelin show that only these tryptophans might be accessible to solvent (Liu ***et al.,*** 2000; Deng ***et al.,*** 2004; Deng ***et al.,*** 2005; Liu ***et al.,*** 2006). It should be noted, however, that the spatial structure of apo-photoprotein is not yet known.

In this chapter we outline for the first time the intrinsic fluorescence of apo-obelin and apo-aequorin and use of its quenching for the characterization of coelenterazine binding.

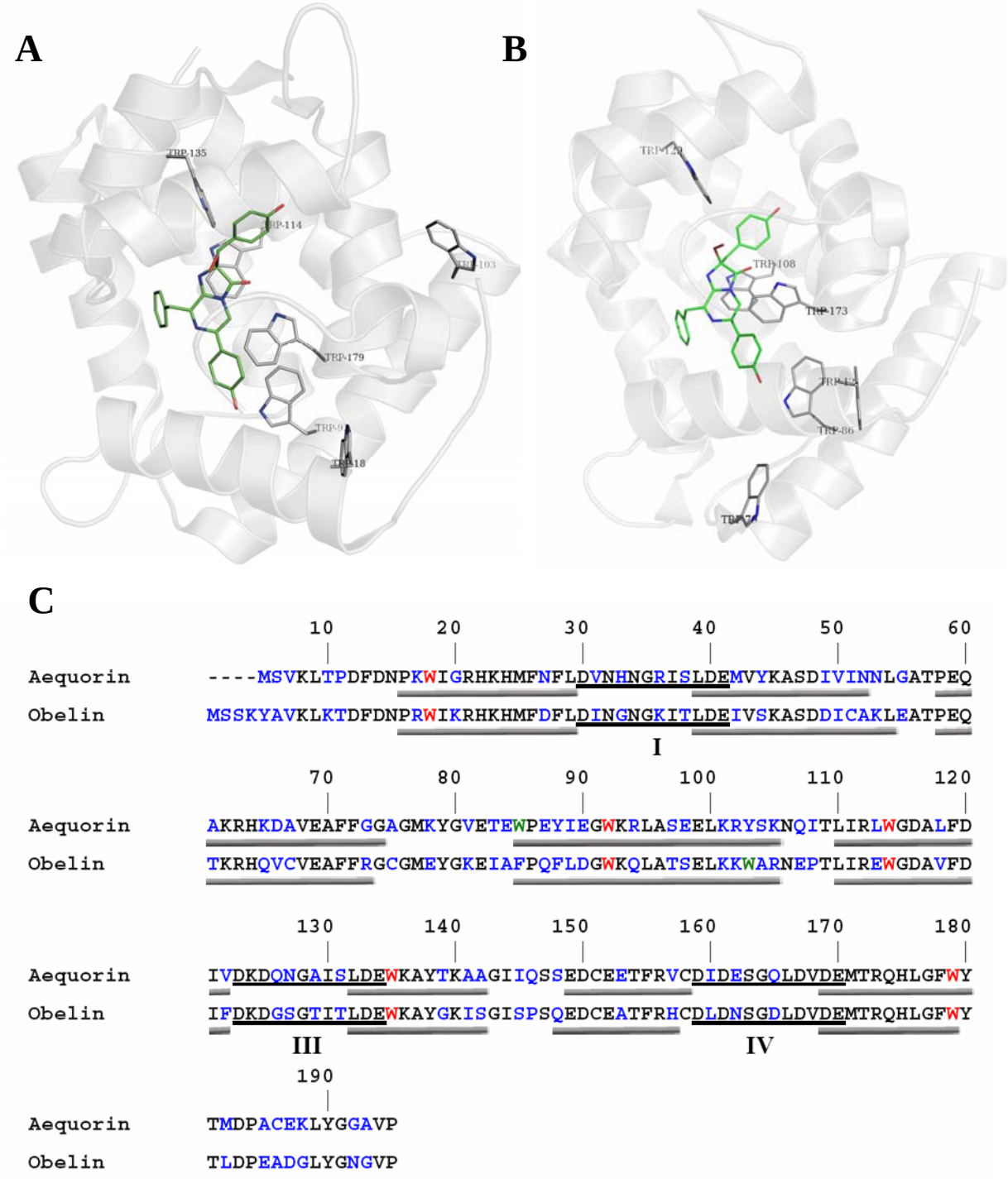

Figure 3.1 Spatial structures of obelin (PDB code 1QV0) (A) and aequorin (PDB code 1EJ3) (B), and their sequence alignment (C). The residues of aequorin structure (B) are numbered according to 1EJ3. The 2-hydroperoxycoelenterazine molecule (green) is shown in the center as a stick model. The identical and variable residues are in black and blue letters, respectively. The conservative and nonconservative Trp residues are colored by red and green, respectively; Ca^{2+}-binding loops I, III, and IV are underlined. The gray cylinders show -helices according to photoprotein structures.

Materials and Methods

Site-directed mutagenesis - The site-directed mutagenesis was done on the template pET19-OL8 *E. coli* expression plasmid carrying the *Obelia longissima* wild-type apo-obelin gene (Markova *et al.,* 2000). Mutations resulting in the changes – W18F, W92F, W103F, W114F, W135F, or W179F – were carried out with the QuickChange site-directed mutagenesis kit (Stratagene, USA) according to the protocol supplied with the kit. The plasmids harboring the mutations were verified by DNA sequencing.

Protein expression and purification - The apo-obelin and apo-aequorin truncated by six residues from the N-terminus as well as obelin mutants were expressed as previously reported (Deng *et al.,* 2005; Markova *et al.,* 2002). For protein production, the transformed *E. coli* BL21-Gold was cultivated with vigorous shaking at 37 ^{o}C in LB medium containing 200 µg/ml ampicillin and induced with 1 mM IPTG when the culture reached an OD_{600} of 0.5-0.6. After addition of IPTG, the cultivation was continued for 3 hours. Most of the apo-photoproteins produced were accumulated in inclusion bodies.

Apo-obelin and apo-aequorin were purified from inclusion bodies as described (Illarionov *et al.,* 2000). The apo-photoproteins obtained after extraction with 6 M urea and purification on a DEAE-Sepharose Fast Flow column, were concentrated by Amicon Ultra Centrifugal Filters (Millipore). To fold apo-photoproteins, the concentrated samples containing 6 M urea were diluted approximately 20-fold with a solution containing 1 mM EDTA, 20 mM Tris-HCl pH 7.0, again concentrated, and then "washed" several times with the same buffer to remove any impurities of urea and salts. The apo-photoproteins (~1 mg/ml) were 0.5 ml-aliquoted into plastic tubes and frozen at -80^{o}C.

All the experiments with apo-photoproteins were carried out with freshly thawed samples. Thawed samples were centrifuged (20,000 g × 10 min) at 4^{o}C, incubated overnight with 10 mM DTT, again centrifuged, and then passed through a Superdex 200 column (Amersham Bioscience) equilibrated with freshly prepared 10 mM DTT, 5 mM EDTA, 20 mM Tris-HCl pH 7.0 to produce monomeric apo-photoprotein containing no disulfide bonds and aggregates (Ohmiya *et al.,* 1993; Masuda *et al.,* 2003). The final preparations of apo-photoproteins were homogeneous according to SDS-PAGE and gel

filtration. Obelin and aequorin, charged with coelenterazine, were produced as previously reported (Markova ***et al.,*** 2002; Illarionov ***et al.,*** 2000; Vysotski ***et al.,*** 2001).

The coelenterazine concentration in the methanol stock solution was determined spectrophotometrically using the extinction coefficient ($_{434\ nm}$ = 8900 cm^{-1} M^{-1} (Hori ***et al.***, 1977). The apo-obelin and apo-aequorin concentrations were determined using $_{280\ nm}$ = 40450 and 43430 $M^{-1}cm^{-1}$ respectively as calculated with the ProtParam tool (http://us.expasy.org/tools/ protparam-doc.html) which uses Edelhoch's method (Edelhoch, 1967).

Fluorescence measurements - Fluorescence measurements were carried out with an AMINCO spectrofluorimeter (Thermo Spectronic, USA) in 5 mM EDTA, 10 mM DTT, 20 mM Tris-HCl pH 7.0 at 20 ^{o}C. Excitation was at 295 nm (slit 4 nm). The fluorescence emission spectra were corrected with the computer program supplied with the instrument. To assess fluorescence quenching only the changes of fluorescence intensity at 336 nm were used. All spectra were taken using a standard quartz cuvette (1 × 1 cm) in a 1-ml initial volume with varied coelenterazine additions in 1- to 5-μl portions up to saturation. The fluorescence intensities were corrected for dilution due to the addition of coelenterazine, for the methanol influence on Trp fluorescence, scattered light, and for inner filter effects of protein and added coelenterazine. To evaluate the inner filter effects, absorbance measurements were performed at excitation and emission wavelengths and fluorescence (*F*) was corrected using the equation:

$$F = F_{unc} e^{\frac{A_{295}+A_{336}}{2}} \qquad (3.1)$$

where A_{295} and A_{336} are absorbance of protein and ligand at excitation and emission wavelengths, respectively, and F_{unc} is uncorrected fluorescence.

Determination of apparent dissociation constant of the apo-photoprotein-coelenterazine complex - The apparent dissociation constant of the apo-photoprotein-coelenterazine complex was determined using the quenching of apo-obelin and apo-aequorin Trp fluorescence upon binding to coelenterazine. Our analysis assumed that the fraction of

bound ligand is equal to the ratio of the fluorescence quenching ($Q = F_o - F_q$) to maximum quenching ($Q_{max} = F_o - F_{qmax}$), where F_o, F_q, and F_{qmax} are fluorescence intensity at 336 nm measured in the absence of added ligand, the quenched fluorescence intensity in the presence of ligand, and the maximum fluorescence quenching at a saturating level of ligand, respectively. The apparent dissociation constants were calculated by fitting the relative fluorescence emission to Equation 3.2, a modified equation compared with the one described elsewhere (Bollen ***et al.,*** 2005):

$$\frac{Q}{Q_{\max}} = \frac{(C + L + K_D) - \sqrt{(C + L + K_D)^2 - 4CL}}{2} \qquad (3.2)$$

where C, L, and K_D are apo-photoprotein and coelenterazine concentrations, and apparent dissociation constant, respectively.

Stopped-flow measurements **-** Stopped-flow measurements were carried out using a temperature-controlled Hi-Tech SF-51 apparatus equipped with a Hi-Tech SU-40 spectrometer (dead time 1.5 ms) (Salisbury, United Kingdom) at 20 ^{o}C. The changes in apo-photoprotein fluorescence emission upon coelenterazine binding were detected between 300 and 400 nm (using Corning WG320 and UG380 filters) with excitation set at 280 nm. The spectral excitation bandwidth was 10 nm. The stopped-flow measurements were carried out by mixing of 1.2 M apo-obelin or 1.2 M apo-aequorin in 5 mM EDTA, 10 mM DTT, 20 mM Tris-HCl pH 7.0 with either 1.2 or 6.0 M coelenterazine prepared in the same buffer.

Results and Discussion

Intrinsic fluorescence of apo-obelin and apo-aequorin - Both apo-photoproteins have typical UV absorption properties characteristic for proteins without any organic ligand with a maximum absorbance at 280 nm and a shoulder at 295 nm (Fig. 3.2A). The active photoproteins, i.e. having bound 2-hydroperoxycoelenterazine, in addition display a shoulder at 310 nm and a maximum at 460 nm. Freshly prepared coelenterazine shows absorption maxima at 275 and 425 nm, and a shoulder at 340 nm.

With excitation at 295 nm, the intrinsic fluorescence of apo-photoproteins is observed with a maximum at 336 nm (Fig. 3.2B). Given that the excitation is at 295 nm, the observed fluorescence is due exclusively to Trp fluorescence. The photoprotein preparations, separated from uncharged apo-proteins by ion-exchange chromatography on Mono Q (Markova *et al.*, 2002; Vysotski *et al*, 2001), display only a very weak fluorescence with an intensity of about 5-6% of apo-photoprotein fluorescence and with the same maximum (336 nm).

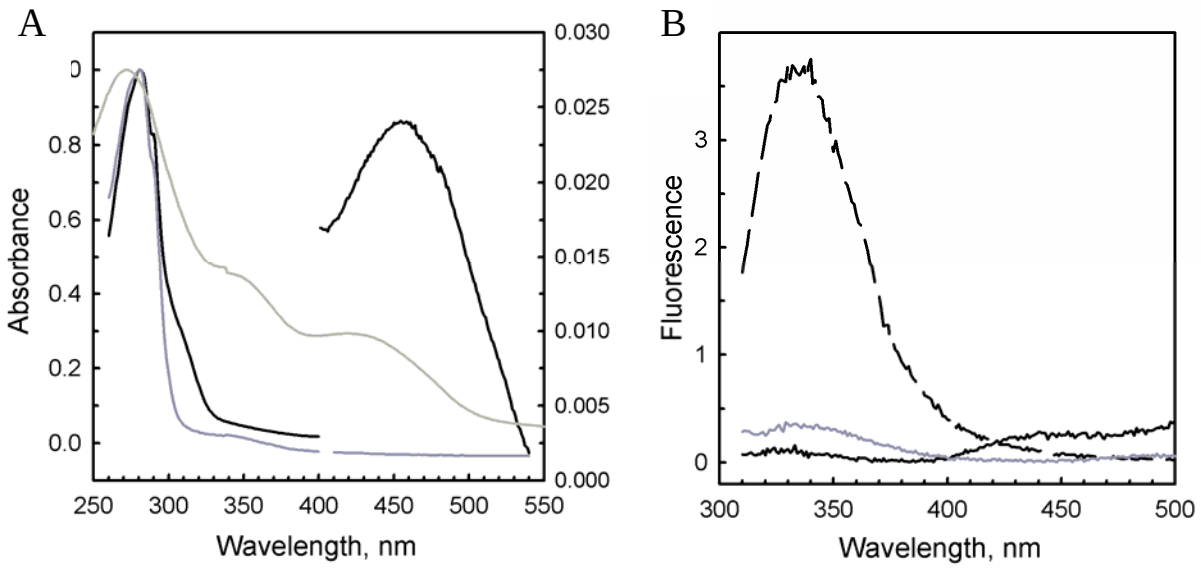

Figure 3.2. Absorption and fluorescence properties of photoproteins. (A) Normalized absorption spectra of apo-aequorin (dark gray line), active aequorin (black line), and free coelenterazine (gray line). The right black and dark grey spectra (after break) belong to the right scale. (B) Fluorescence emission spectra of apo-obelin (dashed black line), active obelin (dark gray), and free coelenterazine with excitation at 295 nm. All samples were in 1 mM EDTA, 20 mM Tris-HCl pH 7.0. To minimize effect of autooxidation, the coelenterazine in buffer was prepared immediately before spectral measurements from methanol stock solution.

Free coelenterazine does not display any fluorescence in the range from 310 to 400 nm; a very weak fluorescence is observed beginning at 400 nm with low intensity maxima at 440 and 520 nm (Fig. 3.2B). These results evidently show that coelenterazine binding to apo-photoproteins quench Trp fluorescence.

The very low fluorescence of active photoproteins is rather surprising because one of the Trp residues of obelin (Trp103) and aequorin (Trp79) (Fig. 3.1) is found on the surface of the protein and is accessible to solvent. Examination of the surroundings of these tryptophans in the crystal structures of obelin (PDB code 1QV0) and aequorin (PDB code 1EJ3) gives a possible explanation for the low intensity of the intrinsic fluorescence. Nearby the indole rings of Trp103 in obelin and Trp79 in aequorin are found the side chains of Arg173 and Lys17, respectively. Although in the crystal structures the atoms of these residues do not form electrostatic interactions with Trp atoms, dynamic interactions with these polar residues might be present in solution and effectively quench the fluorescence.

Intrinsic fluorescence of Trp mutants of obelin - To estimate the influence of each tryptophan on the intrinsic fluorescence properties of apo-photoprotein we produced six obelin mutants by replacing each Trp in turn by Phe (Fig. 3.3). The substitutions do not change the wavelength of the fluorescence emission maxima in comparison with those of wild-type apo-obelin but influence the fluorescence intensity. Although Trp92 deeply resides within the coelenterazine-binding pocket (Fig. 3.1), the decrease in relative intensity on its substitution amounts to ~ 40% of the total fluorescence signal. The substitution of the other two tryptophans of the coelenterazine-binding cavity, Trp114 and Trp179, as well as Trp18 situated in the first -helix, results in a decrease of nearly 20% of the total fluorescence of apo-obelin. Substitution of Trp135, the fourth tryptophan of the coelenterazine-binding cavity, has practically no effect on the overall intensity, indicating that most probably the fluorescence from this Trp is severely quenched by interactions within the protein. Trp103 is the only tryptophan on the surface of the photoprotein molecule (Fig. 3.1). Its substitution reduces the intrinsic fluorescence approximately by 5%. It is quite possible that this Trp is responsible for the weak fluorescence of the active photoproteins (Fig. 3.2B). The different effects of Trp substitutions on the total intrinsic

fluorescence of apo-obelin are likely due to different efficiencies of their fluorescence quenching which might depend on local environments of each Trp.

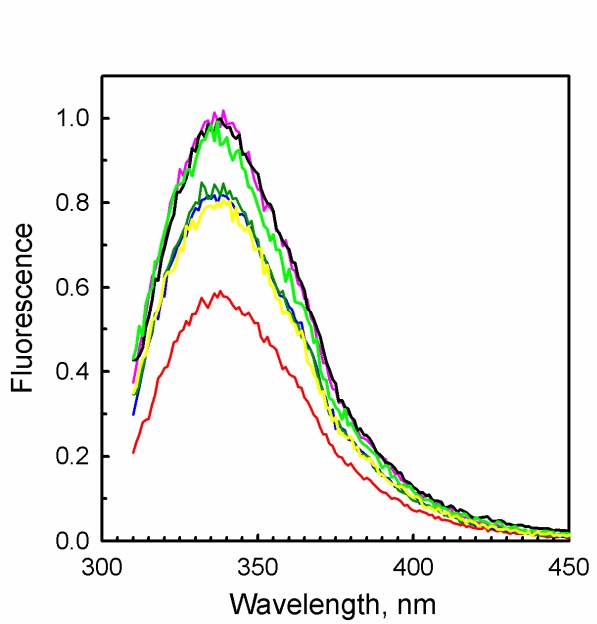

Figure 3.3 Normalized fluorescence emission spectra of wild-type apo-obelin (black line) and its tryptophan mutants: W18F, yellow; W92F, red; W103F, light green; W114F, blue; W135F, pink; and W179F, dark green. The excitation wavelength is 295 nm. The concentrations of wild-type apo-obelin and its mutants are 1.22 M.

Quenching of Trp fluorescence of apo-obelin and apo-aequorin with coelenterazine - Addition of coelenterazine to apo-obelin induces a strong concentration-dependent decrease of Trp fluorescence (Fig. 3.4A). Similar results were obtained with apo-aequorin (not shown). However, even a 7-fold molar excess of coelenterazine does not quench the intrinsic fluorescence of apo-photoproteins completely; always there is residual fluorescence constituting approximately 20-30% of the initial fluorescence. The residual fluorescence practically does not change even after four hours (time required to form an active photoprotein); the fluorescence intensity is decreased by only 2-4%. In contrast, the intrinsic fluorescence of photoproteins after ion-exchange chromatography on Mono Q column is very weak (5-6% of apo-photoprotein intensity) (Fig. 3.2).

This might indicate that approximately a quarter of apo-photoprotein is incompetent for coelenterazine binding despite the fact that monomeric apo-photoproteins reduced with DTT have been used. It is tempting to equate this quarter with the empirical observation that on charging the recombinant apo-photoprotein with coelenterazine, there is always

about the same fraction of uncharged protein, which can be separated by ion-exchange chromatography (Markova *et al.*, 2002; Vysotski *et al*, 2001). It should be noted that the residual (20-30%) fluorescence has approximately the same maximum (336 nm) indicating that the Trp residues of binding-incompetent apo-photoprotein have a very similar environment.

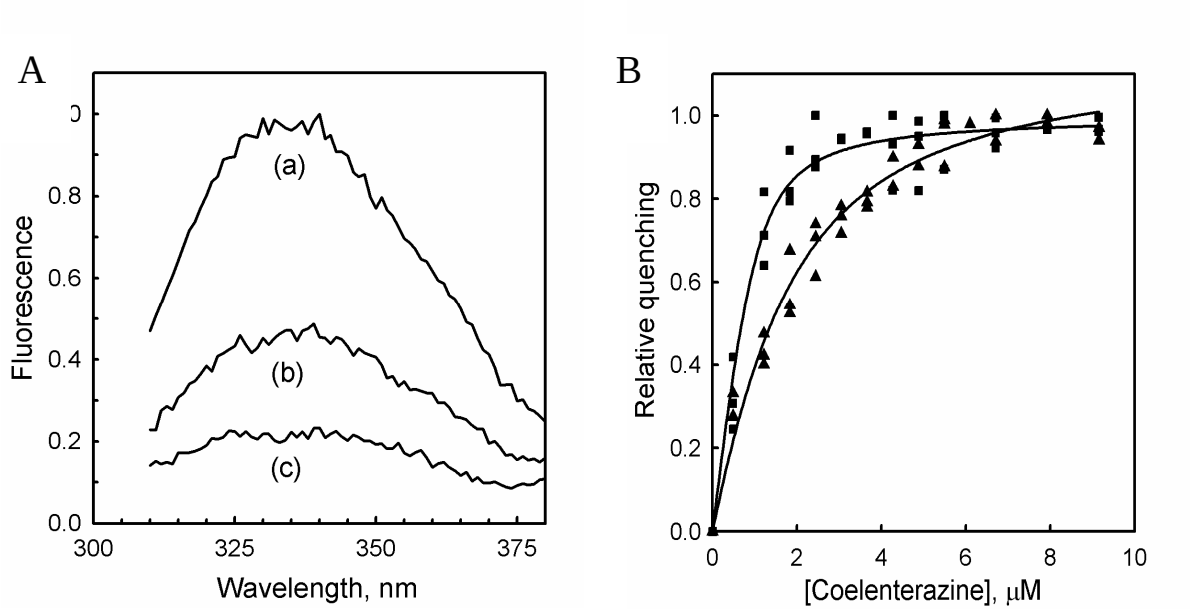

Figure 3.4 Quenching of intrinsic apo-photoprotein fluorescence by coelenterazine. (A) Scans exhibiting the effect of coelenterazine on apo-obelin fluorescence measured between 310 and 380 nm: (a) in absence of coelenterazine; (b) and (c) with 1.22 and 9.15 M of coelenterazine, respectively. (B) Determination of the apparent dissociation constants of apo-obelin- (■) and apo-aequorin-coelenterazine (▲) complexes using the quenching of intrinsic fluorescence of apo-photoproteins upon coelenterazine binding. Equation 3.2 is fitted to the fluorescence intensity data as described under Materials and Methods. The concentrations of apo-obelin and apo-aequorin were 1.22 M. All titrations were performed in triplicate.

The dissociation constant of the apo-photoprotein-coelenterazine complex was determined using the above quenching tryptophan fluorescence data by fitting the relative fluorescence emission to Eq. 3.2 (see Materials and Methods) (Fig. 3.4B). The estimated dissociation constants turn out to be 1.2 ± 0.12 and 0.2 ± 0.04 M for apo-aequorin and apo-obelin, respectively indicating that the affinity of apo-aequorin to coelenterazine is lower than that of apo-obelin. This result is somewhat surprising because according to the spatial structures of these photoproteins the residues lining the coelenterazine-binding cavity are practically the same; there is a distinction in only three amino acids (Liu *et al.*, 2000; Head *et al.*, 2000). In obelin instead of Met42, Val50, and Tyr88 which occupy these

positions in aequorin, Ile42, Ile50, and Phe88 are found (Fig. 3.1). Probably two of these residues (Met and Tyr) might affect aequorin affinity to coelenterazine because the properties of their side chains differ from those of Ile and Phe. This assumption seems quite reasonable because, for example, only one substitution of Tyr88 in aequorin by Phe (or Phe88 in obelin by Tyr) leads to changes in bioluminescence and fluorescence maxima (Stepanyuk ***et al.***, 2005).

It should be noted that the determined dissociation constants for coelenterazine are not equilibrium dissociation constants in the strict sense. When the quenched apo-photoprotein (it was tested with apo-obelin and apo-aequorin) was diluted by a factor of two immediately after coelenterazine addition an exactly two-fold decrease of fluorescence was observed that obviously shows that coelenterazine remains tightly associated with apo-photoprotein. Most likely the strong association of coelenterazine with apo-photoprotein results from hydrophobic interactions of coelenterazine with nonpolar residues lining the coelenterazine-binding cavity placing this substrate in proximity to Trp residues. Hence it is more appropriate to use the term “apparent dissociation constant”.

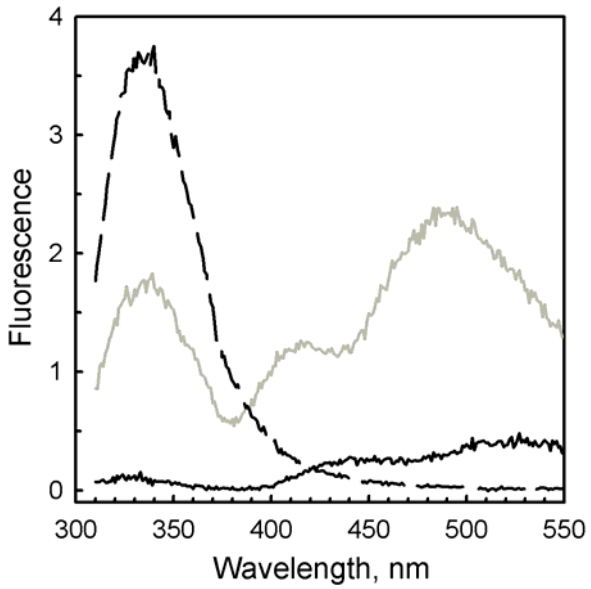

Figure 3.5 Fluorescence emission spectra of 1.22 M apo-obelin (dashed black line), freshly prepared 1.22 M coelenterazine in the same buffer (solid black line) and their mixture at equimolar concentrations of 1.22 M (gray line). Excitation wavelength is 295 nm.

A methanol solution of coelenterazine displays weak yellow fluorescence (Shimomura, 2006). A similar weak fluorescence is observed with freshly prepared coelenterazine in buffer (Fig. 3.5). However, the fluorescence intensity of coelenterazine is noticeably increased upon binding to apo-photoprotein and is accompanied with a blue shift in emission. Because the absorption spectrum of coelenterazine in buffer has a shoulder at 340 nm (Fig. 3.2A) corresponding to the tryptophan fluorescence maximum of apo-photoproteins we might reasonably assume that the increase of coelenterazine fluorescence results from resonance energy transfer between tryptophans and bound coelenterazine. Since the fluorescence of coelenterazine is very weak we might also surmise it is RET that results in the quenching of apo-photoprotein intrinsic fluorescence by coelenterazine.

The quenching of intrinsic fluorescence by coelenterazine and therefore coelenterazine binding with apo-photoprotein is very fast because the Trp fluorescence of apo-obelin and apo-aequorin measured right after adding a 5-fold molar excess of coelenterazine is immediately quenched and no further significant change of fluorescence is observed. Experiments using the stopped-flow technique showed that coelenterazine binding takes place within the dead-time (1.5 ms) of the instrument (not shown). Thus, we can conclude that the coelenterazine binding with apo-photoproteins is a very fast process occurring on submillisecond time scale.

Conclusion

For the first time we have characterized the intrinsic fluorescence of two apo-photoproteins and demonstrated that the quenching of Trp fluorescence by coelenterazine can be applied for studying its binding with apo-protein. Using the effect of concentration-dependent quenching of the intrinsic fluorescence of apo-photoproteins upon binding of coelenterazine we have determined the apparent dissociation constants for coelenterazine binding with apo-aequorin and apo-obelin. The values of apparent dissociation constants imply a high affinity of the apo-photoprotein substrate-binding cavity for coelenterazine. The binding of coelenterazine is shown to be a fast process taking less than milliseconds. This indicates that the rate-limiting step of active photoprotein complex formation is the relatively slow conversion of coelenterazine into its peroxy adduct.

Acknowledgements

We thank Prof. John Lee for valuable suggestions and providing constructive criticisms. The work was supported by Wageningen University Sandwich PhD-Fellowship Program, Grants 02.512.12. 2006 and 1211.2008.4 of Ministry of Education and Science of Russian Federation, MCB Program of RAS, and by Grant No. 2 of SB RAS.

Chapter 4

Oxygen activation of apo-obelin-coelenterazine complex

Eremeeva, E.V.; Natashin, P.V.; van Berkel, W.J.H.; Vysotski, E.S.; and Liu, Z.J.

Abstract

Ca^{2+}-regulated photoproteins use a non-covalently bound 2-hydroperoxycoelenterazine ligand to emit light in response to Ca^{2+} binding. To better understand the mechanism of formation of active photoprotein from apo-protein, coelenterazine and molecular oxygen, we have investigated the spectral properties of the anaerobic apo-obelin-coelenterazine complex and after reaction with oxygen. Our studies suggest that coelenterazine bound within the anaerobic complex might be a mixture of N7 protonated and C2 anionic forms. Proton subtraction from N7 and further reprotonation of C2 followed by 2-hydroperoxy-coelenterazine formation might occur with the assistance of His175. It is proposed that His175 might play a key role both in formation of active obelin and in Ca^{2+} triggering of the bioluminescence reaction.

Keywords: bioluminescence, coelenterazine, photoprotein, oxygen activation

Abbreviations: DTT, dithiothreitol; EDTA, ethylenediaminetetraacetate; IPTG, isopropyl thio-β-D-galactopyranoside

Introduction

Ca^{2+}-regulated photoproteins are responsible for the light emission of a variety of bioluminescent marine organisms, mostly coelenterates (Morin, 1974). The best known of these is aequorin isolated from the jellyfish *Aequorea* (Shimomura *et al*, 1962). Ca^{2+}-regulated photoproteins consist of a single polypeptide chain to which an imidazopyrazinone derivative (2-hydroperoxycoelenterazine) is tightly bound. The light-yielding reaction proceeds at a very low rate in the absence of Ca^{2+} but is greatly accelerated upon Ca^{2+} binding (Allen *et al.,* 1977). Bioluminescence formation involves the oxidative decarboxylation of 2-hydroperoxycoelenterazine, generating protein-bound coelenteramide in its excited state (Shimomura and Johnson, 1972; Cormier *et al.,* 1973). The excited coelenteramide relaxes to its ground state with the production of blue light showing emission maxima around 465–495 nm depending on the source organism (Vysotski and Lee, 2004).

The main use of Ca^{2+}-regulated photoproteins has been for the detection of calcium ions in biological systems (Blinks *et al.,* 1982; Knight *et al.,* 1991; Rizzuto *et al.,* 1992; Baubet *et al.*, 2000; Mithofer and Mazars, 2002; Moscatiello *et al.,* 2009). Photoproteins have been successfully applied in many different types of living cells, both to estimate the intracellular Ca^{2+} concentration under steady-state conditions and to study the role of calcium transients in the regulation of cellular function. Photoproteins were initially injected into cells for these studies or delivered by liposome-mediated transfer, but since the cloning of cDNA genes (Knight *et al.,* 1991; Rizzuto *et al.,* 1992), expression of recombinant photoproteins within cells is preferred. The success of such photoprotein applications, however, depends on various factors among which are the rate and efficacy of the generation of active photoprotein from apo-photoprotein, coelenterazine, and oxygen, as well as any influence of the cellular environment on these processes.

From the determination of different ligand-dependent photoprotein conformational states (Liu *et al.,* 2000; Head *et al.,* 2000; Liu *et al.,* 2003; Deng *et al.,* 2004; Deng *et al.,* 2005; Liu *et al.,* 2006), significant insight has been obtained into the mechanism of bioluminescence (Vysotski and Lee, 2004; Tomilin *et al.,* 2008; Isobe *et al.,* 2009). At the same time much less is known about the mechanism of active photoprotein complex

formation from apo-protein, coelenterazine, and oxygen. Investigations thus far have dealt with the relative rates of active photoprotein complex formation from wild-type apo-aequorin with coelenterazine and its analogs as well as the effect of temperature, pH, incubation time, reducing agent concentrations, and some additives on this process (Shimomura and Johnson, 1975; Inouye *et al.,* 1986; Shimomura *et al.,* 1993; Knight *et al.,* 1993).

Recently, using intrinsic protein fluorescence quenching, we demonstrated that coelenterazine binding to apo-photoprotein occurs within milliseconds in contrast to the formation of active photoprotein complex which requires minutes to hours (Eremeeva *et al.,* 2009). It evidently showed that the rate-limiting step of active photoprotein formation is the conversion of coelenterazine into its peroxy derivative which takes place within the substrate-binding cavity. However, what is happening with coelenterazine after its binding to apo-photoprotein, and what coelenterazine intermediates precede 2-hydroperoxy-coelenterazine generation, is unknown.

In this study we explored for the first time the absorption spectral properties of the anaerobic apo-obelin–coelenterazine complex as well as the kinetics of conversion of bound coelenterazine into 2-hydroperoxycoelenterazine after exposure of the protein-ligand complex to air.

Materials and Methods

Chemicals – Unless stated otherwise, chemicals were from Sigma-Aldrich and the purest grade available. High purity coelenterazine was purchased from JNC Corporation (Yokohama, Japan).

Protein expression and purification - Apo-obelin was expressed and purified as previously reported (Illarionov *et al.,* 2000; Vysotski *et al.,* 2001). For protein production, transformed *E. coli* BL21-Gold was cultivated with vigorous shaking at 37 ºC in LB medium containing 200 µg/mL ampicillin and induced with 0.5 mM IPTG when the culture reached an OD_{600} of 0.5-0.6. After addition of IPTG, the cultivation was continued for 3 h. Most of the apo-obelin produced was accumulated in inclusion bodies. The apo-photoprotein obtained after extraction with 6 M urea and purification on a DEAE-Sepharose Fast Flow column (GE Healthcare) with 6 M urea was concentrated by ultracentrifugal filtration using Amicon Ultra Centrifugal Filters (Millipore).

Apo-obelin concentrations were determined spectrophotometrically using a molar absorption coefficient $_{280\ nm}$ = 40450 M^{-1} cm^{-1} as calculated with the ProtParam tool (http://us.expasy.org/tools/protparam-doc.html) which uses Edelhoch's method (Edelhoch, 1967). The concentration of coelenterazine in the methanol stock solution was determined using a molar absorption coefficient $_{435\ nm}$ = 9800 M^{-1} cm^{-1} (Shimomura, 2006).

Preparation of anaerobic apo-obelin–coelenterazine complex - To remove oxygen solutions were degassed using an anaerobic station (Forma anaerobic system, Thermo Electron Corporation). For that, solutions in the sealed bottles were subjected to 10-15 successive cycles of vacuum treatment and nitrogen flushing.

All steps of preparation of the apo-obelin–coelenterazine complex were carried out within the anaerobic station. First and foremost, all solutions placed into the anaerobic chamber were tested for the presence of oxygen. The conversion of apo-obelin into active photoprotein was used as an indicator of oxygen since oxygen is required for bioluminescence of obelin. For that, 15 L-aliquots of every degassed solution placed within the chamber (i.e. chromatography buffers, calcium solution, activation buffer) were

mixed with 5 L of concentrated apo-obelin and 5 L of charging buffer 5 mM EDTA, 10 mM DTT, 20 mM Tris-HCl pH 7.0 containing 50 µM coelenterazine. After 15 min of incubation 2 L of Ca^{2+} solution (100 mM $CaCl_2$, 100 mM Tris-HCl pH 7.0) was injected. Lack of visible light indicated that the degassing procedure was performed successfully.

To produce the anaerobic apo-obelin–coelenterazine complex, approximately 2 ml of 2 mg/ml degassed apo-obelin in 6 M urea was diluted 10-fold with buffer (5 mM EDTA, 10 mM DTT, 20 mM Tris-HCl pH 7.0) containing coelenterazine (1.1 molar excess to protein) and kept in an anaerobic chamber overnight. The following steps were also performed in the anaerobic station. To remove free apo-obelin and unbound coelenterazine (Vysotski *et al.,* 2001), the sample was loaded on a degassed Q-Sepharose FF column (160 x 10 mm) equilibrated with 5 mM EDTA, 20 mM Tris-HCl pH 7.0. After washing with 2 column volumes starting buffer, the apo-obelin–coelenterazine complex was eluted with 0.3 M NaCl in the same buffer. The fraction having yellowish color was collected and concentrated by ultracentrifugal filtration. Purified protein samples were placed in special anaerobic quartz cells (Hellma Analytics) and tightly sealed to prevent oxygen contamination. Finally, samples were taken out from the anaerobic station for further measurements.

Anaerobic apo-obelin-coelenterazine complex was produced only from apo-obelin kept in 6 M urea. Attempts to obtain the oxygen-free complex from refolded apo-obelin failed.

Spectral measurements - Absorption spectra of apo-obelin–coelenterazine complex in the absence and presence of oxygen were obtained with a Hitachi U-2010 double-beam spectrophotometer (Hitachi). Absorption spectra of apo-obelin–coelenterazine complex were measured against 20 mM Tris-HCl, 2 mM EDTA, 0.3 M NaCl, pH 7.8. Coelenterazine spectra were taken in 5 mM EDTA, 0.3 M NaCl, 20 mM Tris-HCl, pH 7.8 or 10.0, and in 5 mM EDTA, 0.3 M NaCl, 50 mM Bis-Tris-HCl, pH 6.5. Difference absorption spectra of the apo-obelin–coelenterazine complex and coelenterazine were obtained by measuring absorption of the sample in the open cuvette with excess of air against sealed sample (containing the complex or coelenterazine, respectively) every 5 min during 30 min and then every 10 or 15 min during 400 min at 25 ºC.

Bioluminescence measurements **-** Bioluminescence of obelin during its activation was measured with a Varioskan Flash luminometer (Thermo Electron Corporation). Bioluminescence was triggered by forceful injection of 190 L of 100 mM $CaCl_2$, 20 mM Tris-HCl pH 7.0 into 10 L of photoprotein solution taken from anaerobic apo-obelin–coelenterazine complex, rapidly premixed with 20 mM Tris-HCl, 2 mM EDTA, 0.3 M NaCl, pH 7.8 and excess of air. The bioluminescence signal was integrated during 4 s at 25 ºC.

Results and Discussion

Interaction between coelenterazine and apo-obelin - Addition of coelenterazine to apo-obelin induces a strong concentration-dependent decrease of intrinsic protein fluorescence (Eremeeva *et al.,* 2009). When quenched apo-photoprotein was diluted by a factor of two immediately after coelenterazine addition, an exactly two-fold decrease of protein fluorescence was observed, showing that coelenterazine remains tightly associated with apo-photoprotein (Eremeeva *et al.,* 2009). The strong association of coelenterazine with apo-protein is attributed to hydrophobic interaction of coelenterazine with non-polar residues lining the coelenterazine-binding cavity. The successful purification of the anaerobic apo-obelin–coelenterazine complex with ion-exchange chromatography supports that apo-photoprotein and coelenterazine form a tight complex before modification of coelenterazine by oxygen occurs.

Spectral properties of anaerobic coelenterazine - Figure 4.1 shows absorption spectra of coelenterazine at anaerobic conditions in buffers of different pH. Coelenterazine displays absorption maxima at ~265, 345 and 430 nm (pH 6.5), at ~268, 340, and 410 nm (pH 7.8), and at 290 and ~390 nm (pH 10.0), respectively. Thus, alterations in pH result in evident changes in absorption properties of free coelenterazine.

Based on earlier studies of the solvent and pH-dependent spectral properties of coelenterazine derivatives (Scheme 4.1), the absorption spectra at pH 6.5 and 10.0 can be attributed to the N7 protonated and C2 anionic forms of coelenterazine, respectively (Hori *et al.,* 1975; Nakai *et al.,* 2003). Since the absorption spectrum of coelenterazine at 7.8 resembles a superposition of the spectra at pH 6.5 and 10.0, it is reasonable to assume that at pH 7.8, coelenterazine is present mainly as a mixture of N7 protonated and C2 anionic forms under anaerobic conditions (Fig. 4.1).

Reaction of free coelenterazine with oxygen - Coelenterazine emits light in the presence of oxygen when dissolved in aprotic solvents containing a trace amount of base. It was suggested that the first step in this process involves deprotonation of N7 of coelenterazine with a base yielding its C2 anionic form (Goto, 1968; Goto *et al.,* 1968; Kondo *et al.,*

2005). Then oxygen is bound at the C2-position of coelenterazine, giving the peroxide adduct (Scheme 4.2), which following cyclization leads to formation of dioxetanone. The dioxetanone then promptly decomposes with loss of CO_2 generating the singlet excited state of the amide product (Kondo *et al.,* 2005).

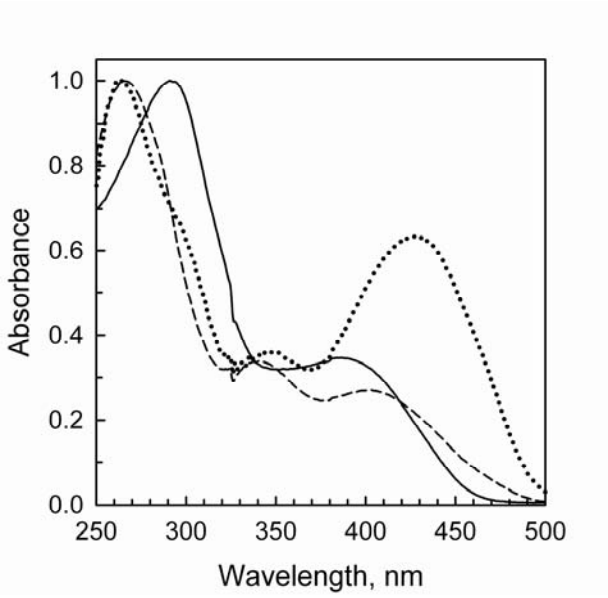

Figure 4.1 Anaerobic absorption spectra of coelenterazine at pH 6.5 (dotted line), 7.8 (dashed line), and 10.0 (solid line). Coelenterazine spectra were taken in buffer 5 mM EDTA, 0.3 M NaCl, 20 mM Tris-HCl, pH 7.8 or 10.0, and in buffer 5 mM EDTA, 0.3 M NaCl, 50 mM Bis-Tris-HCl, pH 6.5. Coelenterazine concentration was 25 M.

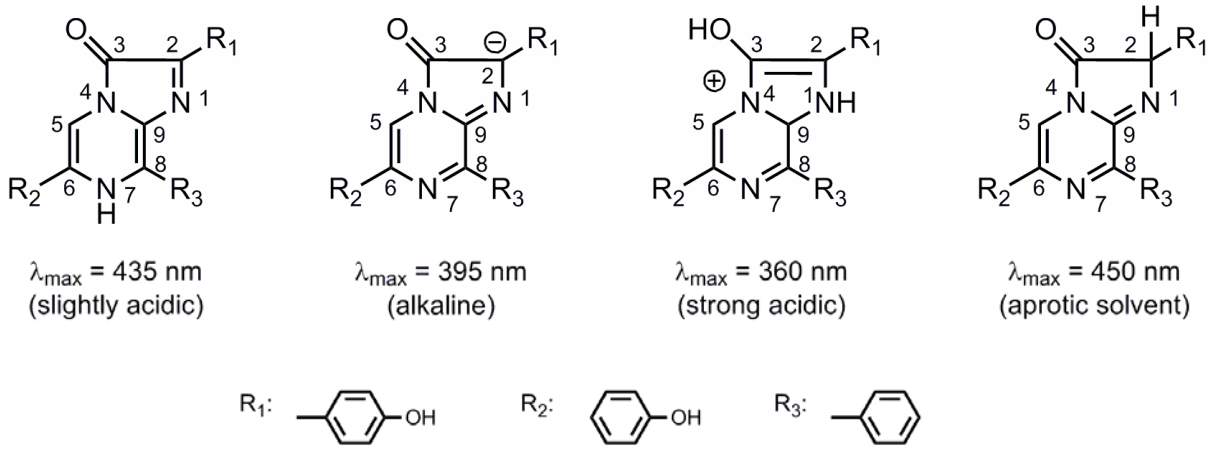

Scheme 4.1 Tautomeric and ionic forms of coelenterazine suggested by (Hori *et al.,* 1975).

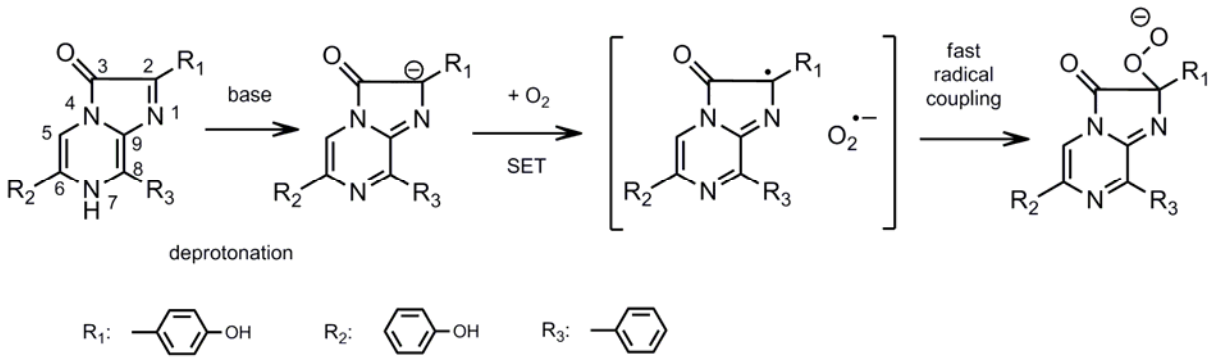

Scheme 4.2 A plausible mechanism for 2-hydroperoxycoelenterazine formation (Kondo *et al.,* 2005).

Figure 4.2 represents the changes in spectral properties of coelenterazine occurring under influence of oxygen at pH 7.8. After being exposed to air, the coelenterazine solution displays a gain of absorption at ~340 nm which, in fact, corresponds to appearance of the chemiluminescence reaction product, coelenteramide, and a disappearance of the absorption maximum at 414 nm that matches the decrease of some tautomeric form of coelenterazine existing at pH 7.8 (Scheme 4.1). It should be noted that the kinetics of the absorption changes (Fig. 4.2) show sigmoidal behavior.

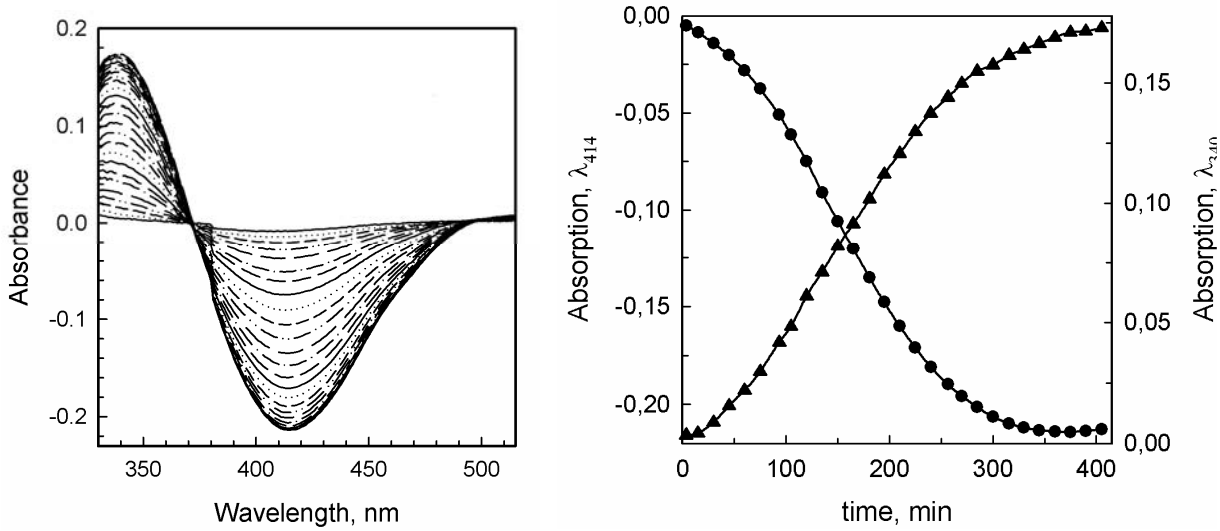

Figure 4.2 Difference spectrum (left panel) representing the changes of coelenterazine tautomeric form and kinetics (right panel) of its conversion into product monitored at 340 nm (▲) and 414 nm (•) occurring under influence of oxygen at pH 7.8. Spectrum was taken from the sample in the open cuvette against anaerobic sample in the sealed cuvette every 5 and then 15 min during 435 minutes. Before taking the first spectrum the sample in cuvette was forcedly mixed by pipette during several minutes for its saturation by air to avoid a diffusion limit. Concentration of coelenterazine was 25 μM.

The protonated tautomeric form of coelenterazine which, according to spectral data, is present in solution at pH 6.5 (Fig. 4.1) also reacts with oxygen. When anaerobic coelenterazine is exposed to air at pH 6.5, again an absorption increase at ~340 nm and an absorption decrease at 430 nm (instead of 414 nm in case of pH 7.8) are observed (data not shown).

Spectral characterization of anaerobic apo-obelin-coelenterazine complex - Apo-obelin has typical UV/VIS absorption properties characteristic for proteins without any organic ligand with a maximum at 280 nm and a shoulder at 295 nm (Eremeeva ***et al.,*** 2009). Active obelin, i.e. with bound 2-hydroperoxycoelenterazine, displays in addition an absorption maximum at ~470 nm and a shoulder at 310 nm (Eremeeva ***et al.,*** 2009).

The absorption spectrum of anaerobic apo-obelin–coelenterazine complex displays an extra absorption maximum at 355 nm and a shoulder at ~400 nm which can be attributed to bound coelenterazine (Fig. 4.3A). This spectrum of the anaerobic apo-obelin–coelenterazine complex does not significantly change in the sealed cuvette during several

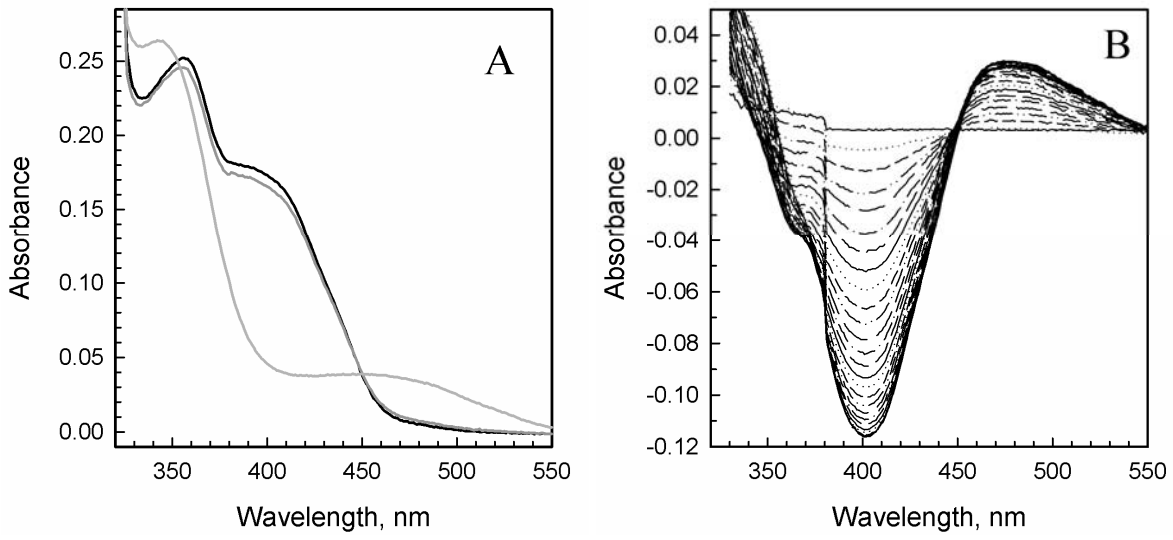

Figure 4.3 Absorption spectra of apo-obelin–coelenterazine complexes. (A) Absorption spectra of anaerobic apo-obelin–coelenterazine complex in sealed cuvette (black line), anaerobic apo-obelin–coelenterazine complex in sealed cuvette after 435 min (dark gray line), active obelin after 435 min (gray line); (B) Difference spectra showing the kinetics of active obelin formation from apo-obelin–coelenterazine complex and oxygen. Spectra were taken from the sample in the open cuvette against anaerobic sample in the sealed cuvette every 5 and then 15 min during 435 min. Before taking the first spectrum, sample was forcedly mixed by pipette during several minutes for saturation with air to avoid diffusion limitation. Concentration of the anaerobic protein-ligand complex was 45 μM.

hours (Fig. 4.3A).

Kinetics of conversion of apo-obelin-coelenterazine complex into active photoprotein – Aerated apo-obelin–coelenterazine complex has an absorption spectrum with a maximum at ~470 nm indicating the presence of bound 2-hydroperoxycoelenterazine (Shimomura, 2006) (Fig. 4.3A). Difference spectra representing the absorption changes of apo-obelin–coelenterazine complex during its activation by oxygen were taken from the sample in the open cuvette against the anaerobic sample in the sealed cuvette. In the course of conversion of apo-obelin–coelenterazine complex into active obelin the shoulder at 400 nm disappears, the maximum at 355 nm shifts to 345 nm, and a new absorption band characteristic for 2-hydroperoxycoelenterazine appears at ~470 nm (Fig. 4.3B). The apparent rate constants of conversion of apo-obelin–coelenterazine complex into active obelin which were calculated using the absorption changes at 400 and 470 nm amount to $k_{400\ nm} = 5.3 \pm 0.3 \times 10^{-3}$ min^{-1} and $k_{470\ nm} = 8.6 \pm 0.6 \times 10^{-3}$ min^{-1}, respectively.

To eliminate the potential limiting effect of oxygen diffusion on the rate of active photoprotein formation, we also performed the oxygen activation experiment under another condition. For this, the concentrated anaerobic sample of apo-obelin–coelenterazine complex was diluted ten times by air-saturated buffer and extensively mixed. After that, absorption spectra were recorded against buffer (Fig. 4.4A).

The spectra clearly demonstrate that there is no significant difference between the two formats of the oxygen activation experiment: in both cases (Fig. 4.3 and 4.4A) the shoulder at 400 nm disappears in time, the maximum at 355 nm shifts to 345 nm, and a new absorption band appears at ~470 nm. However, the $k_{400\ nm}$ and $k_{470\ nm}$ apparent rate constants estimated from the second experiment ($9.0 \pm 0.05 \times 10^{-3}$ min^{-1} and $15.8 \pm 0.3 \times 10^{-3}$ min^{-1}, respectively; Fig. 4.4B), are higher than those calculated from data shown in Fig. 4.3B. This indicates the dependence of apparent rate on oxygen concentration. Noteworthy is that the $k_{470\ nm}/k_{400\ nm}$ ratio is approximately the same in both cases, i.e. the apparent rate constants calculated from the absorption changes at 470 nm are ~1.6-1.7 times higher than those determined from the absorption changes at 400 nm.

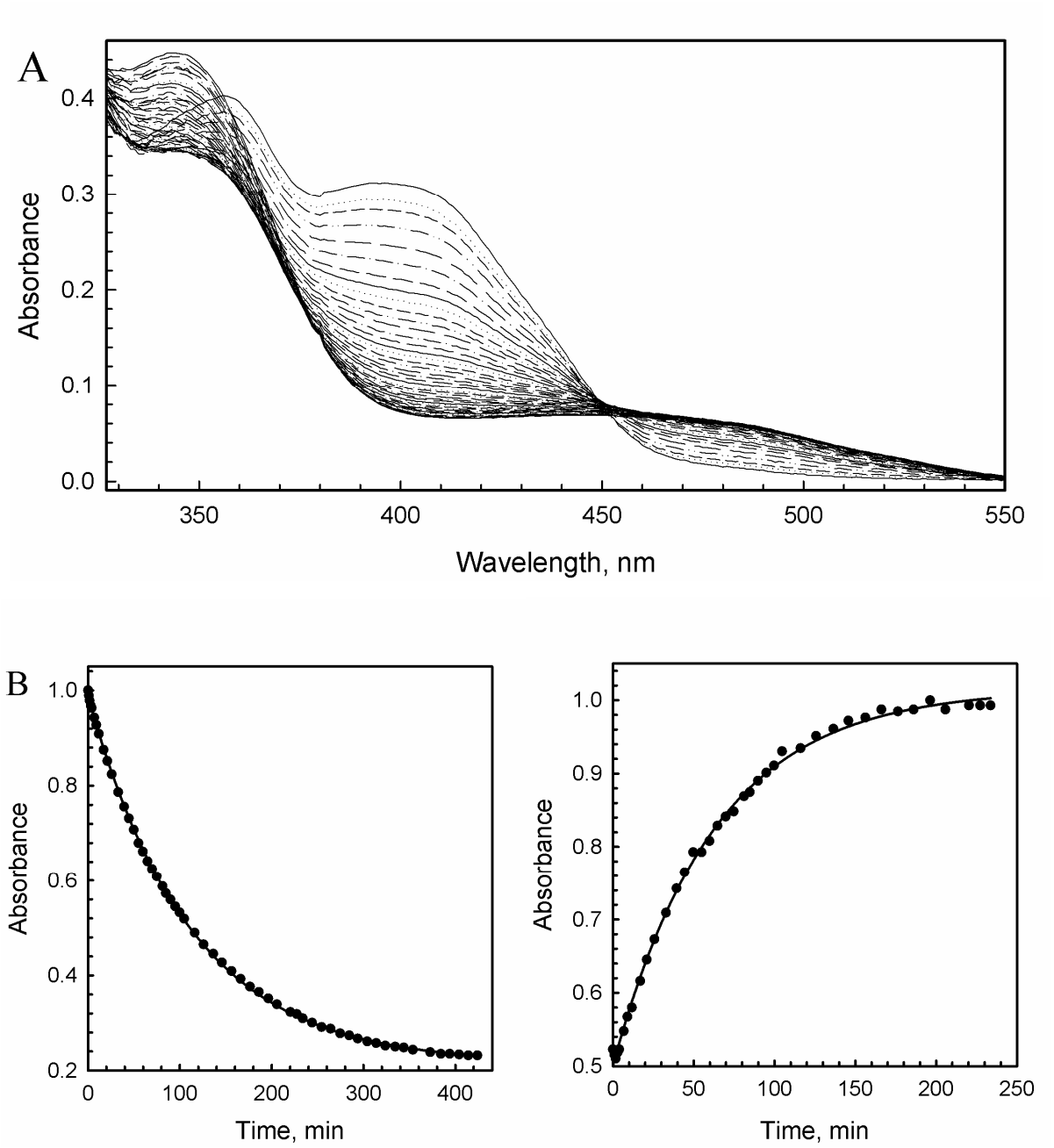

Figure 4.4 Reaction of anaerobic apo-obelin–coelenterazine complex with oxygen. (A) Absorption spectra taken from the air saturated sample against buffer every 5 and then 10 min during 430 min. (B) Kinetics of conversion of apo-obelin-coelenterazine complex into active photoprotein monitored at 400 nm (left panel) and at 460 nm (right panel). Concentration of the anaerobic complex was 68 μM.

Since the increase of absorption at 470 nm corresponds to the accumulation of 2-hydroperoxycoelenterazine in the substrate-binding cavity of obelin we compared the kinetics of active obelin formation monitored by absorbance at 470 nm with the kinetics

determined by bioluminescence (Fig. 4.5). Concentrated anaerobic sample of apo-obelin–coelenterazine complex was diluted ten times by air-saturated buffer, extensively mixed and then bioluminescence kinetics was measured by injection of calcium solution into sample aliquots with different incubation time. The apparent rate constant of bioluminescence formation k_{BL} was estimated to be $24.7 \pm 1.4 \times 10^{-3}$ min^{-1} which value is somewhat higher than that calculated from the absorption changes at 470 nm.

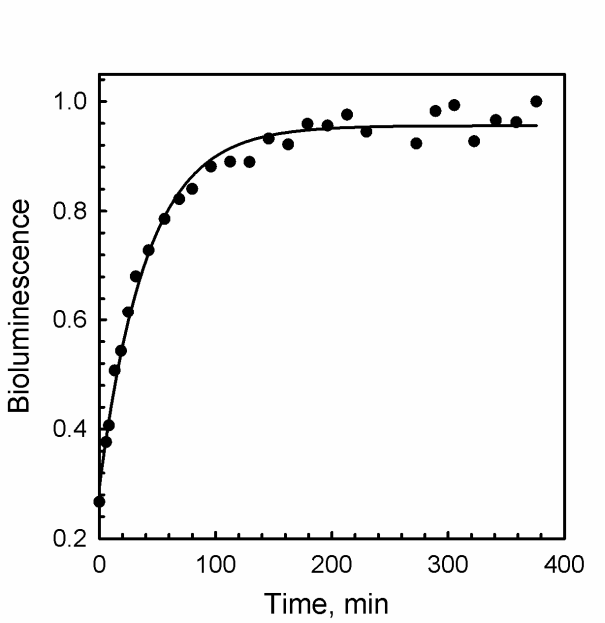

Figure 4.5 Kinetics of apo-obelin-coelenterazine complex activation by oxygen monitored by bioluminescence. Concentration of the anaerobic complex was 74 μM.

Assignment of coelenterazine derivative bound within anaerobic apo-obelin-coelenterazine complex – Comparison of the spectral properties of free coelenterazine and apo-obelin-coelenterazine complex at pH 7.8 allows us to speculate on the molecular structure of the coelenterazine derivative bound within the anaerobic apo-obelin-coelenterazine complex. Although not identical, the absorption spectrum of free coelenterazine at pH 7.8 (Fig. 4.1) is very similar to that of the anaerobic apo-obelin–coelenterazine complex (Fig. 4.3A). The maximum around 410 nm observed in the absorption spectrum of free anaerobic coelenterazine is shifted to 400 nm in case of the apo-obelin-coelenterazine complex. Since the absorption spectrum of coelenterazine at pH 7.8 represents a mixture of protonated and ionic forms, we can propose that coelenterazine bound within the anaerobic complex might be an equilibrium between N7(H) and C2(-) forms.

During the conversion of apo-obelin–coelenterazine complex into active obelin two main absorption changes are observed. The shoulder at 400 nm disappears (Fig. 4.3B) which can be attributed to the diminution of coelenterazine derivative bound within anaerobic apo-obelin-coelenterazine complex, and a new absorption band characteristic for 2-hydroperoxycoelenterazine appears at ~470 nm. The $k_{400\ nm}$ and $k_{470\ nm}$ apparent rate constants are different from each other in case of both experiments (Fig. 4.3B and Fig.4.4B). However, the $k_{470\ nm}/k_{400\ nm}$ ratio is independent on oxygen concentration, i.e. the apparent rate constants calculated from the absorption changes at 470 nm are ~1.6-1.7 times higher than those determined from the absorption changes at 400 nm. Since the coelenterazine bound within the anaerobic complex might be a mixture of C2 anionic and N7 protonated forms and $k_{400\ nm}$ is slower than $k_{470\ nm}$, we can assume that both steps are oxygen dependent and formation of 2-hydroperoxycoelenterazine might shift the equilibrium between initial species.

Photoprotein reaction with oxygen is rather slow (Shimomura and Johnson, 1975) and evidently depends on protein preparation procedure and reaction conditions (see Chapter 5). In contrast, many other monooxygenases and oxidases typically react very rapidly with oxygen (Massey, 1994). The conversion of apo-obelin–coelenterazine complex into photoprotein depends on oxygen concentration and diffusion of O_2 to its targeted binding site might be the rate determining factor. Although oxygen diffusion in water solutions is sufficiently fast (Lakowicz, 2006), in enzymes oxygen diffusion through protein channels can be significantly hindered by steric constraints (Klinman, 2007; Leferink, 2009). In case of apo-obelin–coelenterazine complex oxygen diffusion might be further restricted by the absence of discrete oxygen channels leading to the internal coelenterazine binding site (Liu *et al.,* 2000; Head *et al.,* 2000; Liu *et al.,* 2003). Thus, generation of active obelin involves the rapid binding and re-equilibration of coelenterazine tautomeric forms, followed by slow insertion of dioxygen to yield 2-hydroperoxycolenterazine.

His 175 as a possible proton shuttle - Since active photoprotein forms from apo-protein, coelenterazine, and oxygen at neutral pH, it is likely that some active site residue might act as an acid or base in 2-hydroperoxycoelenterazine formation. According to the crystal

structures of obelin (Liu *et al.*, 2000) and aequorin (Head *et al.*, 2000), His175 in obelin (and the equivalent His169 in aequorin) are located in the C-terminal helix which interacts with the N-terminal helix that assists to close the substrate-binding cavity, not far away from the C2-atom of coelenterazine (Fig. 4.6). This His residue is crucial for photoprotein bioluminescence because its substitution to Ala, Phe, or Trp leads to complete loss of bioluminescence activity, whereas modification of the remaining histidines yields mutant photoproteins with varying bioluminescence activities (Ohmiya and Tsuji, 1993; Eremeeva *et al.*, 2007).

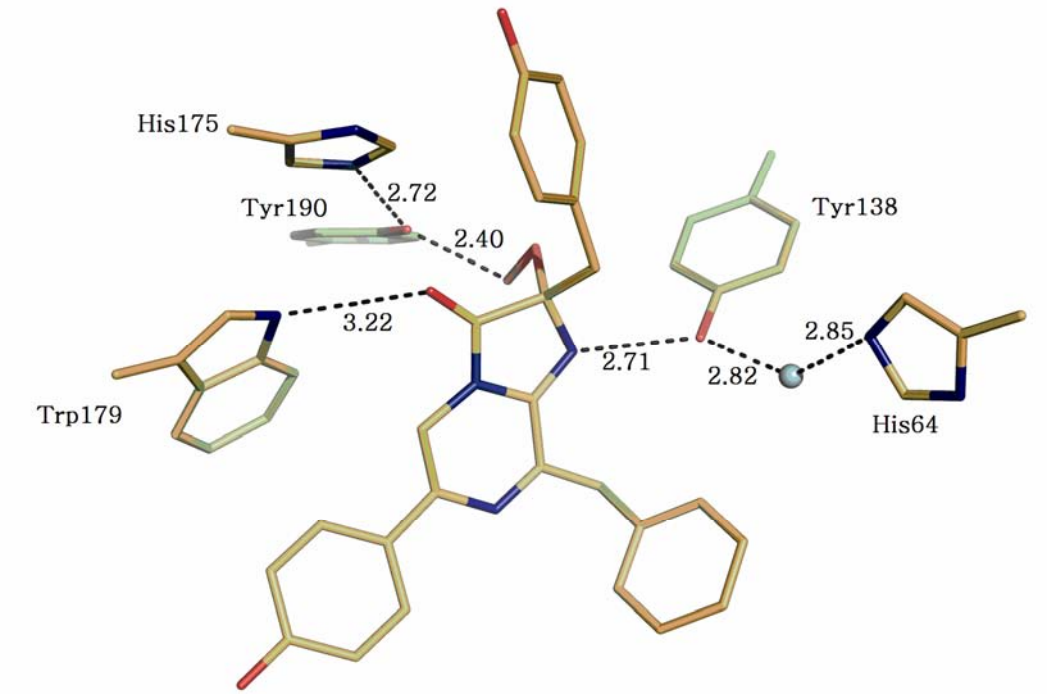

Figure 4.6 Amino acid surroundings of 2-hydroperoxycoelenterazine in obelin (PDB code 1QV0). The blue ball represents a water molecule; Hydrogen bonds (dashed lines) were determined with the PyMOL program. Distances are shown in Å.

For several cofactor-independent oxidases and oxygenases, including *Renilla* luciferase, oxygen activation was also proposed to involve a histidine (Prokop *et al.*, 2003; Steiner *et al.*, 2010; Fetzner and Steiner, 2010). In these enzymes, the histidine plays a key role in the proton relay system acting as a general base and proton donor/acceptor. In obelin, His175 might have a similar function by subtracting a proton from N7 yielding the coelenterazine C2 anion, and then giving this proton back yielding coelenterazine protonated at C2 which further reacts with oxygen giving the 2-hydroperoxy adduct and

consequently active photoprotein.

Conclusion

In summary, this study brings further insight into the mechanism of active photoprotein complex formation from apo-protein, coelenterazine, and oxygen. We show for the first time the formation of a tight complex between apo-photoprotein and coelenterazine in the absence of oxygen. Our spectroscopic studies suggest that at pH 7.8, coelenterazine bound within the anaerobic complex might be a mixture of N7 protonated and C2 anionic forms. Proton subtraction from N7 and further reprotonation of C2 might occur with the assistance of His175, suggesting that this residue plays a key role both in active photoprotein formation and in Ca^{2+} triggering of photoprotein bioluminescence.

Acknowledgements

The work was supported by grants of RFBR 12-04-91153, by the Programs of the Government of Russian Federation “Measures to Attract Leading Scientists to Russian Educational Institutions” (grant 11.G34.31.058), “Molecular and Cellular Biology” of RAS, President of Russian Federation “Leading science school” (grant 1044.2012.2). E.V.E. was supported by Wageningen University Sandwich PhD-Fellowship Program.

Chapter 5

Molecular mechanism of active photoprotein formation

Eremeeva, E.V.; Tomilin, F.N.; Antipina, L.U., Kuzubov, A.A.; Mezhevikin, V.V.; Markova, S.V.; van Berkel, W.J.H.; Ovchinnikov, S.G.; and Vysotski, E.S.

Abstract

Ca^{2+}-regulated photoproteins are responsible for the bioluminescence of a variety of marine organisms. All photoproteins consist of a single polypeptide chain to which the substrate, 2-hydroperoxycoelenterazine, is tightly bound. Although significant insight has been attained into the mechanism of photoprotein bioluminescence, the mechanism of formation of active photoprotein from coelenterazine, apo-protein and oxygen is poorly studied. Based on quantum chemical calculations and kinetic studies of wild-type obelin and selected obelin variants, we propose a mechanism of 2-hydroperoxycoelenterazine formation as well as the function of two key residues (His175 and Tyr138) in this process. Initial binding of coelenterazine to apo-obelin results in formation of the coelenterazine-binding cavity and is accompanied by coelenterazine protonation at C2. His175 likely acts as a proton shuttle in this process. Tyr138 is suggested to contribute to the formation of a stable van der Waals complex between coelenterazine and molecular oxygen, leading to 2-hydroperoxycoelenterazine generation. A similar mechanism of oxygen activation might also be operative with certain cofactor-independent monooxygenases.

Keywords*:* bioluminescence, coelenterazine, oxygen activation, monooxygenase, photoprotein

Abbreviations: CI, Configuration interaction method; CIS, correlation interaction single exciting method; CLZ, coelenterazine; DMF, dimethylformamide; DMSO, dimethyl sulfoxide; DTT, dithiothreitol; EDTA, ethylenediaminetetraacetate; IPTG, isopropyl thio-β-D-galactopyranoside; MO, molecular orbital; PCM, polarized continuum model; PM3, Parameterization method 3; PM6, Parameterization method 6; ROHF, restricted open-shell Hartree-Fock; SET, single electron transfer; TDDFT, time dependent density functional theory.

Introduction

Ca^{2+}-regulated photoproteins are responsible for the bioluminescence of a variety of marine organisms, mostly coelenterates (Morin, 1974). All photoproteins consist of a single polypeptide chain of about 22 kDa to which the substrate, 2-hydroperoxycoelenterazine, is tightly bound. Thus they can be regarded as luciferases containing a stable oxygenated reaction intermediate (Hastings and Gibson, 1963). Bioluminescence is triggered upon binding of Ca^{2+} which induces the oxidative decarboxylation of 2-hydroperoxycoelenterazine with generation of protein-bound coelenteramide in its excited state (Shimomura and Johnson, 1972; Cormier *et al.,* 1973). The excited coelenteramide relaxes to its ground state with the production of blue light with maxima around 465-495 nm depending on the type of photoprotein (Vysotski and Lee, 2004).

Because photoproteins are highly sensitive to detect calcium and harmless when injected into living cells, they have been widely used as probes of cellular Ca^{2+}, either to estimate the intracellular Ca^{2+} concentration under steady-state conditions or to study the role of calcium transients in the regulation of cellular function (Blinks *et al.*, 1982). The successful cloning of cDNAs encoding apo-photoproteins (Prasher *et al.,* 1985; Inouye *et al.,* 1985; Prasher *et al.,* 1987; Inouye and Tsuji, 1993; Fagan *et al.,* 1993; Illarionov *et al.,* 1995; Markova *et al,* 2002) has opened new avenues for utilizing photoproteins. By expressing the recombinant apo-photoprotein intracellularly and adding coelenterazine (CLZ) externally, cells with active photoprotein can be obtained (Knight *et al.,* 1991; Rizzuto *et al.,* 1992). Such cells have, in effect, a "build-in" calcium indicator. Major advantage of this approach is that it does not require robust procedures like microinjection or liposome-mediated transfer. However, the success of these applications depends on various factors among which are the rate and efficiency of the generation of active photoprotein from apo-photoprotein, coelenterazine, and oxygen, as well as any influence of the cellular environment on these processes.

During the past years, significant insight has been obtained into the ligand-dependent conformational states of the photoproteins and their mechanism of bioluminescence (Vysotski and Lee, 2004; Liu *et al.,* 2000; Liu *et al.,* 2003; Deng *et al.,* 2004; Deng *et al.,* 2005; Liu *et al.,* 2006; Vysotski and Lee, 2007; Tomilin *et al.,* 2008). At the same time much less is known about the molecular mechanism of formation of the

active photoprotein complex (Scheme 5.1). During the past years investigations focused primarily on the regeneration of wild-type apo-aequorin with coelenterazine derivatives as well as the effect of temperature, pH, incubation time and some additives on this process (Shimomura and Johnson, 1975; Inouye *et al.*, 1986; Shimomura *et al.*, 1993; Knight *et al.*, 1993). For example, it was shown that dithiothreitol (DTT) or -mercaptoethanol is required to reduce disulfide bonds in the recombinant apo-aequorin (Ohmiya *et al.*, 1993). Furthermore it was established that the binding of coelenterazine to apo-protein occurs within milliseconds (Eremeeva *et al.*, 2009), in contrast to the formation of active photoprotein complex (Shimomura and Johnson, 1975). This finding evidently showed that the rate-limiting step of active photoprotein formation is the conversion of coelenterazine into its peroxy derivative.

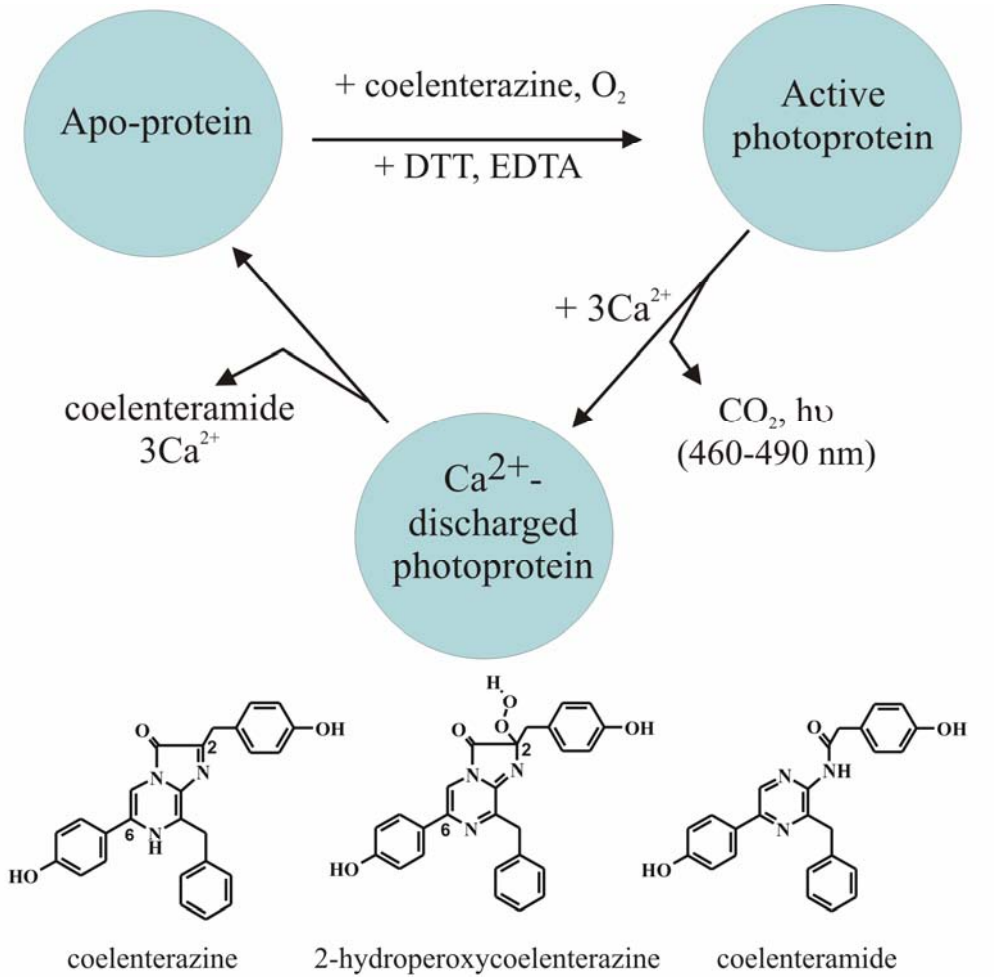

Scheme 5.1 Stages of the photoprotein bioluminescence reaction with corresponding coelenterazine forms.

Studies of the chemiluminescence reaction of imidazopyrazinones with molecular oxygen in basic aprotic solvents have given a plausible mechanism for formation of peroxy derivatives of imidazopyrazinones (Goto, 1968; Goto *et al.,* 1968; Kondo *et al.,* 2005). According to the suggested reaction mechanism, the first step involves deprotonation of the N7-nitrogen of imidazopyrazinone yielding the imidazopyrazinone C2 anion (Scheme 5.2). Then, single electron transfer (SET) from imidazopyrazinone anion to triplet oxygen affords the caged imidazopyrazinone superoxide anion biradical pair. The SET process requiring spin conversion is considered to be rate-limiting. Fast coupling of imidazopyrazinone radical and superoxide anion leads to the peroxide anion of imidazopyrazinone. In case of bioluminescent reactions catalyzed by luciferases subsequent cyclization of imidazopyrazinone peroxide anion takes place. The cyclization gives dioxetanone which decomposes with loss of carbon dioxide, generating the singlet excited state of a product (Kondo *et al.,* 2005). In essence, the mechanism of formation of 2-hydroperoxycoelenterazine during conversion of apo-photoprotein into photoprotein might be the same with one distinction: the coelenterazine peroxide anion resulting from biradical coupling must be quickly protonated to prevent cyclization into dioxetanone (Prendergast, 2000). A similar protonation of a peroxy adduct is operative in flavin-dependent aromatic hydroxylases (Entsch and van Berkel, 1995).

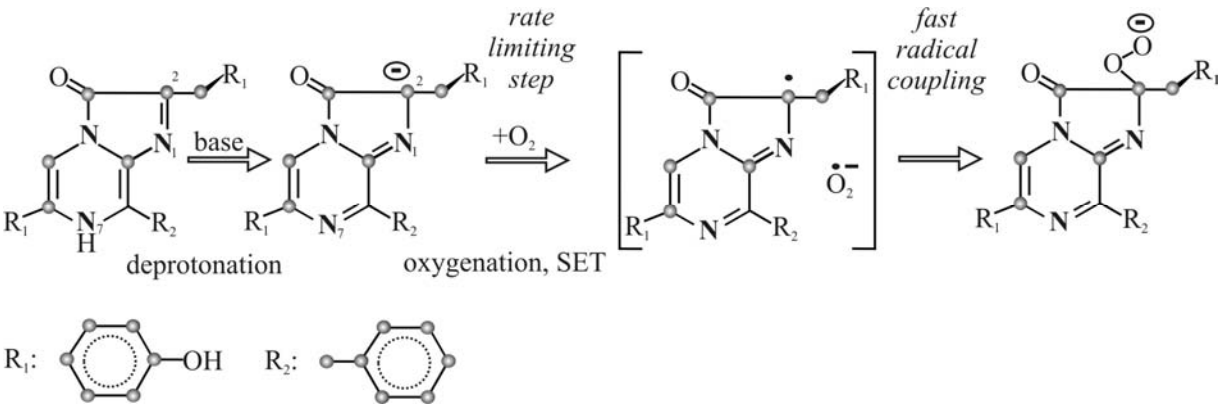

Scheme 5.2 Mechanism of formation of peroxy derivatives of imidazopyrazinones.

Next to the mechanism outlined above an alternative mechanism for the formation of 2-hydroperoxycoelenterazine might be considered. Cormier and co-authors studied the effect of pH and solvents on the spectral properties of coelenterazine analogs under

anaerobic conditions (Hori *et al.,* 1975). They found that the visible absorption spectrum of coelenterazine in aprotic solvent is red-shifted compared to methanol. The different absorption maxima were attributed to tautomeric forms of coelenterazine protonated at the N7 and C2 positions, respectively. Because the coelenterazine-binding cavities of photoproteins are formed by mostly hydrophobic amino acid side chains (Liu *et al.,* 2000; Liu *et al.,* 2003; Head *et al.,* 2000), we may assume that following binding coelenterazine undergoes tautomerization consistent with proton transfer from the N7 to the C2 position. Then this tautomeric form reacts with oxygen to yield 2-hydroperoxycoelenterazine which next is stabilized by hydrogen bonding with the hydroxyl group of tyrosine (Vysotski and Lee, 2004; Vysotski and Lee, 2007).

In this chapter, we have explored both pathways by quantum chemical calculations to discriminate the most reliable one. Insight into the electronic mechanisms can provide detailed information about electronic properties and energies of unstable intermediates and transition states which may serve as an essential and complementary tool to interpret the experiment. Next, the possible role of hydrogen bonding is addressed by using simple model complexes to grasp some important aspects that may affect the electronic mechanism operating within the coelenterazine-binding site during the formation of active photoprotein. To verify the conclusions arising from quantum chemical calculations some experimental studies of active photoprotein complex formation have been carried out as well. Based on theoretical calculations and experimental results, a plausible mechanism of coelenterazine peroxy adduct formation within the apo-photoprotein globule is proposed. Furthermore, functions of key residues within the coelenterazine-binding cavity are highlighted.

Materials and Methods

Apo-photoprotein preparation - Apo-obelin and its mutants were expressed and purified as previously reported (Illarionov *et al.,* 2000; Eremeeva *et al.,* 2009). The apo-photoproteins obtained after extraction with 6 M urea and purification on a DEAE-Sepharose Fast Flow column, were concentrated by Amicon Ultra Centrifugal Filters (Millipore). To fold apo-proteins, the concentrated samples containing 6 M urea were diluted approximately 20-fold with a solution containing 1 mM EDTA, 20 mM Tris-HCl pH 7.0, again concentrated, and then "washed" several times with the same buffer to remove any impurities of urea and salts. The apo-photoproteins (~1 mg/mL) were 0.5 mL-aliquoted into plastic tubes and frozen at -80^{o}C. All the experiments were carried out with freshly thawed samples. Thawed samples were centrifuged (20,000 g × 10 min) at 4 ^{o}C, incubated overnight with 10 mM DTT, again centrifuged, and then passed through a Superdex 200 column (Amersham Bioscience) equilibrated with freshly prepared 10 mM DTT, 5 mM EDTA, 20 mM Tris-HCl pH 7.0 to produce monomeric apo-photoprotein containing no disulfide bonds and aggregates (Eremeeva *et al.,* 2009). The final preparations of apo-photoproteins were homogeneous according to SDS-PAGE and gel filtration. The apo-obelin (and apo-H175N) and apo-Y138F concentrations were determined using $_{280\ nm}$ = 40450 and 38960 $M^{-1}cm^{-1}$, respectively as calculated with the ProtParam tool (http://us.expasy.org/tools/ protparam-doc.html) which uses Edelhoch's method (Edelhoch, 1967).

Bioluminescence measurements - Light emission was measured with a luminometer equipped with neutral-density filters with different transmission coefficients to extend the dynamic range. The bioluminescence was triggered by forceful injection of 10 L of photoprotein solution into 490 L solution of 10 mM $CaCl_2$, 100 mM Tris-HCl pH 8.8. The measurements were carried out at 20 °C.

Kinetics of apo-photoprotein charging with coelenterazine - Activation kinetics were studied using 50 nM apo-photoprotein and 750 nM coelenterazine in air-saturated 5 mM EDTA, 10 mM DTT, 20 mM Tris-HCl pH 6.5 buffer. Coelenterazine was added from a concentrated stock solution in methanol. To eliminate any effect of methanol on apo-

photoprotein activation, the methanol concentration in activation buffer never exceeded 1% (v/v). The coelenterazine concentration in the methanol stock solution was determined spectrophotometrically using the molar absorption coefficient $_{435\ nm}$ = 9800 $M^{-1}cm^{-1}$ in methanol (Shimomura, 2006). To monitor the activation kinetics, a 10- L aliquot of the mixture containing apo-photoprotein and coelenterazine was taken from the activation solution and injected into the cuvette of the luminometer as described above. To study the apo-obelin activation kinetics against temperature the mixtures containing apo-photoprotein and coelenterazine were incubated at constant temperature while aliquots were taken for bioluminescent measurements. The solutions before mixing with coelenterazine were pre-equilibrated at the appropriate temperature for 10 min in advance. The oxygen concentrations in activation buffers at different temperatures were calculated using Henry's equation at 0.97 atm atmospheric pressure. Henry's law constants for oxygen in water at different temperatures were taken from http://www.henrys-law.org. No corrections were made for the effect of ionic strength on oxygen solubility since in experiments low ionic strength buffer was used.

Calculations - To investigate the reaction mechanism of obelin activation, we performed Perdew-Burke-Ernzerhof (PBE) (Perdew *et al.*, 1996) and Parameterization Method 3 (PM3) (Stewart, 1989; Stewart, 2004) calculations using the VASP (the Vienna Ab initio simulation package) (Kresse and Hafner, 1993; Kresse and Hafner, 1994; Kresse and Furthmüller, 1996) and HyperChem-7.52 software packages *(www.hyper.com),* respectively. Stationary points on potential-energy surfaces were located by the energy gradient techniques. Restricted open-shell Hartree-Fock (ROHF) PM3 calculations were used for reactants containing oxygen molecule in triplet state. During the course of the reaction, however, ROHF molecular orbitals (MOs) should be reorganized restricted (RHF PM3) MOs via transition state because products have closed-shell MOs. Restricted density functional theory (R)DFT or RHF PM3 calculations were performed for the closed-shell reactants and products. Reaction pathways for generation of coelenterazine anion, coelenterazine protonated at C2 and 2-hydroperoxycoelenterazine were calculated using PM3 by the quadratic synchronous transit method (Baker, 1986; Peng and Schlegel, 1993).

To determine the transition states and potential barriers for hydrogen hopping yielding coelenterazine protonated at C2, we used a nudged elastic band method (Henkelman ***et al.***, 2000). The reaction pathways were sampled in 10 points from initial to final states. To calculate atomic and electronic structures we used DFT theory (Hohenberg and Kohn, 1964; Kohn and Sham, 1965) within PBE generalized gradient approximation for the exchange–correlation potential and plane wave basis set. The electron–ion interaction was taken into account via ultrasoft Vanderbilt-type pseudopotential formalism (Vanderbilt, 1990) with E_{cutoff} energies equal to 296 eV. To perform electronic structure calculations the VASP code was employed. The size of 3D cell containing coelenterazine was equal to 26 × 26 × 26 Å and vacuum interval between the molecules in neighbor cells was about 10 Å. All calculations were performed for Γ-point. Geometry optimizations were carried out until the forces acting on all atoms became lower than 0.001 eV/Å while applying a 1×10^{-4} eV threshold as self-consistency energy criterion during the individual electronic structure calculations. All values given above were carefully tested and found optimal.

Studying of atomic and electronic structures was carried out at the semi empirical and first-principles level of theory. All semi empirical calculations were performed using the PM3 and the Parameterization Method 6 (PM6) by MOPAC2007 program (Stewart, 2007). Compared to the same semi empirical methods, the PM3 and PM6 are significantly improved for H-, C-, N-, O-containing molecules; they have been demonstrated to be extremely suitable for atomic structures of large organic compounds and biomolecules (Stewart, 2007).

The excitation energies of the optimized geometries were evaluated by semi empirical PM3 and CI approach. The electronic wave functions are of configuration interaction type, with molecular orbitals obtained in a self-consistent field (SCF) calculation with fractional occupation numbers. The ground states of geometry of all structures were optimized using the correlation interaction single exciting method (CIS) by MOPAC2007 and HyperChem-7.52 packages and next step single-point CI calculations for obtaining the exciting energies by HyperChem-7.52. CI calculations were carried out to consider electron correlation. All single excitations from the 10 highest occupied molecular orbitals to the 6 lowest virtual orbitals were included in the configuration

interaction. Applying this strategy at the PM3 CIS level of theory for a number of conjugated systems resulted in excitation energies, which agreed reasonably well with experimental data and high-level ***ab initio*** calculations. To take into account the solvation effects three isomeric forms of coelenterazine were surrounded by 10 molecules of solvent (DMSO or methanol) and geometries of these complexes were calculated by PM3. The excitation energies of the optimized geometries were obtained for coelenterazines using semiempirical PM3 and CI approaches.

The equilibrium structure on ***ab initio*** level of theory was found by using Hartree-Fock (HF) and hybrid DFT by the GAMESS package (Schmidt ***et al.***, 1993). DFT calculations were performed with Becke's hybrid exchange functional B3 and the correlation functional of Lee, Yang, and Parr (LYP) (Becke, 1993; Lee ***et al.***, 1988). The GAMESS program was also used for second-order Møller-Plesset perturbation calculations (MP2). These calculations were performed in both the gas phase and DMSO or methanol solution. To mimic the DMSO or methanol environment, a polarized continuum model (PCM) was used to take into account the solvation effects (Miertus ***et al.***, 1981; Miertus and Tomasi, 1982; Cossi ***et al.***, 1996; Barone ***et al.***, 1997). The dielectric constants of DMSO (46.70) and methanol (32.63) were applied. The structures were calculated by PCM HF/6-31(d) and PCM DFT B3LYP/6-31(d) by the GAMESS program.

The excited-state energy predictions by high-level theory were carried out using the rigorous time-dependent hybrid DFT scheme implemented in the GAMESS package (Gross and Kohn, 1990; Casida and Chong, 1995). The ground state geometry of all structures were optimized using DFT B3LYP/6-31(d) method. We considered the solvent effect in order to predict excited-state energy in solution. The polarized continuum model (PCM) with DMSO or methanol solvent optimized the geometries of all isomeric forms by the DFT B3LYP/6-31(d) method and single-point calculations by PCM TDDFT/6-31(d).

Results and Discussion

Kinetics of active obelin complex formation - Recombinant apo-photoproteins can be converted to the active photoproteins by incubating with coelenterazine under calcium-free conditions in the presence of oxygen and reducing agents like DTT or -mercaptoethanol (Shimomura and Johnson, 1975). It was proposed that the reducing agent is needed to prevent the formation of disulfide bonds in recombinant apo-photoproteins which might lead to conformational constraints hindering coelenterazine binding (Ohmiya *et al.*, 1993). The thiol-reducing agents are not strictly required for formation of active photoprotein because an aequorin mutant, in which all three cysteines were replaced with serine is converted into active photoprotein in the absence of these agents (Kurose *et al.*, 1989; Lewis *et al.*, 2000).

We found that at 20 ^{o}C the concentration of active obelin reaches a maximum after 15 min (Fig. 5.1, left panel), instead of several hours as reported before (Shimomura and Johnson, 1975). This essential shortening in activation time is conditioned by the method of apo-protein preparation. In our studies, the apo-obelin was pre-incubated with DTT overnight and then its monomeric form was isolated by gel filtration on a Superdex 200

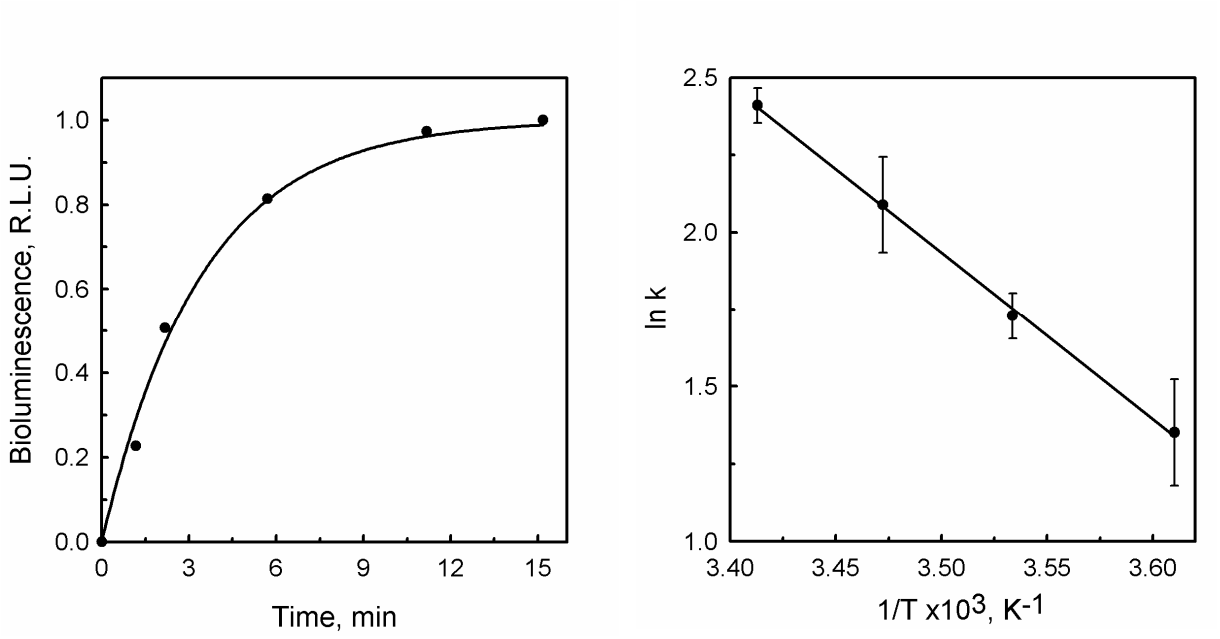

Figure 5.1 Kinetics of activation of monomeric apo-obelin by coelenterazine at 20 ^{o}C monitored by bioluminescence (left panel). Arrhenius plot of photoprotein activation over a 4 to 20 ^{o}C temperature range (right panel). Experimental errors were estimated from the standard deviation determined from the average of three trials performed with a single apo-obelin monomer preparation.

column. This procedure allows the removal of apo-photoprotein aggregates (Masuda *et al.*, 2003) that are responsible for the slow kinetics of apo-photoprotein activation. It should be noticed that the pre-incubation with DTT has no noticeable effect on the rate of apo-obelin activation.

Since coelenterazine binding with apo-photoproteins takes only milliseconds (Eremeeva *et al.*, 2009), the rate-limiting step in formation of active photoprotein complex appears to be some step in the pathway of conversion of bound coelenterazine into its 2-hydroperoxy derivative. The simplest kinetic scheme describing the formation of active photoprotein includes two steps:

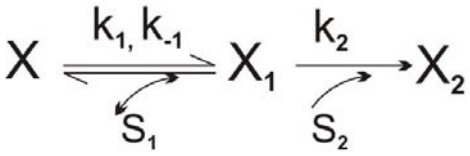

where S_1, coelenterazine; S_2, molecular oxygen; X, apo-photoprotein; X_1, complex of apo-photoprotein with coelenterazine; X_2, active photoprotein; k_1, k_{-1} and k_2, reaction rate constants. The first step corresponds to the formation of apo-photoprotein complex with coelenterazine which is very fast taking only milliseconds (Eremeeva *et al.*, 2009). The second step is the conversion of bound coelenterazine into 2-hydroperoxycoelenterazine; this process takes minutes (Fig. 5.1).

We do not consider reverse processes (k_{-1}, and k_{-2}) because: (i) dissociation of coelenterazine from its complex with apo-photoprotein has not been observed and (ii) 2-hydroperoxycoelenterazine formation is irreversible. We also do not include formation of the intermediate binary XS_2 and ternary XS_1S_2 complexes in the scheme because in the three-dimensional structures of photoproteins (Liu *et al.*, 2000; Liu *et al.*, 2003; Deng *et al.*, 2004; Deng *et al.*, 2005; Liu *et al.*, 2006) no specific binding site for molecular oxygen has been observed. Furthermore, reaction of the anaerobic apo-obelin coelenterazine complex with oxygen follows no bimolecular kinetics (Chapter 4). With the constraints that the concentrations of substrates are much higher than the concentration of apo-photoprotein (i.e. S_1 and $S_2 >> X$) and $k_1S_1 >> k_2S_2$, active photoprotein complex formation can be described by the following equation:

$$X_2(t) = X \cdot (1 - e^{-k_2 S_2 t}) \tag{5.1}$$

where X_2 is a concentration of active photoprotein, X is the initial concentration of apo-photoprotein and S_2 is the initial concentration of molecular oxygen. Using this equation and kinetic data of apo-obelin activation (Fig. 5.1, left panel) the apparent rate constant of active obelin formation (k_2) was evaluated to be 11.0 ± 0.4 $M^{-1}s^{-1}$ at 20 ºC and pH 6.5. It should be noted that the equation for $X_2(t)$ at $k_1 S_1 >> k_2 S_2$ corresponds to the equation describing an irreversible bimolecular chemical reaction. Thus, in effect, the formation of 2-hydroperoxycoelenterazine might be considered as a chemical reaction of coelenterazine with molecular oxygen occurring in a protein environment.

Determination of the apparent rate constants for active obelin formation over a 4 to 20 ºC temperature range allowed us to calculate the activation energy (E_a = 45.0 kJ mol^{-1}) (Fig. 5.1, right panel) and estimate the enthalpy of activation (ΔH = 42.6 kJ mol^{-1}) at 20 ºC.

Formation of 2-hydroperoxycoelenterazine through imidazopyrazinone anion generation - According to Scheme 5.2 the first step of 2-hydroperoxycoelenterazine formation is the generation of imidazopyrazinone anion CLZ(7^-) through deprotonation of N7-nitrogen of coelenterazine. Theoretically, deprotonation of coelenterazine might proceed by three different ways including either direct deprotonation, or with assistance of a base – OH(-) or amino acid side chain (e.g. histidine) which might function as a base.

Direct deprotonation of coelenterazine seems unlikely because of the high activation energy barrier (430 kJ mol^{-1}) (Fig. 5.2). In case of OH(-) or His(-) assistance, E_a of coelenterazine deprotonation becomes essentially lower and equals to 56 kJ mol^{-1} and 11 kJ mol^{-1}, respectively. The E_a values calculated for the reactions with OH(-) and His(-) compare favorably to typical biological processes. It should be noted that the products of these reactions are more stable than the initial reactants. Because the appearance of OH(-) during active photoprotein formation is hardly feasible, we can reasonably conclude that deprotonation of coelenterazine within the photoprotein cavity most probably takes place with the assistance of His(-).

Deprotonation of coelenterazine at N7 with subsequent formation of CLZ(7^-) results in the fast rearrangement of bonds yielding the coelenterazine ionized at C2. The calculated

energy barrier is only 1.5 kJ mol^{-1}. C2 is the only potential position for charge to be transferred since nitrogen has a lone-electron pair.

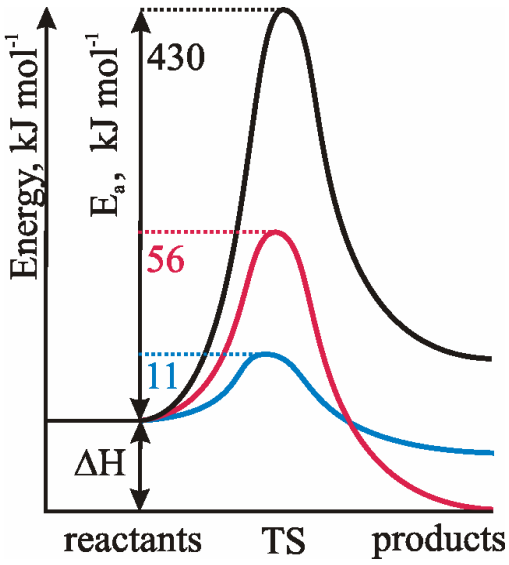

Figure 5.2 Energy reaction profile of coelenterazine anion (7^-) generation. E_a, activation energy barriers; TS, transition state. Black line, direct CLZ deprotonation; red line, CLZ deprotonation with assistance of OH(-) yielding CLZ(7^-) and H_2O; blue line, CLZ deprotonation with assistance of His(-) yielding CLZ(7^-) and His. The activation energies were calculated using PM3 by quadratic synchronous transit method.

Next, modeling of the reaction of dioxygen addition to CLZ(-) was carried out. When the dioxygen molecule is placed close to ionized C2 the geometry optimization of the system immediately leads to the generation of coelenteramide and CO_2, escaping 2-hydroperoxycoelenterazine formation. In other words, oxygen binding results in the formation of peroxycoelenterazine anion followed by fast cyclization. It leads to C3-N4 bond opening yielding dioxetanone (Fig. 5.3A). Thus, in fact, we observe the chemiluminescent reaction presented in Scheme 5.1.

Calculations for the reaction of 2-hydroperoxycoelenterazine formation were carried out in the presence of Tyr or His placed at distances from C2-carbon of coelenterazine corresponding to those in the obelin crystal structure for His175 and Tyr190 (PDB code 1QV0) (Fig. 5.3B). Furthermore, all these calculations were performed with and without the presence of a water molecule placed near N1 of coelenterazine to examine the influence of any polar molecule. In the presence of Tyr or His side chains, which have been suggested to participate in stabilization of the peroxide group (Vysotski and Lee, 2004;

Vysotski and Lee, 2007), optimization of intermediate geometries only resulted in dioxetanone formation (Fig. 5.3B). Thus, it can be concluded that no proton of His175 or Tyr190 is transferred to the distal oxygen of the adduct in order to stabilize 2-hydroperoxycoelenterazine formation. Therefore, 2-hydroperoxycoelenterazine formation in obelin is unlikely to proceed through the peroxy anion intermediate as it would lead to chemiluminescence reaction with production of coelenteramide and carbon dioxide missing the 2-hydroperoxycoelenterazine state.

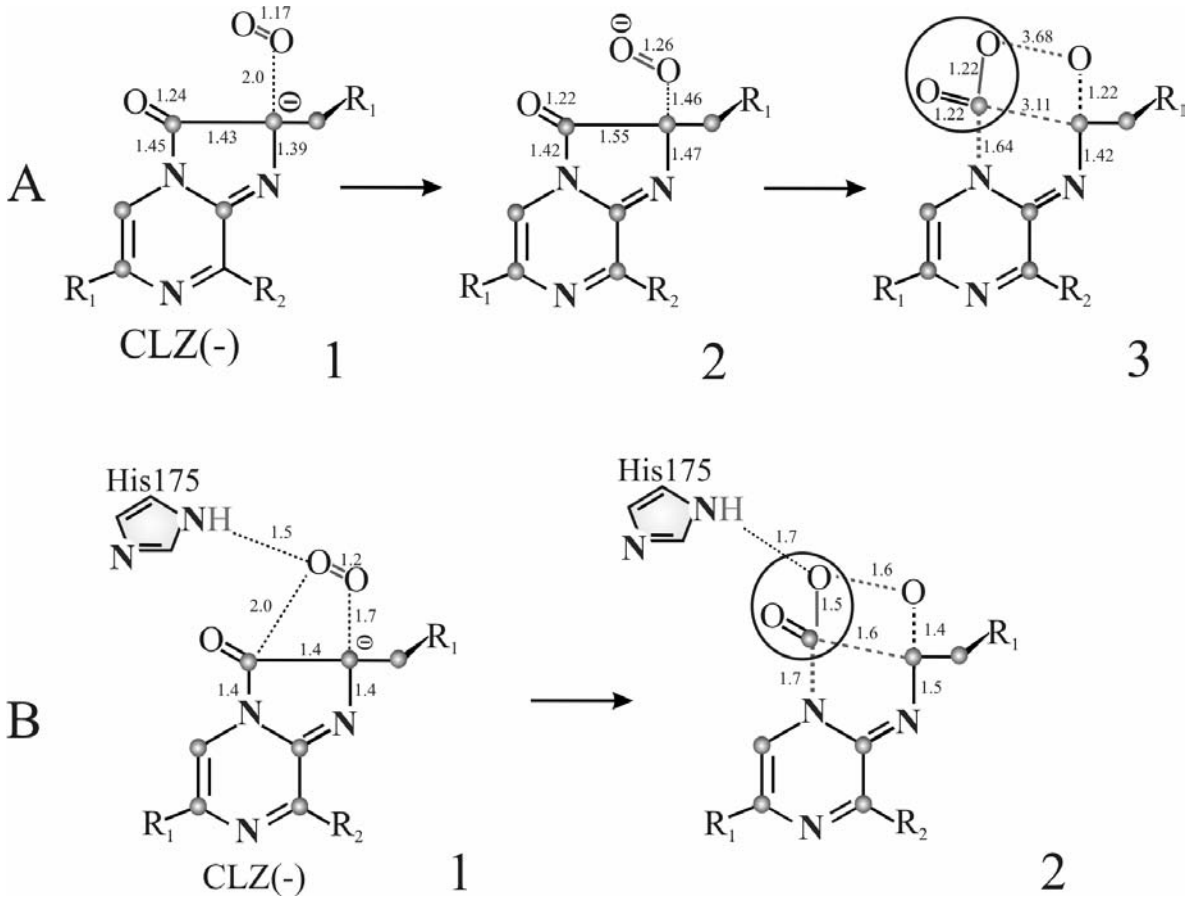

Figure 5.3 Modeling of interactions between coelenterazine anion (CLZ(–)) and oxygen molecule by the PM3 method: (A) reaction between CLZ(–) and oxygen molecule; (B) reaction between CLZ(–) and oxygen molecule in the presence of His175. A1 and B1, initial positions for the optimization processes, where oxygen is in triplet state; A2, final position, where oxygen is in triplet state; A3 and B2, final structures after the geometry optimization processes, where oxygen is in singlet state.

The results of our calculations are in good agreement with experimental observations that the chemiluminescence reaction of coelenterazine in solution with the assistance of base proceeds much faster than without it (Goto *et al.*, 1968; Kondo *et al.*,

2005). The activation energy barrier calculated for generation of imidazopyrazinone anion with the assistance of base is only 56 kJ mol^{-1} and therefore could be easy overcome.

Formation of 2-hydroperoxycoelenterazine from coelenterazine protonated at C2-carbon - At present, several three-dimensional structures of obelin-ligand complexes have been solved, but the structure of apo-obelin remains unknown. We believe that apo-obelin loses conformational freedom upon binding with coelenterazine and that the conformation of this complex does not change considerably upon activation with oxygen (Chapter 4). This assumption seems reasonable because the hydroperoxy derivative becomes stabilized through hydrogen bonding with surrounding residues (Vysotski and Lee, 2004). Thus, for modeling the protein environment during 2-hydroperoxycoelenterazine formation we used the amino acid residue positions observed in the crystal structure of active obelin (Liu ***et al.,*** 2000; Liu ***et al.,*** 2003).

Optimization of the geometry of coelenterazines protonated at N7 and C2 (CLZ(7H) and CLZ(2H)) with an amino acid environment corresponding to that of active obelin (Liu ***et al.,*** 2000; Liu ***et al.,*** 2003) was carried out with the DFT B3LYP/6-31(p,d) method. The calculations were performed for an amino acid cluster consisting of residues at a distance of about 4 Å from each atom of the 2-hydroperoxycoelenterazine molecule. Residues included were His22, Met25, Phe28, Leu29, Lys45, Ala46, Asp49, Ile50, Cys51, Lys53, Leu54, His64, Phe72, Phe88, Trp92, Trp114, Gly115, Val118, Phe122, Trp135, Ser142, Gly143, Ile144, Met171, Thr172, His175, Trp179 and Tyr190 (overall, about 500 atoms including one water molecule).

In case of CLZ(7H) our attempts were unsuccessful because the geometry optimization always resulted in breaking of the coelenterazine molecule. The non-optimal geometry resulted from a lack of space for one of the phenolic moieties of coelenterazine due to steric hindrance of the His175 and Trp135 side chains (Fig. 5.4, left panel) and because the C2-carbon which is in ***sp2*** configuration cannot change the bond angle between the phenol and imidazopyrazinone rings in order to fit in the available space. It is also supported by the fact that the linker CH_2 group connecting the phenol and imidazopyrazinone is essential for photoprotein activity (Qi ***et al.,*** 1991). In contrast, when we optimized the CLZ(2H) molecule under the same conditions, a stable molecular

structure was obtained (Fig. 5.4, right panel). Since C2 is in *sp3* configuration, the angle between the phenol and imidazopyrazinone rings might bend from planar geometry thereby enabling its fitting within the substrate-binding cavity.

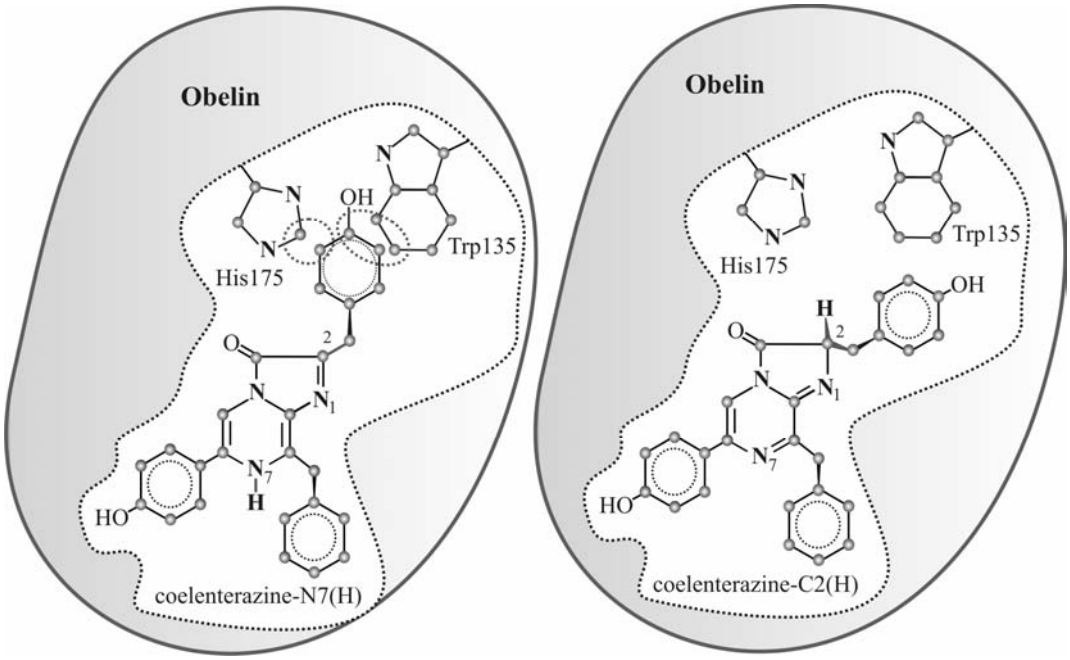

Figure 5.4 Initial positions for the geometry optimization of coelenterazine protonated at either N7 or C2 embedded in the coelenterazine-binding cavity with amino acid environment corresponding to that of active obelin (PDB code 1QV0).

Figure 5.5 summarizes the energy reaction scheme of 2-hydroperoxycoelenterazine formation from coelenterazine protonated at C2-carbon. This process can be described as a one-stage reaction with generation of an intermediate state when the C2 proton of coelenterazine transfers to oxygen followed by 2-hydroperoxycoelenterazine formation. The activation barrier of the reaction is calculated to be 68 kJ mol^{-1}, enthalpy – 60 kJ mol^{-1}. These values are in a good agreement with those determined from experimental kinetic data (E_a – 45.0 kJ mol^{-1}, enthalpy – 42.6 kJ mol^{-1} at 20 ºC).

Tautomeric forms of coelenterazine - The mechanism described above raises the question how coelenterazine protonated at C2-carbon might be formed upon binding with obelin. Theoretically coelenterazine can exist in three tautomeric forms: protonated at N7 (CLZ(7H)), N1 (CLZ(1H)), or C2 (CLZ(2H)) (Fig. 5.6).

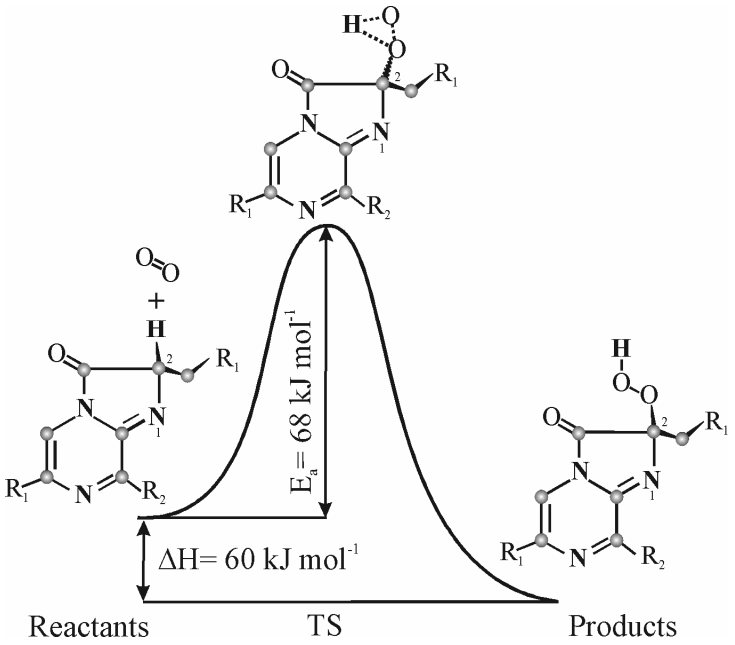

Figure 5.5 Energy reaction scheme of 2-hydroperoxycoelenterazine formation from CLZ(2H) and dioxygen. E_a, activation energy barrier; TS, transition state. Reactants and TS are in triplet state, product is in singlet state. The activation energy is calculated using PM3 by quadratic synchronous transit method.

CLZ(2H) has an angle between the R1 moiety and the imidazopyrazinone ring equal to 120^o, whereas for coelenterazine protonated at N7 or N1 the angle is 180^o, i.e. the bond lies in the same plane as the imidazopyrazinone ring. Thus, the appearance of hydrogen at C2 results in alteration of its configuration ($sp^2 \rightarrow sp^3$) followed by changing of bond length and angles. The geometry difference between the CLZ(7H) and CLZ(1H) structures is considered to be minor because the change of hydrogen position leads only to rearrangement of electron density between the coelenterazine atoms.

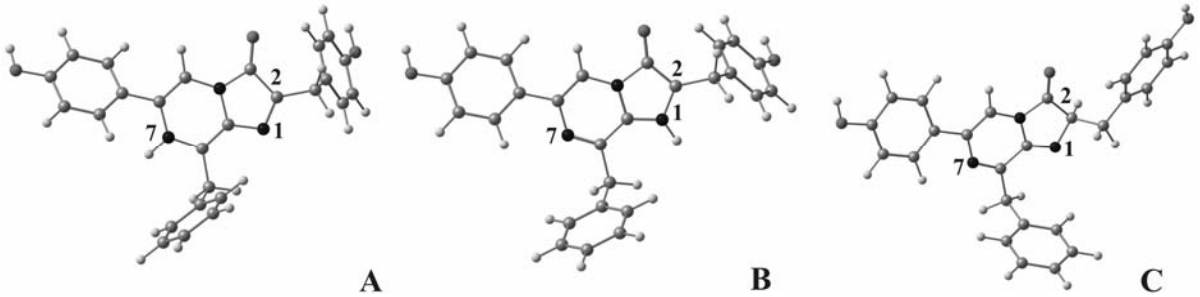

Figure 5.6 Structures of coelenterazine molecules protonated at N7, N1 or C2 optimized in vacuum. (A) CLZ(7H); (B) CLZ(1H); (C) CLZ(2H).

We have calculated structures of all three tautomeric forms of coelenterazine under different conditions: in vacuum, in methanol, and in DMSO. Influence of solvents has been calculated with both direct and indirect methods. For direct calculations, coelenterazine was surrounded by 10 molecules of solvent (semiempirical PM3 and PM6 methods). Indirect solvent effect computations were performed using the PCM by *ab initio* HF/6-31(d) and DFT-B3LYP/6-31(d) methods.

As mentioned above, Cormier and co-workers investigated the effect of pH and solvents on the spectral properties of coelenterazine and its analogs under anaerobic conditions (Hori *et al.,* 1975). They found that the absorption spectrum of coelenterazine in DMF is red-shifted (454 nm) compared to methanol (435 nm). The different absorption maxima were attributed to tautomeric forms of coelenterazine protonated at C2 and N7, respectively.

Taking in mind Cormier's supposition we calculated the absorption maxima of coelenterazine tautomers in vacuum, methanol and DMSO using the TD procedure on the basis of DFT-B3LYP/6-31(d) geometry (Table 5.1). Since TDDFT is a very powerful tool for the calculation of absorption spectra of finite systems, it has become a popular method to solve this kind of problems in quantum chemistry. However, the accuracy of the TDDFT method was shown to be out of the required accuracy for photobiology, so TDDFT could be useless for clarifying the underlying principle behind the photobiological phenomena (Nakatani *et al.*, 2007; Casida *et al.*, 1998; Casida and Salahub, 2000; Appel *et al.*, 2003; Hsu *et al.*, 2001; Dreuw *et al.*, 2003; Milet *et al.*, 1999; Fujimoto *et al.*, 2007).

Table 5.1 Absorption maxima of coelenterazine tautomers in vacuum, methanol and DMSO calculated by TDDFT-B3LYP/6-31(d) and PM3-CI geometries

	TDDFT			PM3-CI		
	vacuum	methanol	DMSO	vacuum	methanol	DMSO
CLZ(7H)	450 nm	435 nm	437 nm	475 nm	499 nm	540 nm
CLZ(1H)	470 nm	435 nm	434 nm	440 nm	433 nm	430 nm
CLZ(2H)	440 nm	442 nm	444 nm	363 nm	362 nm	369 nm

Our calculations based on the indirect PCM model (TDDFT-B3LYP method) did not reveal differences between the absorption maxima in both solvents, most likely because

methanol and DMSO possess similar polarization properties (Table 5.1). In principle results of our TDDFT calculations could be well explained by Cormier's supposition since the absorption maximum of CLZ(2H) is red-shifted (443 nm) with respect to CLZ(7H) and CLZ(1H) which are both calculated to be 435 nm.

We also calculated the absorption maxima of coelenterazine tautomeric forms in vacuum using the CI procedure on the basis of semiempirical PM3-CI geometry with 10 occupied and 6 vacant orbitals. This procedure allows taking into account the electronic correlations and therefore is believed to be more reliable for this type of calculations. Moreover, PM3 method includes van der Waals and hydrogen bonds as parameters; hence, it is more accurate for calculations of our system of interest. The absorption maximum of CLZ(2H) is calculated to be 363 nm (Table 5.1). This means that we can exclude the CLZ(2H) structure from our considerations since the calculated absorption maximum dramatically differs from the experimental one. The absorption maximum of the CLZ(1H) is calculated to be 440 nm in vacuum, the one of CLZ(7H) is red-shifted to 475 nm. The same pattern is shown for methanol and DMSO (Table 5.1). Thus we can conclude that coelenterazine is present as CLZ(1H) in methanol and CLZ(7H) in DMSO or DMF. Thus, proton exchange given by protic solvents such as methanol or water provides the transition from CLZ(7H) to the CLZ(1H) form.

Both PM3 and PM6 methods show CLZ(1H) to be more preferable than CLZ(7H) because the energy of CLZ(1H) is calculated to be lower than that of CLZ(7H). N(7)-H and N(1)-H bonds are energetically similar, therefore transition from CLZ(7H) to the CLZ(1H) form seems plausible. On the contrary, C-H bond essentially differs from N-H bond in terms of energy, hence the transition from CLZ(7H) to the CLZ(2H) form in protic solvent is considered to be hardly probable.

Formation of coelenterazine protonated at C2-carbon - In fact, formation of CLZ(2H) via tautomerization can involve several pathways. Three of them are summarized in Figure 5.7.

Hydrogen from N7-nitrogen of coelenterazine can be transferred to C2-carbon via C8-carbon followed by transfer to C9-carbon and then to N1-nitrogen (Fig. 5.7A). This reaction pathway was calculated using both PM3 by HyperChem 7.52 package and DFT by VASP. The first energy barrier equals to 250 kJ mol^{-1} resulting from the breaking of the

N7-H bond. The second pathway (Fig. 5.7B) involves a hydrogen transfer to C2-carbon from N7-nitrogen via C9-carbon of coelenterazine. Calculations performed using PM3 by HyperChem showed two reaction barriers of 120 kJ mol^{-1} and 195 kJ mol^{-1}, respectively. Formation of CLZ(2H) can proceed not only from CLZ(7H) but from CLZ(1H) as well (Fig. 5.7C). Energy barriers were calculated to be 220 kJ mol^{-1} and 180 kJ mol^{-1} in the case of using the PM3 or DFT method, respectively.

Thus, all three reaction pathways described above seem rather unlikely because of high energy barriers. Therefore, formation of CLZ(2H) through tautomerization or with involvement of any extraneous molecules is hardly feasible. This suggests that CLZ(2H) can be generated only while coelenterazine is captured by apo-obelin, apparently with assistance of some His side chain acting as a base at neutral pH. Catalytic mechanisms, involving His as a proton shuttle and Asp or Glu as a general acid, have been proposed for several oxygenases, for example, dioxygenases from *Arthrobacter nitroguajacolicus* and *Pseudomonas putida*, and *Renilla* luciferase (Prokop *et al.*, 2003; Steiner *et al.*, 2010).

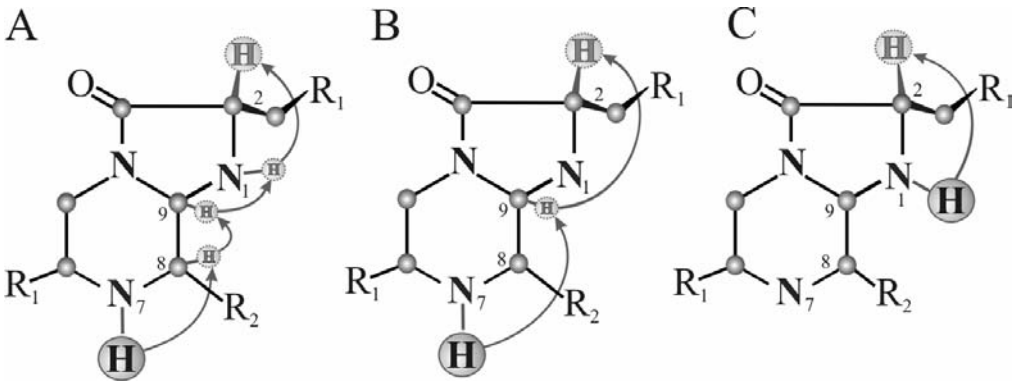

Figure 5.7 Modeling of proton transfer in coelenterazine from N7-nitrogen to C2-carbon yielding CLZ(2H). (A) four stage process, (B) two stage process, (C) one stage process. Calculations were performed by DFT and PM3 methods.

We carried out calculations considering that coelenterazine protonated at C2-carbon is formed from imidazopyrazinone anion CLZ(-) (Fig. 5.8). Formation of CLZ(2H) from CLZ(-) might proceed by four different pathways: (i) direct protonation: CLZ(-) + H(+) → CLZ(2H), (ii) with assistance of a water molecule: CLZ(-) + H_2O → CLZ(2H) + OH(-), (iii) with assistance of His in neutral state: CLZ(-) + His → CLZ(2H) + His(-), or (iv) with assistance of protonated His: CLZ(-) + His(+) → CLZ(2H) + His. The first three pathways

seem unlikely because of high activation energy barriers of 265 kJ mol^{-1}, 120 kJ mol^{-1}, and 340 kJ mol^{-1}, respectively (Fig. 5.8).

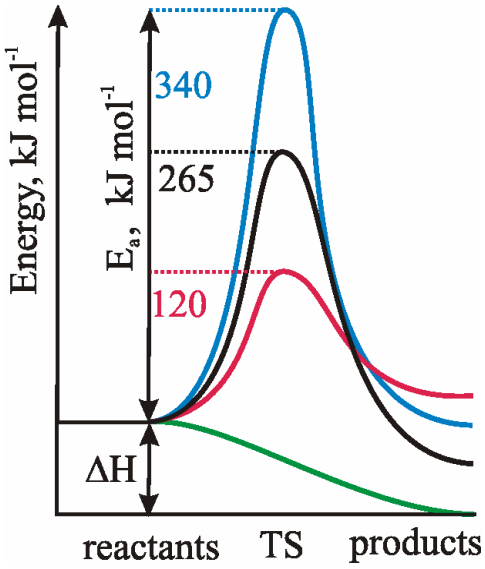

Figure 5.8 Energy reaction profile of CLZ(2H) generation from coelenterazine anion. E_a, activation energy barriers; TS, transition state. Black line, reaction between CLZ(-) and H(+) yielding CLZ(2H); red line, reaction between CLZ(-) and H_2O yielding CLZ(2H) and OH(-); blue line, reaction between CLZ(-) and His yielding CLZ(2H) and His(-); green line, reaction between CLZ(-) and His(+) yielding CLZ(2H) and His. The activation energies were calculated using PM3 by the quadratic synchronous transit method.

Generation of CLZ(2H) with the assistance of His(+) proceeds without energy barrier and represents the most reliable pathway. According to the obelin crystal structure, the best candidate for transferring the proton from N7 to C2-carbon is His175 (Fig. 5.9).

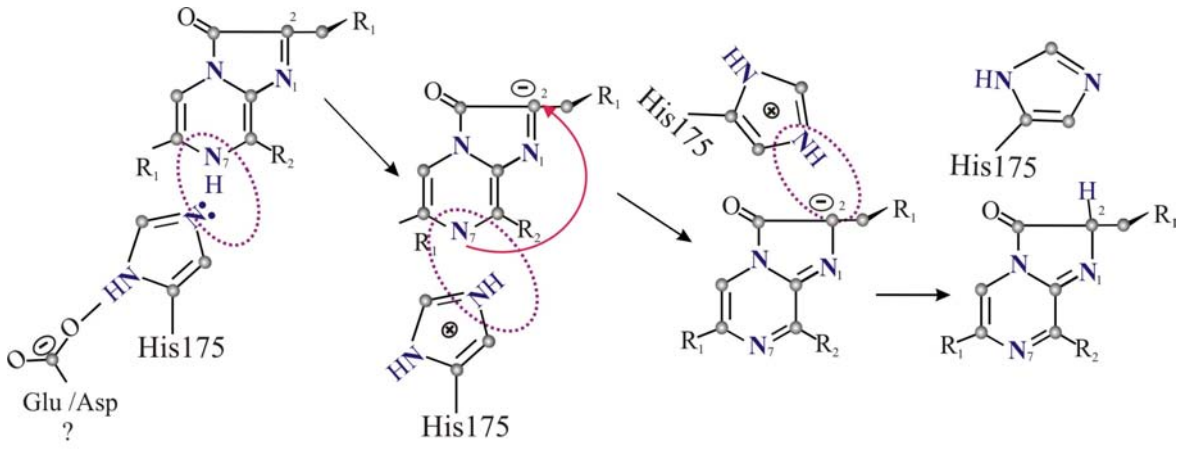

Figure 5.9 Tentative scheme of His175 operation in transferring the proton from N7-nitrogen to C2-carbon of coelenterazine within the substrate binding cavity of obelin.

Substitutions of His175 to residues with different side chain properties (Gln, Asn, Ala, Glu, Asp, Arg, Lys, Phe) revealed either extremely low or no bioluminescence activity (Eremeeva ***et al.***, 2007). For one of the His175 variants, H175N, we estimated the apparent dissociation constant for the apo-photoprotein–coelenterazine complex. The determined value (K_d = 0.15 ± 0.01 M) corresponds to the apparent dissociation constant of the wild type complex (K_d = 0.2 ± 0.04 M) (Eremeeva ***et al.***, 2009), indicating relatively strong binding. However, in case of H175N, bound coelenterazine is easily removed from the complex during Mono Q anion exchange chromatography. Consequently, H175N is eluted from the Mono Q column in the apo-protein form with minor amount of active obelin and coelenterazine remaining bound to the column. This observation can be explained with the results of quantum chemical calculations showing that the ultimate coelenterazine-binding pocket can be formed only after coelenterazine protonation at C2-carbon has taken place. Thus, H175N mutant properties and quantum chemical calculations of the coelenterazine-binding pocket geometry confirm that His175 could act as a proton shuttle participating in the formation of coelenterazine protonated at carbon C2.

Activation of bound coelenterazine protonated at C2-carbon by oxygen - Above, we discussed the possible mechanisms of 2-hydroperoxycoelenterazine formation in the coelenterazine-binding cavity of photoproteins and the thermodynamic properties of this process. However, one of the most intriguing questions is how the activation of coelenterazine by oxygen takes place.

In order to reveal what the driving force of 2-hydroperoxycoelenterazine formation is and what microenvironment is obligatory for CLZ(2H) activation by oxygen, we carried out the geometry optimization of a system including coelenterazine, oxygen, water and a few active site residues. The starting geometry of the system was based on structural data for active obelin (PDB code 1QV0), providing accurate information about the environment of the coelenterazine-binding cavity. We assume that van der Waals forces play a key role in the process of coelenterazine activation. Hence we used semiempirical quantum chemical calculations including van der Waals forces and hydrogen bonds as the parameters.

First we built the CLZ(2H) structure, placed molecular oxygen at different distances nearby C2 and started geometry optimization calculations of the cluster (Fig. 5.10A). According to these calculations the energy of the coelenterazine–dioxygen cluster is less than 1 kJ mol^{-1}. Moreover, oxygen always moves away from coelenterazine at a minimal distance of 3.6 Å, even if we placed it closer at an initial distance equal to 1.5 – 2.0 Å. These results indicate that coelenterazine and molecular oxygen do not form the chemical complex.

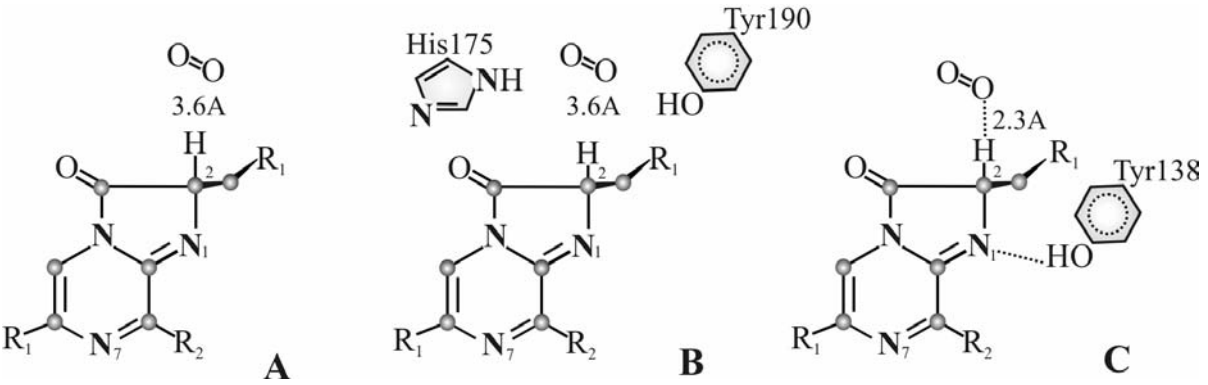

Figure 5.10 Modeling of interactions between CLZ(2H) and dioxygen depending on microenvironment. (A) coelenterazine and oxygen in vacuum; (B) and (C) coelenterazine and dioxygen in presence of either His175 and Tyr190, or Tyr138.

Subsequently we added certain amino acids to the CLZ(2H)–dioxygen cluster: histidine and tyrosines in different positions and combinations (Fig. 5.10). The amino acids were placed into starting positions according to the position of the corresponding His175, His64, Tyr138 and Tyr190 in the obelin crystal structure (PDB code 1QV0) (Fig. 5.11).

Geometry optimization of the cluster including CLZ(2H), dioxygen, His175 and/or Tyr190 results in certain energy gain but dioxygen is situated at 3.6 Å from C2 of coelenterazine as before (Fig. 5.10B). In case of the CLZ(2H), dioxygen and Tyr138 cluster, the dioxygen molecule is getting closer at 2.3 Å as the result of geometry optimization (Fig. 5.10C). Addition of His175 and/or Tyr190 to this cluster and following geometry optimization do not change the distance between dioxygen and CLZ(2H).

As the next step we carried out calculations with a water molecule situated near Tyr138 and His64, as observed in the obelin crystal structure (Fig. 5.11). Water possesses strong polarizing properties and might participate in or influence the activation of

coelenterazine. Since the water molecule has relatively small size and might therefore be found in different positions we placed it in few locations around coelenterazine. Addition of the water molecule to coelenterazine and dioxygen leads to decreasing the distance between dioxygen and CLZ(2H) to 2.3 Å as in the presence of Tyr138 and 0.3 eV energy gain. Addition of His175 and/or Tyr190 to the coelenterazine – oxygen – water cluster leads to stable complex formation as well. Regardless of initial distances between water, dioxygen and coelenterazine used in the geometry optimization, they have tendency to order in certain way: dioxygen situates above the imidazopyrazinone ring of coelenterazine opposite C2-carbon and water is placed opposite N1-nitrogen.

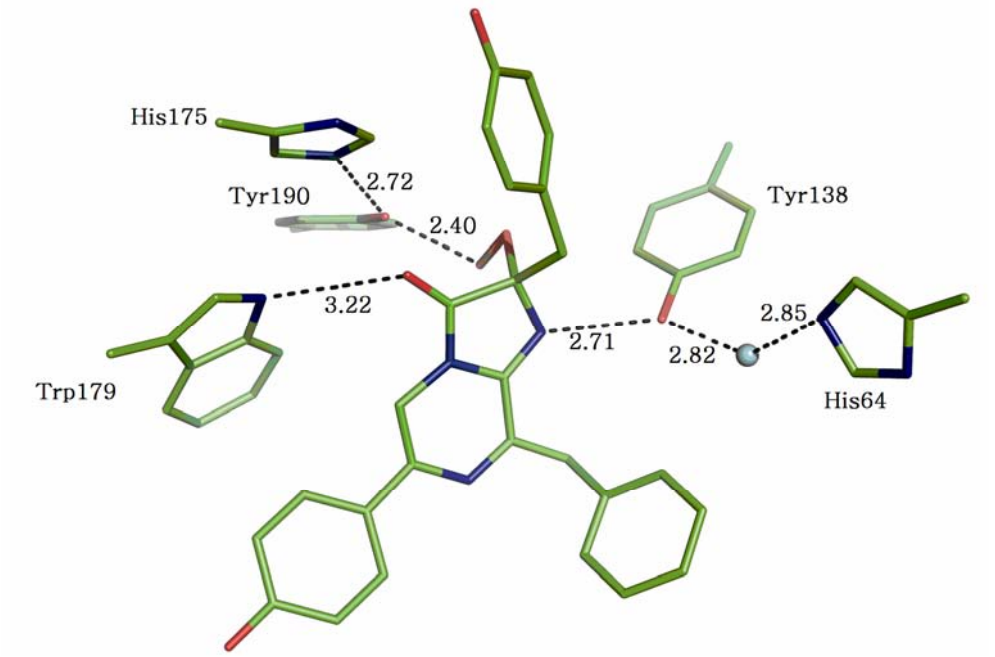

Figure 5.11 Binding mode of 2-hydroperoxycoelenterazine in obelin (PDB code 1QV0). The blue ball represents a water molecule; Hydrogen bonds (dashed lines) were determined with the PyMOL program. Distances are shown in Å.

Formation of a stable chemical complex is characterized by two factors: the energy of the complex and the distances between molecules. In the system consisting of coelenterazine, dioxygen, water, Tyr138 and His175 the energy gain is calculated to be 0.95 eV, without dioxygen it turns out to be 0.92 eV, without water – 0.7 eV. However, the distance between dioxygen and coelenterazine is determined to be 2.3 Å in all these cases.

The calculations show that the partial charges on the coelenterazine atoms change in

the presence of water and/or amino acid residues. The negative charge of N1-nitrogen changes from -0.38 to -0.42 under the influence of water and Tyr138. The negative charge of O18 also changes from -0.44 to -0.49. Presence of dioxygen increases the positive charge of the C2-bound hydrogen from +0.20 to +0.21; presence of water changes it to +0.24. As for charge of C2-carbon, addition of water changes it from +0.07 to -0.07, with Tyr138 and dioxygen it becomes -0.09.

Geometry optimization of the cluster including coelenterazine, dioxygen, water and His64 results in H-bonding of the water molecule with His64. The distance between the oxygen atom of the water molecule and the hydrogen atom of His64 is estimated to be 1.93-1.95 Å in vacuum, which is in good agreement with the 1.85 Å distance found in the obelin crystal structure. The computation shows that the His64-water complex placed close to N1-nitrogen of coelenterazine makes the dioxygen molecule move close to C2-carbon of coelenterazine at 2.4 Å via polarizing features of water. If the His64-water complex is placed at a distance of 4 to 5 Å from N1-nitrogen then the dioxygen molecule tends to move away from C2-carbon of coelenterazine at more than 3.6 Å.

Next we performed geometry optimization of the coelenterazine-dioxygen-water cluster excluding His64, sequentially placing the water molecule at different initial distances from N1-nitrogen of coelenterazine: 3, 4, 5, 6, 7, 10 Å, and keeping the distance between dioxygen and C2-carbon fixed at 2.4 Å. Geometry optimization showed that the water molecule is getting closer to N1-nitrogen of coelenterazine at 3 Å when it is placed at an initial distance up to 5 Å. As a result of this closer interaction the N1-nitrogen of coelenterazine is polarized and a stable complex between coelenterazine and dioxygen is formed.

It is reasonable to assume that the water molecule and/or Tyr138 redistribute the charges of the coelenterazine molecule via polarizing the N1-nitrogen and changing its partial atomic charge. As a result of this inductive effect the C2-H bond becomes also polarized and the dioxygen molecule becomes situated at 2.4 Å from C2-protonated carbon under London dispersion force (part of the van der Waals forces) influence. The London dispersion force is a weak intermolecular force arising from quantum induced instantaneous polarization multipoles in molecules. London forces are exhibited by nonpolar molecules because of the correlated movements of the electrons in interacting molecules. We believe

that formation of van der Waals complex between CLZ(2H) and oxygen could create a pre-condition for further oxygenation of coelenterazine. Our calculations show that molecular oxygen can undergo a spin transition from the triplet to singlet state during reaction with coelenterazine, for example, as a result of spin-orbit coupling (Isobe *et al.*, 2008).

Y138F replacement - To verify the supposition stated above we calculated the atomic structure of the coelenterazine – dioxygen cluster with addition of Phe138 instead of Tyr138 (Fig. 5.12). As a result of geometry optimization the dioxygen molecule moves away from C2-H at a distance of more than 5.0 Å. Addition of His175 and/or Tyr190 to this cluster does not change the result (Fig. 5.12A). When the His64 – water complex is added to the coelenterazine-dioxygen-Phe138 cluster being placed at a distance between the oxygen atom of water and N1-nitrogen of coelenterazine of 4 Å or farther, it also makes dioxygen move away from C2-H (Fig. 5.12B).

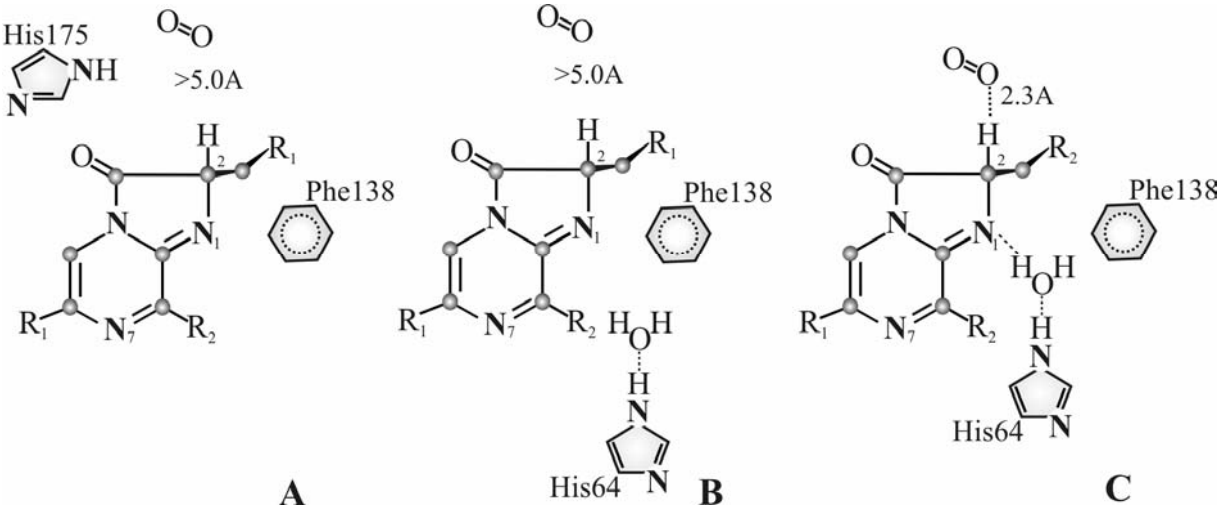

Figure 5.12 Modeling of interactions between coelenterazine protonated at C2 (CLZ(2H)) and dioxygen depending on microenvironment in Y138F obelin. (A) coelenterazine and dioxygen with His175, (B) coelenterazine and dioxygen with His64 - water complex, (C) coelenterazine and dioxygen with His64 - water complex placed closer than 4 Å.

However, if we placed His64 – water complex closer (less than 4 Å) to the coelenterazine-dioxygen-Phe138 cluster, then Phe138 is forced to move aside from its original position and dioxygen occupies the position near C2-carbon of coelenterazine at a distance of 2.3 Å (Fig. 5.12C). Thus the calculations show that the stable van der Waals

complex of CLZ(2H) with dioxygen can be formed only in the presence of a polar molecule near N1-nitrogen of coelenterazine: either water or a polar amino acid.

To experimentally verify the relevance of a polar molecule near N1-nitrogen of coelenterazine we produced the Y138F obelin mutant and studied its kinetic properties. It was found that the concentration of active Y138F reaches a maximum after 160 min of activation instead of 15-20 min of wild type obelin. The apparent rate constant of active Y138F formation (k_2) was evaluated to be 0.8 $M^{-1}s^{-1}$ at pH 6.5 and 20 ºC which is almost 14 times less than that of wild type obelin. Thus, the appearance of the dioxygen molecule near C2-carbon of coelenterazine is still possible in case of Y138F obelin, however it occurs with smaller probability than in the presence of a polar molecule near N1-nitrogen.

Based on the kinetic properties of the Y138 variant and quantum chemical calculations Tyr138 is supposed to provide the positioning of the dioxygen molecule near C2-carbon, increasing the probability of stable van der Waals complex formation between CLZ(2H) and oxygen for 2-hydroperoxycoelenterazine generation (Fig. 5.12C).

Conclusion

The reaction between triplet molecular oxygen and singlet carbon in organic compounds is spin-forbidden. However, a large number of enzymes do use O_2 to oxygenate an organic substrate being able to activate molecular oxygen (Torres Pazmino *et al.*, 2010). The majority of O_2-metabolizing enzymes involve transition metals, e.g. in P450 monooxygenase, or organic cofactors for catalysis, e.g. flavin-dependent monooxygenases (van Berkel *et al.*, 2006). Transition metals, mostly iron and copper, are able to form complexes with dioxygen or/and organic substrate when being in lower oxidation states and thus influence the electronic structure of the bound compound changing its reactivity. Organic cofactors like dihydroflavin and tetrahydropterin are thought to donate an electron to dioxygen, generating an activated oxygen species.

In the oxidation reaction catalyzed by flavin-dependent monooxygenases an electron is transferred from singlet reduced flavin to triplet dioxygen (Massey, 1994). This yields a caged radical pair of superoxide and the flavin radical, which collapses into an unstable hydroperoxyflavin after spin inversion. Flavin-dependent monooxygenases have found a way to stabilize this reactive peroxyflavin and to use it for oxygenation of a substrate.

Depending on the protonation state of the peroxyflavin, either a nucleophilic or electrophilic attack on the substrate is performed (van Berkel et al., 2006). As a result, a single atom of molecular oxygen is incorporated into the substrate, while the other oxygen atom is reduced to water.

Several enzymes have been recently reported to catalyze dioxygen incorporation without any requirement for cofactors or metal ions (Fetzner, 2002; Fetzner and Steiner, 2010). There are, for example, quinone-forming monooxygenases, ***Renilla*** luciferase, and several bacterial dioxygenases involved in the degradation of quinolones or the biosynthesis of vancomycin and teicoplanin antibiotics. Photoproteins, e.g. obelin and aequorin, can also be considered as cofactor-independent monooxygenases, but they stabilize a peroxygenated substrate extremely effectively, in contrast to other enzymes. It is believed that the common initial step for cofactor-independent monooxygenases is the abstraction of a proton from the organic substrate by an active site base, to form a conjugated anion intermediate (Fetzner and Steiner, 2010).

As an alternative mechanism one could propose the non-radical bimolecular dioxygenation mechanism, based on the process known as intersystem crossing when energy gap between the singlet and triplet state of the organic substrate is diminished. In case of the enediol oxygenation reaction catalyzed by RUBISCO enzyme spin coupling yields activated oxygen, singlet peroxide, attacking the organic compound (Oliva ***et al.***, 2001).

Basically, the reaction mechanism proposed for flavin-dependent monooxygenases up to peroxyflavin formation resembles the one for reaction of imidazopyrazinones with dioxygen in aprotic solvent containing base resulting in the formation of peroxy derivatives of imidazopyrazinones (Scheme 5.2). Possible catalytic mechanisms for several cofactor-independent monooxygenases are proposed focusing on the amino acid residues involved. ***Renilla*** luciferase is considered to belong to the α,β-hydrolase fold superfamily, which usually employs a catalytic triad consisting of a nucleophilic residue, a histidine acting as a general base and an acidic residue for making the histidine a better proton acceptor (Prokop ***et al.***, 2003; Steiner ***et al.***, 2010). Hod and Qdo dioxygenases, other members of α,β-hydrolase fold superfamily, do not depend on a catalytic triad but use a His–Asp pair instead.

Based on the studies of obelin activation kinetics and quantum chemical calculations we suggest the following mechanism of 2-hydroperoxycoelenterazine formation and the role of His175 and Tyr138 in this process (Fig. 5.13).

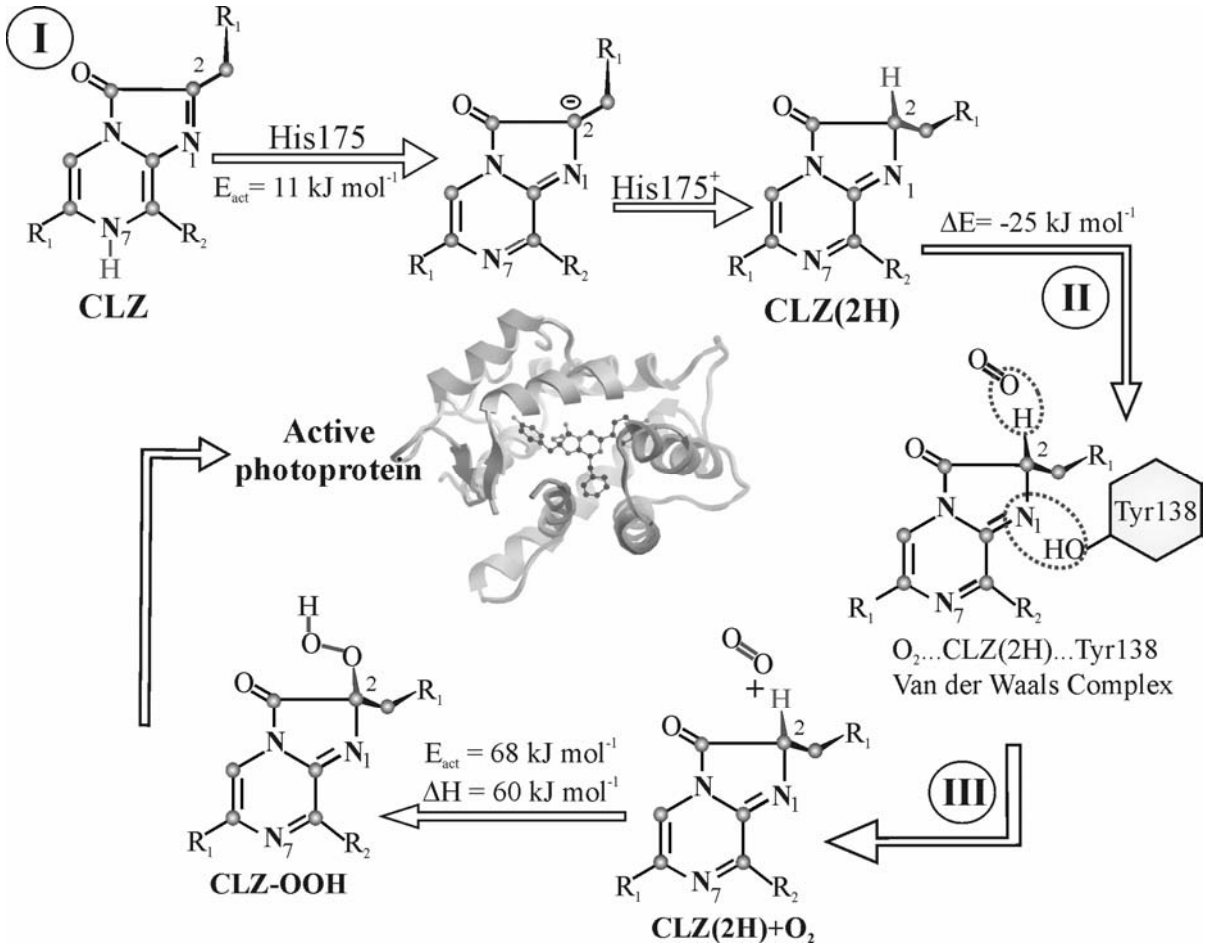

Figure 5.13 Proposed mechanism of coelenterazine conversion into its peroxy adduct at generation of active photoprotein.

Initial formation of the complex between apo-photoprotein and coelenterazine occurs within milliseconds (Eremeeva *et al.,* 2009) (Chapter 3). Apo-obelin undergoes conformational rearrangement upon binding with coelenterazine (Chapter 2), which involves coelenterazine-binding cavity formation along with coelenterazine protonation at carbon C2. His175 acts as a proton shuttle in this process by transferring the proton from N7-nitrogen to C2-carbon of coelenterazine (Fig. 5.13, step I). The next step is the conversion of bound coelenterazine into 2-hydroperoxycoelenterazine; this process takes minutes and might require additional structural rearrangements (Chapter 4). Tyr138 is

supposed to provide the positioning of the dioxygen molecule near C2-carbon, increasing the possibility of stable van der Waals complex formation between coelenterazine and dioxygen for proper 2-hydroperoxycoelenterazine generation (Fig. 5.13, steps II and III). A similar mechanism of oxygen activation might also be operative with certain cofactor-independent monooxygenases especially with those with slow reaction rates and stable intermediates.

Acknowledgements

This work was supported by grants of SB RAS No. 2, RFBR 09-04-00172, 09-04-12022, MCB program of RAS, and Ministry of Education and Science of the Russian Federation No. 64987.2010.4. E.V.E. was supported by Wageningen University Sandwich PhD Fellowship program. F.N.T. was supported by FCP GK-P333 and FCP GK-P213. We are grateful for the use of computation facilities of Joint Supercomputer Center of the Russian Academy of Sciences MVS-100K (Moscow) and Center of high-efficiency calculations of IKIT SFU (Krasnoyarsk).

Chapter 6

Bioluminescent and spectroscopic properties of obelin and aequorin coelenterazine-binding pocket mutants

Eremeeva, E.V.; Markova, S.V.; Frank, L.A.; Visser, A.J.W.G.; van Berkel, W.J.H.; and Vysotski, E.S.

Abstract

Ca^{2+}-regulated photoproteins are responsible for the bioluminescence of several marine organisms, mostly coelenterates. The best studied photoproteins, obelin and aequorin, consist of a single polypeptide chain (~ 22 kDa) having a hydrophobic cavity in which the "pre-activated" ligand, 2-hydroperoxycoelenterazine, is bound. According to spatial structures the side chains of His175, Trp179 and Tyr190 form hydrogen bonds with the peroxy and carbonyl groups of the 2-hydroperoxycoelenterazine ligand. We replaced these amino acid residues in both photoproteins by residues with different hydrogen bond donor-acceptor capacity. All mutants exhibited luciferase-like bioluminescence activity, hardly present in the wild-type proteins. Most o(belin) and a(equorin) mutants, except for aH176Q (24% of wild type activity), oW179Y (23%), oW179F (67%), oY190F (14%) and aY191F (22%), showed low or no photoprotein activity. The results indicate that His175, Trp179, and Tyr190 participate in positioning of the 2-hydroperoxycoelenterazine intermediate and provide the H-bond network stabilizing the substrate and participating in the emitter formation process.

Keywords: bioluminescence, photoprotein, mutants, active site

Abbreviations: DTT, dithiothreitol; EDTA, ethylenediaminetetraacetate; IPTG, isopropyl thio-β-D-galactopyranoside

Introduction

Aequorin and obelin are members of a family of Ca^{2+}-regulated photoproteins that are responsible for the bioluminescence of certain marine organisms, mostly coelenterates (Morin, 1974). The need of Ca^{2+} to trigger bioluminescence distinguishes photoproteins from luciferases (Hastings and Morin, 1969). Calcium is not essential for the bioluminescence reaction: calcium-free photoproteins emit a very low level of light named "the calcium-independent bioluminescence". The light intensity increases to 1-million fold or even more after the addition of calcium. The light-emitting reaction of photoproteins involves the oxidative decarboxylation of the coelenterazine ligand, followed by the emission of a photon (Cormier ***et al.***, 1973). The bioluminescence spectra of the emitted light are broad with maxima ranging from 465-495 nm depending on the type of photoprotein (Vysotski and Lee, 2004). The oxygen required for this reaction is derived from the "pre-activated" coelenterazine, 2-hydroperoxycoelenterazine, which is tightly but not covalently bound to the 22 kDa polypeptide chain.

Studies of coelenteramide, the product of the photoprotein-induced bioluminescence reaction, and its analogs have revealed a number of possible ionic species (Shimomura and Teranishi, 2000). A neutral species with a fluorescence emission maximum around 400 nm, the amide mono-anion with a maximum around 450 nm, the phenolate anion with a maximum around 480-490 nm and some other species with maxima at longer wavelengths. The amide mono-anion excited state is assumed to be the source of the bioluminescence. However, there is a small emission band at 400 nm (Markova ***et al.***, 2001) in the obelin spectra (maximum at 485 nm), presumably arising from the excited neutral species (Shimomura and Teranishi, 2000).

Resemblance between the bioluminescence and fluorescence spectra of aequorin (λ_{max}=465 nm) was one of the evidences used for the assignment of the amide mono-anion to be the primary excited state. But with obelin, the fluorescence maximum is at a longer wavelength than that of the bioluminescence (Markova ***et al.***, 2001). Therefore, the phenolate anion of coelenteramide has been suggested to be the source of Ca^{2+}-discharged obelin fluorescence.

The crystal structures of several photoproteins have been determined: aequorin from *Aequoria victoria* with a resolution of 2.3 Å (Head ***et al.***, 2000), obelin from *Obelia*

longissima with a resolution of 1.7 Å (Liu *et al.*, 2000) and 1.1 Å (Liu *et al.*, 2003), and some other obelins. Both photoproteins have spatial characteristics of the superfamily of Ca^{2+}-regulated proteins: four helix-turn-helix motifs, with only three of them being actual Ca^{2+}-binding EF-hands. The coelenterazine binding pocket is highly hydrophobic and is formed by residues originating from each of the helices. Besides, several hydrophobic side chains are directed into the active site (His22, Tyr139, His175 and Tyr190).

The importance of certain amino acid residues for the photoprotein bioluminescence was apparent before the crystal structures were solved. Ohmiya with coworkers constructed a number of Trp to Phe aequorin mutants and found that replacement of some tryptophans (Trp108, Trp173) led to loss of bioluminescence activity (Ohmiya *et al.*, 1992). Studies of several His mutants of aequorin showed that most of them have fair to good (15–70%) bioluminescence activity, but that mutants with substitutions of His169 to Ala, Phe and Trp had slight or no activity (Ohmiya *et al.*, 1993).

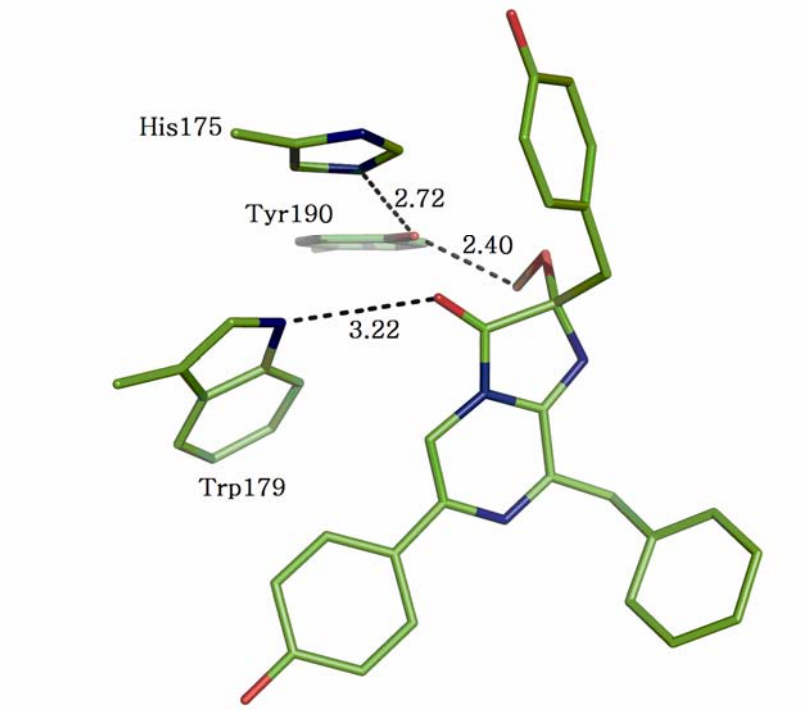

Figure 6.1 Hydrogen bonds between 2-hydroperoxycoelenterazine and His175, Trp179, and Tyr190 of obelin.

In the binding cavity of aequorin and obelin the hydrogen bond network around the 2-hydroperoxycoelenterazine is very similar (Vysotski and Lee, 2004). According to the obelin three-dimensional structure, the side chains of His175, Trp179, and Tyr190 form

hydrogen bonds with the peroxy- and carbonyl groups of the ligand (Fig. 6.1). To study the role of these interactions in the bioluminescence reaction in more details, we have replaced His175, Trp179, and Tyr190 of obelin and corresponding residues in aequorin by residues with different side chain hydrogen bond donor-acceptor properties. An account of the activity and spectroscopic properties of these mutants is presented.

Materials and Methods

Molecular biology - Site-directed mutagenesis was done on the template pET19-OL8 *E. coli* expression plasmid carrying the *O. longissima* wild-type apo-obelin gene (Markova *et al.*, 2001) and pET19-Aq7 *E. coli* expression plasmid carrying the *A. victoria* wild-type apo-aequorin gene. Mutations resulting in the desired amino acid change were carried out using the QuickChange site-directed mutagenesis kit (Stratagene, La Jolla, CA, USA) according to the protocol supplied with the kit. The plasmids harboring the mutations were verified by DNA sequencing.

Protein purification - For protein production, transformed *E. coli* BL21-Gold was cultivated with vigorous shaking at 37ºC in LB medium containing ampicillin. Induction was initiated with 1 mM IPTG when the culture reached an OD_{600} of 0.6-0.8. After addition of IPTG the cultivation of cells was continued for 3 h. Obelin and aequorin mutants were purified and activated with coelenterazine as previously reported for recombinant WT obelin (Vysotski *et al.*, 1999; Illarionov *et al.*, 2000). We observed that efficacy of activation with coelenterazine varied for the different mutants. However, in the last step of protein purification by ion-exchange chromatography using a Mono Q column (Amersham Bioscience), active mutants were clearly separated from their apo-forms. The purified mutant proteins were homogeneous according to SDS-PAGE.

Bioluminescence assay - The bioluminescence of obelin and aequorin was measured with a Luminoskan Ascent (Thermo Electron, Finland) by injection of 50 µl 100 mM $CaCl_2$, 100 mM Tris-HCl, pH 8.8, into the well containing 100 µl of 5 mM EDTA, 100 mM Tris-HCl

pH 8.8 and the photoprotein aliquot. The bioluminescence signal was integrated during 6 sec.

Spectral analysis - Absorption spectra were obtained with an UVIKON 943 Double Beam ultraviolet-visible (UV/VIS) spectrophotometer (Kontron Instruments, Italy). Bioluminescence and fluorescence spectra were measured with an AMINCO spectrofluorimeter (Thermo Spectronic, USA). The fluorescence emission spectra were corrected with the computer program supplied with the instrument. The bioluminescence spectra were measured in 1 mM EDTA, 20 mM Tris-HCl pH 7.0. Bioluminescence was initiated by injection of the $CaCl_2$ solution in the same buffer. The concentration of free calcium was around 0.5 μM to provide constant light level during the spectral scans.

Results and Discussion

Bioluminescence activities and kinetics of coelenterazine-binding pocket mutants – Bioluminescent activity is an important parameter characterizing the ability of bioluminescent proteins and their mutants to transfer chemical reaction energy to the light. The bioluminescent activities of mutant photoproteins are summarized in Table 6.1. His175 in obelin and the corresponding His176 in aequorin were substituted by Gln, Asn, Ala, Glu, Asp, Arg, Lys, Phe; Trp179 in obelin (Trp180 in aequorin) was substituted by Ala, Tyr, Arg, Lys, Glu, Phe; and Tyr190 in obelin (Tyr 191 in aequorin) was substituted by Arg, Lys, Phe, Glu. All mutants reveal low (or no) photoprotein bioluminescent activity except for aH176Q (23.8 %), oW179Y (23%), oW179F (67%), oY190F (14.3%) and aY191F (22%).

Table 6.1 Bioluminescent activities of obelin and aequorin mutants

Mutant[a]	Obelin bioluminescent activity [b] (%)	Aequorin bioluminescent activity [b] (%)	Mutant[a]	Obelin bioluminescent activity [b] (%)	Aequorin bioluminescent activity [b] (%)
			W179A	0.02	0.03
			W179Y	23.0	0.25
H175Q	0.80	23.80	W179R	0.02	0.001
H175N	1.70	3.30	W179K	0.70	0.18
H175A	0.50	0.18	W179E	0.60	0.004
H175E	0.20	0.02	W179F	67.0	3.50
H175D	0.01	6.00			
H175R	0.02	0.76	Y190R	0.01	0.40
H175Y	0.30	0.16	Y190K	0.03	1.00
H175F	0.30	0.98	Y190F	14.3	22.0
			Y190E	1.90	1.50

[a] Numbering according to the obelin sequence
[b] Relative to wild type

Basically, the bioluminescence activities of the aequorin mutants tend to agree with those of the corresponding obelin mutants. Substitution of Tyr190/Tyr191 for Phe results in similar activities (oY190F retains 14.3% of WT obelin activity, aY191F – 22.0% of WT aequorin activity). However, in some cases there are clear distinctions between mutants with equal substitutions. oW179Y and oW179F show relatively high (23% and 67%)

bioluminescence activities whereas the corresponding aW180Y and aW180F have rather low activities (0.25% and 3.5%). A clear difference is also seen between the bioluminescence activities of oH175Q (0.8%) and aH176Q (23.8%).

Substitutions of His175 in obelin and His176 in aequorin lead to complete loss of the bioluminescent activity (except for aH176Q). This suggests that His175 is needed for stabilizing the photoprotein-2-hydroperoxycoelenterazine complex through hydrogen bond formation with coelenterazine and Tyr190. His175 may play a key role in the oxidative decarboxylation of 2-hydroperoxycoelenterazine, initiating the bioluminescence reaction. The supposition that His175 is essential for the bioluminescence activity is in agreement with previous observations of aequorin mutants. It was shown that substitution of this His to Ala, Trp or Phe results in complete loss of the activity whereas modification of the remaining four His residues results in varying bioluminescence activities (Ohmiya ***et al.,*** 1993).

oW179Y and oW179F show relatively high bioluminescence activities (23% and 67% respectively) whereas the other Trp179 mutants have low activities. This suggests that the conservation of a hydrophobic aromatic moiety at this position is crucial for the spatial orientation of the 2-hydroxyperoxycoelenterazine molecule in the binding pocket.

A proton-relay hypothesis has been formulated to explain how Ca^{2+} binding triggers the bioluminescent reaction (Vysotski and Lee, 2004). According to this hypothesis, H-bonds between Tyr190 and His175 and between Tyr190 and 2-hydroperoxycoelenterazine are indispensable. Therefore, the substitution of Tyr190 to non-hydrogen bond forming amino acids was expected to result in impaired proton transfer. Hence it was surprising to find that Y190F mutants in both photoproteins retain significant bioluminescent activity. Thus it can be supposed that an isosteric hydrophobic aromatic side chain at this position partially compensates the deficiency of these H-bonds. However, this result may be not simply interpretable without knowledge of the spatial structure of this mutant.

In contrast to wild-type, all mutants display a luciferase-like bioluminescence activity upon incubation with coelenterazine under Ca^{2+}-free conditions (Fig. 6.2). Furthermore, when Ca^{2+} is injected into the solution containing photoprotein and coelenterazine a flash-like bioluminescence activity of photoprotein is observed. It is important to note that the photoprotein activities of the obelin and aequorin mutants are

substantially higher than their luciferase-like activities. This suggests that substitution of one of these amino acid residues leads to the formation of an unstable pre-activated photoprotein complex which can be destroyed slowly through Ca^{2+}-independent bioluminescence.

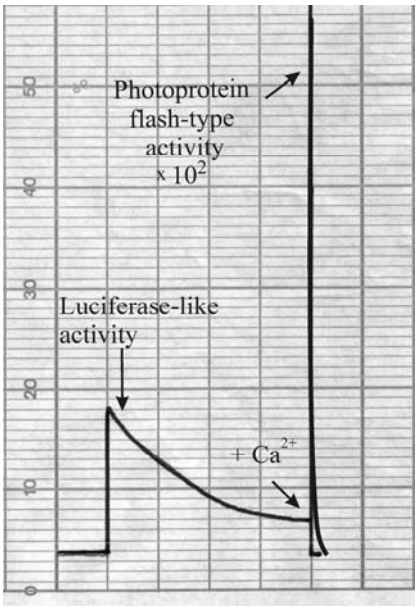

Figure 6.2 Simultaneous luciferase-like and photoprotein bioluminescent activities of Y190E obelin. Measurements are taken within 10 minutes after mixing apo-protein with coelenterazine.

This idea is supported by the fact that the absorption spectra of photoproteins with low activities have a shoulder around 350 nm in most cases, indicating the presence of coelenteramide, the product of the bioluminescence reaction (Fig. 6.3). At the same time these mutants have almost no 2-hydroperoxycoelenterazine absorbance around 460 nm. Some spectra have no near-UV absorbance at all (for example oW179A), apparently due to dissociation of coelenteramide.

The bioluminescence decay curves of the obelin and aequorin variants are depicted in Fig. 6.4. All mutants as well as wild type photoproteins have a high rate of rise of light intensity. However, the decay rates of the mutants are different from those of the wild-type proteins in most cases and the bioluminescence decay kinetics cannot be characterized with a single rate constant (Table 6.2). This could be due to either heterogeneous protein populations with different rates or one population consisting of two conformations that very slowly interconvert.

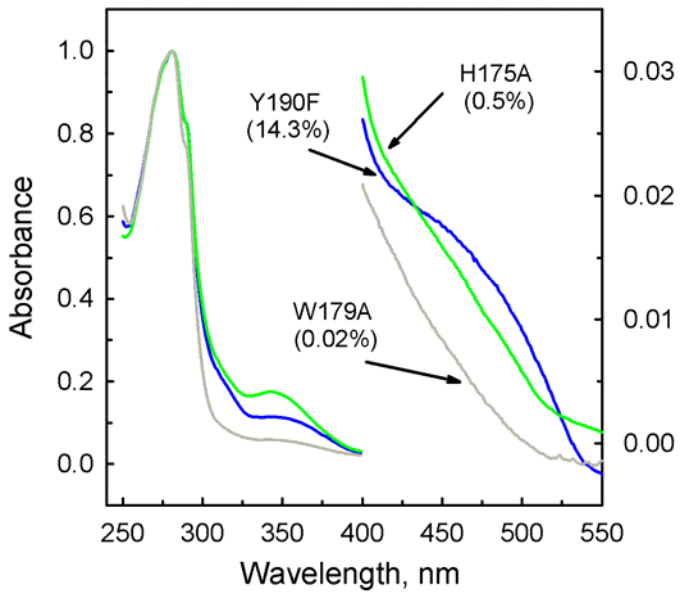

Figure 6.3 Normalized absorption spectra of selected obelin mutants. The corresponding relative bioluminescent activities are indicated between brackets**.**

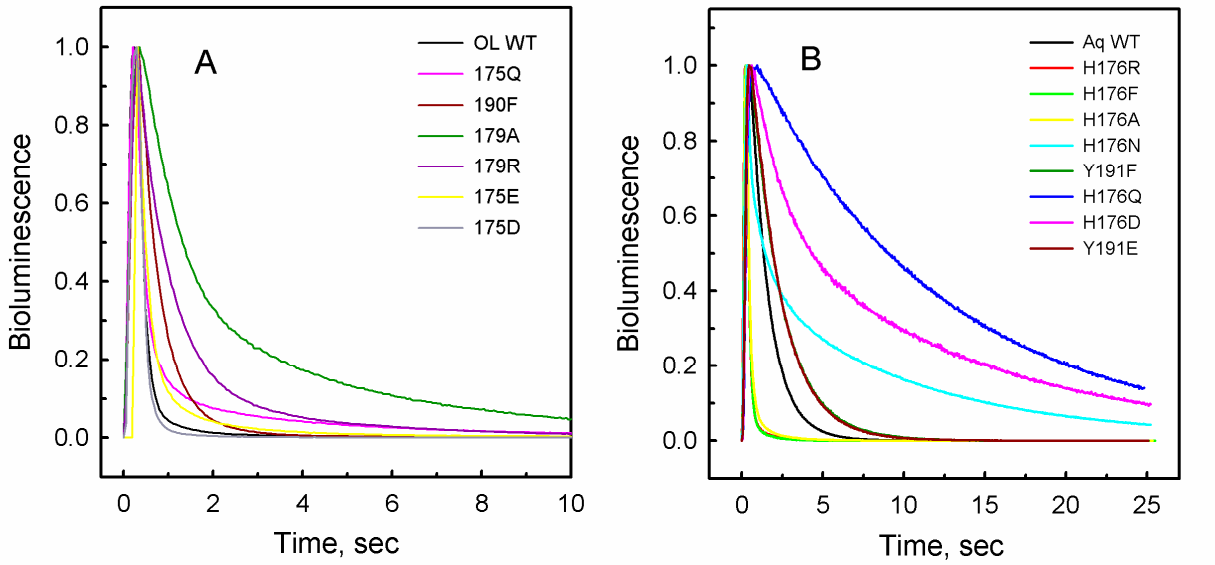

Figure 6.4 Normalized kinetics of bioluminescent reaction of obelin (A), aequorin (B) and their mutants.

There are three groups of mutants that can be classified according to their decay properties: with lower rate - oW179A, oY190F, oH175Q and aH176D, aH176Q, aW180R, with higher rate – oY190K and aH176R, aH176A, aH176F, aW180A, aW180K, aY191K, and with decay rates, which is close to that of the corresponding wild type photoprotein - oH175R, oH175D and aY191R.

Table 6.2 Bioluminescence decay rates of obelin and aequorin variants

Obelin mutants	Decay rate[a,b], s^{-1}		Decay rate[a,b], s^{-1}		Aequorin mutants
	k_1	k_2	k_1	k_2	
WT	7.0	-	0.9	-	WT
H175Q	4.7 (0.96)	0.4 (0.04)	0.1	-	H176Q
H175N	5.6	-	1.3 (0.64)	0.1 (0.36)	H176N
H175A	5.7	-	6.0 (0.98)	0.9 (0.02)	H176A
H175E	4.9 (0.96)	0.7 (0.04)	4.3 (0.97)	0.2 (0.03)	H176E
H175D	6.8 (0.99)	0.4 (0.01)	0.5 (0.5)	0.1 (0.5)	H176D
H175R	7.1 (0.99)	0.8 (0.01)	4.9	-	H176R
H175Y	4.6 (0.99)	0.5 (0.01)	0.8 (0.92)	0.2 (0.08)	H176Y
H175F	5.2 (0.98)	0.7 (0.02)	6.5 (0.99)	0.8 (0.01)	H176F
W179F	0.9	-	0.8	-	W180F
W179K	6.0 (0.97)	0.9 (0.03)	3.9 (0.96)	0.4 (0.04)	W180K
W179E	6.4 (0.98)	0.8 (0.02)	0.5 (0.83)	0.1 (0.17)	W180E
W179A	1.2 (0.76)	0.2 (0.24)	5.5 (0.97)	0.7 (0.03)	W180A
W179Y	3.7 (0.89)	1.1 (0.11)	0.3	-	W180Y
W179R	1.5 (0.89)	0.3 (0.11)	0.6 (0.75)	0.2 (0.25)	W180R
Y190R	4.9 (0.98)	0.6 (0.02)	0.9 (0.92)	0.2 (0.08)	Y191R
Y190K	7.7 (0.99)	0.9 (0.01)	5.2 (0.98)	0.8 (0.02	Y191K
Y190F	2.2 (0.97)	0.6 (0.03)	0.5	-	Y191F
Y190E	5.2	-	0.5	-	Y191E

[a] Rate constants have maximum error values of 10%.
[b] The relative amplitudes for two-exponential decay with sum normalized to 1 are indicated in parentheses

Bioluminescence and fluorescence spectra of coelenterazine-binding pocket mutants – The bioluminescence spectra of the mutants with a relatively high activity are all virtually the same as those of the corresponding wild type photoproteins with a maximum at 482 ± 10 nm and a shoulder at 390 nm in case of obelin, and with maximum at 473 ± 10 nm in case of aequorin (Table 6.3, Fig. 6.5). The bioluminescence maxima of the obelin mutants oW179K and oW179E are shifted to 460 nm while the shoulder keeps its position at 390 nm. The same shoulder appears in the spectra of several aequorin mutants, for example aH176A, aH176F, aW180K, aW180A and aY191K, indicating the presence of the neutral

coelenteramide excited state, which is supposed to be the initial emitter generated in the reaction (Vysotski and Lee, 2004).

Table 6.3 Bioluminescence maxima of obelin and aequorin variants

Obelin mutant	Bioluminescence, max / shoulder, nm	Bioluminescence, max / shoulder, nm	Aequorin mutant
WT	482 / 390	473	WT
H175Q	490 / 390	482	H176Q
H175N	476 / 390	475	H176N
H175A	474 / 390	475 / 390	H176A
H175E	470 / 390	-	H176E
H175D	-	477	H176D
H175R	-	475	H176R
H175Y	480 / 390	-	H176Y
H175F	478 / 390	480 / 390	H176F
W179F	473	460	W180F
W179K	460 / 390	466 / 390	W180K
W179E	460 / 390	-	W180E
W179A	-	475 / 390	W180A
W179Y	486 / 390	-	W180Y
W179R	-	-	W180R
Y190R	-	-	Y191R
Y190K	-	469 / 390	Y191K
Y190F	475 / 390	475	Y191F
Y190E	469 / 390	473	Y191E

The second emitter, which is responsible for the blue bioluminescence (λ_{max} = 460-495 nm), is generated as the result of proton transfer from the hydroxyl group of the 5-(*n*-hydroxy)-phenyl moiety of coelenteramide to His22. It is believed that in case of aequorin the proton transfer occurs more effectively because of the additional H-bond between Tyr89 (there is a Phe in this position in obelin) and the 6-(*n*-hydroxy)-phenyl group of 2-hydroperoxycoelenterazine. This is the reason why the aequorin bioluminescence spectrum lacks the shoulder at 390 nm.

His176, Trp180 and Tyr191 are situated far enough from the site where the proton transfer is supposed to occur. However, it is obviously the disturbance of proton transfer that leads to the appearance of the 390 nm shoulder in the mutant spectra in case of aH176A, aH176F, aW180K, aW180A and aY191K. Probably these particular substitutions result in improper orientation of 2-hydroperoxycoelenterazine in the active site, which might lead to breaking of the H-bond between Tyr89 and the 6-(*n*-hydroxy)-phenyl group or to an increasing distance between His22 and the 6-(*n*-hydroxy)-phenyl group. It is interesting to note that the appearance of the 390 nm shoulder in a few aequorin mutant spectra correlates with their faster decay rates in comparison to those of wild type aequorin.

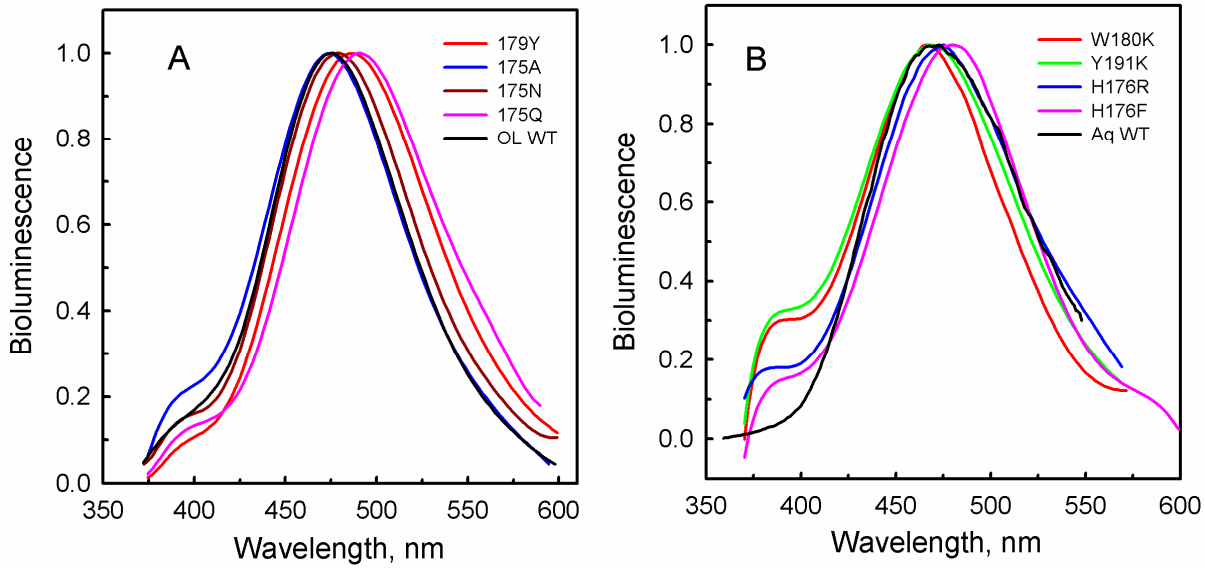

Figure 6.5 Normalized bioluminescence spectra of obelin (A), aequorin (B) and their mutants at pH 7.0.

While active photoproteins are hardly fluorescent, Ca^{2+}-discharged photoproteins have strong fluorescence with maxima at 470 nm in case of aequorin and at 505 nm in case of obelin. All mutants can be divided into groups according to their fluorescent properties (Table 6.4, Fig. 6.6). There are four groups for obelin mutants: with bimodal fluorescence – violet and green, with violet maximum, with green maximum and with no fluorescence. Aequorin mutants fall into five groups: non-fluorescent, with violet, green and blue maxima, and with bimodal fluorescence (violet and blue). These spectral changes may result from the disturbance of proton transfer between the 5-(*n*-hydroxy)-phenyl moiety of

coelenteramide and His22. This explains the appearance of violet peaks in the fluorescence spectra of several mutants.

Any substitution within the photoprotein active center might also lead to a change of emitter microenvironment influencing the spectral distribution. For example, it is known that a more polar environment can shift the coelenteramide spectrum to the green region and this is what we observe in case of H176E aequorin. The absence of fluorescence in case of some mutants can be due to quenching or dissociation of coelenteramide from the coelenterazine-binding pocket.

Table 6.4 Fluorescence maxima of Ca^{2+}-discharged obelin and aequorin variants

Obelin mutant	Fluorescence, max / shoulder, nm	Fluorescence, max / shoulder, nm	Aequorin mutant
WT	505	470	WT
H175Q	502 / 419	-	H176Q
H175N	417 / 504	476 / 418	H176N
H175A	502 / 417	471	H176A
H175E	498 / 423	502	H176E
H175D	420	496 / 419	H176D
H175R	481	-	H176R
H175Y	415	-	H176Y
H175F	418	-	H176F
W179F	504	415	W180F
W179K	-	430	W180K
W179E	-	416	W180E
W179A	420	410	W180A
W179Y	505	415	W180Y
W179R	414	415	W180R
Y190R	-	-	Y191R
Y190K	425 / 500	422	Y191K
Y190F	501/ 416	420 / 480	Y191F
Y190E	480 / 420	-	Y191E

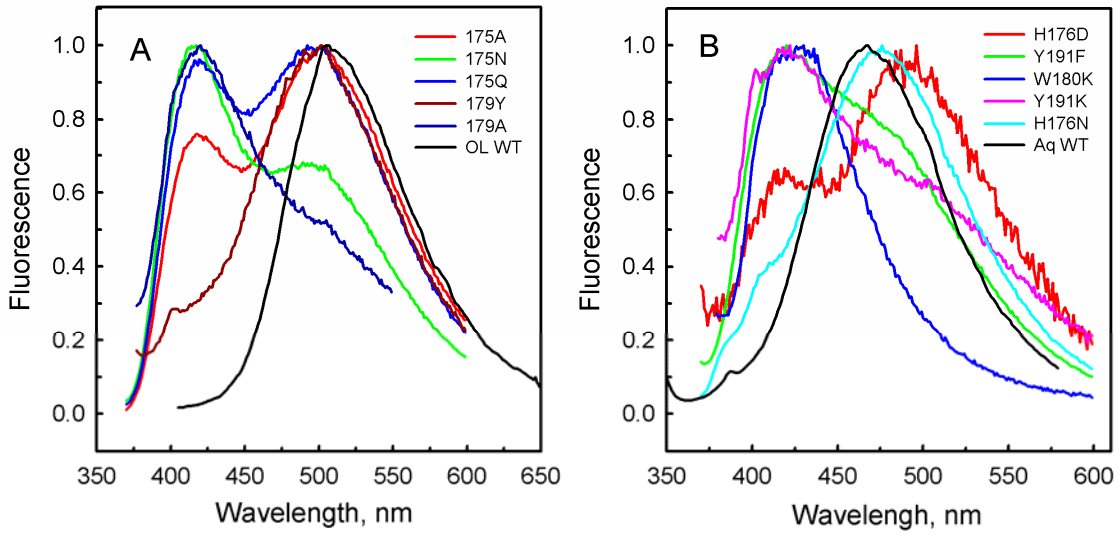

Figure 6.6 Normalized fluorescence spectra of Ca^{2+}-discharged obelin (A), aequorin (B) and their mutants at pH 7.0.

Apparent dissociation and rate constants of coelenterazine-binding pocket mutants – Apparent dissociation constants of apo-protein – coelenterazine complex and apparent rate constants of active photoprotein formation for obelin and its mutants are summarized in Table 6.5. A 5- to 6-fold increase of the apparent dissociation constant of the apo-protein – coelenterazine complex is observed for all Trp179 mutants and oY190E. In contrast, oH175N and oY190F have almost the same dissociation constants as wild type obelin.

Table 6.5 Dissociation constants and apparent rate constants of active photoprotein formation for obelin variants

	Bioluminescent activity, %	Dissociation constant K_D, μM	Rate constant k_2, $M^{-1}s^{-1}$
Obelin WT	100.0	0.2 ± 0.04	11.0 ± 0.4
H175N	1.7	0.15 ± 0.01	1.3 ± 0.1
W179Y	23.0	1.0 ± 0.07	1.6 ± 0.06
W179A	0.02	1.1 ± 0.09	1.5 ± 0.4
W179F	67.0	1.2 ±0.07	1.5 ± 0.2
Y190E	1.9	1.0 ± 0.08	1.4 ± 0.3
Y190F	14.3	0.2 ± 0.01	0.4 ± 0.03

The apparent rate constants of active photoprotein formation of the mutants are almost ten times (and more for Y190F) less than in case of wild type obelin. This suggests that binding of coelenterazine is still effective for oH175N and oY190F but that malfunctioning of oxygen activation leads to a decrease in the rate of formation of 2-hydroperoxycoelenterazine.

Conclusion

The results of the present study indicate that His175, Trp179 and Tyr190 of obelin and the corresponding residues of aequorin position the 2-hydroperoxycoelenterazine intermediate and provide the H-bond network stabilizing the substrate and participating in the emitter formation process.

Acknowledgements

The work was supported by Wageningen University Sandwich PhD-Fellowship Program, Grants 02.512.12. 2006 and 1211.2008.4 of Ministry of Education and Science of Russian Federation, MCB Program of RAS, and by Grant No. 2 of SB RAS.

Chapter 7

Picosecond fluorescence relaxation spectroscopy of the calcium-discharged photoproteins aequorin and obelin

van Oort, B.; Eremeeva, E.V.; Koehorst, R.B.M.; Laptenok, S.P.; van Amerongen, H.; van Berkel, W.J.H.; Malikova, N.P.; Markova, S.V.; Vysotski, E.S.; Visser, A. J.W.G.; and Lee; J. (2009) *Biochemistry*, 48, 10486-10491.

Abstract

Addition of calcium ions to the Ca^{2+}-regulated photoproteins, such as aequorin and obelin, produces a blue bioluminescence originating from a fluorescence transition of the protein-bound product, coelenteramide. The kinetics of several transient fluorescent species of the bound coelenteramide is resolved after picosecond-laser excitation and streak camera detection. The initially formed spectral distributions at picosecond-times are broad, evidently comprised of two contributions, one at higher energy (~25000 cm^{-1}) assigned as from the Ca^{2+}-discharged photoprotein-bound coelenteramide in its neutral state. This component decays much more rapidly (t½ ~ 2 ps) in the case of the Ca^{2+}-discharged obelin than aequorin (t½ ~ 30 ps). The second component at lower energy shows several intermediates in the 150-500 ps times, with a final species having spectral maxima 19400 cm^{-1}, bound to the Ca^{2+}-discharged obelin, and 21300 cm^{-1}, bound to the Ca^{2+}-discharged aequorin, and both have a fluorescence decay lifetime of 4 ns. It is proposed that the rapid kinetics of these fluorescence transients on the picoseconds time scale, correspond to times for relaxation of the protein structural environment of the binding cavity.

Keywords: bioluminescence, fluorescence, Ca^{2+}-discharged photoprotein, obelin, aquorin

Abbreviations: DMSO, dimethyl sulfoxide; TRES, time-resolved emission spectra

Introduction

Bioluminescent animals are found in a variety of types occurring both terrestrially and in the ocean. More often than not, the chemistry of their light emission processes and the proteins involved are found quite unrelated. Well-studied cases, for example, are the bioluminescence of firefly, which involves ATP and a substrate firefly luciferin, a benzthiozole derivative, and that of the photoprotein aequorin from the bioluminescent jellyfish *Aequorea*, which is triggered for light emission by Ca^{2+}. Coelenterazine, an imidazopyrazinone derivative (Fig. 7.1), is the luciferin (a generic term for the substrate) involved in many marine bioluminescent systems, including the ones subject to this present study, the Ca^{2+}-regulated photoproteins, aequorin and obelin from the hydrazoan *Obelia* (Shimomura, 2006; Vysotski and Lee, 2004; Vysotski and Lee, 2007).

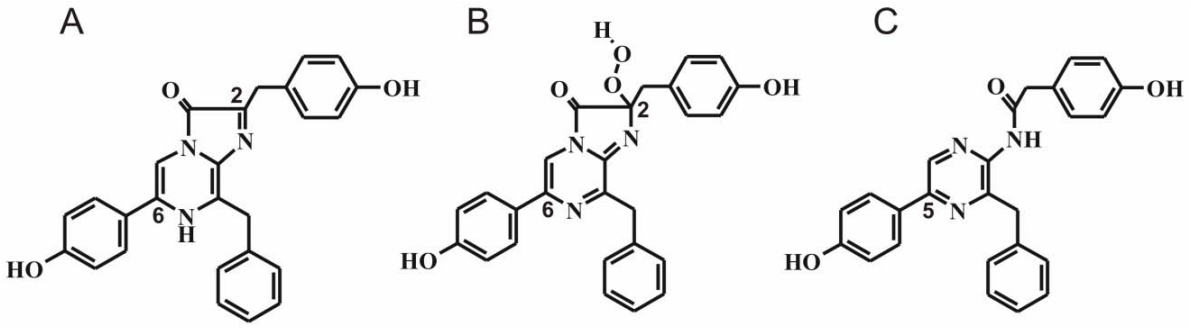

Figure 7.1 Chemical structures of coelenterazine (A), 2-hydroperoxycoelenterazine (B) and coelenteramide (C).

A significant advance in uncovering the mechanism of bioluminescence from aequorin and obelin resulted from the determination of the high-resolution spatial structure of the two photoproteins (Head *et al.*, 2000; Liu *et al.*, 2000; Liu *et al.*, 2003). The coelenterazine was revealed residing in an internal cavity substituted with a peroxy group (Fig. 7.1B), as long suspected from earlier indirect evidence (Shimomura and Johnson, 1978). Such a compound would be very unstable in free solution, but in the protein it appears to be frozen in place via a H-bond network to amino acid residues comprising the binding cavity. Model chemiluminescence studies with coelenterazine analogs had shown such a peroxide to be an intermediate, closing to a dioxetanone in the reaction pathway (McCapra and Chang, 1967). The free energy produced by decarboxylation of this

dioxetanone around 70 kcal/mol is sufficient to account for the energy of the photons of blue bioluminescence.

Aequorin and obelin are EF-hand proteins belonging to the large family of Ca^{2+}-binding proteins. They each contain three Ca^{2+}-ligating loops and the spatial structure revealed how Ca^{2+} binding could lead to residue shifts in the binding site to interfere with the H-bond network and cause the decarboxylation reaction to proceed to the product coelenteramide (Fig. 7.1C) in its first singlet electronic excited state (Vysotski and Lee, 2004). The bioluminescence spectrum then originates from the fluorescence transition of coelenteramide.

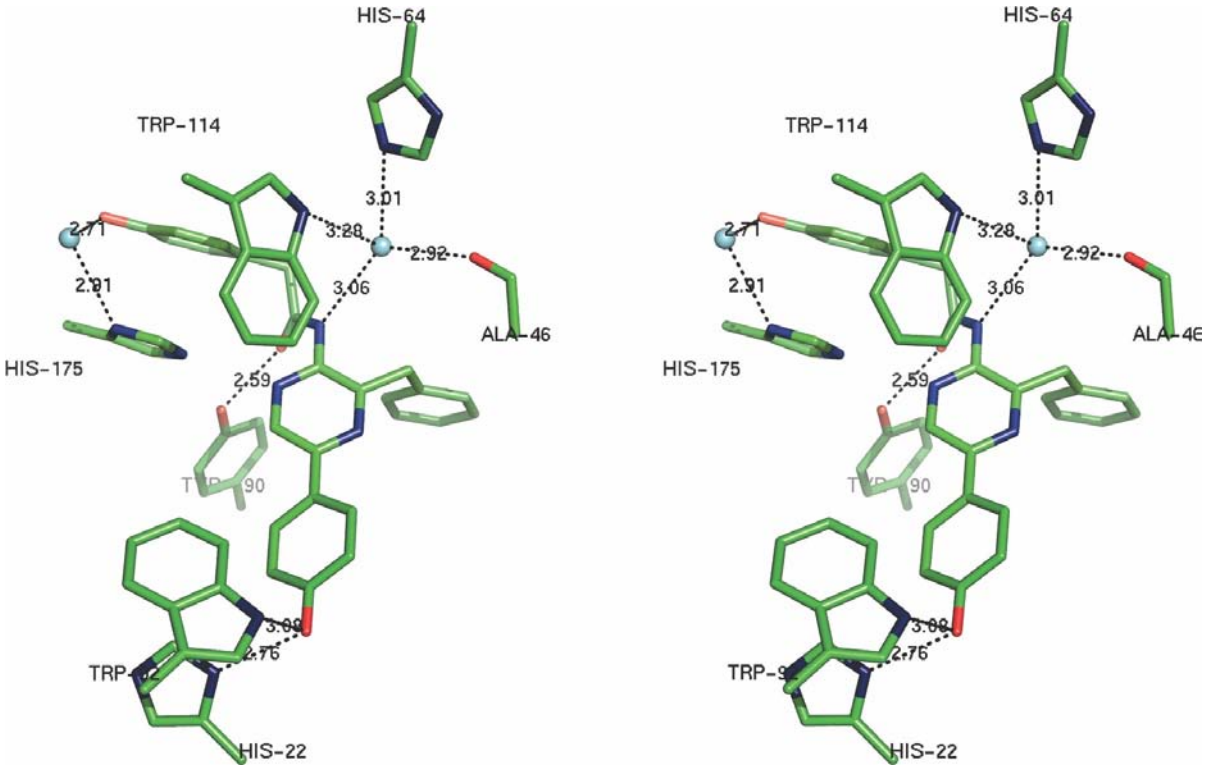

Figure 7.2 Stereoview showing the interactions of coelenteramide within the binding cavity of Ca^{2+}-discharged obelin (PDB code 2F8P). The blue balls represent water molecules; dotted lines indicate H-bonds. The distances are shown in Ångstroms. Hydrogen bonds (dotted lines) were determined with the PyMOL program (DeLano, 2002).

The bioluminescence spectra are broad with maxima depending on the type of organism. Aequorin has a maximum at 469 nm and various obelins – at 475-495 nm (Markova *et al.*, 2002). The photoproteins are hardly fluorescent themselves but following the bioluminescence reaction, the Ca^{2+}-discharged photoproteins exhibit strong

fluorescence. For Ca^{2+}-discharged aequorin the fluorescence spectral distribution is very similar to the bioluminescence spectrum. In contrast, the Ca^{2+}-discharged obelins show fluorescence maxima about 25 nm to longer wavelength than their bioluminescence. Furthermore, the obelin bioluminescence spectrum is bimodal, with a minor higher energy band having a maximum around 400 nm, not evident in aequorin bioluminescence (Markova *et al.*, 2002; Stepanyuk *et al.*, 2005). From spectral studies of model compounds this high energy band is identified as from the excited level of coelenteramide in its neutral state (Shimomura and Teranishi, 2000). More controversial has been the characterization of the lower energy blue bioluminescence band because the evidence from fluorescence model diagnostics is somewhat ambiguous. The spatial structures of obelin and its product however, directly implicate the origin of the blue band as from the excited coelenteramide 5-phenoxy anion. The primary excited neutral coelenteramide should be quickly transformed to the anion due to the proximity of a His22 residue, H-bonded to the phenolic oxygen and poised to act a proton acceptor (Fig. 7.2) (Vysotski and Lee, 2004). By such a mechanism, the bioluminescence spectrum is "tuned" to most efficiently satisfy the biological survival function of the light emission.

It is the purpose of this work to investigate the excited state dynamics of coelenteramide bound in the protein cavity, to test this proton transfer idea and also to account for the variations in steady state emission properties.

Materials and Methods

Preparation of proteins - The apo-obelin and apo-aequorin truncated by residues from the N-terminus were produced in transformed *E. coli* BL21-Gold (Markova *et al.*, 2001; Deng *et al.*, 2005) and purified and charged with coelenterazine to form the active photoproteins, all as previously reported (Illarionov *et al.*, 2000; Vysotski *et al.*, 2001). The final products were homogeneous according to SDS-PAGE. To prepare the Ca^{2+}-discharged samples, the concentrated solutions of photoproteins were diluted to a concentration of 0.26 mg/mL (aequorin) and 0.32 mg/mL (obelin) with 50 mM Bis-Tris propane pH 7.0 containing $CaCl_2$ (final concentration of calcium in a sample = 1 mM). Fluorescence was measured after bioluminescence reaction ceased (OD was 0.06 - 0.07 at the excitation wavelength) and samples were deoxygenated by flushing with argon then applying vacuum.

Time-resolved fluorescence - Time resolved fluorescence was measured at room temperature with a streak camera setup as described in detail in (van Oort *et al.*, 2009). In brief, the sample is excited by ~0.2 ps duration pulses (340 nm, ~1 mW) at a repetition rate of 250 kHz. Pulses were generated in an optical parametric amplifier that was fed by pulses from a mode-locked titanium-sapphire laser, amplified by a regenerative amplifier. Polarization was set vertical by a Berek polarizer. The samples were in a static fluorescence cuvette (10x10 mm). Fluorescence was collected under magic angle polarization and focused by a set of achromatic lens assemblies onto the slit of the imaging spectrograph. The spectrograph focused the output light (horizontal spectral dispersion) directly onto the stripe-shaped cathode of the streak camera. The resulting photoelectrons are accelerated and deflected by a time-dependent vertical electric field, and detected by a multichannel plate, phosphorescent screen, and a CCD camera. Scale, linearity and curving of the time and wavelength axes, were extensively treated as described in (van Oort *et al.*, 2009). For more details on streak camera experiments and data analysis, see (van Stokkum *et al.*, 2008).

The CCD images are two-dimensional data sets of fluorescence intensity as a function of time and wavelength. For the experiments described here, the time windows were 160 ps or 2 ns, and the spectral window ranged from 330 nm to 650 nm (using a grating with 40 grooves/mm ruling and 500 nm blaze). The images contain the initial part of the decay (directly after excitation), overlapped with the decay at a delay of 6.6 ns (backsweep). The backsweep is treated explicitly in data analysis and gives information on slower relaxation processes. In addition to fluorescence, the CCD images also show Rayleigh and Raman scatter. Wavelengths at which the scatter intensity was high relative to the fluorescence were omitted from analysis. When the scatter intensity was of the same order as fluorescence intensity, the scatter was included explicitly in the fitting as a component with an infinitely fast decay as described in (van Stokkum *et al.*, 2008).

Data analysis - Streak data were analyzed in two distinct ways. Firstly, the data were fitted to a sequential model, in which a spectral species i evolves into species $i+1$ with rate k_i, and then into $i+2$ with rate k_{i+2}, and so on. The fitting procedure is described in detail in (Mullen and van Stokkum, 2007). In this procedure spectral shapes are unconstrained. To

increase the signal to noise ratio, the decays were averaged over 5 nm prior to fitting (this corresponds to 313 cm^{-1} at 400 nm and 139 cm^{-1} at 600 nm).

Secondly, the data were converted to an energy scale (dividing the fluorescence intensity at each detection wavelength by the square of the detection wavelength). The data were then fitted to a sum of two spectral bands: one with a Gaussian shape and one with a log-normal shape. Position and intensity of the two bands were fitted to exponential functions. The fitting procedure and software are described in detail elsewhere (Koehorst ***et al.***, 2009). The data could also be fitted with a sum of three or four Gaussian shapes, however that required more fit parameters and led to strong correlations (and large uncertainties) between the fitted values. Fitting with two log-normal functions yields one distribution with skewness close to unity, and this function was therefore replaced by a Gaussian. Gaussian and log-normal lineshapes very adequately describe fluorescence emission spectra for a range of (bio)organic chromophores (Burstein and Emelyanenko, 1996). As a consequence this fitting procedure has the advantage over the first fitting procedure that it is closer to a physically meaningful description of the data. Unfortunately it has a reduced time resolution (~25 ps).

The estimated errors of the peak positions were calculated as standard errors from the fits of the spectra. The uncertainty of the lifetimes cannot by judged from the standard errors due to strong correlations between the fit parameters. Instead the uncertainty of a lifetime is deduced from the fit quality of the best fit obtained when that lifetime is fixed at a range of different values.

Results and Discussion

Fig. 7.3 shows that the fluorescence decay function of the Ca^{2+}-discharged aequorin, is multiexponential and depends on the wavelength of detection. This indicates that the excitation of protein-bound coelenteramide populates at least two excited states, with a rapidly decaying high-energy state. The data can also be presented as spectra at different times after excitation.

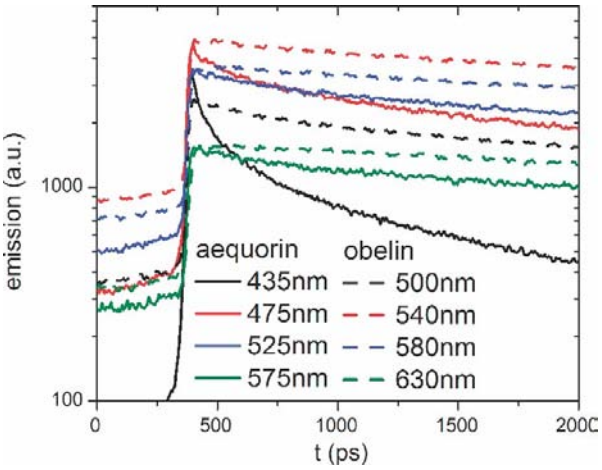

Figure 7.3 Fluorescence decay curves of Ca^{2+}-discharged aequorin and obelin (dashed) at several detection wavelengths. The decays are averaged over 3 nm around the indicated central wavelengths. The signal before about 300 ps is due to the backsweep.

Fig. 7.4 (top) shows such time-resolved emission spectra (TRES) of Ca^{2+}-discharged aequorin at various times following the excitation and indeed, a fast decaying spectral band does appear at the higher energy side. On the assumption of a lognormal and a Gaussian energy distribution (see above for reasons to use these bandshapes), the TRES are resolved into the two bands, shown for 25 ps and 1500 ps after excitation in Figure 7.4 (bottom). TRES at each detection time were fitted with two bands. The higher energy band (25900(30) cm^{-1} at 25 ps) decays with a 1/e lifetime of approximately 45(15) ps, while redshifting ~2200(100) cm^{-1} with 1/e lifetime of 630(50) ps. Values in brackets are standard errors calculated from the fit of the spectra (for the peak positions) and uncertainties calculated as described in the Materials and Methods (for the lifetimes). In addition to the 45-ps decay component there is a small component with ~4 ns decay. The low energy band (21000(20) cm^{-1} at 25 ps) shifts 670(50) cm^{-1} in 260(50) ps, and shows a slower redshift of

380(30) cm^{-1} in ~4 ns. The intensity of this 21000 cm^{-1}-band decays biexponentially: 40% with a lifetime of 500(50) ps, and 60% 2.7 ns.

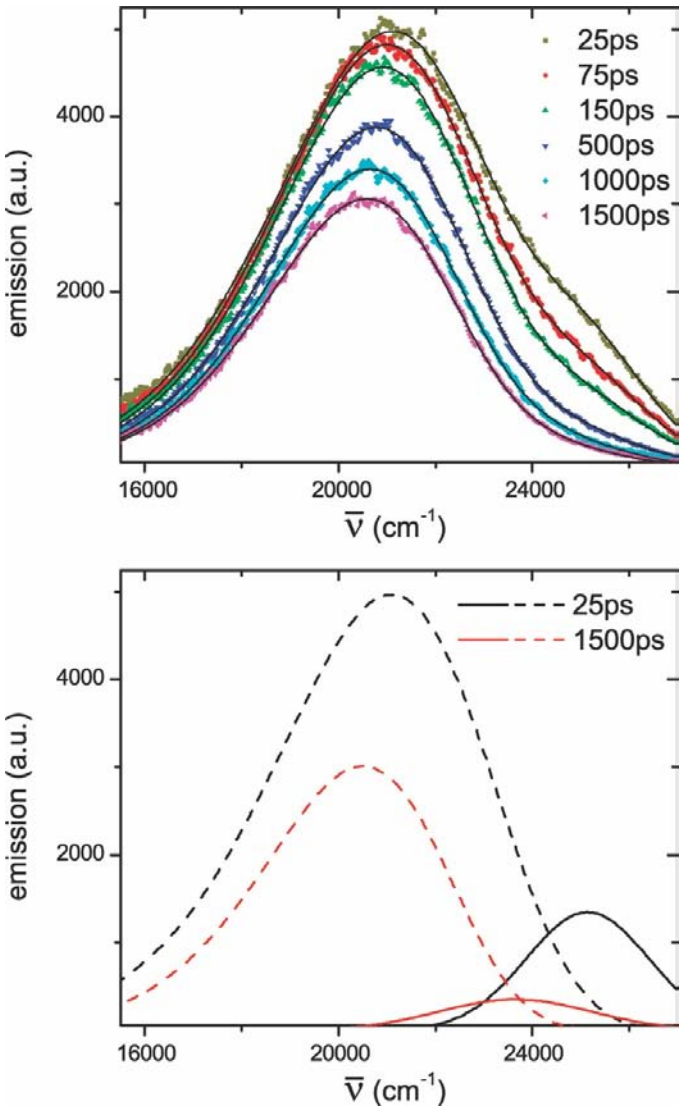

Figure 7.4 Time-resolved emission spectra of Ca^{2+}-discharged aequorin at various times after excitation. The spectrum at each time is fitted as a sum of a log-normal (dashed) and Gaussian function. The lower panel shows the two functions at 25 ps and 1.5 ns after excitation. At 25 ps the log-normal function peaks at 21100 cm^{-1} (465 nm), and the Gaussian function at 25900 cm^{-1} (396 nm). At 1.5 ns this is 20500 cm^{-1} (480 nm) and 23600 cm^{-1} (419 nm). The peak positions in nm were obtained from converting the fitted functions to a wavelength scale using $F(\ ) = (dN/d\ ) = {}^{-2}(dN/d\bar{\nu}) = {}^{-2}F(\bar{})$, with in m and $\bar{}$ in m^{-1} (Seliger, 1978).

Ca^{2+}-discharged obelin exhibits less spectral change with time than Ca^{2+}-discharged aequorin. Fig. 7.5 shows the TRES for Ca^{2+}-discharged obelin at various times after

excitation. The main (low energy) band (19070(50) cm^{-1} at 25 ps) shifts ~230(30) cm^{-1}, with a 1/e lifetime of approximately 190 ps, with a slower (~4 ns) further shift of 100(10) cm^{-1}. In addition there is a small high energy band (22770(50) cm^{-1} at 25 ps), that shifts ~490(50) cm^{-1} in 200 ps. This band lies between the two bands of Ca^{2+}-discharged aequorin. A band with higher energy (> 24000 cm^{-1}) may be present, but must then be very shortlived.

This is verified by an experiment using < 3 ps resolution in Fig. 7.6. This figure shows the results of fitting the fluorescence decay data with a four-component sequential model. The evolution of the initial Ca^{2+}-discharged obelin spectrum (dashed black curve in Fig. 7.6) to the second spectrum occurs on a time scale that is on the limit of the time resolution of the setup. As a consequence, both the time and spectrum of this initial component are not determined very accurately. It is however clear that the Ca^{2+}-discharged obelin spectrum shows significant intensity up to at least 24400 cm^{-1} (~300 cm^{-1} resolution). The second spectrum, peaking at 20000 cm^{-1}, evolves into a spectrum peaking at 19660 cm^{-1} in 22(1) ps, and then into the final emitting state at 19400 cm^{-1} in 423(17) ps. Values in parentheses are standard errors obtained from the fit. The fluorescence lifetime of the final emitting species is ~4 ns. The streak camera setup is not very sensitive for the amplitude and lifetime of fluorescence decays longer that 1 ns (for details see (van Stokkum ***et al.***, 2008)). This is probably why the amplitude of the final emitting species is higher than that of the third species. The presence of a ~4 ns fluorescence decay time is confirmed by time-correlated single-photon counting experiments using the setup described in (van Oort ***et al.***, 2007; Borst ***et al.***, 2005) (data not shown).

The spectral evolution of Ca^{2+}-discharged aequorin on this fast timescale is very different. The initial fluorescence emission spectrum of aequorin red-shifts from 25400 cm^{-1} to 23000 cm^{-1} in 12.0(0.1) ps (black curve in Fig. 7.6), and then further to the final emitting state at 21300 cm^{-1} in 164(3) ps. The fluorescence lifetime of the final emitting state is ~4 ns, again confirmed by time-correlated single-photon counting experiments.

Most published spectra are in units of photons/wavelength interval versus wavelength. For comparison, the wavenumber maxima $\bar{\nu}_M$ in the present results can be converted to the equivalent wavelength maximum, λ_M by the expression (Seliger, 1978):

$$\bar{\nu}_M = \bar{\nu}_M^{-1}\left[1 - 0.36\left(\frac{FWHM}{\bar{\nu}_M}\right)^2\right] \qquad (7.1)$$

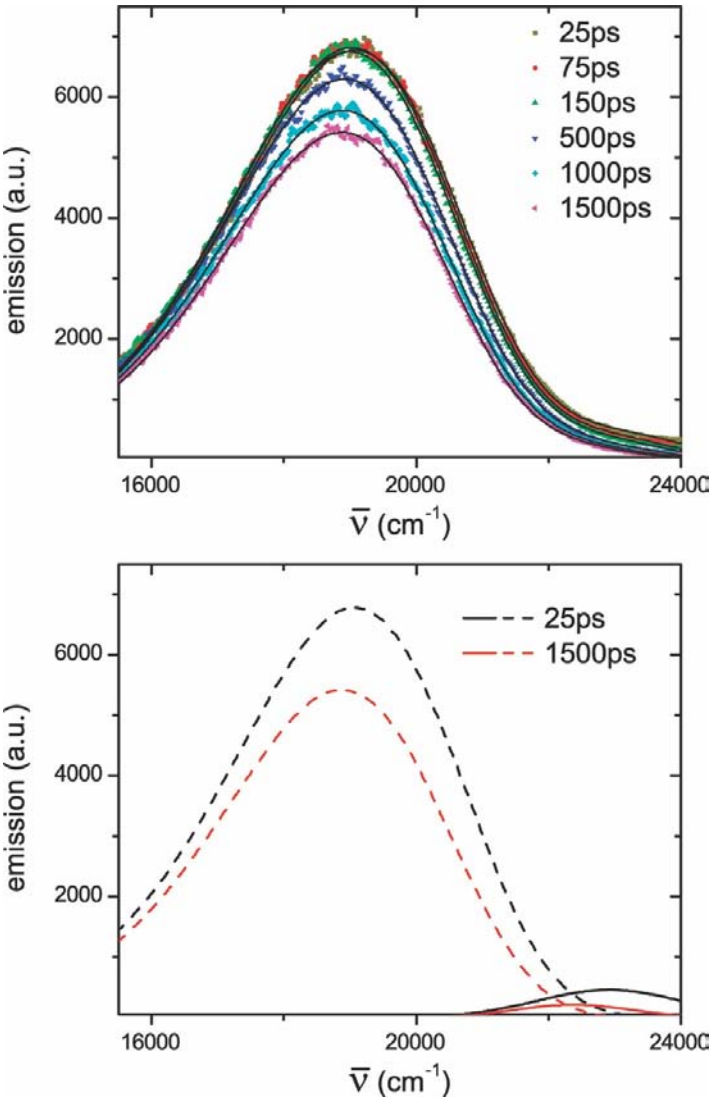

Figure 7.5 Time-resolved emission spectra of Ca^{2+}-discharged obelin at various times after excitation. The spectrum at each time is fitted as a sum of a log-normal and Gaussian function. The lower panel shows the two functions at 25 ps and 1.5 ns after excitation. At 25 ps the log-normal function peaks at 19000 cm^{-1} (517 nm), and the Gaussian function at 22900 cm^{-1} (435 nm). At 1.5 ns this is 18900 cm^{-1} (522 nm) and 22400 cm^{-1} (446 nm). The peak positions in nm were obtained from converting the fit functions to a wavelength scale, see legend of Figure 7.4.

in which FWHM is the full width at half maximum of the spectral (Gaussian) band. Although this equation is formally not correct for log-normal distributions, in practice it provides accurate results. For our fits it gives deviations of less than 1 nm, when compared with the maxima derived from conversion of the log-normal distribution from an energy to a wavelength scale, using $F(\ ) = (dN/d\ ) = {}^{-2}(dN/d\bar{\nu}) = {}^{-2}F(\bar{\ })$, with in m and $\bar{\ }$ in m^{-1} (Seliger, 1978).

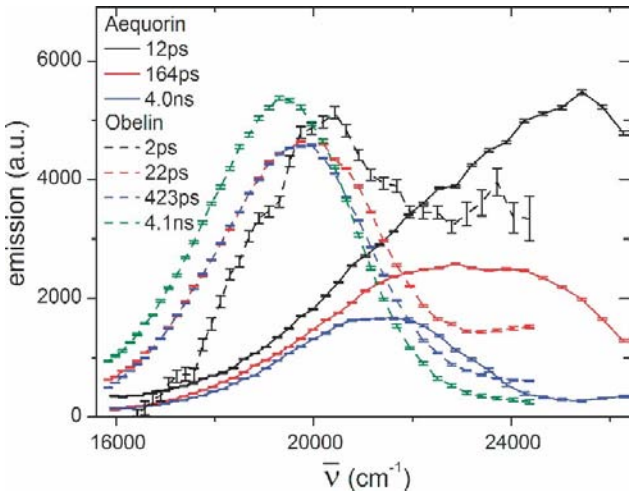

Figure 7.6 Fit results of streak data with a 180 ps time basis for evolution associated fluorescence decay spectra (I($\bar{\ }$)) of Ca^{2+}-discharged aequorin and obelin. The initial spectrum of Ca^{2+}-discharged obelin (black dashed line) is bimodal with significant intensity of the higher energy band in the same region as the initial spectrum of Ca^{2+}-discharged aequorin (black full line). The lower energy band of obelin after spectral deconvolution analysis (Fig. 7.4) overlaps with the 12 ps band from Ca^{2+}-discharged aequorin spectrum. It can be concluded that if a high-energy form of Ca^{2+}-discharged obelin is present shortly after excitation, it does not exist for longer than ~1 ps. The bars indicate standard errors.

In this work we have investigated the excited state dynamics of coelenteramide bound in the protein cavities of the calcium-discharged photoproteins aequorin and obelin. Excitation at 340 nm into the lowest energy absorption band, generates the neutral coelenteramide in its lowest electronically excited (S_1) state. In aqueous solution the fluorescence of free coelenteramide is quenched but in less polar solvents the inhomogeneously broadened spectrum has a maximum spanning the range 386-423 nm, depending on solvent polarity. Free coelenteramide in solutions that are made basic however, display a new fluorescence band at lower energy, spectral maxima 465–520 nm,

again depending on solvent polarity and also somewhat on basicity. This lower energy band is identified as the 5-phenoxy anion based on the fact that in the excited state, the p*K** of phenols is known to be 5 or more units more acidic than the ground state p*K* around 10, and this is where dissociation is likely to occur as the other phenol, the 2-hydroxybenzyl substituent, is not conjugated to the main ring system. The amide is not considered acidic although, using analogs with the phenoxy blocked say by methylation, or absent altogether, the amide proton can be dissociated with a very strong base such as tertiary butoxide in DMSO, to produce what is apparently the coelenteramide amide anion, having a fluorescence band maxima in the range 420-450 nm.

Therefore, the two excited states suggested as being formed in the binding site cavities of the Ca^{2+}-discharged photoproteins (Fig. 7.3 - 7.6), are first the neutral coelenteramide, which reverts to the anion on a picosecond time scale. Unfortunately, any corresponding rise in the longer wavelength band is not recoverable in the analysis suggesting an ultrafast kinetic process. In the binding site cavity of Ca^{2+}-discharged obelin (Fig. 7. 2), it is observed that His22 is in a strong H-bond interaction with the 5-phenolic oxygen, inferred by the N-O separation of 2.76 Å (Liu ***et al.,*** 2006). An elementary picture of such an H-bond is one in which partial positive charge is deposited from the donor oxygen onto the acceptor nitrogen, in other words, some partial dissociation of the phenol even in the ground state, so that in the excited state having the lowered p*K**, a more complete transfer of charge takes place. This idea is supported by a computational study (Tomilin ***et al.,*** 2008) and it has been suggested from properties of fluorescence models (Mori ***et al.,*** 2006), that a complete ion-pair is formed. In any case, the time–scale for such a proton shift within the already formed H-bond, must be sub-picosecond. The decay of the neutral band intensity as the excited anion band increases over a time about 45 ps (Fig. 7.4), is more likely a measure of the structural relaxation of the binding cavity, the origin of the inhomogeneous broadening of the protein-bound fluorescence (Petushkov ***et al.,*** 2003).

It has already been proposed that the bioluminescence reaction generates these same two excited states (Liu ***et al.,*** 2006). The structural evidence suggests that the primary excited species populated by the free energy released by the decarboxylation of the peroxy-coelenterazine in obelin, is the neutral coelenteramide which, as already described, rapidly dissociates to the excited anion by means of the proximity of His22 to the 5-phenol group.

This His22 is found in the same position in the structure of the cavity in both obelin and Ca^{2+}-discharged obelin, and also an equivalent His16 is in the same position in the aequorin cavity. Further evidence for the presence of two excited species comes from the bioluminescence of obelin, which reveals a small contribution at the high energy end, not seen in aequorin bioluminescence. It was suggested that the total bioluminescence spectrum results from a competition between the radiation rate from the primary neutral excited state and the rate of population of the excited anion.

Qualitative support for the idea that H-bonding to the oxygen at the 6-phenol position controls the emission spectra, has been obtained from study of a number of aequorin and obelin mutants (Ohmiya *et al.*, 1992; Deng *et al.*, 2001; Vysotski *et al.*, 2003; Malikova *et al.*, 2003; Stepanyuk *et al.*, 2005). The substitution of Trp92 in obelin and Trp86 in aequorin which are found not far away from the oxygen atom of the 6-(*p*-hydroxyphenyl) group of coelenterazine (Fig. 7.7, right) to phenylalanine, led to the appearance of bimodal bioluminescence with a prominent contribution from the 400-nm neutral species of coelenteramide. The substitution W92R in obelin gives an almost monomodal emission around 400 nm, with almost no contribution from the excited anion.

Fig. 7.7 (left) shows that aequorin has two H-bonds to the 6-phenol oxygen of coelenterazine. Replacing aequorin's Tyr82 by phenylalanine, thus removing that hydrogen bond, shifts its emissions to lower energy mimicking obelin, with bioluminescence maximum at 500 nm, fluorescence - at 495 nm. Likewise, changing obelin's Phe88 to tyrosine, adding the hydrogen bond as in aequorin, upshifts the energy levels near those from aequorin, the bioluminescence maximum now being at 453 nm and the fluorescence maximum at 487 nm.

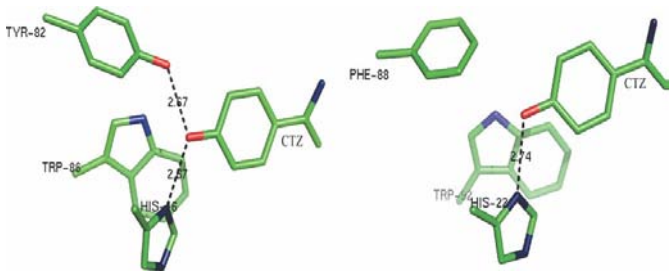

Figure 7.7 Interactions between the hydroxyl moiety of the 6-hydroxyphenyl substituent of coelenterazine within the binding cavity of aequorin (left) and obelin (right). Hydrogen bonds (dotted lines) were determined with the PyMOL program (DeLano, 2002). The distances are shown in Ångstroms.

It needs to be appreciated that the properties of the excited states and their corresponding emissions, will depend to some extent on the process of excitation. Fluorescence excitation (photon absorption) is a Franck-Condon transition, therefore the initial hot state is on the energy envelope of the cavity interactions which have to cool to the lowest level of the excited state. The bioluminescence energetic process goes by an adiabatic crossing of the reaction coordinate with the cavity relaxation energy envelope of the bound product coelenteramide, a crossing so as to direct the reaction energy to efficiently populate the excited state of the product (Ohmiya ***et al.***, 1992). Evidently, from the 25-nm shift of the fluorescence maxima over the bioluminescence, the final equilibrated state of Ca^{2+}-discharged obelin must lie at somewhat lower energy than the bioluminescence emitting state.

Rationalization of these perturbation effects needs to be done with caution in the absence of spatial structures for each of these mutants. Especially conjectural is any explanation of how the H-bonds control the probability of excited anion emission. It can be expected that a combination of the structural and fluorescence dynamics measurements, perhaps combined with theoretical computation (Tomilin ***et al.***, 2008), could lead to a quantitative account of how protein cavity structure quantitatively modulates the spectral properties.

Acknowledgements

This work was supported by NATO Collaborative Linkage Grant No. 979229, Grants of SB RAS and RFBR 09-04-12022, MCB program of RAS. B.v.O. was supported by “Stichting voor Fundamenteel Onderzoek der Materie (FOM)”, which is financially supported by the NWO, and by a Rubicon grant of NWO. E.V.E. was supported by Wageningen University Sandwich Ph.D.-Fellowship program. S.P.L was supported by Wageningen University Sandwich Ph.D.-Fellowship program, European Community (Marie Curie Research Training Network MRTN-CT-2005-019481 (From FLIM to FLIN), and Computational Science Grant 635.000.014 from the Netherlands Organization for Scientific Research.

Chapter 8

Fast kinetics of W92F obelin emitting species

Eremeeva, E.V.; Leferink, N.G.H.; Markova, S.V.; Visser, A.J.W.G.; van Berkel, W.J.H.; and Vysotski, E.S.

Abstract

Next to the usual blue emission around 480 nm, Ca^{2+}-regulated photoprotein obelin shows a small violet emission around 400 nm. From studies of W92F obelin, which displays an even stronger violet emission, it was argued that the calcium-induced bioluminescence originates from the coelenteramide phenolate ion-pair excited state with a small admixture of the neutral excited state. Here we applied rapid mixing stopped-flow spectroscopy to investigate the nature and fate of the emitting species of W92F obelin in further detail. The rise and fall kinetics observed revealed that the violet species is formed slower and decomposes earlier than the blue species. The rates of bioluminescence generation were moderately influenced by temperature, yielding activation energies of 59.9 ± 3.5 kJ mol^{-1} and 65.2 ± 4.8 kJ mol^{-1} for the violet and blue component of W92F obelin, respectively. The implications of these results for the photoprotein bioluminescence mechanism are discussed.

Keywords: bioluminescence, coelenterazine, obelin, fast kinetics

Abbreviations: DTT, dithiothreitol; EDTA, ethylenediaminetetraacetate; IPTG, isopropyl thio-β-D-galactopyranoside

Introduction

Obelin from *Obelia longissima* is a member of a family of Ca^{2+}-regulated photoproteins responsible for the bioluminescence of certain marine organisms, mostly coelenterates (Morin, 1974). The light-emitting reaction of these photoproteins involves calcium-induced oxidative decarboxylation of the oxygenated coelenterazine ligand, followed by emission of a photon (Cormier *et al.*, 1973). The bioluminescence spectra of the emitted light are broad with maxima around 465-495 nm depending on the type of photoprotein (Vysotski and Lee, 2004). The oxygen atoms released in the decarboxylation reaction are derived from 2-hydroperoxycoelenterazine, which is tightly non-covalently bound to the 22 kDa polypeptide chain (Head *et al.*, 2000; Liu *et al.*, 2000).

Coelenteramide, the product of the photoprotein-induced bioluminescence reaction, can exist in different ionic forms (Shimomura and Teranishi, 2000): a neutral species with a fluorescence emission maximum around 400 nm, the amide mono-anion with a maximum around 450 nm, the phenolate anion with a maximum around 480-490 nm, and the pyrazine-N(4) anion resonance form with a maximum in the 535-550 nm range (Fig. 8.1).

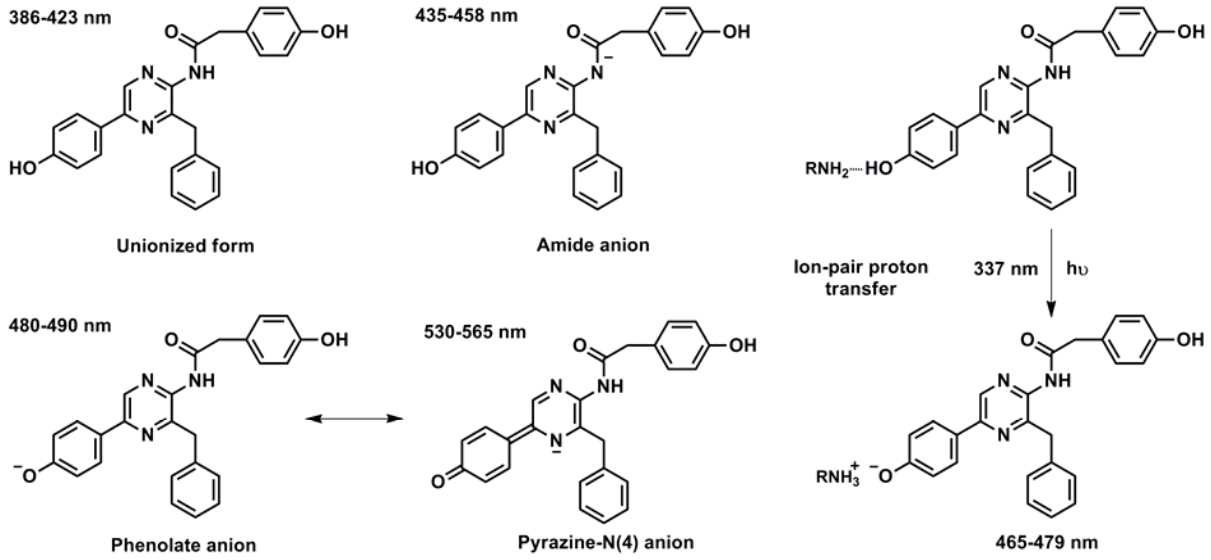

Figure 8.1 Coelenteramide forms.

Addition of *n*-butylamine to a benzene solution of coelenteramide produces a bimodal fluorescence spectrum with maxima at 397 and 467 nm. The maximum at 467 nm originates from an ion-pair excited state that has intramolecular charge-transfer character

(Imai *et al.*, 2001).

Originally, the amide anion excited state of coelenteramide was consented to be the primary chemical product generated in its excited state from which the photoprotein bioluminescence emission occurs (Shimomura and Teranishi, 2000). In this scenario, it would be energetically infeasible to populate the neutral excited state at higher energy. Later, based on fluorescence studies of the singlet-excited state of the phenolate form, it was concluded that the coelenteramide phenolate anion in ion pair contact with a histidine side chain is the light emitter in aequorin and obelin bioluminescence (Imai *et al.*, 2001; Kondo *et al.*, 2005; Mori *et al.*, 2006).

Next to the usual emission around 480 nm, obelin shows an emission band around 400 nm, presumably arising from the excited neutral species (Markova *et al.*, 2001). This violet emission is not observed in aequorin (Shimomura *et al.*, 1962). The W86F variant of aequorin has an enhanced bioluminescence emission at 400 nm (Ohmiya *et al.*, 1992) and the equivalent mutation in obelin, W92F, produces an even greater enhancement at 400 nm without changing the geometry of the photoprotein active site (Deng *et al.*, 2001). It was proposed that the violet emission of W92F obelin results from impaired hydrogen bonding between Phe92 and the phenolic moiety of 2-hydroperoxycoelenterazine. From further studies of W92F obelin, it was argued that the bioluminescence of WT obelin originates from the coelenteramide phenolate ion-pair excited state with a small admixture of the neutral excited state, both rapidly formed from the primary excited amide anion (Vysotski *et al.*, 2003). However, based on the crystal structure of Ca^{2+}-discharged obelin with coelenteramide bound, it was suggested that the primary excited species formed might be the neutral coelenteramide which rapidly dissociates to the phenolate anion (Liu *et al.*, 2006).

The purpose of this work was to investigate the fast kinetics of W92F obelin emitting species. The results show that the violet species is formed slower and decomposes earlier than the blue species. The implications of this finding for the photoprotein bioluminescence mechanism are discussed.

Materials and Methods

Site-directed mutagenesis - Site-directed mutagenesis was done on the template pET19-OL8 *E. coli* expression plasmid carrying the *Obelia longissima* WT apo-obelin gene (Markova *et al.*, 2001). The mutation, resulting in the amino acid substitution W92F, was carried out with the QuickChange site-directed mutagenesis kit (Stratagene, USA) according to the protocol supplied with the kit. The plasmid harboring the mutation was verified by DNA sequencing.

Protein expression and purification - The W92F mutant protein was expressed and purified as previously reported for WT recombinant obelin (Markova *et al.*, 2002; Illarionov *et al.*, 2000). For protein production, transformed *E. coli* BL21-Gold was cultivated with vigorous shaking at 37 ºC in LB medium containing 200 µg/ml ampicillin. Induction was initiated by adding 0.5 mM IPTG when the culture reached an OD_{600} of 0.5-0.6. After IPTG addition, cultivation was continued for 3 h. Most of the apo-photoprotein produced was accumulated in inclusion bodies.

W92F apo-protein was purified from inclusion bodies as described (Illarionov *et al.*, 2000). The apo-photoprotein obtained after ion exchange chromatography was concentrated by Amicon Ultra Centrifugal Filters (Millipore). To obtain active photoprotein, the concentrated W92F apo-photoprotein containing 6 M urea was diluted approximately 20-fold with a solution containing 5 mM DTT, 5 mM EDTA, 20 mM Tris-HCl pH 7.0 and molar excess of coelenterazine. The final preparation of protein was homogeneous according to SDS-PAGE and analytical gel filtration.

The coelenterazine concentration in the methanol stock solution was determined spectrophotometrically using a molar absorption coefficient at 435 nm of 9800 M^{-1} cm^{-1} (Shimomura, 2006). The concentration of apo-W92F was determined using a molar absorption coefficient at 280 nm of 34950 $M^{-1}cm^{-1}$, as calculated with ProtParam tool (http://us.expasy.org/tools/protparam-doc.html) which uses Edelhoch's method (Edelhoch, 1967).

Spectral analysis - Bioluminescence spectra were recorded with an AMINCO spectrofluorimeter (Thermo Spectronic, USA). Samples contained 1 mM EDTA, 20 mM

Tris-HCl pH 7.0. Bioluminescence was initiated by injection of $CaCl_2$ solution in the same buffer. The concentration of free calcium was around 0.5 μM to provide constant light level during the spectral scans.

Stopped-flow kinetics - An Applied Photophysics SX.18MV stopped-flow machine with a dead-time of $\leq$1ms was used for all measurements. Long pass filters (WG360 and GG455) and band pass filter (400 bp filter EALING 35-3201 T-BLQ (FWHM 10 nm)) were used to obtain signals from different parts of the bioluminescence spectrum. The temperature was controlled with a circulating water bath. Temperature was set at 20 °C, unless indicated otherwise. Protein syringe (2 ml) contained 1 mM EDTA and 9 μM W92F in 20 mM Tris-HCl, pH 7.0. Ca^{2+} syringe (2 ml) contained 2 mM $CaCl_2$ in 20 mM Tris-HCl, pH 7.0. Final concentrations after mixing were 0.5 mM EDTA, 4.5 μM W92F and 1 mM Ca^{2+}.

Rise and decay rate constants were calculated separately by one- or two-exponential fitting with SigmaPlot software using averaging of 3 shots with particular time scale.

Results and Discussion

W92F obelin displays a bimodal bioluminescence spectrum (Deng *et al.*, 2001): along with the emission around 480 nm, there is a relatively strong emission around 400 nm (Fig. 8.2).

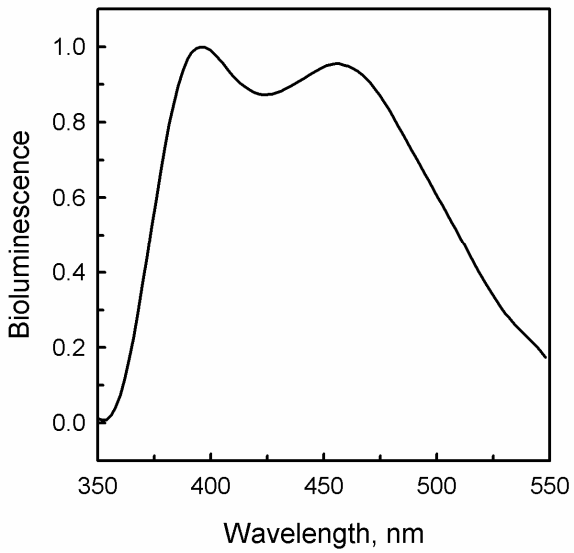

Figure 8.2 Bioluminescence spectrum of W92F obelin.

Figure 8.3 shows the kinetics of formation and decay of W92F obelin bioluminescence at 20 °C. The 400 band pass filter allows recording only the violet part of the signal originating from the neutral excited state (Fig. 8.3A) whereas the 455 long pass filter allows to specifically detect blue emission from the coelenteramide phenolate ion-pair excited state (Fig. 8.3B).

By fitting a single exponential to the rising phase of each light signal recorded with 0.025 sec time frame, we estimate that the rate constant for the rise of total W92F luminescence is 1350 ± 15 s^{-1} at 20°C. This value is 1.36 times higher than the one reported for W92F obelin before (Vysotski *et al.*, 2003). This could be due to different experimental conditions as well as due to different instruments: the one used in previous measurements had longer dead-time, prohibiting detection of part of the signal. The rise constants for the violet and blue components were calculated to be 760 ± 30 s^{-1} and 1100 ± 12 s^{-1} at 20°C, respectively.

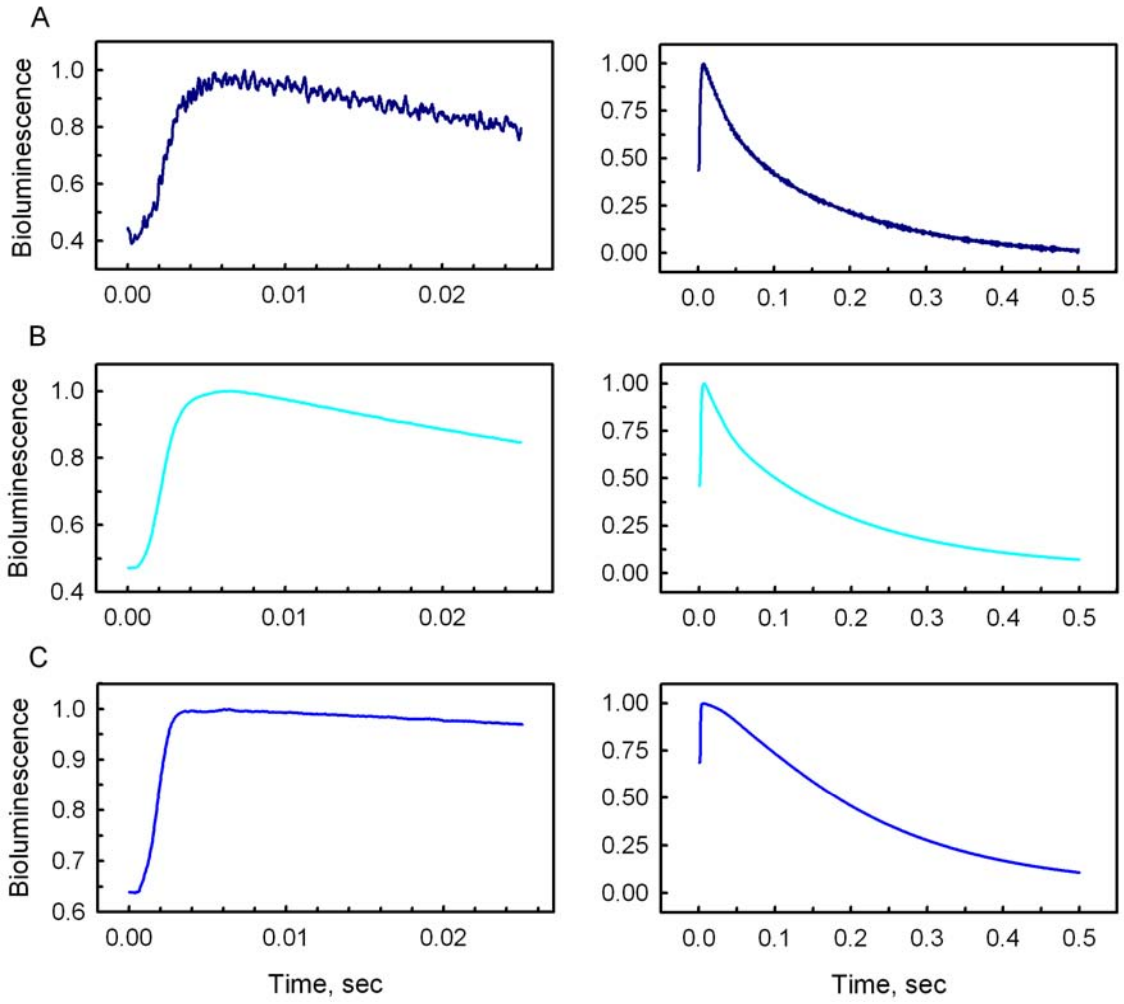

Figure 8.3 Stopped-flow kinetics of rise and fall bioluminescence intensity upon 1 mM Ca^{2+} addition to 4.5 µM W92F obelin mutant (0.025 sec time frame – left panel, 0.5 sec time frame – right panel) at 20°C. (A) recorded with 400 band pass filter - violet component; (B) recorded with 455 long pass filter - blue component; (C) recorded with 360 long pass filter - total light. The curves are individual shots.

The rate of bioluminescence rise of different components of W92F obelin is moderately influenced by temperature (Fig. 8.3, 8.4, 8.5). Rate constants for the formation of violet component are calculated to be 184 ± 5 s^{-1} at 4°C, 470 ± 10 s^{-1} at 12°C, and 760 ± 30 s^{-1} at 20°C; rate constants for the formation of blue component are 236 ± 3 s^{-1} at 4°C, 713 ± 14 s^{-1} at 12°C, and 1100 ± 12 s^{-1} at 20°C (Table 8.1). Assuming a linear Arrhenius correlation, activation energies for bioluminescence generation are estimated to be 59.9 ± 3.5 kJ mol^{-1} and 65.2 ± 4.8 kJ mol^{-1} for the violet and blue component, respectively.

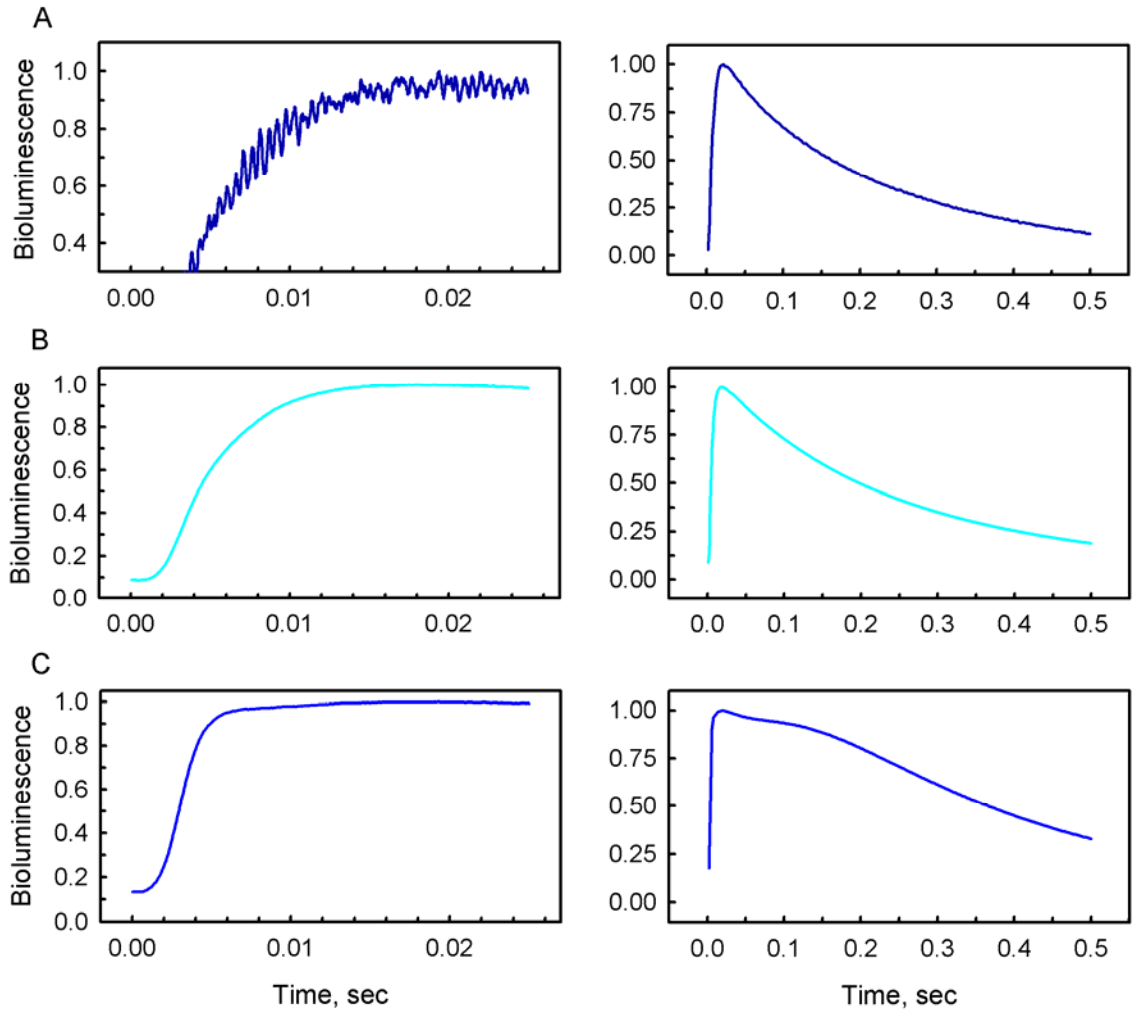

Figure 8.4 Stopped-flow kinetics of rise and fall bioluminescence intensity upon 1 mM Ca^{2+} addition to 4.5 µM W92F obelin mutant (0.025 sec time frame – left panel, 0.5 sec time frame – right panel) at 4°C. (A) recorded with 400 band pass filter - violet component; (B) recorded with 455 long pass filter - blue component; (C) recorded with 360 long pass filter - total light. The curves are individual shots.

Table 8.1 Rate constants for formation of W92F obelin bioluminescence

	4 °C	12 °C	20 °C
Violet component	184 ± 5 s^{-1}	470 ± 10 s^{-1}	760 ± 30 s^{-1}
Blue component	236 ± 3 s^{-1}	713 ± 14 s^{-1}	1100 ± 12 s^{-1}

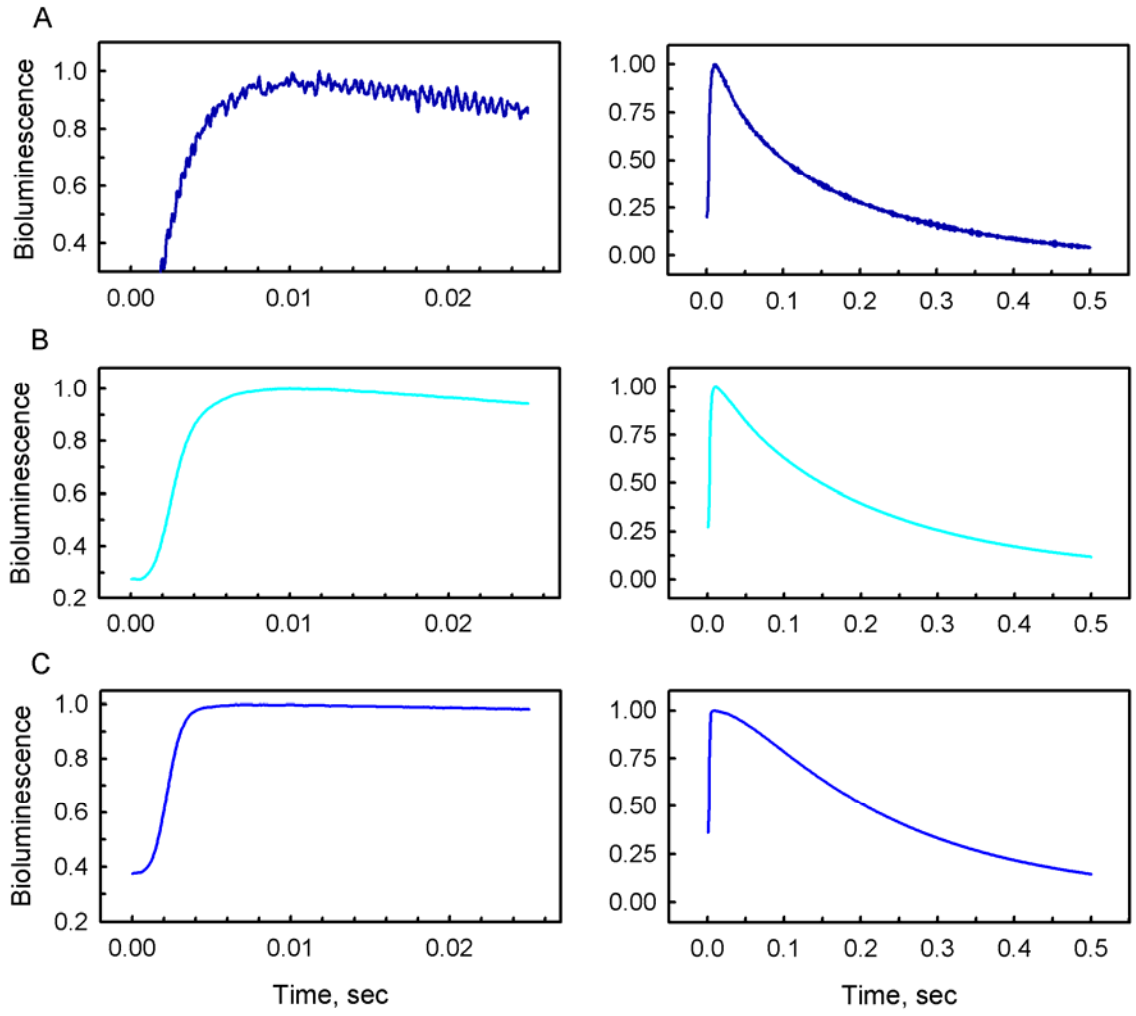

Figure 8.5 Stopped-flow kinetics of rise and fall bioluminescence intensity upon 1 mM Ca^{2+} addition to 4.5 µM W92F obelin mutant (0.025 sec time frame – left panel, 0.5 sec time frame – right panel) at 12°C. (A) recorded with 400 band pass filter - violet component; (B) recorded with 455 long pass filter - blue component; (C) recorded with 360 long pass filter - total light. The curves are individual shots.

The decay rate of W92F bioluminescence obtained by fitting a single exponential to the decay phase of the light signal recorded with 0.5 sec time frame is estimated to be 4.4 ± 0.2 s^{-1} at 20°C (Fig. 8.3). The decay rates of the separate violet and blue components are different from that calculated for the total light signal and cannot be characterized with single rate constants. This might be due to either heterogeneous protein populations or one population consisting of two conformations that slowly interconvert. Decay rate constants obtained from two exponential fitting were estimated to be 46 ± 0.5 s^{-1} and 7 ± 0.2 s^{-1} for the violet component, and 32 ± 2.5 s^{-1} and 5 ± 0.1 s^{-1} for the blue component, respectively.

Based on structural studies of photoproteins (Liu *et al.*, 2000; Liu *et al.*, 2003; Liu *et al.*, 2006) and chemical studies of coelenterazine and its analogs (McCapra and Chang, 1967; Shimomura, 2000), a proton-relay hypothesis has been formulated as to how Ca^{2+} binding could trigger the bioluminescence reaction and how the product excited states form (Vysotski and Lee, 2004; Vysotski and Lee, 2007). In Ca^{2+}-discharged obelin, a water molecule near the coelenteramide amide group seems favorably oriented to donate a proton to the dioxetanone anion prior to its decomposition to the excited state product (Liu *et al.*, 2006). Based on this assumption, the primary product of obelin was proposed to be the neutral excited coelenteramide (emission maximum in the range 390-405 nm). The mainly observed lower energy excited state (460-495 nm) might result from an excited state proton transfer from the 5-hydroxyl group of coelenteramide to a nearby histidine acting as proton acceptor. Thus, it was suggested that the bioluminescence spectrum of obelin results from a competition between the rate of formation of the primary neutral excited state and the rate of population of the excited anion.

Thermal decomposition studies of peroxidized coelenterazines have indicated that both homolytic and charge-transfer biradical mechanisms of dioxetanone decomposition are energetically feasible and that the balance between these pathways in the photoprotein active site depends on the protonation state of the peroxy substrate as modulated by the polarity and hydrogen bonding capacity of the protein environment (Isobe *et al.*, 2009). This proposition was supported by the properties of aequorin and obelin variants (Ohmiya *et al.*, 1992; Deng *et al.*, 2001). Replacement of Trp92 in obelin with Phe resulted in an enhanced bioluminescence emission at 400 nm due to the bicyclic ring of tryptophan being important for pK_a regulation (Dougherty, 1996).

The results presented in this paper show that the blue component of the W92F bioluminescence emission assigned to the coelenteramide phenolate anion species rises approximately 1.4 times faster and decays 1.4 times slower than the violet component which is attributed to the neutral species. This observation casts doubt on the previous explanations on the nature of the light emitter involved in photoprotein bioluminescence (Vysotski and Lee, 2007). Taking into account the results of thermal decomposition of peroxidized coelenterazines (Isobe *et al.*, 2009), it is reasonable to assume that a mixture of neutral and phenolate ion-pair excited states, probably resulting from different pathways of

dioxetanone decomposition, act as independent emitters in photoprotein bioluminescence. This idea is supported by the chemiluminescence properties of a coelenterazine model compound in protic solvent at -78 ºC (Usami and Isobe, 1996). Using low-temperature NMR, the structure of the photo-oxygenation product was established to be two peroxidic species. In addition, two independent pathways for decarboxylation were proposed: one is dioxetanone decomposition to emit light (400 nm) through neutral amide, the other is 2-hydroperoxide decomposition through anionic amide (with emission at 470 nm).

Acknowledgements

This work was supported by the Program of the Government of Russian Federation "Measures to Attract Leading Scientists to Russian Educational Institutions" (grant No 11. G34.31.058) and Wageningen University Sandwich PhD-Fellowship program.

Chapter 9

Summary and General Discussion

Summary

This thesis focuses on the structure-function relationship of the Ca^{2+}-regulated photoprotein obelin from the hydroid *Obelia longissima*.

Chapter 1 presents an introduction to Ca^{2+}-regulated photoproteins and their occurrence in a variety of marine organisms, mostly coelenterates. The spatial structure, proton-relay mechanism of bioluminescence, biological partners and applications of Ca^{2+}-regulated photoproteins are reviewed.

Chapter 2 reports on the various ligand-dependent conformational states of obelin. Fluorescence and far-UV circular dichroism data show that these states differ significantly in stability against thermal unfolding. Apo-obelin containing no ligand is an ensemble of interconverting conformational states and the least stable obelin form. Binding of coelenterazine and calcium considerably protect obelin from thermal unfolding.

Chapter 3 describes the characterization of coelenterazine binding to apo-obelin and apo-aequorin using the quenching of their tryptophan fluorescence. The apparent dissociation constants for the obelin and aequorin complexes are found to be in the low micromolar range. Stopped-flow measurements of fluorescence quenching show that coelenterazine binding is a millisecond-scale process. The subsequent formation of active photoprotein complex is far slower taking at least minutes. The conclusion is drawn that the rate-limiting step of active photoprotein formation is the conversion of coelenterazine into its peroxy derivative.

In **Chapter 4** the spectral properties of anaerobic coelenterazine and apo-obelin-coelenterazine complex and their reactivity with oxygen are investigated. Kinetic studies on the formation of active photoprotein from anaerobic apo-obelin-coelenterazine complex and oxygen suggest that bound coelenterazine might be a mixture of N7 protonated and C2 anionic forms. The possible role of His175 as proton shuttle in obelin complex formation is discussed.

Chapter 5 presents further study on the process of active photoprotein complex formation using quantum chemical calculations combined with kinetic and site-directed mutagenesis studies. A plausible mechanism of coelenterazine peroxy adduct formation within the apo-photoprotein globule is proposed and the possible role of some coelenterazine-binding cavity residues in this process is highlighted.

After fast binding to apo-obelin and subsequent conformational rearrangements of the protein, coelenterazine is proposed to become protonated at carbon C2 with the assistance of His175 acting as a proton shuttle. Then the bound coelenterazine slowly converts into 2-hydroperoxycoelenterazine in presence of oxygen; this process takes minutes and might require additional structural rearrangements of the protein. Van der Waals forces are assumed to play a key role in the process of coelenterazine activation. Tyr138 is proposed to provide the effective positioning of the oxygen molecule, increasing the probability of stable van der Waals complex formation between coelenterazine protonated at C2 and oxygen to yield 2-hydroperoxycoelenterazine.

In **Chapter 6** bioluminescent and spectroscopic properties of several obelin and aequorin coelenterazine-binding pocket mutants are summarized. Substitutions of His175, Trp179 and Tyr190 by residues with different side chain hydrogen bond donor-acceptor properties decrease the yield of active photoprotein complex and its bioluminescence activity. In contrast to wild-type, all mutants display a luciferase-like bioluminescence activity upon incubation with coelenterazine under Ca^{2+}-free conditions. Thus, His175, Trp179, and Tyr190 are proposed to orient 2-hydroperoxycoelenterazine in the binding cavity by forming a proper hydrogen bond network for substrate stabilization.

Chapter 7 describes a fluorescence relaxation spectroscopy study on the excited state dynamics of the calcium-discharged photoproteins aequorin and obelin. Two excited states are confirmed to be formed in the coelenterazine-binding cavity, the first one representing the neutral coelenteramide which reverts to the anionic state on a picosecond time scale.

Chapter 8 presents a further study on the nature of light emitters involved in photoprotein bioluminescence. Using rapid mixing stopped-flow kinetics it is demonstrated that the bimodal bioluminescence of the W92F obelin variant can be employed to determine the rate constants for the formation of neutral and phenolate anion emitting species. It is proposed that the neutral and phenolate excited states are independent emitters in photoprotein bioluminescence originating from different pathways of dioxetanone decomposition.

General discussion

Ca^{2+}-regulated photoproteins

Ca^{2+}-regulated photoproteins are attractive analytical tools for many areas of research. Due to the high sensitivity of the bioluminescence signal, photoprotein applications allow monitoring changes in calcium concentrations from 10^{-7} to 10^{-3} M with no need of external illumination. Detailed insight into the mechanisms of active photoprotein complex formation and bioluminescence provides the fundamental basis for improving various assays involving photoproteins.

Ca^{2+}-regulated photoproteins consist of a single polypeptide chain of about 22 kDa to which the "pre-activated" coelenterazine, 2-hydroperoxycoelenterazine, is tightly bound (Shimomura and Johnson, 1978; Head *et al.*, 2000; Liu *et al.*, 2000). The bioluminescence reaction of photoproteins is triggered by calcium. Binding of this sensor ion induces the oxidative decarboxylation of 2-hydroperoxycoelenterazine with generation of protein-bound coelenteramide in its excited state, and subsequent production of blue light (λ_{max} = 465-495 nm). The tertiary structures of several photoproteins are known in atomic detail (e.g., Head *et al.*, 2000, Liu *et al.*, 2000), and significant insight has been attained into the mechanism of photoprotein bioluminescence (Fig. 1.9) (Vysotski and Lee, 2004; Vysotski and Lee, 2007). Ca^{2+}-regulated photoproteins are successfully applied as reporters or labels in various binding assays and are widely used to monitor calcium levels in biological systems (Roda *et al.*, 2004; Rowe *et al.*, 2009; Grienberger and Konnerth, 2012).

Conformational states of photoprotein obelin

According to its "circle of life" photoprotein obelin populates five conformational states: apo-protein, active photoprotein with bound 2-hydroperoxycoelenterazine, Ca^{2+}-discharged photoprotein containing coelenteramide and calcium, Ca^{2+}-discharged photoprotein containing coelenteramide, and apo-protein containing calcium (Fig. 2.1).

Previous attempts to solve the apo-obelin structure were not successful because no suitable crystals could be obtained. Results presented in **Chapter 2** shed light on the reason why apo-obelin is so difficult to crystallize**.** By using fluorescence and far-UV CD spectroscopy it was found that the binding of different ligands considerably stabilizes

obelin against thermal unfolding. Apo-obelin containing no ligand turned out to be an ensemble of conformational states and the least stable obelin form. Our results suggest that the artificially produced apo-protein might not represent the natural state of obelin in *Obelia* cells and that binding of coelenterazine is required to protect the protein from degradation and aggregation.

Formation of 2-hydroperoxycoelenterazine

Recombinant apo-photoproteins can be converted to their active 2-hydroperoxy-coelenterazine-liganded forms upon incubation with coelenterazine, molecular oxygen and thiol-reducing agents under calcium-free conditions (Shimomura and Johnson, 1975). However, how the active photoprotein complex actually is formed has for a long time remained a black box.

Using the quenching of apo-photoprotein intrinsic fluorescence we could demonstrate that coelenterazine binding is a fast process, completed within the dead time of the stopped-flow instrument. Tryptophan fluorescence binding studies showed an apparent dissociation constant for the complex in the low micromolar range and also revealed that coelenterazine remains tightly associated with apo-photoprotein (**Chapter 3**). The successful purification of the anaerobic apo-obelin–coelenterazine complex allowed us to confirm that apo-photoprotein and coelenterazine form a tight complex before modification of coelenterazine by oxygen occurs (**Chapter 4**). According to the spectroscopic and kinetic data, bound coelenterazine might be a mixture of N7 protonated and C2 anionic forms. Further kinetic studies on the activation of apo-obelin and its selected mutants together with quantum chemical calculations allowed us to propose a mechanism of 2-hydroperoxycoelenterazine formation as well as the function of two key residues (His175 and Tyr138) in this process (**Chapter 5**). After initial binding of coelenterazine, apo-obelin undergoes conformational rearrangements, involving coelenterazine-binding cavity formation along with coelenterazine protonation at carbon C2. His175 presumably acts as a proton shuttle in the latter process. The next step is the oxygen-dependent conversion of bound coelenterazine into 2-hydroperoxycoelenterazine; this process takes minutes and might require additional structural rearrangements. Van der Waals complex formation

between coelenterazine protonated at C2 and oxygen might be stimulated with assistance of Tyr138 (Fig. 5.13).

The slow reaction with oxygen (Shimomura and Johnson, 1975; **Chapter 4 and 5**) discriminates Ca^{2+}-regulated photoproteins from other monooxygenases and oxidases which typically react extremely fast with oxygen (Massey, 1994). Site-directed mutagenesis studies on various flavin-dependent enzymes revealed that substitution of just one amino acid residue can change the rate for flavin oxidation up to 8000-fold (Zhao *et al.*, 2008; Leferink *et al.*, 2009). A positive charge around the flavin binding site was shown to play an important role in enhancing the oxygen reactivity in several flavoprotein oxidases (Klinman, 2007; Jorns *et al.*, 2010; Gadda, 2012) and in N-hydroxylating monooxygenase SidA (Franceschini *et al.*, 2012). However, as demonstrated for dihydroorotate dehydrogenase, simply placing a positive charge near flavin N5 does not guarantee an increase in oxygen reactivity (McDonald *et al.*, 2011).

Oxygen may diffuse into an enzyme active site via discrete channels and this step can be rate-limiting (Klinman, 2007). Recently, multiple diffusion pathways were proposed for the delivery of oxygen into the active sites of several flavoenzymes (Baron *et al.*, 2009). Close study of oxygen diffusion patterns during photoprotein formation as well as modeling of the local environment of the C2-carbon of coelenterazine might help to explain why the rate of coelenterazine oxidation is so slow and provide clues how to improve it.

Stabilization of 2-hydroperoxycoelenterazine

According to the obelin three-dimensional structure (Liu *et al.*, 2000), the side chains of His175, Trp179, and Tyr190 and some other residues form hydrogen bonds with bound 2-hydroperoxycoelenterazine (Fig. 1.4). Site-directed mutagenesis studies revealed that replacement of His175, Trp179, or Tyr190 in most cases leads to significant loss of photoprotein bioluminescence activity and appearance of luciferase-like bioluminescence activity, hardly present in wild-type obelin (**Chapter 6**). The conclusion was drawn that His175, Trp179, and Tyr190 position the 2-hydroperoxycoelenterazine in the binding cavity and provide the H-bond network for stabilizing the substrate.

Flavin-dependent monooxygenases also form and stabilize peroxy intermediates to oxygenate a substrate, while flavoprotein oxidases produce hydrogen peroxide without

detectable stabilization of a peroxy adduct (Chaiyen et al., 2012). Flavoprotein monooxygenases such as Baeyer–Villiger monooxygenases, flavin-containing monooxygenases, and N-hydroxylating monooxygenases require the presence of bound $NADP^+$ in their oxidative half-reaction to stabilize the peroxyflavin (van Berkel, 2006). In bacterial luciferase, the peroxyflavin is remarkably stable in the absence of the long chain aldehyde substrate, allowing its isolation (Hastings ***et al.***, 1973) and characterization by ^{13}C NMR (Vervoort ***et al.***, 1986).

Ca^{2+}-regulated photoproteins go much further: they stabilize the 2-hydroperoxy-coelenterazine within the protein active site so effectively that the activated protein can be kept for months and used as a tool for various assays. ***Renilla*** luciferase (RLuc) is another bioluminescent protein using coelenterazine as a substrate (Karkhanis and Cormier, 1971). While in the photoproteins the peroxy anion must be quickly protonated, in RLuc, it is unstable and immediately undergoes cyclization to a dioxetanone with further decomposition to coelenteramide, CO_2 and light (Hart ***et al.***, 1978). So for the luciferases, there should be a different hydrogen bond network around the peroxy anion, one that favors its decomposition, rather than effective stabilization via protonation as in the photoproteins.

The different stabilization of oxygenated coelenterazine in bioluminescent proteins has an ecological meaning: species containing luciferases glow continuously in the presence of oxygen rather than producing discrete photoprotein flashes under Ca^{2+} release. In general, bioluminescent glows are thought to function as attractant signals, and sudden flashes are thought to be repellent (Haddock ***et al.,*** 2010). Such difference in bioluminescence kinetics between luciferases and photoproteins also provides diversity in their analytical applications. Thus, luciferases can conveniently be applied for ***in vivo*** imaging or in reporter assays, while Ca^{2+}-regulated photoproteins are extensively used in various immunoassays and DNA hybridization assays as well as Ca^{2+}-indicators.

RLuc has a α/β-hydrolase fold (Loening ***et al.,*** 2007), which is different from the compact globular structure of photoproteins with helix-turn-helix motifs (Head ***et al.***, 2000; Liu ***et al.***, 2000). Although rich in aromatic residues, the RLuc active site lacks the catalytic triad of photoproteins (Woo ***et al.,*** 2008), and especially a residue equivalent to Tyr190, which stabilizes the 2-hydroperoxycoelenterazine in obelin by direct H-bonding. Additional work is needed to reveal the factors that determine the stability of oxygen adducts in

photoproteins. This knowledge might help to stabilize the peroxy intermediate in proteins that only transiently form such adduct and might especially be useful in cases where the reaction needs to be optimized towards the synthesis of valuable oxyfunctionalized products.

Light emitters in photoprotein bioluminescence

The nature of light emitters involved in photoprotein bioluminescence has been an intriguing topic for researches for years. Based on site-directed mutagenesis and structural studies of photoproteins (Liu *et al.*, 2000; Deng *et al.*, 2001; Liu *et al.*, 2003; Vysotski *et al.*, 2003; Liu *et al.*, 2006) together with chemical studies of coelenterazine model compounds (McCapra and Chang, 1967; Shimomura and Teranishi, 2000; Imai *et al.*, 2001; Kondo *et al.*, 2005; Mori *et al.*, 2006) it was suggested that photoprotein-bound coelenteramide populates at least two excited states, the neutral and phenolate anionic state. The total bioluminescence spectrum results from a competition between the radiation rate from the primary neutral excited state and the rate of population of the excited phenolate anion (Fig. 1.9) (Vysotski and Lee, 2007).

The results of excited state dynamics of photoprotein-bound coelenteramide suggested neutral coelenteramide to be the first excited state formed, which reverts to the anion on a picosecond time scale (**Chapter 7**). However, rapid mixing stopped-flow spectroscopy showed that in W92F obelin the blue component of bioluminescence corresponding to the coelenteramide phenolate anion species rises faster and decays slower than the violet component which is attributed to the neutral species (**Chapter 8**). Thus the mixture of neutral and phenolate excited states could originate from different pathways of dioxetanone decomposition (Isobe *et al.*, 2009) and consequently might act as independent emitters in photoprotein bioluminescence. Further spectroscopic studies combined with theoretical computation could lead to better understanding of the origin of light emitters involved in photoprotein bioluminescence.

In conclusion the knowledge obtained in this thesis improves our insight into the process of active photoprotein complex formation and the nature of light emitting species involved in photoprotein bioluminescence. Ca^{2+}-regulated photoproteins can be regarded as cofactor-independent monooxygenases. However, they have a few unique distinctive properties such as the slow rate of substrate oxygenation and the ability to effectively stabilize the peroxy adduct. Knowledge on the mechanism of formation and stabilization of the 2-hydroperoxycoelenterazine adduct in the active site of photoproteins obtained in this thesis can be applied for studies of other monooxygenases, for example, in the field of oxygen reaction rate control or stabilization of oxygenated intermediates. The results emerged in this thesis also provide a solid basis for further studies on different aspects of photoprotein bioluminescence and may be useful for improving *in vivo* and *in vitro* assays involving photoproteins.

References

A

Adamczyk, M., Moore, J.A. and Shreder, K., (2002) Dual analyte detection using tandem flash luminescence. *Bioorg. Med. Chem. Lett.*, 12, 395–398.

Aghamaali, M.R., Jafarian, V., Sariri, R., Molakarimi, M., Rasti, B., Taghdir, M., Sajedi, R.H. and Hosseinkhani, S., (2011) Cloning, sequencing, expression and structural investigation of mnemiopsin from *Mnemiopsis leidyi*: an attempt toward understanding Ca^{2+}-regulated photoproteins. *Protein J.*, 30, 566-574.

Allen, D.G., Blinks, J.R. and Prendergast, F.G., (1977) Aequorin luminescence: Relation of light emission to calcium concentration—a calcium-independent component. *Science*, 195, 996–998.

Appel, F. Gross, E.K.U. and Burke, K., (2003) Excitations in time-dependent density-functional theory. *Phys. Rev. Lett.*, 90, 043005.

B

Bakayan, A., Vaquero, C.F., Picazo, F. and Llopis, J., (2011) Red fluorescent protein-aequorin fusions as improved bioluminescent Ca^{2+} reporters in single cells and mice. *PLoS One*, 6, e19520.

Baker, J., (1986) An algorithm for the location of transition states. *J. Comp. Chem.*, 7, 385-395.

Baron, R., Riley, C., Chenprakhon, P., Thotsaporn, K., Winter, R.T., Alfieri, A., Forneris, F., van Berkel, W.J.H., Chaiyen, P., Fraaije, M.W., Mattevi, A. and McCammon, J.A., (2009) Multiple pathways guide oxygen diffusion into flavoenzyme active sites. *Proc. Natl. Acad. Sci. USA*, 106, 10603-10608.

Barone, V., Cossi, M., Mennucci, B. and Tomasi, J., (1997) A new definition of cavities for the computation of solvation free energies by the polarizable continuum model. *J. Chem. Phys.*, 107, 3210-3221.

Baubet, V., Le Mouellic, H., Campbell, A.K., Lucas-Meunier, E. and Fossier P., (2000) Chimeric green fluorescent protein-aequorin as bioluminescent Ca^{2+} reporters at the single-cell level. *Proc. Natl. Acad. Sci. USA*, 97, 7260–7265.

Becke, A.D., (1993) Density-functional thermochemistry. III. The role of exact exchange. *J. Chem. Phys.*, 98, 5648-5652.

Becktel, W.J. and Schellman, J.A., (1987) Protein stability curves. *Biopolymers*, 26, 1859-1877.

Blinks, J.R., Wier, W.G., Hess, P. and Prendergast, F.G., (1982) Measurement of Ca^{2+}

concentrations in living cells. *Prog. Biophys. Mol. Biol.*, 40, 1-114.

Bollen, Y.J.M., Nabuurs, S.M., van Berkel, W.J.H. and van Mierlo, C.P.M., (2005) Last in, first out: the role of cofactor binding in flavodoxin folding. *J. Biol. Chem.*, 280, 7836–7844.

Bollen, Y.J., Westphal, A.H., Lindhoud, S., van Berkel, W.J.H. and van Mierlo, C.P.M., (2012) Distant residues mediate picomolar-binding affinity of a protein cofactor. *Nat. Commun.*, doi: 10.1038/ncomms2010.

Bondar, V.S., Frank, L.A., Malikova, N.P., Inzhevatkin, E.V., Illarionova, V.A. and Vysotski, E.S., (1999) Bioluminescent activity of the recombinant obelin after chemical modification of histidine and cysteine residues. In *Bioluminescence and Chemiluminescence: Perspectives for the 21st century* (Roda, A., Pazzagli, M., Kricka, L.J. and Stanley, P.E., eds.). John Wiley & Sons, Chichester, pp. 400–403.

Borst, J.W., Hink, M.A., van Hoek, A. and Visser, A.J.W.G., (2005) Effects of refractive index and viscosity on fluorescence and anisotropy decays of enhanced cyan and yellow fluorescent proteins. *J. Fluoresc.*, 15, 153-160.

Burstein E.A. and Emelyanenko V.I., (1996) Log-normal description of fluorescence spectra of organic fluorophores. *Photochem. Photobiol.*, 64, 316-320.

C

Campbell, A.K., (1974) Extraction, purification and properties of obelin, the calcium – activated protein from the hydroid *Obelia geniculate. Biochemistry*, 143, 411-418.

Casida, M.E. and Chong D.P., (1995) Time-dependent density functional response theory for molecules. In *Recent Advances in Density Functional Methods* (Chong, D.P., eds.), World Scientific, Singapore, pp. 155.

Casida, M.E., Jamorski, C., Casida, K.E. and Salahub, D.R., (1998) Molecular excitation energies to high-lying bound states from time-dependent density-functional response theory: Characterization and correction of the time-dependent local density approximation ionization threshold. *J. Chem.Phys.*, 108, 4439-4449.

Casida, M.E. and Salahub, D.R., (2000) Asymptotic correction approach to improving approximate exchange-correlation potentials: time dependent density-functional theory calculations of molecular excitation spectra. *J. Chem. Phys.*, 113, 8918-8935.

Chaiyen, P., Fraaije, M.W. and Mattevi, A., (2012) The enigmatic reaction of flavins with oxygen. *Trends Biochem. Sci.*, 37, 373-380.

Chung, L.W, Hayashi, S., Lundberg, M., Nakatsu, T. Kato, H. and Morokuma, K., (2008) Mechanism of efficient firefly bioluminescence via adiabatic transition state

and seam of sloped conical intersection. *J. Am. Chem. Soc.,* 130, 12880–12881.

Cormier, M.J., Hori, K., Karkhanis, Y.D., Anderson, J.M., Wampler, J.M., Morin, J.G. and Hastings, J.W., (1973) Evidence for similar biochemical requirements for bioluminescence among the coelenterate. *J. Cell Physiol.*, 81, 291-297.

Cossi, M., Barone, V., Cammi, R. and Tomasi, J., (1996) *Ab initio* study of solvated molecules: a new implementation of the polarizable continuum model. *Chem. Phys. Lett.*, 255, 327-335.

D

de la Fuente, S., Fonteriz, R.I., de la Cruz, P.J., Montero, M. and Alvarez, J., (2012) Mitochondrial free [Ca(2+)] dynamics measured with a novel low-Ca(2+) affinity aequorin probe. *Biochem. J.,* 445, 371-376.

DeLano, W. L., (2002) The PyMOL Molecular Graphics System, DeLano Scientific, San Carlos, CA.

Deng, L., Vysotski, E.S., Liu, Z.J., Markova, S.V., Malikova, N.P., Lee, J., Rose, J. and Wang, B.C., (2001) Structural basis for the emission of violet bioluminescence from a W92F obelin mutant. *FEBS Lett.,* 506, 281-285.

Deng, L., Markova, S.V., Vysotski, E.S., Liu, Z.J., Lee, J., Rose, J. and Wang, B.C., (2004) Crystal structure of a Ca^{2+}-discharged photoprotein: implications for mechanisms of the calcium trigger and bioluminescence. *J. Biol. Chem.,* 279, 33647-33652.

Deng, L., Vysotski, E.S., Markova, S.V., Liu, Z.J., Lee, J., Rose, J. and Wang, B.C., (2005) All three Ca^{2+}-binding loops of photoproteins bind calcium ions: The crystal structures of calcium-loaded apo-aequorin and apo-obelin. *Protein Sci.,* 14, 663-675.

Dougherty, D.A., (1996) Cation-pi interactions in chemistry and biology: a new view of benzene, Phe, Tyr, and Trp. *Science*, 271, 163-168.

Dreuw, A., Weisman, J.L. and Head-Gordon, M., (2003) Long-range charge transfer excited states in time-dependent density functional theory require non-local exchange. *J. Chem. Phys*., 119, 2943-2946.

E

Entsch, B. and van Berkel, W.J.H., (1995) Structure and mechanism of para-hydroxybenzoate hydroxylase. *FASEB J.*, 9, 476-483.

Edelhoch, H., (1967) Spectroscopic determination of tryptophan and tyrosine in proteins. *Biochemistry,* 6, 1948-1954.

Eremeeva, E.V., Markova, S.V., Frank, L.A. and Vysotski, E.S., (2007) The main function of His175, Trp179 and Tyr190 residues of the obelin binding site is to stabilize the hydroperoxy-coelenterazine intermediate. In *Bioluminescence & Chemiluminescence: Chemistry, Biology and Application* (Szalay, A.A.., Hill, P.J., Kricka, L.J. and Stanley, P.E., eds.), Singapore, World Scientific, pp. 7-10.

Eremeeva, E.V., Markova, S.V., Westphal, A.H., Visser, A.J., van Berkel, W.J.H. and Vysotski, E.S., (2009) The intrinsic fluorescence of apo-obelin and apo-aequorin and use of its quenching to characterize coelenterazine binding. *FEBS Lett.*, 583, 1939-1944.

F

Fagan, T.F., Ohmiya, Y., Blinks, J.R., Inouye, S. and Tsuji, F.I., (1993) Cloning, expression and sequence analysis of cDNA for the Ca(2+)-binding photoprotein, mitrocomin. *FEBS Lett.*, 1, 301-305.

Fetzner, S., (2002) Oxygenases without requirement for cofactors or metal ions. *Appl. Microbiol. Biotechnol.*, 60, 243-257.

Fetzner, S. and Steiner, R.A., (2010) Cofactor-independent oxidases and oxygenases. *Appl. Microbiol. Biotechnol*., 86, 791-804.

Fisher, W.R., Taniuchi, H. and Anfinsen, C.B., (1973) On the role of heme in the formation of the structure of cytochrome *c. J. Biol. Chem.*, 248, 3188–3195.

Franceschini, S., Fedkenheuer, M., Vogelaar, N.J., Robinson, H.H., Sobrado, P. and Mattevi, A., (2012) Structural insight into the mechanism of oxygen activation and substrate selectivity of flavin-dependent N-hydroxylating monooxygenases. *Biochemistry*, 51, 7043-7045.

Fujimoto, K., Hayash, S., Hasegawa, J. and Nakatsuji, H., (2007) Theoretical studies on the color-tuning mechanism in retinal proteins. *J. Chem. Theory Comput.*, 3, 605-618.

G

Gadda, G. (2012) Oxygen activation in flavoprotein oxidases: the importance of being positive. *Biochemistry*, 51, 2662-2669.

Goto, T. (1968) Chemistry of bioluminescence. *Pure Appl. Chem.*, 17, 421-441.

Goto, T., Inoue, S. and Sugiura, S., (1968) *Cypridina* bioluminescence. IV. Synthesis and chemiluminescence of 3,7-dihydroimidazo[1,2-a]pyrazin-3-one and its 2-methyl derivative. *Tetrahedron Lett.*, 3873-3876.

Gross, E.K.U. and Kohn, W., (1990) Time-dependent density functional theory. *Ad. Quantum Chem.*, 21, 255-291.

Grienberger, C. and Konnerth, A., (2012) Imaging calcium in neurons. *Neuron*, 73, 862-885.

H

Haddock, S.H., Moline, M.A. and Case, J.F., (2010) Bioluminescence in the sea. *Ann. Rev. Mar. Sci.*, 2, 443-493.

Hart, R.C., Stempel, K.E., Boyer, P.D. and Cormier, M.J. (1978) Mechanism of the enzyme-catalyzed bioluminescent oxidation of coelenterate-type luciferin. *Biochem. Biophys. Res. Commun*., 81, 980-986.

Hastings, J.W. and Gibson, Q.H., (1963) Intermediates in the bioluminescent oxidation of reduced flavin mononucleotide. *J. Biol. Chem.*, 238, 2537-2554.

Hastings, J.W. and Morin, J.G., (1969) Calcium-triggered light emission in *Renilla*. A unitary biochemical scheme for coelenterate bioluminescence. *Biochem. Biophys. Res. Commun*., 37, 493-498.

Hastings, J.W., Balny, C., Peuch, C.L. and Douzou, P., (1973) Spectral properties of an oxygenated luciferase-flavin intermediate isolated by low-temperature chromatography. *Proc. Natl. Acad. Sci. USA*, 70, 3468-3472.

Hastings, J.W., (1996) Chemistries and colors of bioluminescent reactions: a review. *Gene*, 173, 5-11.

Head, J.F., Inouye, S., Teranishi, K. and Shimomura, O., (2000) The crystal structure of the photoprotein aequorin at 2.3 Å resolution. *Nature*, 405, 372-376.

Henkelman, G., Uberuaga, B.P. and Jónsson, H., (2000) A climbing image nudged elastic band method for finding saddle points and minimum energy paths. *J. Chem. Phys.*, 113, 9901.

Hohenberg, P. and Kohn, W., (1964) Inhomogeneous electron gas. *Phys. Rev. B*, 136, 864-871.

Hori, K., Wampler, J.E., Matthews, J.C. and Cormier, M.J., (1973) Identification of the product excited states during the chemiluminescent and bioluminescent oxidation of *Renilla* (sea pansy) luciferin and certain of its analogs. *Biochemistry*, 12, 4463–4468.

Hori, K., Anderson, J.M., Ward, W.W. and Cormier, M.J., (1975) *Renilla* luciferin as the substrate for calcium induced photoprotein bioluminescence. Assignment of

luciferin tautomers in aequorin and mnemiopsis. *Biochemistry*, 14, 2371-2376.

Hori, K., Charbonneau, H., Hart, R.C. and Cormier, M.J., (1977) Structure of native *Renilla reniformis* luciferin. *Proc. Natl. Acad. Sci. USA,* 74, 4285-4287.

Hsu, C.-P., Hirata, S. and Head-Gordon, M., (2001) Excitation energies from time-dependent density functional theory for linear polyene oligomers: butadiene to decapentaene. *J. Phys. Chem. A*, 105, 451-458.

I

Illarionov, B.A., Bondar, V.S., Illarionova, V.A. and Vysotski, E.S., (1995) Sequence of the cDNA encoding the Ca(2+)-activated photoprotein obelin from the hydroid polyp *Obelia longissima*. *Gene*, 153, 273-274.

Illarionov, B.A., Frank, L.A., Illarionova, V.A., Bondar, V.S., Vysotski, E.S. and Blinks, J.R., (2000) Recombinant obelin: cloning and expression of cDNA, purification and characterization as a calcium indicator. *Methods Enzymol.,* 227, 223-249.

Imai, Y., Shibata, T., Maki, S., Niwa, S., Ohashi, M. and Hirano T., (2001) Fluorescence properties of phenolate anions of coelenteramide analogues: the light-emitter structure in aequorin bioluminescence. *Photochem. Photobiol. A.*, 146, 95–107.

Inouye, S., Noguchi, M., Sakaki, Y., Takagi, Y., Miyata, T., Iwanaga, S., Miyata, T. and Tsuji, F.I., (1985) Cloning and sequence analysis of cDNA for the luminescent protein aequorin. *Proc. Natl. Acad. Sci. USA*, 82, 3154-3158.

Inouye, S., Sakaki, Y., Goto, Y. and Tsuji, F.H., (1986) Expression of apoaequorin complementary DNA in *Escherichia coli*. *Biochemistry,* 25, 8425-8429.

Inouye S. and Tsuji, F.I., (1993) Cloning and sequence analysis of cDNA for the Ca(2+)-activated photoprotein, clytins. *FEBS Lett.* 11, 343–346.

Isobe, H., Yamanaka, S., Kuramitsu, S., Yamaguchi, K., (2008) Regulation mechanism of spin-orbit coupling in charge-transfer-induced luminescence of imidazo-pyrazinone derivatives. *J. Am. Chem. Soc.*, 130, 132-149.

Isobe, H., Yamanaka, S., Okumura, M. and Yamaguchi, K., (2009) Theoretical investigation of thermal decomposition of peroxidized coelenterazines with and without external perturbations. *J. Phys. Chem. A,* 113, 15171-15187.

J

Jorns, M.S., Chen, Z.W. and Mathews, F.S., (2010) Structural characterization of

mutations at the oxygen activation site in monomeric sarcosine oxidase. *Biochemistry*, 49, 3631-3639.

K

Karkhanis, Y.D. and Cormier, M.J., (1971) Isolation and properties of *Renilla reniformis* luciferase, a low molecular weight energy conversion enzyme. *Biochemistry,* 10, 317-326.

Klinman, J.P., (2007) How do enzymes activate oxygen without inactivating themselves? *Acc. Chem. Res.*, 40, 325-333.

Knight, M.R., Campbell, A.K., Smith, S.M. and Trewavas, A.J., (1991) Transgenic plant aequorin reports the effects of touch and cold-shock and elicitors on cytoplasmic calcium. *Nature,* 352, 524-526.

Knight, M.R., Read, N.D., Campbell, A.K. and Trewavas, A.J., (1993) Imaging calcium dynamics in living plants using semi-synthetic recombinant aequorins. *J. Cell. Biol.,* 121, 83-90.

Koehorst, R.B.M., Laptenok, S., van Oort, B., van Hoek, A., Spruijt, R.B., van Stokkum, I.H., van Amerongen, H. and Hemminga, M., (2010) Profiling of dynamics in protein-lipid-water systems: A time-resolved fluorescence study of a model membrane protein with the label BADAN at specific membrane depths. *Eur. Biophys. J.*, 39, 647-656.

Kohn, W. and Sham, L.J., (1965) Self-consistent equations including exchange and correlation effects. *Phys. Rev. A*, 140, 1133-1138.

Kondo, H., Igarashi, T., Maki, S., Niwa, H., Ikeda, H. and Hirano T., (2005) Substituent effects on the kinetics for the chemiluminescence reaction of 6-arylimidazo[1,2-a]pyrazin-3(7H)-ones (*Cypridina* luciferin analogues): support for the single electron transfer (SET)–oxygenation mechanism with triplet molecular oxygen. *Tetrahedron Lett.*, 46, 7701–7704.

Kresse, G. and Hafner, J., (1993) *Ab initio* molecular dynamics for liquid metals. *Phys. Rev. B.*, 47, 558-561.

Kresse, G. and Hafner, J., (1994) *Ab initio* molecular-dynamics simulation of the liquid-metal-amorphous-semiconductor transition in germanium. *Phys. Rev. B.*, 49, 14251-14269.

Kresse, G. and Furthmüller, J., (1996) Efficient iterative schemes for *ab initio* total-energy calculations using a plane-wave basis set. *Phys. Rev. B.*, 54, 11169-11186.

Kudryavtsev, A.N., Krasitskaya, V.V., Petunin, A.I., Burakov, A.Y. and Frank, L.A.,

(2012) Simultaneous bioluminescent immunoassay of serum total and IgG-bound prolactins. *Anal. Chem.*, 84, 3119-3124.

Kurose, K., Inouye, S., Sakaki, Y. and Tsuji, F.I., (1989) Bioluminescence of the calcium-binding photoprotein aequorin after cysteine modification. *Proc. Natl. Acad. Sci. USA*, 86, 80-84.

L

Lakowicz, J.R., (2006) *Principles of Fluorescence Spectroscopy*, Third Edition, Springer, Singapore.

Lee, C., Yang, W. and Parr, R.G., (1988) Development of the Colle-Salvetti correlation energy formula into a functional of the electron density. *Phys. Rev. B*, 37, 785-789.

Lee, J., (2001) Bioluminescence. Nature Encyclopedia of Life Sciences online (www.els.net).

Lee, J., Glushka, J.N., Markova, S.V., and Vysotski, E.S., (2001) Protein conformational changes in obelin shown by ^{15}N-HSQC nuclear magnetic resonance. In *Bioluminescence & Chemiluminescence* (Case J.F., Herring P.J., Robison B.H., Haddock S.H.D., Kricka L.J. and Stanley P.E., eds.), World Scientific, Singapore, pp. 99–102.

Leferink, N.G., Fraaije, M.W., Joosten, H.J., Schaap, P.J., Mattevi, A. and van Berkel, W.J.H., (2009). Identification of a gatekeeper residue that prevents dehydrogenases from acting as oxidases. *J. Biol. Chem.*, 284, 4392-4397.

Levine, L.D. and Ward, W.W., (1982) Isolation and characterization of a photoprotein, "phialidin," and a spectrally unique green-fluorescent protein from the bioluminescent jellyfish *Phialidium gregarium*. *Comp. Biochem. Physiol. B.*, 72, 77–85.

Lewis, J.C., Lopez-Moya, J.J. and Daunert S., (2000) Bioluminescence and secondary structure properties of aequorin mutants produced for site-specific conjugation and immobilization. *Bioconjug. Chem.*, 11, 65-70.

Liu, Z.J., Vysotski, E.S., Chen, C.J., Rose, J.P., Lee, J. and Wang, B.C., (2000) Structure of the Ca^{2+}-regulated photoprotein obelin at 1.7 Å resolution determined directly from its sulfur substructure. *Protein Sci.*, 11, 2085-2093.

Liu, Z.J., Vysotski, E.S., Deng, L., Lee, J., Rose, J. and Wang, B.C., (2003) Atomic resolution structure of obelin: soaking with calcium enhances electron density of the second oxygen atom substituted at the C2-position of coelenterazine. *Biochem. Biophys. Res. Commun*., 311, 433–439.

Liu, Z.J., Stepanyuk, G.A., Vysotski, E.S., Lee, J., Markova, S.V., Malikova, N.P. and Wang, B.C., (2006) Crystal structure of obelin after Ca^{2+}-triggered bioluminescence suggests neutral coelenteramide as the primary excited state. *Proc. Natl. Acad. Sci. USA*, 103, 2570-2575.

Loening, A.M., Fenn, T.D. and Gambhir, S.S., (2007) Crystal structures of the luciferase and green fluorescent protein from *Renilla reniformis*. *J. Mol. Biol.*, 374, 1017-1028.

M

Malikova, N.P., Stepanyuk, G.A., Frank, L.A., Markova, S.V., Vysotski, E.S. and Lee, J., (2003) Spectral tuning of obelin bioluminescence by mutations of Trp92. *FEBS Lett.*, 554, 184-188.

Malikova, N.P., Visser, N.V., van Hoek, A., Skakun, V.V., Vysotski, E.S., Lee, J., Visser, A.J., (2011) Green-fluorescent protein from the bioluminescent jellyfish *Clytia gregaria* is an obligate dimer and does not form a stable complex with the Ca(2+)-discharged photoprotein clytin. *Biochemistry*, 50, 4232-4241.

Markova, S.V., Vysotski, E.S. and Lee, J., (2001) Obelin hyperexpression and characterization. In *Bioluminescence and Chemiluminescence* (Case, J.F., Herring, P.J., Robison, B.H., Haddock, S.H.D., Kricka, L.J. and Stanley, P.E., eds), World Scientific, Singapore, pp. 115-118.

Markova, S.V., Vysotski, E.S., Blinks, J.R., Burakova, L.P., Wang, B.C. and Lee, J., (2002) Obelin from the bioluminescent marine hydroid *Obelia geniculata*: cloning, expression, and comparison of some properties with those of other Ca^{2+}-regulated photoproteins. *Biochemistry,* 41, 2227–2236.

Markova, S.V., Burakova, L.P., Golz, S., Malikova, N.P., Frank, L.A. and Vysotski, E.S., (2012) Light-sensitive photoprotein berovin from the bioluminescent ctenophore *Beroe abyssicola*: A novel type of Ca(2+)-regulated photoprotein. *FEBS J.*, 279, 856-870.

Massey, V., (1994) Activation of molecular oxygen by flavins and flavoproteins. *J. Biol. Chem.*, 269, 22459-22462.

Masuda, H., Takenaka, Y., Shikamoto, Y., Kagawa, M., Mizuno, H. and Tsuji, F.I., (2003) Chromatography of isoforms of recombinant apoaequorin and method for the preparation of aequorin. *Protein Expr. Purif.*, 31, 181-187.

McCapra, F. and Chang, Y.C., (1967) The chemiluminescence of a *Cypridina* luciferin analogue. *Chem. Commun.*, 19, 1011–1012.

McDonald, C.A., Fagan, R.L., Collard, F., Monnier, V.M. and Palfey, B.A., (2011) Oxygen reactivity in flavoenzymes: context matters. *J. Am. Chem. Soc.*, 133, 16809-

16811.

Miertus, S., Scrocco, E. and Tomasi, J., (1981) Electrostatic interaction of a solute with a continuum. A direct utilization of *ab initio* molecular potentials for the prevision of solvent effects. *Chem. Phys.*, 55, 117-129.

Miertus, S. and Tomasi, J., (1982) Approximate evaluations of the electrostatic free energy and internal energy changes in solution processes. *Chem.Phys.*, 65, 239-241.

Milet, A., Korona, T., Moszynski, R. and Kochanski, E., (1999) Anisotropic intermolecular interactions in van der Waals and hydrogen-bonded complexes: What can we get from density functional calculations? *J. Chem. Phys.*, 111, 7727-7735.

Mirasoli, M., Deo, S.K., Lewis, J.C., Roda, A. and Daunert, S., (2002) Bioluminescence immunoassay for cortisol using recombinant aequorin as a label. *Anal. Biochem.*, 306, 204–211.

Mithofer, A and Mazars, C., (2002) Aequorin-based measurements of intracellular Ca^{2+}-signatures in plant cells. *Biol. Proceed. Online,* 4, 105–118.

Moncrief, N.D., Kretsinger, R.H. and Goodman, M. (1990) Evolution of EF-hand calcium-modulated proteins. I. Relationships based on amino acid sequences. *J. Mol. Evol.*, 30, 522-562.

Mori, K., Maki, S. Niwa, H, Ikeda, H. and Hirano, T., (2006) Real light emitter in the bioluminescence of the calcium-activated photoproteins aequorin and obelin: light emission from the singlet-excited state of coelenteramide phenolate anion in a contact ion pair. *Tetrahedron,* 62, 6272–6288.

Morin, J.G., (1974) Coelenterate bioluminescence. In: *Coelenterate biology: Reviews and new perspectives* (Muscatine, L. and Lenhoff, H.M., eds.), Academic Press, New York, pp. 397-438.

Moscatiello, R., Alberghini, S., Squartini, A., Mariani, P. and Navazio, L., (2009) Evidence for calcium-mediated perception of plant symbiotic signals in aequorin-expressing *Mesorhizobium loti. BMC Microbiol.* 9, 206.

Mullen, K.M. and van Stokkum, I.H.M., (2007) TIMP: an R package for modeling multi-way spectroscopic measurements. *J. Stat. Soft.,*18, 2007.

N

Nakai, S., Yasui, M., Nakazato, M., Iwasaki, F., Maki, S., Niwa, H., Ohashi, M. and Hirano, T., (2003) Fundamental studies on the structures and spectroscopic properties of imidazo[1,2-a]pyrazin-3(7H)-one derivatives. *Bull. Chem. Soc. Jpn.*, 76, 2361–2387.

Nakatani, N., Hasegawa, J. and Nakatsuji, H., (2007) Red light in chemiluminescence and yellow-green light in bioluminescence: color-tuning mechanism of firefly, *Photinus pyralis*, studied by the symmetry-adapted cluster-configuration interaction method. *J. Am. Chem. Soc.*, 129, 8756-8765.

Nelson, M.R. and Chazin, W.J., (1998) Structures of EF-hand Ca(2+)-binding proteins: diversity in the organization, packing and response to Ca^{2+} binding. *Biometals*, 11, 297–318.

O

Ohmiya, Y., Ohashi, M. and Tsuji, F.I., (1992) Two excited states in aequorin bioluminescence induced by tryptophan modification. *FEBS Lett.*, 301, 197-201.

Ohmiya, Y., Kurono, S., Ohashi, M., Fagan, T.F. and Tsuji, F.I., (1993) Mass spectrometric evidence for a disulfide bond in aequorin regeneration. *FEBS Lett.*, 332, 226-228.

Ohmiya, Y., and Tsuji, F.I., (1993) Bioluminescence of the Ca^{2+}-binding photoprotein, aequorin, after histidine modification. *FEBS Lett.*, 320, 267-70.

Oliva, M., Safont, V.S., Andrés, J. and Tapia, O., (2001) Transition structures for D-ribulose-1,5-bisphosphate carboxylase/oxygenase-catalyzed oxygenation chemistry: Role of carbamylated lysine in a model magnesium coordination sphere. *J. Phys. Chem. A.*, 105, 4726–4736.

P

Pace, C.N. and Laurents, D.V., (1989) A new method for determining the heat capacity change for protein folding. *Biochemistry*, 28, 2520-2525.

Peng, C. and Schlegel, H.B., (1993) Combining synchronous transit and quasi-Newton methods to find transition states. *Israel J. Chem.*, 33, 449-454.

Perdew, J.P., Burke, K. and Ernzerhof, M., (1996) Generalized gradient approximation made simple. *Phys. Rev. Lett.*, 77, 3865-3868.

Petushkov V.N., van Stokkum, I.H.M., Gobets, B., van Mourik, F., Lee, J., van Grondelle, R. and Visser. A.J.W.G., (2003) Ultrafast fluorescence relaxation spectroscopy of 6,7-dimethyl-(8-ribityl)-lumazine and riboflavin, free and bound to antenna proteins from bioluminescent bacteria. *J. Phys. Chem. B.*, 107, 10934-10939.

Prasher, D., McCann, R.O. and Cormier, M.J., (1985) Cloning and expression of the cDNA coding for aequorin, a bioluminescent calcium-binding protein. *Biochem. Biophys. Res. Commun.*, 126, 1259-1268.

Prasher, D.C., McCann, R.O., Longiaru, M. and Cormier, M.J., (1987) Sequence comparisons of complementary DNAs encoding aequorin isotypes. *Biochemistry*, 26, 1326-1332.

Prendergast, F.G., (2000) Bioluminescence illuminated. *Nature*, 405, 291-293.

Privalov, P.L. and Khechinashvili, N.N., (1974) A thermodynamic approach to the problem of stabilization of globular protein structure: a calorimetric study. *J. Mol. Biol.*, 86, 665-684.

Prokop, Z., Monincová, M., Chaloupková, R., Klvana, M., Nagata, Y., Janssen, D.B. and Damborský, J., (2003) Catalytic mechanism of the maloalkane dehalogenase LinB from *Sphingomonas paucimobilis* UT26. *J. Biol. Chem.*, 278, 45094–45100.

Q

Qi, C.F., Gomi, Y., Ohashi, M., Ohmiya, Y. and Tsuji, F.I., (1991) Chemi- and bioluminescence, of coelenterazine analogues. Effects of substituents at the C2 position. *Chem. Commun.*, 18, 1307-1309.

R

Ray, B.D., Ho, S., Kemple, M.D., Prendergast, F.G. and Nageswara Rao, B.D., (1985) Proton NMR of aequorin. Structural changes concomitant with calcium-independent light emission. *Biochemistry*, 24, 4280-4287.

Rizzuto, R., Simpson, A.W.M., Brini, M. and Pozzan, T., (1992) Rapid changes of mitochondrial Ca^{2+} revealed by specifically targeted recombinant aequorin. *Nature*, 358, 325-327.

Roda, A., Pasini, P., Mirasoli, M., Michelini, E. and Guardigli, M., (2004) Biotechnological applications of bioluminescence and chemiluminescence. *Trends Biotechnol*. 22, 295-303.

Rowe L., Dikici, E. and Daunert S., (2009) Engineering bioluminescent proteins: expanding their analytical potential. *Anal. Chem.*, 81, 8662–8668.

S

Schmidt, M.W., Baldridge, K.K., Boatz, J.A., Elbert, S.T., Gordon, M.S., Jensen, J.H., Koseki, S., Matsunaga, N., Nguyen, K.A., Su, S., Windus, T.L., Dupuis, M. and Montgomery J.A.Jr., (1993) General atomic and molecular electronic structure system. *J. Comput. Chem.*, 14, 1347–1363.

Seliger, H.H., (1978) Excited states and absolute calibrations in bioluminescence. *Methods*

Enzymol., LVII, 560-600.

Shimomura, O., Johnson, F.H. and Saiga, Y., (1962) Extraction, purification and properties of aequorin, a bioluminescent protein from the luminous hydromedusan, *Aequorea*. *J. Cell. Comp. Physiol.,* 59, 223–240.

Shimomura, O. and Johnson, F.H., (1972) Structure of the light-emitting moiety of aequorin. *Biochemistry*, 11, 1602–1608.

Shimomura, O. and Johnson, F.H., (1973) Chemical nature of light emitter in bioluminescence of aequorin. *Tetrahedron Lett.,* 2963-2966.

Shimomura, O. and Johnson, F.H., (1975) Regeneration of the photoprotein aequorin. *Nature,* 256, 236-238.

Shimomura, O. and Johnson, F.H., (1978) Peroxidized coelenterazine, the active group in the photoprotein aequorin. *Proc. Natl. Acad. Sci. USA*, 75, 2611–2615.

Shimomura, O., Kishi, Y. and Inouye, S., (1993) The relative rate of aequorin regeneration from apoaequorin and coelenterazine analogues. *Biochem. J.,* 296, 549-551.

Shimomura, O. and Teranishi, K., (2000) Light-emitters involved in the luminescence of coelenterazine. *Luminescence,* 15, 51–58.

Shimomura, O., (2006) *Bioluminescence: chemical principles and methods.* World Scientific, Singapore.

Shropshire, W.Jr. and Gettens, R.H., (1966) Light induced concentration changes of adenosine-triphosphate in phycomyces sporangiophores. *Plant Physiol.*, 41, 203-207.

Steensma, E., Nijman, M.J.M., Bollen, Y.J.M., de Jager, P.A., van den Berg, W.A.M., van Dongen, W.M.A.M. and van Mierlo, C.P.M., (1998) Apparent local stability of the secondary structure of *Azotobacter vinelandii* holoflavodoxin II as probed by hydrogen exchange: implications for redox potential regulation and flavodoxin folding. *Protein Sci.,* 7, 306–317.

Steensma, E. and van Mierlo, C.P.M., (1998) Structural characterization of apoflavodoxin shows that the location of the stable nucleus differs among proteins with a flavodoxin-like topology. *J. Mol. Biol.,* 282**,** 653–666.

Steiner, R.A., Janssen, H.J., Roversi, P., Oakley, A.J. and Fetzner, S., (2010) Structural basis for cofactor-independent dioxygenation of N-heteroaromatic compounds at the alpha/beta-hydrolase fold. *Proc. Natl. Acad. Sci. USA.*, 107, 657–662.

Stepanyuk, G.A., Golz, S., Markova, S.V., Frank, L.A., Lee, J. and Vysotski, E.S., (2005) Interchange of aequorin and obelin bioluminescence color is determined by substitution of one active site residue of each photoprotein. *FEBS Lett.*, 579, 1008-1014.

Stewart, J.J.P., (1989) Optimization of parameters for semiempirical methods I. Method. *J. Comput. Chem.*, 10, 209-220.

Stewart, J.J.P., (2004) Optimization of parameters for semiempirical methods IV: Extension of MNDO, AM1, and PM3 to more main group elements. *J. Mol. Model.*, 10, 155-164.

Stewart, J.J.P., (2007) Optimization of parameters for semiempirical methods V: Modification of NDDO approximations and application to 70 elements. *J. Mol .Model.*, 13, 1172-1213.

T

Titushin, M.S., Feng, Y., Stepanyuk, G.A., Li, Y., Markova, S.V., Golz, S., Wang, B.C., Lee, J., Wang, J., Vysotski, E.S and Liu, Z.J., (2010) NMR-derived topology of a GFP-photoprotein energy transfer complex. *J. Biol. Chem.*, 285, 40891–40900.

Titushin, M.S., Feng, Y., Lee, J., Vysotski, E.S and Liu, Z.J., (2011) Protein-protein complexation in bioluminescence. *Protein Cell,* 2, 957–972.

Tomilin, F.N., Antipina, L.Y., Vysotski, E.S., Ovchinnikov S.G. and Gitelzon I.I., (2008) Fluorescence of calcium-discharged obelin: the structure and molecular mechanism of emitter formation. *Dokl. Biochem. Biophys.*, 422, 279-284.

Torres Pazmiño, D.E., Winkler, M., Glieder, A. and Fraaije, M.W., (2010) Monooxygenases as biocatalysts: Classification, mechanistic aspects and biotechnological applications. *J. Biotechnol.*, 146, 9-24.

Tsuji, F.I., Ohmiya, Y., Fagan, T.F., Toh, H. and Inouye S., (1995) Molecular evolution of the Ca^{2+}-binding photoproteins of the *Hydrozoa*. *Photochem. Photobiol.*, 62, 657–661.

U

Usami, K. and Isobe, M., (1996) Low-temperature photooxygenation of coelenterate luciferin analog synthesis and proof of 1,2-dioxetanone as luminescence intermediate. *Tetrahedron,* 52, 12061–12090.

V

van Berkel, W.J.H., Kamerbeek, N.M. and Fraaije, M.W., (2006) Flavoprotein monooxygenases, a diverse class of oxidative biocatalysts. *J. Biotechnol.*, 124, 670-689.

van Oort B., van Hoek A., Ruban A.V. and van Amerongen H., (2007) Equilibrium between quenched and nonquenched conformations of the major plant light-harvesting complex studied with high-pressure time-resolved fluorescence. *J. Phys. Chem. B,* 111, 7631-7637.

van Oort, B., Murali, S., Wientjes, E., Koehorst, R.B.M., Spruijt, R., van Hoek, A., Croce, R. and van Amerongen, H., (2009) Ultrafast resonance energy transfer from a site-specifically attached fluorescent chromophore reveals the folding of the N-terminal domain of CP29. *Chem. Phys.*, 357, 113-119.

van Stokkum, I.H.M., van Oort, B., van Mourik, F., Gobets, B. and van Amerongen, H., (2008) (Sub-)Picosecond spectral evolution of fluorescence studied with a synchroscan streak-camera system and target analysis. In *Biophysical Techniques in Photosynthesis*, Volume II (Aartsma, T.J. and Matysik, J., eds.), Springer, Dordrecht, pp. 223-240.

Vanderbilt, D. (1990) Soft self-consistent pseudopotentials in a generalized eigenvalue formalism. *Phys. Rev. B.*, 41, 7892-7895.

Vervoort, J., Müller, F., Lee, J., van den Berg, W.A.M. and Moonen, C.T., (1986) Identification of the true carbon-13 NMR spectrum of the stable intermediate II in bacterial luciferase. *Biochemistry*, 25, 8062-8067.

Vysotski, E.S., Bondar, B.S. and Letunov, V.N., (1989) Isolation and purification of Ca^{2+}-dependent photoprotein – obelin from hydroid *Obelia longissima*. *Biochemistry* (in Russian), 54, 965-973.

Vysotski, E.S., Liu, Z.J., Rose, J., Wang, B.C. and Lee, J., (1999) Preparation and preliminary study of crystals of the recombinant calcium-regulated photoprotein obelin from the bioluminescent hydroid *Obelia longissima*. *Acta Crystallogr. D.*, 55, 1965-1966.

Vysotski, E.S., Liu, Z.J., Rose, J., Wang, B.C. and Lee, J., (2001) Preparation and X-ray crystallographic analysis of recombinant obelin crystals diffracting to beyond 1.1 Å. *Acta Crystallogr. D Biol. Crystallogr.*, 57, 1919-1921.

Vysotski, E.S., Liu, Z.J., Markova, S.V., Blinks, J.R., Deng, L., Frank, L.A., Herko, M., Malikova, N.P., Rose, J.P., Wang, B.C. and Lee, J., (2003) Violet bioluminescence and fast kinetics from W92F obelin: Structure-based proposals for the bioluminescence triggering and the identification of the emitting species.

Biochemistry, 42, 6013-6024.

Vysotski, E.S. and Lee, J., (2004) Ca^{2+}-regulated photoproteins: Structural insight into the bioluminescence mechanism. *Acc. Chem. Res.,* 37, 405-415.

Vysotski, E.S. and Lee, J., (2007) Bioluminescent mechanism of Ca^{2+}-regulated photoproteins from three-dimensional structures. In *Luciferases and Fluorescent Proteins: Principles and Advances in Biotechnology and Bioimaging* (Viviani, V.R. and Ohmiya, Y., eds.), Transworld Research Network, Kerala, India, pp. 19-41.

W

Ward, W.W. and Seliger, H.H., (1974) Properties of mnemiopsin and berovin, calcium-activated photoproteins from the ctenophores *Mnemiopsis sp*. *Biochemistry,* 13, 1500–1510.

Woo, J., Howell, M.H. and von Arnim, A.G., (2008) Structure-function studies on the active site of the coelenterazine-dependent luciferase from *Renilla*. *Protein Sci*., 17, 725-735.

Z

Zhao, G., Bruckner, R.C. and Jorns, M.S., (2008) Identification of the oxygen activation site in monomeric sarcosine oxidase: role of Lys265 in catalysis. *Biochemistry*, 47, 9124-9135.

Samenvatting en Algemene Discussie

Samenvatting

Dit proefschrift beschrijft onderzoek naar de structuur-functie relatie van het Ca^{2+}-gereguleerde foto-eiwit obelin uit de zeepoliep *Obelia longissima*.

In Hoofdstuk 1 wordt beschreven wat Ca^{2+}-gereguleerde foto-eiwitten zijn, wat ze doen en waar ze in de natuur voorkomen. Naast het verstrekken van informatie over hun ruimtelijke structuur en bioluminiscentie eigenschappen wordt er aandacht besteed aan de biologische partners en mogelijke toepassingen van deze eiwitten.

Hoofdstuk 2 beschrijft de verschillende ligand-afhankelijke conformaties van obelin**.** Steady-state fluorescentie en circulair dichroisme gegevens tonen aan dat deze conformaties verschillen in temperatuur stabiliteit. Apo-eiwit zonder ligand is de minst stabiele vorm van obelin welke bestaat uit een ensemble van conformaties die in elkaar kunnen overgaaan. Binding van coelenterazine en calcium beschermen obelin aanzienlijk tegen temperatuur-geinduceerde ontvouwing.

Hoofdstuk 3 beschrijft het bindingsgedrag van coelenterazine aan apo-obelin en apo-aequorin. Fluorescentie titratie studies tonen aan dat de dissociatie-constanten van de eiwit-coelenterazine complexen liggen in het laag micromolaire gebied. Snelle kinetiek metingen laten zien dat coelenterazine binding aan apo-obelin plaatsvindt binnen milliseconden. Vorming van het actieve obelin-2-hydroperoxycoelenterazine complex duurt vervolgens minuten. Hieruit kan worden afgeleid dat de reactie met zuurstof de snelheidsbeperkende stap is tijdens het activatieproces.

In **Hoofdstuk 4** worden de spectrale eigenschappen van het anaerobe obelin-coelenterazine complex beschreven en na reactie met zuurstof. In het anaerobe obelin-coelenterazine complex bestaat coelenterazine waarschijnlijk uit een mengsel van de N7 geprotoneerde en C2 anionische vorm. Vorming van 2-hydroperoxycoelenterazine wordt gestimuleerd door proton overdracht van N7 naar C2 en gebeurt waarschijnlijk met hulp van His175. Deze histidine is niet alleen belangrijk voor de vorming van actief obelin maar ook voor het triggeren van de bioluminescentie reactie door calcium.

Hoofdstuk 5 geeft een meer verdiepend inzicht in de vorming van het geactiveerde obelin-2-hydroperoxycoelenterazine complex. Op basis van kwantum chemische berekeningen en kinetische studies van geselecteerde mutant eiwitten wordt een

mechanisme voorgesteld voor de vorming van het peroxy adduct. Tevens wordt ingegaan op de mogelijke rol van kritische residuen in de coelenterazine bindingsplaats.

Na binding aan apo-obelin en een conformationele herrangschikking zorgt His175 er voor dat coelenterazine op C2 wordt geprotoneerd. Vervolgens wordt coelenterazine met behulp van zuurstof omgezet in 2-hydroperoxycoelenterazine. Dit proces verloopt langzaam en vereist mogelijk een verdere structurele aanpassing van het eiwit. Van der Waals krachten spelen een sleutelrol in het activeringsproces. Tyr138 zorgt voor een optimale positionering van het zuurstof molecuul waardoor de kans op een stabiel Van der Waals complex tussen C2 geprotoneerd coelenterazine en zuurstof, en dus de kans op vorming van 2-hydroperoxycoelenterazine, wordt vergroot.

In **Hoofdstuk 6** worden de bioluminescente en spectroscopische eigenschappen van verschillende obelin en aequorin varianten beschreven. Het vervangen van His175, Trp179 en Tyr190 door residuen met andere waterstofbrug donor-acceptor eigenschappen verlaagt de opbrengst aan actief foto-eiwit en de bioluminescentie activiteit. In afwezigheid van calcium vertonen alle mutanten in tegenstelling tot de wild type eiwitten luciferase-achtige bioluminescentie activiteit. Dit geeft aan dat His175, Trp179 en Tyr190 via waterstofbrug netwerken zorgen voor de juiste orientatie van 2-hydroperoxycoelenterazine in het actieve centrum.

Hoofdstuk 7 beschrijft een fluorescentie relaxatie studie over de dynamische eigenschappen van de aangeslagen toestand in de door calcium ontladen foto-eiwitten aequorin en obelin. De initieel gevormde fluorescente producten worden toegekend aan de neutrale vorm van eiwit-gebonden coelenteramide die op picoseconde tijdschaal door relaxatie van de eiwtomgeving wordt omgezet in de anionische vorm.

Hoofdstuk 8 beschrijft een verdere studie naar de identiteit van de licht uitzendende deeltjes in het obelin bioluminescentie proces. Door middel van stopped-flow snelle reactie kinetiek is aangetoond dat de unieke bimodale bioluminescentie van de W92F obelin variant kan worden gebruikt voor het bepalen van de snelheid van vorming en afbraak van de neutrale (blauwe) en anionische (paarse) licht uitzendende deeltjes. Er wordt voorgesteld dat beide aangeslagen toestanden afkomstig zijn van verschillende ontledingsroutes van dioxetanon en dat ze onafhankelijk licht uitzenden.

Algemene Discussie

Ca^{2+}-gereguleerde foto-eiwitten

Ca^{2+}-gereguleerde foto-eiwitten zijn aantrekklijke analytische gereedschappen voor vele onderzoeksgebieden. Vanwege de hoge gevoeligheid van het bioluminescentie signaal kunnen foto-eiwit applicaties veranderingen in calcium concentratie waarnemen van 10^{-7} to 10^{-3} M zonder dat er extra belichting nodig is. Gedetailleerd inzicht in het mechanisme van bioluminescentie en een beter begrip van hoe Ca^{2+}-gereguleerde foto-eiwitten worden geactiveerd vormen de fundamentele basis voor het verbeteren van de diverse toepassingsmogelijkheden van foto-eiwtten.

Ca^{2+}-gereguleerde foto-eiwitten bestaan uit een enkele polypeptide keten van ongeveer 22 kDa met daarin een stevig gebonden 2-hydroperoxycoelenterazine molecuul (Shimomura en Johnson, 1978; Head *et al.,* 2000; Liu *et al.,* 2000). Het startschot voor de bioluminescentie reactie van foto-eiwitten wordt gegeven door calcium. Binding van deze sensor induceert de oxidatieve decarboxylering van 2-hydroperoxycoelenterazine tot coelenteramide in zijn aangeslagen toestand, wat vervolgens leidt tot productie van blauw licht met een golflengte van 465-495 nm.

Er zijn verschillende tertiaire structuren van foto-eiwitten bekend (bijvoorbeeld Head et al. 2000, Liu et al. 2000), en er is al veel inzicht verkregen in het mechanisme van de door foto-eiwitten gekatalyseerde bioluminescentie reactie (Fig. 1.9) (Vysotski and Lee, 2004; Vysotski and Lee, 2007). Ca^{2+}-gereguleerde foto-eiwitten worden succesvol toegepast als reporters en labels in bindings assays en worden alom gebruikt voor het bepalen van calcium concentraties in biologische systemen (Roda *et al.,* 2004; Rowe *et al.,* 2009; Grienberger and Konnerth, 2012).

Conformatietoestanden van obelin

Tot nu toe zijn vijf conformatietoestanden van obelin geisoleerd: apo-eiwit, eiwit met gebonden 2-hydroperoxycoelenterazine (actief obelin), eiwit met gebonden coelenteramide en gebonden calcium (calcium ontladen obelin), eiwit met gebonden coelenteramide, en eiwit met gebonden calcium. Alleen van de geligandeerde vormen zijn 3D-structuren bekend (Fig. 2.1).

Pogingen om de 3D-structuur van apo-obelin op te lossen zijn gestrand omdat er geen geschikte kristallen konden worden verkregen. De fluorescentie en circulair dichroisme experimenten die beschreven staan in **Hoofdstuk 2** verduidelijken waarom apo-obelin niet goed kristallisseert. Het uit inclusion bodies verkregen apo-obelin bestaat uit een mengsel van verschillende conformaties en is erg labiel. Binding van coelenterazine en/of calcium beschermt obelin aanzienlijk tegen temperatuur geinduceerde ontvouwing en brengt het eiwit in een meer gedefinieerde conformatie. De in dit hoofdstuk verkregen resultaten suggereren ook dat het artificieel geproduceerde apo-eiwit niet de werkelijke conformatie weergeeft van apo-obelin in *Obelia* cellen en dat binding van coelenterazine nodig is om het eiwit te beschermen tegen afbraak en aggregatie.

Vorming van 2-hydroperoxycoelenterazine

Recombinante apo foto-eiwitten kunnen in afwezigheid van calcium omgezet worden in de actieve 2-hydroperoxycoelenterazine geligandeerde vorm door incubatie met coelenterazine, moleculaire zuurstof en thiol-reducerende agentia (Shimomura en Johnson, 1975). Echter, hoe het actieve foto-eiwit precies wordt gevormd is lange tijd volledig duister gebleven.

Door gebruik te maken van de intrinsieke fluorescentie van het apo-obelin konden we voor het eerst aantonen dat de binding van coelenterazine plaatsvindt binnen milliseconden (**Hoofdstuk 3**). Tryptofaan fluorescentie binding studies gaven dissociatieconstanten voor het obelin-coelenterazine complex in het laag micromolaire gebied en toonden aan dat coelenterazine stevig gebonden blijft aan het apo-eiwit. Uit deze studie kon echter niet worden afgeleid of de stevige interactie wordt veroorzaakt door het feit dat het eiwit-gebonden coelenterazine langzaam met zuurstof wordt omgezet tot 2-hydroperoxycoelenterazine.

Door zuivering van het anaerobe apo-obelin–coelenterazine complex kon vastgesteld worden dat apo-obelin en coelenterazine inderdaad een stevig complex vormen voordat de modificatie van coelenterazine met zuurstof plaatsvindt (**Hoofdstuk 4**). De verkregen spectroscopische en kinetische gegevens suggereerden tevens dat het initieel gebonden coelenterazine in evenwicht is tussen een N7 geprotoneerde en een C2 anionische vorm.

De activering van apo-obelin is verder onderzocht door kinetische studies aan geselecteerde mutant eiwtten te combineren met gedetailleerde kwantum chemische berekeningen (**Hoofdstuk 5**). Via deze aanpak kon een hypothese worden opgesteld voor het mechanisme van de 2-hydroperoxycoelenterazine vorming en de rol van twee sleutelresiduen (His175 and Tyr138) tijdens dit proces. Na de initiële binding van coelenterazine treedt er in obelin een conformationele herrangschikking plaats waardoor het coelenterazine reactiecentrum wordt gevormd en protonering op C2 kan plaatsvinden. His175 fungeert bij dit laatste proces waarschijnlijk als proton shuttle. De volgende stap is de zuurstof-afhankelijke omzetting van het gebonden coelenterazine in 2-hydroperoxycoelenterazine; dit proces duurt minuten en mogelijk treden hierbij additionele conformatieveranderingen op. Vorming van het Van der Waals complex tussen de geprotoneerde C2 vorm van coelenterazine en zuurstof wordt waarschijnlijk gestimuleerd met hulp van Tyr138 (Fig. 5.13).

De langzame reactie met zuurstof (Shimomura en Johnson, 1975; **Hoofdstuk 4 en 5**) onderscheidt Ca^{2+}-gereguleerde foto-eiwitten van andere monooxygenases en oxidases die meestal bijzonder snel met zuurstof reageren (Massey, 1994). Studies aan flavine-afhankelijke enzymen hebben laten zien dat vervanging van een enkel aminozuur residue de reactiesnelheid van gereduceerd flavine met zuurstof enorm kan opkrikken. (Zhao *et al.,* 2008; Leferink *et al.,* 2009). Een positieve lading nabij de flavine bindingsplaats verhoogt de reactiesnelheid met zuurstof in verschillende oxidases (Klinman, 2007; Jorns *et al.,* 2010; Gadda, 2012) en ook in de monooxygenase SidA (Franceschini *et al.,* 2012). In dihydroorotate dehydrogenase daarentegen heeft het inbrengen van een positieve lading in het actieve centrum niet het gewenste effect (McDonald *et al.,* 2011).

Zuurstof kan een eiwit in diffunderen via discrete kanalen en deze gelimiteerde diffusie kan de snelheidsbeperkende stap zijn in de katalyse (Klinman, 2007). Recent is voorgesteld dat er meerdere diffusie routes zijn voor zuurstof in flavoenzymen en dat deze wegen samenkomen bij de toegangspoort tot het actieve centrum (Baron *et al.,* 2009). Een verdiepende studie naar het diffusie gedrag van zuurstof en een betere omschrijving van de locale omgeving rondom het C2 atoom van coelenterazine zou een verklaring kunnen

geven waarom de oxidatie reactie in foto-eiwitten zo langzaam is en zou mogelijk ook een hint kunnen opleveren hoe deze reactie te verbeteren.

Stabilisatie van 2-hydroperoxycoelenterazine

Volgens de ruimtelijke structuur van obelin (Liu *et al.*, 2000), vormen de zijketens van His175, Trp179, Tyr190 en enkele andere residuen waterstofbruggen met het gebonden 2-hydroperoxycoelenterazine (Fig. 1.4). Plaatsgerichte mutagenese studies toonden aan dat de vervanging van His175, Trp179, of Tyr190 door andere residuen in de meeste gevallen resulteerde in een significant verlies van bioluminescentie activiteit en het opkomen van luciferase activiteit, die nauwelijks aanwezig is in wild-type obelin (**Hoofdstuk 6**). Hieruit kon worden opgemaakt dat His175, Trp179, en Tyr190 een waterstofbrug netwerk vormen die het substraat stabiliseert en dat deze triade belangrijk is voor de juiste positionering van 2-hydroperoxycoelenterazine.

Flavine-afhankelijke monooxygenases stabiliseren ook peroxy intermediairen tijdens hun reactiecyclus, maar deze stabilisatie is sterk afhankelijk van het type enzym. In hydroxylases is de geprotoneerde flavine peroxide erg labiel (Chaiyen et al., 2012). Baeyer–Villiger monooxygenases en verwante enzymen maken gebruik van gebonden $NADP^+$ om de anionische peroxyflavine te stabiliseren (van Berkel, 2006). In bacterieel luciferase is de peroxyflavine in afwezigheid van het aldehyde substraat zodanig stabiel dat isolatie (Hastings *et al.*, 1973) en identificatie (Vervoort *et al.*, 1986) mogelijk is.

Ca^{2+}-gereguleerde foto-eiwtten gaan veel verder: zij stabiliseren de 2-hydroperoxycoelenterazine in het actieve centrum zodanig dat het geactiveerde eiwit maandenlang gebruikt kan worden voor allerlei assays. *Renilla* luciferase (RLuc) is een ander bioluminescent eiwit dat coelenterazine gebruikt als substraat (Karkhanis en Cormier, 1971). In de foto-eiwitten wordt het peroxy anion geprotoneerd, terwijl in RLuc de peroxy anion onmiddellijk cycliseert tot een dioxetanon en vervolgens uiteen valt in coelenteramide, kooldioxide en licht (Hart *et al.*, 1978). Het waterstofbrug netwerk rondom de peroxy anion moet in luciferases dus anders zijn dan in de foto-eiwitten zodat een stabilisatie van het adduct voorkomen wordt.

De verschillen in stabiliteit van het peroxycoelenterazine in bioluminescente eiwitten heeft ook ecologische betekenis. Organismen die luciferases bevatten gloeien

continu in aanwezigheid van zuurstof en produceren geen calcium-afhankelijke lichtflitsen. Het gloeien wordt algemeen beschouwd als een lokmiddel terwijl de lichtflitsen meer als een afweermiddel worden gezien (Haddock ***et al.***, 2010). Het verschil in bioluminescentie kinetiek tussen luciferases en foto-eiwitten geeft ook diversiteit in de analytische toepassingen. Luciferases zijn zeer geschikt voor ***in vivo*** imaging en reporter assays, terwijl Ca^{2+}-gereguleerde foto-eiwitten uitgebreid gebruikt worden in immuno- en DNA hybridisatie assays en als Ca^{2+} indicators.

RLuc heeft een α/β-hydrolase vouwingspatroon (Loening ***et al.***, 2007), wat afwijkt van de compacte globulaire structuur van foto-eiwitten met helix-turn-helix motieven (Head ***et al.***, 2000; Liu ***et al.***, 2000). RLuc bezit vele aromatische residuen maar mist de katalytische His-Trp-Tyr triade van foto-eiwitten (Woo ***et al.***, 2008), en vooral een residue dat equivalent is met Tyr190 in obelin. Deze tyrosine stabiliseert de 2-hydroperoxycoelenterazine via een waterstofbrug. Er is meer onderzoek nodig naar de factoren die de stabiliteit van zuurstofadducten in foto-eiwitten bepalen. Hierdoor wordt het misschien mogelijk om peroxy intermediairen te stabiliseren in eiwitten die deze adducten normaal slechts mondjesmaat stabiliseren. Dit is vooral nuttig in gevallen waarbij de reactie geoptimaliseerd moet worden voor de synthese van waardevolle (chirale) producten.

Lichtgevende deeltjes in foto-eiwitten

De aard van de lichtgevende deeltjes in foto-eiwitten is al jarenlang een intrigrerend onderwerp voor onderzoekers. Op basis van plaatsgerichte mutagenese studies en structuuronderzoek aan foto-eiwitten (Liu ***et al.***, 2000; Deng ***et al.***, 2001; Liu ***et al.***, 2003; Vysotski ***et al.***, 2003; Liu ***et al.***, 2006), en chemische studies van coelenterazine model verbindingen (McCapra and Chang, 1967; Shimomura and Teranishi, 2000; Imai ***et al.***, 2001; Kondo ***et al.***, 2005; Mori ***et al.***, 2006), is voorgesteld dat de geëxciteerde toestand van het eiwit-gebonden coelenteramide uit minstens twee populaties bestaat, nl. de neutrale fenol en anionische fenolaat vorm. Het totale bioluminescentiespectrum is op deze manier het resultaat van een competitie tussen de stralingssnelheid vanuit de neutrale geëxciteerde toestand en de snelheid van populatie van de anionische geëxciteerde toestand (Fig. 1.9) (Vysotski en Lee, 2007).

Fluorescentie relaxatie studies van de geëxciteerde toestand van het eiwit-gebonden coelenteramide deden vermoeden dat eerst de neutrale vorm van de geëxciteerde toestand ontstaat en dat deze vorm wordt omgezet naar de anionische vorm op picoseconde tijdschaal (**Hoofdstuk 7**). Stopped-flow spectroscopie liet echter zien dat in de W92F obelin mutant de blauwe component van de bioluminescentie, die correspondeert met het coelenteramide phenolaat anion, eerder wordt gevormd en sneller wordt afgebroken dan de paarse (neutrale) component (**Hoofdstuk 8**). De neutrale en anionisch geëxciteerde toestanden zouden afkomstig kunnen zijn van verschillende routes voor het uiteenvallen van de dioxetanon (Isobe *et al.,* 2009) en aldus onafhankelijk licht kunnen geven in het bioluminescentie proces. Verdere spectroscopische studies gecombineerd met theoretische berekeningen kunnen mogelijk leiden tot een beter begrip van de afkomst van de lichtgevende deeltjes in de bioluminescentie reactie van foto-eiwitten.

Concluderend kan gesteld worden dat de resultaten beschreven in dit proefschrift meer inzicht hebben verschaft in de vorming van het actieve foto-eiwit complex. Tevens is meer inzicht verkregen in de aard van de lichtgevende deeltjes die betrokken zijn bij het foto-eiwit bioluminescentie proces. De Ca^{2+}-gereguleerde foto-eiwitten kunnen beschouwd worden als cofactor-onafhankelijke monooxygenases. Zij hebben echter enkele unieke kenmerkende eigenschappen zoals de langzame reactie met zuurstof en de effectieve stabilisatie van het peroxy gesubstitueerde coelenterazine substraat. De kennis die in dit proefschrift verkregen is over de vorming en stabilisatie van het 2-hydroperoxycoelenterazine adduct kan toegepast worden in studies van andere monooxygenases, bijvoorbeeld bij het controleren van zuurstof reactiesnelheden of het stabiliseren van zuurstof intermediairen. De resultaten van dit proefschrift vormen ook een solide basis voor verdere studies naar de diverse aspecten van de bioluminescntie reactie van foto-eiwitten en kunnen nuttig zijn voor het verbeteren van in vivo en in vitro assays met deze eiwitten.

Acknowledgements

In 2007, when I came to Wageningen as a fresh Sandwich PhD-student I didn't know how gravely my life would change and how long this journey would be. Now when everything is done I would like to thank all people without whom this thesis would not exist.

My special thanks to my supervisors: Willem van Berkel, Eugene Vysotski and Ton Visser for giving me the chance to do a PhD both in Krasnoyarsk and in Wageningen. Willem and Eugene, thank you for your daily guidance through all these years, for the fruitful discussions and for help and advices you gave me. Dear Ton, I appreciate your contribution to this project and your never ending scientific ideas. I would like to thank Sacco de Vries for providing an excellent working and learning environment at the Biochemistry Department. I will always cherish my memory about our trips to the north of the country and those flights (and landings!).

As a Sandwich PhD-student I have spent most of my project time in the native state – working in the Photobiology Lab of the Institute of Biophysics, Krasnoyarsk. I am greatly indebted to Svetlana Markova and Ludmila Frank who taught me how to handle DNA and proteins in my first year in the lab during supervision of my MSc thesis. Many thanks to my colleagues, former and present, from the Photobiology Lab – Ludmila Burakova, Natalia Malikova, Vasilisa Krasitskaya, Pavel Natashin, Galya Stepanyuk, Maxim Titushin and Nadezhda Veryugina. I feel lucky to have such a nice group of people to work with. I appreciate your scientific help and overall support, and, of course, our fun during tea breaks and travels.

One year and a half of my PhD time that I have spent in Wageningen was great thanks to all my collegues from the Biochemistry Department. Adrie, Nicole, Teunie, Astrid, Carlo, Simon, Jan Willem, Willy, Stefania, Agatha, Antsje, Marije, Mieke, Joseline and Laura – thank you for assistance you always provide, for patiently absorbing all my questions and handling my problems. And special thanks to my officemates – Nicole (2007), Stefania (2011) and Mieke (2012). Daily chats with you were really a nice distraction from lab and computer work!

I would also like to acknowledge all collaborators from different groups all over the world involved in my project. Sergey Laptenok, Bart van Oort, Rob Koehorst and Herbert

van Amerongen from the Biophysics Department in Wageningen were busy with time-resolved measurements. Professor John Lee from University of Georgia, USA was involved in writing a Biochemistry paper and always provided valuable suggestions and constructive criticism. Felix Tomilin, Lyuba Antipina and Alexander Kuzubov from the Institute of Physics in Krasnoyarsk carried out all quantum chemical calculations included in this thesis. Nicole Leferink helped me with stopped-flow experiments in Prof. Nigel Scrutton's lab in University of Manchester.

In 2009 and 2010, I spent few months in Beijing, China in the National Lab of Biomacromolecules of the Institute of Biophysics working on the anaerobic obelin complex and trying to grow some crystals. I would like to thank Prof. Zhijie Liu for giving me the opportunity to work in his lab and for his hospitality. Chongyun Cheng, Heng Ru, Neil Shaw and Ke Chen gave me a lot of scientific and administrative assistance during my stay in Beijing and also broke a language barrier for me.

And last but not least my special thanks to Dmitry Zubov for the help with a cover of the book and for his support and friendship during all these years!

Thank you all for your time and energy devoted to this project!

List of publications

Eremeeva, E.V., Markova, S.V., Frank, L.A., Vysotski, E.S. **(2007)** The main function of His175, Trp179 and Tyr190 residues of the obelin binding site is to stabilize the hydroperoxycoelenterazine intermediate. In: *Bioluminescence & Chemiluminescence: Chemistry, Biology and Application* (Szalay, A.A., Hill, P.J., Kricka, L.J., Stanley, P.E., eds.), Singapore, World Scientific, pp. 7-10.

Eremeeva, E.V., Markova, S.V., Westphal, A.H., Visser, A.J.W.G., van Berkel, W.J.H., Vysotski, E.S. **(2009)** The intrinsic fluorescence of apo-obelin and apo-aequorin and use of its quenching to characterize coelenterazine binding. *FEBS Lett.*, 583, 1939-1944.

van Oort, B., **Eremeeva, E.V.,** Koehorst, R.B.M., Laptenok, S.P., van Amerongen, H., van Berkel, W.J.H., Malikova, N.P., Markova, S.V., Vysotski, E.S., Visser, A.J.W.G., Lee, J. **(2009)** Picosecond fluorescence relaxation spectroscopy of the calcium-discharged photoproteins aequorin and obelin. *Biochemistry*, 48, 10486-10491.

Eremeeva, E.V.; Vysotski, E.S., Westphal, A.H., van Mierlo, C.P.M., van Berkel, W.J.H. **(2012)** Ligand binding and conformational states of the photoprotein obelin. *FEBS Lett.***,** 586, 4173‑4179.

Eremeeva, E.V., Markova, S.V., Frank, L.A., Visser, A.J.W.G., van Berkel, W.J.H., Vysotski, E.S. **(2013)** Bioluminescent and spectroscopic properties of His-Trp-Tyr triad mutants of obelin and aequorin. *In preparation.*

Eremeeva, E.V., Natashin, P.V., van Berkel, W.J.H., Vysotski, E.S., Liu, Z.J. **(2013)** Oxygen activation of apo-obelin-coelenterazine complex. *In preparation.*

Eremeeva, E.V., Tomilin, F.N., Antipina, L.U., Kuzubov, A.A., Mezhevikin, V.V., Markova, S.V., van Berkel, W.J.H., Ovchinnikov, S.G., Vysotski, E.S. **(2013)** Molecular mechanism of active photoprotein formation. *In preparation.*

Curriculum vitae

Elena Eremeeva was born on the 25th of August 1983, in Krasnoyarsk, Russia. In 2000 she finished her high school education and started her studies at Krasnoyarsk State University majoring in Biochemistry. After graduation in 2005 with an MSc she joined the Photobiology Lab in the Institute of Biophysics RAS (Krasnoyarsk, Russia) as a PhD-student under supervision of Dr. Eugene Vysotski. In 2006 she started a Sandwich PhD-fellowship project at Wageningen University (The Netherlands) under the supervision of Prof. Willem van Berkel and Prof. Antonie Visser. During her research Elena took the opportunity to spend a few months in the Dr. ZhiJie Liu's National Lab of Biomacromolecules in the Institute of Biophysics CAS (Beijing, China) performing anaerobic experiments and apo-obelin crystallization attempts. Elena intends to continue working in the Photobiology Lab of the Institute of Biophysics (Krasnoyarsk, Russia) as a postdoc.

Overview of completed training activities

Discipline specific activities

Courses

Photophysics, Photochemistry and Photobiology (Amsterdam, 2007)

Proteomics (Wageningen, 2011)

Imaging Life at the Molecular Level Advanced Light Microscopy Course (Rotterdam-Amsterdam, 2011)

Conferences and meetings

14th Int. Symposium on Bioluminescence and Chemiluminescence (San-Diego, USA, 2006)

15th Int. Symposium on Bioluminescence and Chemiluminescence, (Shanghai, China, 2008) - winner of Marlene DeLuca Prize

35th FEBS Congress (Gothenburg, Sweden, 2010)

17th Int. Symposium on Bioluminescence and Chemiluminescence (Guelph, Canada, 2012)

NWO Study Group Biomolecular Chemistry (Lunteren, The Netherlands, 2012)

General courses

Advanced English (Krasnoyarsk, 2005-2006)

Philosophy and Science (Krasnoyarsk, 2005-2006)

Informatics and Programming (Krasnoyarsk, 2008)

Optional activities

Preparation of PhD propositions

Biochemistry weekly meetings (Wageningen, 2007, 2011, 2012)

Photobiology weekly meetings (Krasnoyarsk, 2006-2012)

The research described in this thesis was financially supported by Wageningen University Sandwich PhD-fellowship program.

Financial support from Wageningen University for printing this thesis is gratefully acknowledged.

Printed by Print Service Ede, Ede, The Netherlands.

Cover picture of *Obelia* by Karen & Nadya Sanamyan.
Cover design by Dmitry Zubov.